Tunisian Republic
Ministry of Higher Education and Scientific Research

University of Sfax
National School of Engineers of Sfax

Doctoral School of Sciences and Technologies

DOCTORAL Thesis

Order Number:

Doctoral Thesis

Presented at

National School of Engineers of Sfax

In partial fulfillment of the requirements to obtain

DOCTORAT

in Mechanical Engineering

Presented by

Maroua HAMMAMI

Efficiency And Wear In Automotive Gear Transmissions

December 8th - 2017

Dissertation committee:

M. Tahar FAKHFAKH	**Professor, National School of Engineers of Sfax - Tunisia**	**President**
M. Mnaouar CHOUCHANE	**Professor, National School of Engineers of Monastir - Tunisia**	**Reviewer**
M. Olivier BAREILLE	**Lecturer, Ecole Centrale of Lyon - France**	**Reviewer**
M. José DIAS RODRIGUES	**Professor, Faculty of Engineers University of Porto - Portugal**	**Member**
M. Mohamed Slim ABBES	**Lecturer, National School of Engineers of Sfax - Tunisia**	**Director**
M. Ramiro Carneiro MARTINS	**Professor, Faculty of Engineers University of Porto - Portugal**	**Director**
M. Jorge SEABRA	**Professor, Faculty of Engineers University of Porto - Portugal**	**Co-supervisor**
M. Mohamed HADDAR	**Professor, National School of Engineers of Sfax - Tunisia**	**Co-supervisor**

1.1Tunisian Republic
Ministry of Higher Education and Scientific Research

University of Sfax
National School of Engineers of Sfax

Doctoral School of Sciences and Technologies

Doctoral Thesis – Order Number:

University of Porto
Engineering Faculty

Doctoral Program in Mechanical Engineering

December 2017

Efficiency and Wear in Automotive Gear Transmissions

Maroua HAMMAMI

Doctoral Thesis
developed under the Co-Supervision Thesis Agreement of November 1st, 2014,
between the University of Sfax, Tunisia, and the University of Porto, Portugal.

Submitted to the National Engineering School of Sfax,
in partial fulfilment of the requirements to obtain the

Doctorat in Mechanical Engineering

Sustained le 8th December 2017, in front of the review committee:

M. Tahar FAKHFAKH	**Professor, National School of Engineers of Sfax - Tunisia**	**President**
M. Mnaouar CHOUCHANE	**Professor, National School of Engineers of Monastir - Tunisia**	**Reviewer**
M. Olivier BAREILLE	**Lecturer, Ecole Centrale of Lyon - France**	**Reviewer**
M. José DIAS RODRIGUES	**Professor, Faculty of Engineers University of Porto - Portugal**	**Member**
M. Mohamed Slim ABBES	**Lecturer, National School of Engineers of Sfax - Tunisia**	**Director**
M. Ramiro Carneiro MARTINS	**Professor, Faculty of Engineers University of Porto - Portugal**	**Director**
M. Jorge SEABRA	**Professor, Faculty of Engineers University of Porto - Portugal**	**Co-supervisor**
M. Mohamed HADDAR	**Professor, National School of Engineers of Sfax - Tunisia**	**Co-supervisor**

Acknowledgements

First of all, I thank God for giving me strength and ability to perform this work.

I would like to express my deepest gratitude to my supervisors Mohamed Slim Abbes, Ramiro Martins, Mohamed Haddar and Jorge Seabra, for the opportunity given and all their patient guidance, caring, permanent support and providing me an excellent atmosphere throughout the course of this work. Their great interest and through understanding my subject has been very inspiring for my work.

I am very much indebted to M. Tahar FAKHFAKH for having accepted to be my president of jury.

I also want to express appreciation to the two examiners M. Mnaouar CHOUCHANE and M. Olivier BAREILLE who kindly agreed to judge this work.

I offer my sincere appreciation and respect to M. José Dias RODRIGUES to be a member in committee of my graduation project and to asses my work.

I would like also to thank with much appreciation the crucial role of to my remarkable colleagues and friends at **CETRIB** (Carlos Fernandes, Pedro Marques, Beatriz Graça, David Gonçalves, José Brandão), they gave me the help to use all required machinery and the necessary material to perform the experimental tests and my colleagues at **LA2MP** especially my great friend Safa Ben Arab for all the help provided when I needed and the great working environment that made everything more enjoyable.

To my family: my parents and my two brothers for providing me with unfailing support and continuous encouragement throughout my years of study and through the process of researching, not only during these years, but my entire life. To my husband, for his continued and unfailing love, support and understanding during my pursuit of Ph.D degree that made the completion of thesis possible. You were always around at times. You helped me to keep things in perspective. I greatly value his contribution and deeply appreciate his belief in me.

It is a pleasure, honour and privilege to have done my work within collaboration between the National Engineering School of Sfax (**ENIS**) and **INEGI** (Instituto Nacional de Engenharia e Gestao Industial). Above all, I would like to acknowledge the financial, academic and technical support of the University of Engineering of Porto (**FEUP**) and **FCT** (Fundacao para a Ciencia e a Tecnologia).

Also, I want gratefully acknowledge the funding supported by:

- National Funds through Fundacao para a Ciencia e a Tecnologia (FCT), under the project EXCL-II/SEM-PRO/0103/2012;
- NORTE-01-0145-FEDER-000022 - SciTech - Science and Technology for Competitive and Sustainable Industries, cofinanced by Programa Operacional Regional do Norte (NORTE2020), through Fundo Europeu de Desenvolvimento Regional (FEDER);
- LAETA under the project UID/EMS/50022/2013.

Abstract

Fuel efficiency is a major concern for automotive manufacturers and the society in general. A lot of effort has been put into the decrease of emissions and fuel consumption. The axle transmission has not been in focus although it is among the components with poorer efficiency on the mechanical transmission. Thus, any improvement in the axle efficiency will have a large impact on the overall fuel economy.

The axle transmission is a key component of the vehicle powertrain. It is a complex mechanical system. Usually, it consists of a hypoid bevel geared transmission, rolling bearings, seals, shafts and axle gear oil.

The main goal of the project is to design an axle that transfer drive to the road surface as efficiently and low mechanical loss as possible.

To reach such ambitious objective, the present work is intended to study power loss in rolling bearings and gears, in particular lubricated with axle gear oils. It will be shown that the oil formulation, as well as the gears and rolling bearings geometry have a very significant influence on the power loss of gearboxes. The most important experimental works that support this thesis are:

- The physical, chemical and rheological characterization of different fully formulated axle oils;
- The traction coefficient and film thickness measurements in a ball-on-disc contact under the three lubrication regimes;
- Tribofilm generation using an axial rolling bearing test rig;
- The power loss measurement using different rolling bearing geometries under a wide range of conditions with different axle oil formulations;
- The power loss measurement of FZG gearboxes with different axle oil formulations and gear geometries.
- The work contains also several analytical and numerical models for:
  - The validation and the calibration of a rolling bearings power losses models based on SKF model;
  - The validation and the calibration of the gears power loss;
  - The characterization of the average coefficient of friction and the lubricant parameter (X_L) between the meshing gears;
  - The development and validation of a gearbox power loss model.

The findings will clearly show that the efficiency of the axle can be improved by modifying the oil formulation, the gear geometry, the rolling bearing geometry and the operating conditions.

Keywords

Axle gear oils
Tribological properties
Lubricating film
Friction behaviour
Tribofilm generation
Sliding coefficient of friction
Rolling bearings power loss
Gears power loss
Total power loss

Contents

List of Figures

List of Tables

Nomenclature

Variable	Units	Description
a	[m]	Radius of the contact circle
a	[mm]	Axis distance
$\overline{AE}.b$	[mm^2]	Plane of action area
a_A	[-]	D341 viscosity parameter
A_c	[m^2]	Surface contact area
A_{base}	[m^2]	Base area of the gearbox
A_{ca}	[m^2]	Area of the gearbox
A_h	[m^2]	Horizontal area of the gearbox
A_v	[m^2]	Vertical area of the gearbox
b	[mm]	Gear face width
B	[mm]	Rolling bearing width
C	[N]	Basic dynamic load rating capacity
C_0	[N]	Basic static load rating
c_f	[-]	Conduction factor
C_{ch}	[Nm]	Churning torque loss
C_m	[-]	Dimensionless drag group of churning losses
COF	[-]	Coefficient of friction
$CPUC$	[-]	Wear Particle Concentration
d	[-]	Dilution factor
d	[mm]	Rolling bearing bore diameter
d	[m]	Reference diameter
d'	[m]	Working pitch diameter
d_a	[m]	Tip diameter
d_b	[m]	Base diameter
d_m	[mm]	Mean diameter of a rolling bearing
d_s	[mm]	Rolling bearing seal counter-face diameter
d_{sh}	[m]	Shaft diameter
D	[mm]	Rolling bearing outside diameter
D_L	[-]	Large wear particles
D_S	[-]	Small wear particles
E	[Pa]	Elastic modulus
E^*	[Pa]	Contact equivalent Young modulus
F_a	[N]	Axial load
F_{bn}	[N]	Normal force to tooth flank
F_{bt}	[N]	Transverse force to tooth flank
F_D	[-]	Viscosity effect factor to calculate seal losses
F_n	[N]	Normal force
F_N	[N/mm]	Local load per unit length
F_r	[N]	Radial load
Fr	[-]	Froude number
f_0	[-]	Load dependent friction torque constant

f_1	[-]	Load dependent friction torque constant
G	[-]	Material parameter
g	[9.8 m/s^2]	Gravitational acceleration
g_α	[-]	Length of path of contact
G_{rr}	[-]	Factor depending on the bearing type, bearing mean diameter and applied load
G_{sl}	[Nmm]	Factor depending on the bearing type, bearing mean diameter and applied load
H	[mm]	Width of the bearing
h	[m]	Gear submersion height
h_{ca}	[m]	Height of gear unit housing
h_m	[μm]	Minimum film thickness
h_t	[m]	Tooth height
h_{t0}	[m]	Reference tooth height
h_0	[μm]	Center film thickness
h_{0C}	[μm]	Thermal corrected center film thickness
H	[-]	Original Hersey number
Hp	[-]	Modified Hersey number
H_V	[-]	Gear loss factor
H_{VL}	[-]	Local gear loss factor using rigid load distribution
$H_V^{Ohlendorf}$	[-]	Gear loss factor according to Ohlendorf
i	[-]	Gear transmission ratio
$ISUC$	[-]	Severity of Wear Particles
k	[-]	Viscosity ratio
K_{FZG}	[-]	FZG load stage
K_L	[W/mK]	Thermal conductivity
K_{rs}	[-]	Starvation constant for oil bath lubrication
K_L, K_Z	[-]	Drag friction torque constants of a rolling bearing
k_v, b_v, c_v	[-]	Vogel's equation constants to calculate kinematic viscosity
K_{S1}, K_{S2}	[-]	Seals friction torque constants of a rolling bearing
K_{ball}	[-]	Ball bearing related constant
K_{roll}	[-]	Roller bearing related constant
l	[m]	Roller element width
L	[-]	Thermal parameter
l^i	[mm]	Length of contact of a tooth
L_{ca}	[m]	Width of gear unit housing
LP	[-]	Lubricant parameter
m	[mm]	Gear normal module
M_0	[Nmm]	Load independent friction torque of a rolling bearing
M_1	[Nmm]	Load dependent friction torque of a rolling bearing
m_A	[-]	D341 viscosity parameter
M_t	[Nmm]	Total friction torque
M_t^{exp}	[Nmm]	Experimental total friction torque of a rolling bearing
M_{r1}	[%]	Peak material ratio
M_{r2}	[%]	Valley material ratio
M'_{rr}	[Nmm]	Rolling friction torque
M_{sl}	[Nmm]	Sliding friction torque

M_{seal}	[Nmm]	Seals friction torque
M_{drag}	[Nmm]	Drag losses
n	[rpm]	Rotational speed
n_A	[-]	D341 viscosity parameter
P	[N]	Load
$P1$	[N]	Bearing load
p_0	[Pa]	Maximum Hertz pressure
p_m	[Pa]	Medium pressure
p_{max}	[Pa]	Maximum contact pressure
p_{bt}	[mm]	Transverse base pitch
P_{IN}	[W]	Gearbox input power
p_H	[Pa]	Hertz contact pressure
P_V	[W]	Gearbox total power loss
P_V^{exp}	[W]	Gearbox total power loss measured
P_{VD}	[W]	Shaft seals power loss
P_{VL}	[W]	Rolling bearings power loss
P_{VL}	[W]	Rolling bearings power loss
P_{VS}	[W]	Slave gearbox power loss
P_{VT}	[W]	Test gearbox power loss
P_{VZ0}	[W]	Load independent meshing gears power loss
$P_{VZ0,acceleration}$	[W]	Power loss due to ventilation due to oil acceleration
$P_{VZ0,squeeze}$	[W]	Power loss due to squeeze or pocketing
$P_{VZ0,ventilation}$	[W]	Power loss due to ventilation
P_{VZP}	[W]	Load dependent meshing gears power loss
P_{VX}	[W]	Auxiliary power loss
PLP	[-]	Percentage of Large Particles
Q_T	[W]	Total heat dissipated
Q_{cond}	[W]	Heat dissipated by conduction
Q_{conv}	[W]	Heat dissipated by convection
Q_{rad}	[W]	Heat dissipated by radiation
R	[m]	Radius
r_1	[m]	Pitch radius of the pinion
$R1, R2, R3$	[-]	Geometry constant for rolling bearing friction torque
R_a	[m]	Average surface roughness
Re_c	[-]	Critical Reynolds number
R_{ku}	[m]	Kurtosis of the roughness profile
R_{max}	[m]	Maximum peak-to-valley height
R_{pk}	[m]	Reduced peak height
R_q	[m]	Root mean square roughness
R_{sk}	[m]	Skewness of the rough profile
R_{vk}	[m]	Reduced valley depth
R_z	[m]	Mean peak-to-valey height
R_x	[m]	Equivalent radius in x direction
R_{x1}	[m]	Radius of curvature raceway
R_{x2}	[m]	Radius of curvature roller

R_y	[m]	Equivalent radius in y direction
s	[-]	Pressure-viscosity parameter
$S1, S2, S3$	[-]	Geometry constant for sliding friction torque
S_a	[m]	Arithmetical mean height
S_{ku}	[-]	Kurtosis of the roughness areal
S_m	[m^2]	Submerged are of the gear
S_p	[m]	Maximum peak height
Sp	[-]	Modified Stribeck parameter [Brandao et al., 2009]
S_q	[m]	Root mean square height
S_{sk}	[-]	Skewness of the rough areal
S_v	[m]	Maximum valley depth
S_z	[m]	Maximum height
SRR	[%]	Slide-to-roll ratio
t	[-]	Pressure-viscosity parameter
T	[°C]	Operating temperature
T_0	[°C]	Reference temperature
T_1	[Nm]	Pinion torque
T_2	[Nm]	Wheel torque
$T_{\%}$	[-]	Direct measurement on Rheomat 115
T_{IN}	[Nm]	Gearbox input torque
T_{ref}	[K]	Reference temperature
T_L	[Nm]	Gearbox total torque loss
T_{VZ0}	[Nm]	Load independent meshing gears torque loss
T_W	[Nm]	Wheel static torque
u	[-]	Gear transmission ratio
$U1$	[m/s]	Raceway speed
$U2$	[m/s]	Roller speed
U	[-]	Speed influence parameter
U_{bob}	[m/s]	Bob rheometer speedd
U_{disc}	[m/s]	Disc speed
U_{ball}	[m/s]	Ball speed
U_r	[m/s]	Rolling speed
V_0	[m^3]	Gearbox oil volume
V_M	[-]	Drag loss factor
v_t	[m/s]	Absolute tangential speed on the pitch point
v_0	[m/s]	Oil jet velocity
v_g	[m/s]	Sliding speed
v_r	[m/s]	Rolling velocity
v_{tb}	[m/s]	Absolute tangential speed on the base plane
$v_{\sum C}$	[m/s]	Sum of the rolling velocities on the pitch point
Ve	[-]	Slip rate
VI	[-]	Viscosity index
W	[-]	Load parameter
x	[-]	Addendum modification coefficients
X_L	[-]	Coefficient of friction lubricant parameter

Y	[-]	Rolling bearing SKF calculation factor
z	[-]	Number of rollers
z_1	[-]	Number of teeth of pinion
α	[Pa^{-1}]	Piezoviscosity coefficient
α_t	[-]	Thermal expansion coefficient
α_W	[°]	Working pressure angle
α_z	[°]	Gear pressure angle
α_{cond}	[W/m°K]	Conduction heat transfer coefficient
α_{conv}	[W/m°K]	Convection heat transfer coefficient
α_{rad}	[W/m°K]	Radiation heat transfer coefficient
β	[$°K^{-1}$]	Thermoviscosity coefficient
β_b	[°]	Gear base helix angle
β_R	[-]	Seals friction torque exponent of a rolling bearing
Λ	[μm]	Specific film thickness
λ_{wand}	[-]	Gearbox geometric factors to calculate the windage losses
η	[Pas]	Dynamic viscosity
η_0	[Pas]	Dynamic viscosity at atmospheric pressure and reference temperature
η_S	[-]	Efficiency of FZG slave gearbox
η_T	[-]	Efficiency of FZG test gearbox
$\eta\%$	[mPas]	Representative factor to calculate dynamic viscosity
η_{Global}	[-]	Global efficiency of FZG gearboxes
ε_1	[-]	Addendum contact ratio of pinion
ε_2	[-]	Addendum contact ratio of wheel
ε_α	[-]	Transverse contact ratio
ε_γ	[-]	Total contact ratio
$\dot{\gamma}$	[s^{-1}]	Shear strain rate
$\dot{Q}_e$	[m^3/s]	Oil jet flow
δ	[m]	Penetration
μ_{bl}	[-]	Coefficient of friction in boundary film lubrication
μ_{EHL}	[-]	Coefficient of friction in full film lubrication
μ_{mz}	[-]	Average coefficient of friction along the path of contact
μ_{sl}	[-]	Sliding coefficient of friction
ν	[cSt]	Kinematic viscosity
ν_1	[cSt]	Required kinematic viscosity
ρ	[g/cm^3]	Density
ρ_0	[g/cm^3]	Density at reference temperature
σ_c	[m]	Composite surface roughness pinion/wheel
σ_1	[m]	Roughness surface roughness of pinion
σ_2	[m]	Roughness surface roughness of wheel
τ	[Pa]	Shear stress
τ_{rep}	[mPas]	Representative shear stress
θ	[°C]	Temperature
θ_a	[°C]	Ambient temperature
θ_{base}	[°C]	Temperature of FZG machine base plate
θ_{oil}	[°C]	Oil temperature

θ_{room}	[°C]	Temperature of FZG machine room
$\theta_{stab,base}$	[°C]	Stabilization temperature of the FZG machine base plate
ϕ_{bl}	[-]	Sliding friction torque weighting factor
ϕ_{ish}	[-]	Inlet shear heating reduction factor
ϕ_{rs}	[-]	Kinematic replenishment/starvation reduction factor
ϕ_T	[-]	Thermal reduction factor
ρ_{redC}	[mm]	Equivalent contact radius on the pitch point
ζ	[-]	Portion of boundary lubrication
ω_1	[rad/s]	Angular velocity of the pinion
ω_2	[rad/s]	Angular velocity of the wheel

1. Introduction

In recent years, environmental issues are interfering more and more often in the industrial world. Indeed, constraints on energy become important and they are now widely considered when developing new products.

Power transmitters or transmissions are mechanisms to accommodate the power needs-based. The automotive axle gear transmission is a typical component of vehicle powertrain which transmits the power and speed of the motor to the power required to maintain vehicle motion on the wheels. The strong growth of constraints of energy savings requires reducing power losses in mechanisms while reducing their masses and dimensions. These considerations enhance to a precisely study the sources and consequences of thermal dissipation level. There are a few research works on thermal aspects in the power transmission gear. Indeed, the industrial concerns of the last thirty years have focused on issues of strength, weight reduction, vibration and noise frequently neglecting the consequences in terms of loss and overheating.

In the automotive sector, the reduction in consumption and environmental polluting emissions are major areas of research. In this context, many efforts are worn on the motorization of vehicles. However, research is also being undertaken on the mechanical transmission and thus the performance of axles. In the design phase, when no prototype has yet been built, it is essential to have a numerical model to estimate the mechanical losses in the axle transmission depending on the chosen technical solutions.

Different organs are potential sources of power loss: gears, rolling bearings and seals. The losses generated by them may be dependent of the load, such as the power loss between gear tooth contact for transmitting the driving torque and the power loss in rolling bearings due to friction between the different parts of the bearings but also independent of the load, then they correspond to the energy needed to bring the moving lubricant and to the shearing caused by elements rotating at differential speeds.

Whatever their type, these losses will be strongly linked to the quality of lubrication implemented in the axle transmission. Particular attention should therefore be paid to the properties of the lubricant and the oil supply of contacts. The oil of automotive axle plays a key role in the successful operation of this mechanical device. Indeed, the oil must ensure both the lubrication of the contact between moving parts and removal of calories that are produced during operation of the axle. But with the development of oil projects transmissions tell "power saving" the identification and understanding of both the nature and the importance of energy losses associated with the lubricant becomes paramount. Thus, to increase, significantly, the efficiency of axle transmissions, it is imperative to minimize simultaneously the load dependent and the load independent losses through improvements in lubrication and in mechanical design. However, higher reliability of the axle transmission is required so, the durability must be warranted of the oil, of the gears and of

the rolling bearings. Overall, all physical, chemical and rheological properties of axle gear oil, rolling bearing design and gear tooth geometry are the key factors influencing the axle torque and efficiency and must be be studied and highlighted.

1.1. Scientific publications

The main thesis results were yet been published on scientific journals or conference proceeding.

As author

Paper I. M. Hammami, R. Martins, M. S. Abbes, M. Haddar, J. Seabra
Axle gear oils: Tribological characterization under full film lubrication
Tribology International (2017), 106, 109-122
DOI: 10.1016/j.triboint.2016.05.051

Paper II. M. Hammami, N. Rodrigues, C. Fernandes, R. Martins, J. Seabra, M. S. Abbes, M. Haddar, Axle gear oils: Friction, wear and tribofilm generation under boundary lubrication regime
Tribology International (2017), 114, 88-108
DOI: 10.1016/j.triboint.2017.04.018

Paper III. M. Hammami, R. Martins, M. S. Abbes, M. Haddar, J. Seabra,
Axle gear oils: Axle gear oils: Friction behaviour under mixed and boundary lubrication regimes
Tribology International (2017), 116, 47-57
DOI: 10.1016/j.triboint.2017.06.028

As co-author

Paper VI. C. Fernandes, M. Hammami, R. Martins, J. Seabra
Power loss prediction: Application to a 2.5 MW wind turbine gearbox
Journal of Engineering Tribology (2016), 230(8), 983-995
DOI: 10.1177/1350650115622362

1.2. Thesis outline

This report is arranged in eight chapters:

- **Chapter 1**: Introduction has presented a general introduction of the work scope in the field of improving axle efficiency . It has also concentrated on the objectives of the current research to understand and diminish losses in automotive axle transmission. It cited the thesis's outline.

- **Chapter 2**: State-of-the-art depicts the prominent information presented in the literature review of the different kinds of automotive transmission systems, types of power transmission system, axles, gearing mechanisms, rolling bearings, lubrication systems, rear wheel axle lubrication and full vehicle modelling. Subsequently, Chapter 2 shows the need for current research which concentrates on the importance of fuel economy required for cars, decreasing the mechanical losses in order to predict a high axle efficiency.

- **Chapter 3**: Axle gear oils focus on the prominence of the lubrication system and gives a general idea about multigrade oils and base stocks. It brings out the main features of the selected axle oil formulations. Their physical, chemical and rheological properties are determined to evaluate their abilities to generate a lubricating film, under boundary and mixed lubrication regimes.

- **Chapter 4**: The tribological properties of the axle oils were characterized. Film thickness and traction coefficients of axle gear oils were measured on ball-on-disc contact. Their ability to generate a lubricating film was evaluated, and their friction properties were determined through traction and Stribeck curves under the three lubrication regimes. The results of this work under full film lubrication regime is published in Paper I and other interesting results under mixed and boundary lubrication regime are published in Paper III. Further experimental tests were carried out on axial rolling bearing test rig in order to analyse the tribofilm generation on the roller bearing surfaces and to establish a relation between axle oil formulations and their additives. This work is published in paper II.

- **Chapter 5**: A literature review about the different sources of power loss occurring in gearboxes were displayed. Several models will be detailed and compared for gears, rolling bearings and seals losses. The model adopted for this study, as well as several parameters necessary to calculate gear power loss (coefficient of friction, gear loss factor and Lubricant Parameter) will be presented.

- **Chapter 6**: Rolling bearings experimental results show the friction torque measurement procedure and the operating conditions and also it includes a brief description of the tested bearings. The new SKF friction torque model is used to validate the experimental results in order to calculate the sliding coefficient of friction. The aim of this chapter is to study the behaviour of the five axle oil formulations in specific type of rolling bearing under different operating conditions and to be able to predict the friction torque of rolling bearings in gearboxes. This work will be published in paper IV.

- **Chapter 7**: The torque loss measurements on FZG gears lubricated with axle gear oils were presented. The tests were performed with type A gear geometry in FZG test gearbox and the spur gears in FZG slave gearbox. The influence of the gear oil will be presented and a power loss model will be calibrated allowing to find the most efficient gear oil for a given situation. To do that the coefficient of friction of the meshing gears will be determined based on experimental results and correlated with formulas from the literature. This work will be published in paper V.

- **Chapter 8**: Conclusions and future work shows the main conclusions that can be obtained until now from the developed thesis's work through a consequent experimental work, as well

as the work that can be developed in the future.

2. State-of-the-art

2.1. Introduction

Learn from the past for the future!

To develop one field, it's necessary to have a grasp of its historical development [Naunheimer, 2011]. Then it's possible to estimate what progress is still achievable and what technological potential the current field development has already realized.

For many years, research has been conducted to estimate the performance of gear [Buckingham, 1958] [Henriot, 1980]. Indeed, given the rotational speeds or transmitted couples that may be important, gears generate losses as heat then it will be removed. However, often a gear takes place in a more complete mechanical system as it is the case for an axle transmission. This element is composed of transmission pinions, bearings, shafts, seals. All of these are lubricated by oil depending on the application. Conventionally, a reduction in loss is divided into two families according to their origin [Hohn et al., 1996] [Martins et al., 2006a] [Schlegel et al., 2009]: the load dependent loss transmitted by the gear unit and the load independent losses. But whatever the losses family considered, it must depend on the used lubricant. The latter ensures effective lubrication of the contacts, either at the gear teeth or contact rings in ball-bearings for example. The lubricant also acts as a coolant fluid whose aim is to remove the heat generated by the losses. Thus, the properties of the oil must enable it to perform these two functions simultaneously.

This chapter offers a hand to list the types of automotive transmission systems, power transmission system, gives an overview of the types of axles, gearing systems, bearings, lubrication systems, rear axle lubrication, and then the full vehicle modelling.

2.2. Different kinds of automotive transmission systems

Gears were doubtlessly used more than 1000 years ago for enhancing human and animal labour. Note that all essential elements and design principles for transmissions had already been developed by 1925 [Naunheimer, 2011].

Since then, further to the progress of driving and transport performance of passenger and commercial vehicles, imperatives imposed upon the development of automotive transmis-

sions through increasing reliability and service life, raising efficiency levels, transport capacity, reducing costs and, above all, reducing fuel consumption and increasing ease of operation and road safety.

A transmission is a system of gears that transfers the engine's power to the drive wheels of the car. The transmission receives torque from the engine through its input shaft when the clutch is engaged. The torque is then transferred through a set of gears, which either multiply it or transfer it directly [Erjavec, 2010]. The resultant torque turns the transmission's output shaft, which is indirectly connected to the drive wheels. All transmission systems have the following requirements:

- Provide means of connection and disconnection of engine with rest of power train without shock and smoothly;
- Provide a varied leverage between the engine and the drive wheels;
- Provide means to transfer power in opposite direction;
- Enable power transmission at varied angles and varied lengths;
- Enable speed reduction between engine and the drive wheels in the ratio;
- Enable diversion of power flow at right angles;
- Provide means to drive the driving wheels at different speeds when required;
- Bear the effect of torque reaction, driving thrust and braking effort effectively.

The transmission system or power train is composed by (see Figure 2.1):

- Clutch
- Gearbox
- Propeller shaft
- Universal joints
- Rear axle
- Wheel

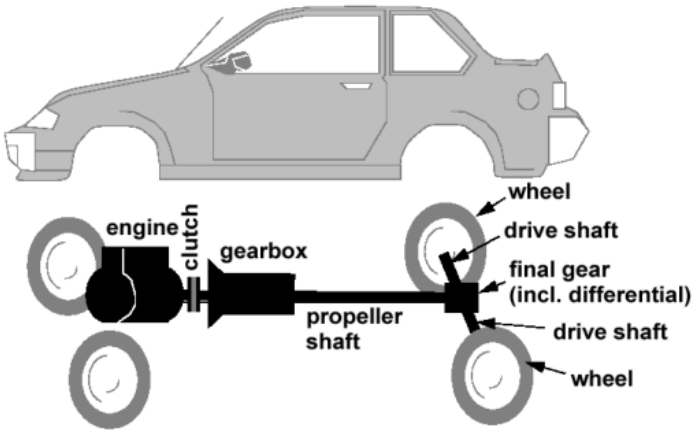

Figure 2.1: The transmission system delivers the engine power to wheels.

In the case of passenger cars, the trend toward individualized designs has caused strong segmentation with numerous vehicle classes. This has also lead to a massive diversification among transmission designs, with individual solutions and competing concepts. No doubt, the ideal transmission design is determined by the intended application, systematic thinking and experience [Naunheimer, 2011].

The most common transmission systems that have been used for the automotive industry are manual transmission (MT), automatic transmission (AT), semi-automatic transmission (AMT), and continuously-variable transmission (CVT) [Naunheimer, 2011]. This work is focused on manual transmission (MT).

2.3. Power transmission system types

The power produced by the engine is used to propel the vehicle by driving the road wheels through a power transmission system [Hillier and Coombes, 2004].

Since the location of the engine and the drive wheels depends on the type of the vehicle, different power transmission system configurations are possible. The engine could be located in the front, in the middle or in the rear, but currently it is found in the front for the most of the passenger vehicle. This case brings an improve of weight distribution and ensure better stability. The drivetrain configuration can be divided in two categories: TWD (two-wheel drive) or AWD (all-wheel drive). The difference between these two types of arrangements is the number of sets of wheels that are responsible of transferring the engine power. On the TWD case, a single pair of wheels is responsible of transmitting the power to the road while on AWD case both pairs transfer the traction. These types are chosen according to a number of factors like the size of vehicle, the purpose of use and the cost of the car.

2.3.1. Two-wheel drive

The TWD configuration is the most common technology on passenger cars and it is divided in two different layouts: FWD (front-wheel drive) and RWD (rear-wheel drive). In rear-wheel drive (see Figure 2.2 (a)), the rear wheels drive the vehicle and the front wheels swivel to allow it to be steered while in front-wheel drive (see Figure 2.2 (b)), the front wheels perform both functions which causes a faster wear of the front tires and the front breaks. Additionally, the rear-wheel drive vehicles feature a longitudinal engine, rather the transverse engine arrangement generally found in front-wheel drive.

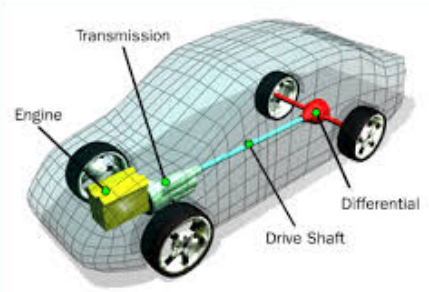

(a) Rear-Wheel Drive.

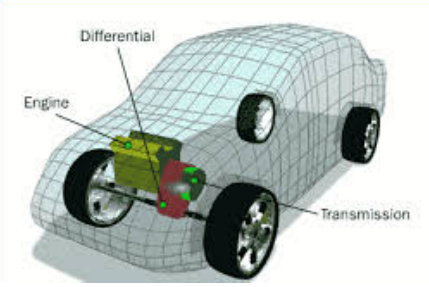

(b) Front-Wheel Drive.

Figure 2.2: Two-Wheel Drive arrangements.

2.3.2. All-wheel drive

In AWD configuration, all wheels are capable of delivering the engine power, once the two axles can be driven at the same time. It is usually seen on sport utility vehicles (SUVs) and trucks, although nowadays a few sedan, coupé and hatchback have this drivetrain. There is two types of all-wheel drive which are AWD and four-wheel drive (4WD).

AWD arrangement could work permanently with two driving axles or only with one. When front and rear axles have open differentials, only a set of wheels has traction. Although, when the wheels begin to slip and spin, the other axle is activated and the car starts to function in AWD mode, through the use of a viscous coupling, as shown in Figure 2.3 (a). When front, rear axles and viscous coupling are replaced by limited slip or TORSEN differentials, as shown in Figure 2.3 (b), the engine torque is distributed permanently for both axles in 50%:50% or 33%:66% ratios. This technology has a huge growth in the last years, due to a more precise handling, similar self-steering properties under different weather conditions and an improved vehicle movement in slippery surfaces. However it has disadvantages associated to greater technical complexity, higher costly maintenance and increased weight related to two added differentials and consequently less fuel efficiency [Naunheimer, 2011]. 4WD layout typically has a transfer box between the gearbox and the rear axle, showed in Figure 2.3 (c), and one open differential in each axle. Normally it works in TWD mode. The function of transfer box is to split the drive from the main gearbox to both front and rear axles. In the most of cases it has some sort of selectable internal differential or viscous coupling to allow

front and rear drives turn at different speeds if needed. This layout is commonly use in trucks and off road vehicles [Garrett et al., 2001].

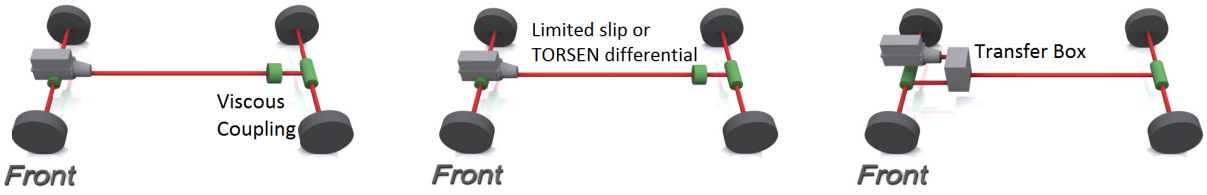

(a) Non-Permanent AWD. (b) Permanent AWD. (c) 4WD.

Figure 2.3: All-Wheel Drive arrangements.

2.4. Axle types

An axle is a cross-support between the wheels [axl, 2000]. Numerous possible axle designs can be composed depending on gear configuration, torque transferred, shaft and flange type, and bearing assembly. The most wheeled vehicles have axles as integral components. Axles are divided in two different types based on independent and dependent suspension systems. An independently suspended system is found mostly in modern cars, sport utility vehicles and also on the front of many light trucks [Hillier and Coombes, 2004] where the axles are used only to transmit driving torque to the wheels but the position and angle of the wheel hubs are an independent function of the suspension system. Independent suspensions always include a spring which allows each wheel to move independently and absorb shock, making for a smoother ride and less wear on the axle.

Other vehicles may still fitted with dependently suspended system (solid axle or beam axle). In a rigid axle suspension, both wheels are connected to a beam and aligned. They cannot move independently. If one wheel is jarred, the beam can be knocked out of alignment. In contrast, they are more homogeneous and more wheel-suited to off-road use compared to dependently-suspended.

The axles in the dependent suspended system are referred to two major types either 'dead' or 'live' and there are fundamental differences between them.

2.4.1. Dead axle

Dead axle is not a part of the drive-train but is instead free rotating. A car with front wheel drive, its rear axle can be a dead axle. Dead axle has sufficient rigidity and strength to support the weight of the vehicle which leads to a considerable reduction in unsprung weight that improves both the ride and road holding [Garrett et al., 2001], but it cannot always hold its wheels perpendicular to the road. These kinds of car axles are usually seen in many trucks and trailers.

2.4.2. Live axle

Live axle has to support the weight of the vehicle and to drive the wheels connected to it [Hillier and Coombes, 2004]. Usually, the front axle of a passenger car is a dead axle and the rear axle is a live axle. In four-wheel drive vehicles, both front and rear axles are live axles which are generally fitted with fully floating shafts that allow the high stress to be exerted on the axle. Live axle contains a final drive gears and the differential gears. The axle shafts pass from the differential to the wheel hubs. The central part of the axle is formed by the pinion and the ring gear in the differential housing. These gears of the axle transmit only turning effort, or torque and are not requested by any other force. The propeller shaft drives the pinion gear which rotates with contacting ring gear. This mechanism involves rotating gear pairs, bearings and seals which will affect transmission efficiency. Axle shafts take the stresses caused by the turning of the wheels. In this process, the energy loss due to friction and drag in the axle system is unavoidable.

Total power loss in the axle [Kolivand et al., 2010, Talbot et al., 2016, Joachim et al., 2011] can be calculated by consideration of:

- Pinion and gear contact frictional loss;
- Churning and windage of lubricant due to gear and bearing losses;
- Rolling, sliding and drag losses in the roller bearings which includes bearing preload.

Three main groups of live axles are used in automotive and construction equipment which are further divided into: semi-floating, three quarter floating and fully floating. They are classified according to the way in which the axle shafts are supported on bearings and assembled with the wheels. The type used will depend on the stresses to which the shaft is subjected during the vehicle's use.

2.4.2.1. Semi-floating axle

A semi-floating axle is a typical axle shaft used on light cars [Hillier and Coombes, 2004]. It is composed of an axle shaft on each side that is splined on the inside end where it mates directly to the differential and for the outside end the wheels are keyed to the flange of the axle as shown in Figure 2.4 (a).

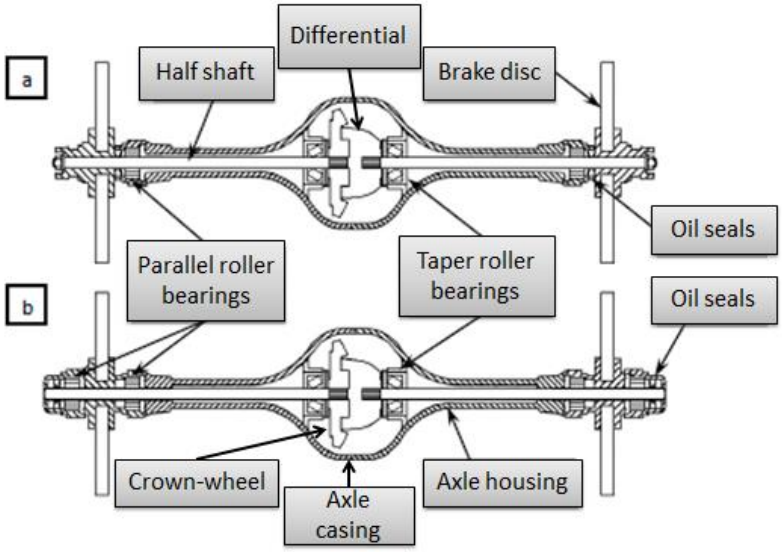

Figure 2.4: Live axles: (a) Semi floating (b) Fully floating [Kolekar et al., 2013].

The axle shaft rides on six bearings, four taper roller bearings for pinion and ring gear and two parallel roller bearings in the end of the axle housing where the wheel is attached directly to the hub as presented in Figure 2.5 which depicts an exploded view of a semi-floating Dana axle with a flanged shaft.

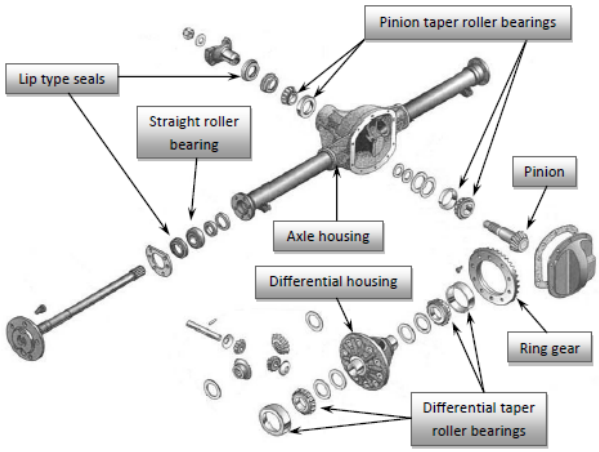

Figure 2.5: Dana 44 Rear Semi-floating Axle exploded view.

The semi floating axle has its differential case independently supported. Therefore, the differential carrier relieves the axle shafts from the weight of the differential assembly and the stresses caused by its operation. The major advantage of this type of axle that it is lighter and cheaper to manufacture and it can be removed after the wheel has been pulled off.

2.4.2.2. Fully-floating axle

A fully floating axle is used in severe duty vehicles and many large trucks due to its inherent strength of the assembly. A small difference in the construction between a fully-floating axle and a three-quarter floating which is the single bearing mounted between the hub and the casing instead of two [Hillier and Coombes, 2004]. A fully floating axle uses on each side an axle shaft splined at both ends. For the same as a semi-floating, the shaft mates the differential but the outer shaft and hub assembly are different. In this style of axle, the wheels are bolted to the axle shaft. So they will not leave the vehicle in the event of a broken axle. The axle contains eight bearings, two taper roller bearings supporting the input pinion, two more supporting the crown-wheel, carrier and differential assembly and two parallel roller bearings on the outboard end of each of the two half-shafts only one of which is in contact with the axle lubricant it is presented in Figure 2.4 (b) [Kolekar et al., 2013]. In a full-float axle, the axle shaft transmits the torque but not carries the weight unlike the semi-floating axle. The axle housing supported the weight of the vehicle, more specifically, a bearing spindle attached to the axle housing, and a set of bearings in a separate wheel hub. This assembly makes the fully-floating axles system more stronger and sturdier than a semi-floating system.

2.5. The differential

The differential is a mechanical device that allows two wheels on the same axle rotate at different rates, divides the torque input between two drive shafts and also acts as the final gear reduction in the driveline [Garrett et al., 2001].

The differential assembly presented in Figure 2.6, is mounted in the axle housing and is bolted to, and driven by, the final drive ring gear. It consists of sets of bevel gears, and pinions within a cage, attached to the large final drive gear [axl, 2000].

As part of drivetrain, the differential is assembled on a live axle. If the vehicle has FWD or RWD layout only one differential is needed, however we have AWD or 4WD arrangement, it's necessary frequently three differentials, one between the gearbox output and the two live axles and one in each axle. This allow the entire front and rear axles to spin at different speeds to each other [Naunheimer, 2011].

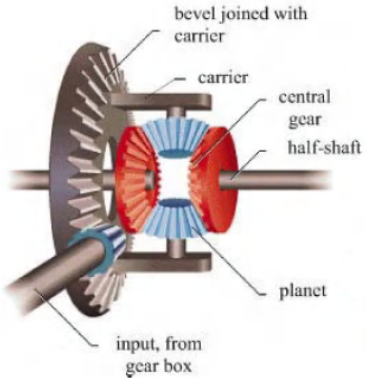

Figure 2.6: 3-D model of a differential [Jelaska, 2012].

2.5.1. Differential types

As mentioned previously, different types of differentials are used. Differentials can be generally classified into three categories: open, limited slip and locking differentials.

2.5.1.1. Open differentials

Open differentials, shown in Figure 2.7 (a), are the most common type encountered in production vehicles and they don't present a connection between the two shafts [Shepard, 2013]. They are characterized with a great on-road manners and performance, and work well for most applications [Palazzolo, 2009]. When the vehicle moves in a straight line, the open differential supply the same torque to both axles and the traction is equal in both sides and the wheels rotate at the same speed as the differential cage and the differential pinions are stopped.

When the vehicle is turning, the open differential pinions rotate on its own axis and the differential cage rotates with different velocity than the bevel output gears. The limitation of the open differential is in this turning situation where the differential send the majority of the power to the wheel with the least amount of resistance. The result is the wheel on the traction-less surface spins free, while the opposite wheel of that axle on the better traction surface provides little or no power [Naunheimer, 2011].

2.5.1.2. Limited slip differentials

Also known as self-locking differential, shown Figure 2.7 (b), looks similar to the open differential on the outside but they are different in the inside. It tries to limit the amount of movement of one axle versus the other. The limited slip differential contains small springs to push on a small clutch pack, including discs and plates in order to overcome the traction difference problem. At high traction wheel side the clutch pack is pressed firmly. Then power from the differential casing flows directly to high traction axle pack assembly. On the low

traction wheel side the clutch is not engaged, so the power limited to that side [Naunheimer, 2011].

2.5.1.3. Locking differentials

Locking differential (locker), shown in Figure 2.7 (c), uses a mechanism that allows right and left wheels to lock relative to each other and force them to rotate at the same speed regardless to the tractional differences at each wheel while still allow them to turn at different speeds when it is required. A locking differential is designed to be used in difficult situation during off road driving and to overcome the limitation of a standard open differential.

Two mains mechanisms are used to provide the lock-up, automatic lockers where the lock and the unlock are operated without direct driver intervention and on-command, or selectable lockers where the previous functions are manually operated via compressed air (pneumatics) or electronic solenoids (electromagnetics).

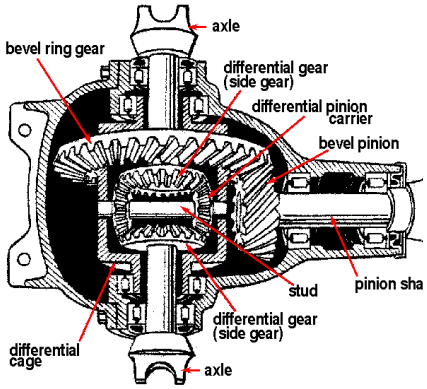

(a) Open Differential.

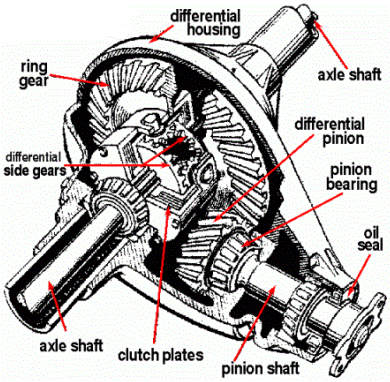

(b) Limited Slip Differential.

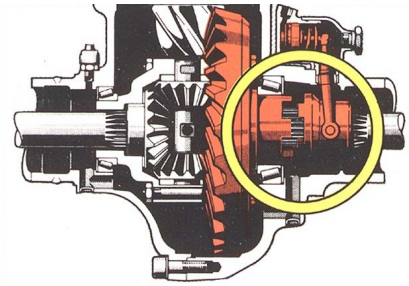

(c) Locking Differential.

Figure 2.7: Different types of differentials.

2.5.2. Differential components

2.5.2.1. Gearing mechanisms

Different kinds of gears and gear arrangements can be seen in differentials depending on its disposition in powertrain and type as shown in Figure 2.8.

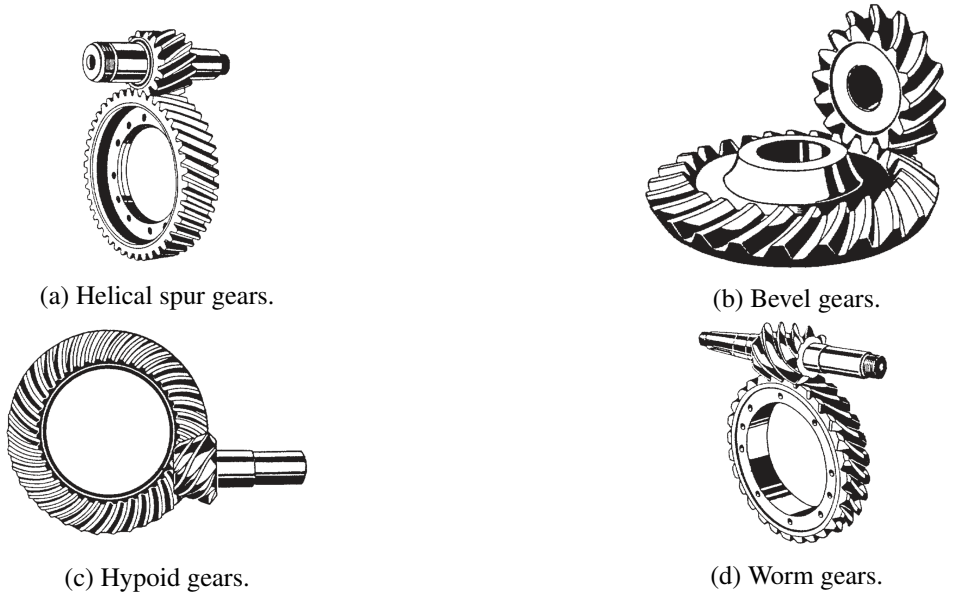

(a) Helical spur gears.

(b) Bevel gears.

(c) Hypoid gears.

(d) Worm gears.

Figure 2.8: Types of gears assembled in differentials [Mang and Dresel, 2007].

Spur gears are commonly used in the popularity of vehicle with transverse front-mounted engines (FWD). The axle drive is driven either directly by the output shaft of the transmission, or by idler gears. It is normally favourable for the differential cage drive if the engine and transmission are mounted side by side, with the disadvantage of having drive shafts of unequal length to the wheels. The reasons for their popularity are the low cost and very good efficiency of 99-99.8 % [Joachim et al., 2011]. They are also used in high speed and high load application in all types of trains and a wide range of velocity ratios.

Helical gears (see Figure 2.8 (a)) are a modification of spur gears where the helical teeth are cut across the gear face at an angle rather than straight, allowing more than two teeth to be in contact at a time. This increases their load-carrying capacity, and they find extensive use in high-speed transmissions. They are more effective in reducing noise and vibration than spur gears due to the high contact ratio. They are needed for very high speeds and loads that's why they are found in wide applications in automotive gearboxes

There are various experimental and numerical studies focused on spur and helical gears in order to develop the efficiency of these gearing mechanisms [Anderson and Loewenthal, 1982,Heingartner and Mba, 2003,Seetharaman and Kahraman, 2009,Fernandes et al., 2014b, Fernandes et al., 2014a].

Bevel gears (see Figure 2.8 (b)) are used in powertrains where the engine is longitudinally mounted (RWD), and in all-wheel drives (AWD), the power flow to the wheels has to be

turned through 90°. According to the engagement of bevel gear and crown gear, the bevel gears can be divided in helical gears and hypoid gears. Commonly they are used in open, locking and self-locking differentials with multi-plate clutches.

Hypoid gear systems (see Figure 2.8 (c)) are used for right angle drive in which two non-intersecting crossed axles. The hypoid gear design is characterized with the high strength and rigidity in the fact that the hypoid pinion has a large diameter and a long base and the crown gear can be smaller for the same load [gea, 2001, Bhandari, 2010]. Its highest-volume applications can be found in front and rear axle of rear-wheel-drive or all-wheel-drive vehicles [Kolivand and Kahraman, 2009]. Thereby the sliding movement appears at the flanks in longitudinal tooth direction which contributes to a noise reduction and difficult lubrication due to the high tooth-contact pressures which reduces efficiency, hypoid gears have lower total efficiency that attains approximately 85-97 % [Joachim et al., 2011, Winter and Wech, 1988, Bhandari, 2010]. Hypoid gears are used on the input pinion and the ring gear, and bevel are used in gears inside differential cage between the differential pinions and the output gears

Published studies on modelling of hypoid tooth contact under loaded conditions are quite sparse see the complex geometry of hypoid gears. Nevertheless, analysis in this topic has been completed by a number of workers [Winter and Wech, 1988, Simon, 2000, Vijayakar, 2004, Xu et al., 2007, Kolivand and Kahraman, 2009, Kolekar et al., 2013, Talbot et al., 2016].

Most of the models on hypoid gear dynamics are limited to experimental or simple, semi-analytical formulation, and the effects of time-varying mesh characteristics are either not considered or only approximately represented [Litvin, 1989, Krenzer, 1981].

Worm gears (see Figure 2.8 (d)) are employed in TORSEN differentials, between the gears inside the differential cage and the output worm gears although this type is rarely used due to the difficult and expensive manufacturing despite its large multiplications in a compact space [Naunheimer, 2011].

2.5.2.2. Rolling bearings

Depending on the axle design, subjected loads, gear contact loads, vehicle weight and operating lifetime different bearings are available to implement.

In differentials (see Figure 2.9), the tapered roller bearing (TRB) is the common type used for this application. Four bearings are needed from this type: two support the differential case and two support the drive pinion shaft. They are always used in pairs facing opposite ways, and are capable of dealing with considerable radial loads [Hillier and Coombes, 2004]. In addition to the radial load, they can carry a large axial component whose magnitude depends on the angularity of the rollers [Bhandari, 2010]. Due to the contact between the roller and the rib, the preload of the tapered roller bearings is reduced which causes a reduction in gear teeth life and noise during operation. That's why a new bearing design which is the angular contact ball bearing (ACBB) appears to replace the tapered roller bearing to meet the requirement of increasing efficiency by reducing friction losses, high rigidity, long life and no preload loss during operation [Spindler and Von Petery, 2003]. These two types of rolling

bearings, tapered roller bearing (TRB) or double-row angular contact ball bearings (ACBB) are shown in Figure 2.10 (a) and 2.10 (b), respectively [Kolekar, 2013].

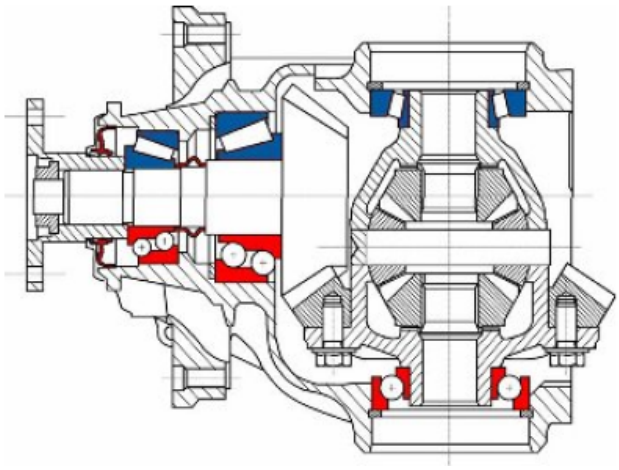

Figure 2.9: Comparison of tapered roller bearings with angular-contact ball bearings in differentials.

(a) Tapered roller bearing.

(b) Double row angular contact ball bearing.

Figure 2.10: Types of bearings assembled in differentials [SKF, 2013].

2.6. Axle lubrication

The lubricant is used to reduce friction sliding surfaces in order to protect the automotive components that it lubricates [J.Shah, 2003]. In some cases this protection diminishes the wear, heat and possibility of seizure parts. Although a layer of oil will eliminate the excessive friction of metal-to-metal contact [Bhandari, 2010]. The lubrication systems are broadly categorized as splash (bath), forced and combined lubrication. Heavy duty axles feature combined lubrication while in some light duty axles a splash lubrication system. The churning and windage losses depend on the depth of immersion and gear rotation. The level filled with the lubricant is reliant to the gear rotational speed and the size of the axle housing.

2.6.1. Splash lubrication

Bath lubrication or splash lubrication may be used for gears, chains, bearings and other moving parts that can be partly submerged in an oil reservoir and it is mainly used in gearboxes and rear axles. In the bath system the gear simply picks up oil as it dips into the reservoir and sprays or carries it to other parts along its path. The splash system contains a special ring gear that splashed up oil from the sump against other parts that need to be lubricated in order to achieve an increased efficiency [Denton, 2011]. Oil bath lubrication is particularly applicable for low speeds. However, at high speeds too much oil is supplied which increase friction and cause the operating temperature to rise [SKF, 2013]. The level filled with lubricant in the axle required the amount of lubrication received by the gears and bearings. A low level can result in insufficient lubrication and the breakdown of the axle and high level results in surplus lubrication and churning power loss.

2.6.2. Combined lubrication

The combined lubrication system is particularly important in the final drive axle, where load and/ or speed transferred are high, the combination of splash and force feed of lubricant is delivered to different components, like in case of heavy duty tandem drive axles [Denton, 2011, Naunheimer, 2011]. In combination splash and force –feed systems, oil is delivered to some parts by means of splash and to other parts through oil galleries under a pressure from the pump as shown in Figure 2.11.

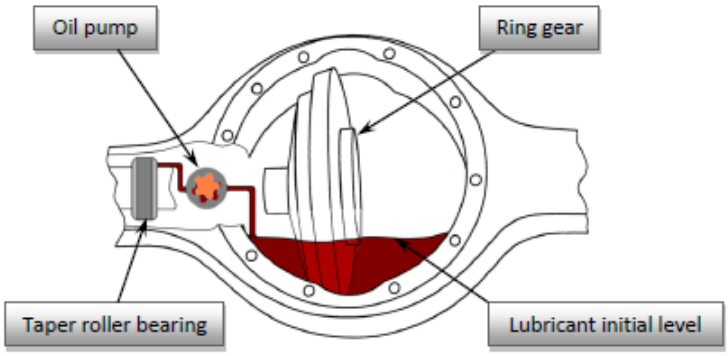

Figure 2.11: Combined lubrication system.

Lubricant is splashed and pumped from the sump so that an adequate lubrication to gears, bearings and seals in the axle is provided [of the Army and of the Air Force, 1956]. Inside the sump lubricant trickles down due to gravity, where it is collected again and the cycle repeats.

2.7. Rear wheel axle lubrication

The axle lubricant plays a prominent role in controlling the energy dissipation. Its development challenge is to bridge the gap between the efficiency and the axle durability [Evans,

2014]. In order to achieve the proper efficiency-durability balance in axle transmissions, some critical factors are needed like oil viscosity, traction properties, fluid film thickness, fluid thermal stability and additive chemistry as well as controlling axle operating temperatures [Vinci et al., 2004, Warden et al., 2010, Evans, 2014]. Since that, vehicles operate in several driving conditions (temperature, climate), so the lubricant should basically provide adequate protection against gear failures, oxidation, rust, corrosion and foaming especially in the mating surfaces [Willermet and Dixon, 1977].

The axle lubricant can be tailored to deliver higher levels of operating efficiency over a wide range of conditions in order to accommodate the both public demand and vehicle manufactures [Vinci et al., 2004].

To develop the efficiency of an axle, some influencing parameters should be determined which are the lubricant itself, the lubrication system, the vehicle drive cycle, the gearing system, the surface finish of the mating components, the working conditions, and the bearing and seals types [Ludwig, 2008].

The primary function of the gear lubricant is to provide a high degree of reliability in the service life of gear equipment [OConnor et al., 1982].

The gear lubricant also has the potential of reducing friction of sliding surfaces in the axles. Moreover, a gear lubricant should diminish the wear, heat dissipated by power loss and possibility of seizure parts in order to protect the axle components. The mean factors which help to get the right selection of gear lubricant for a given requirement can be presented as follows; the gearing type and speed, lubricant additives additives, gear and bearing surface finish, material compatibility, transmitted torque and operating temperature. [Ludwig, 2008].

Investigations continue in this area to achieve minimum energy losses in the same time maintaining or improving the service life of the axle components.

Studies have shown that the semi and full-synthetic base oil generate the maximum benefits compared to the mineral oil based lubricant. It has been presented in earlier studies that the synthetic fluids distinguished itself with chemical and physical properties to provide different viscosity-temperature-pressure features which not the case of mineral lubricant [OConnor et al., 1982, Law and Rowe, 1994].

However the relation of the dependence of temperature on torque efficiencies is quite complicated [Bala et al., 2000b].

Whatever the lubricant used mineral or synthesized, the temperature decreases when the churning force as the speed as the lubricant viscosity all of them increase. At low temperature with a low viscosity fluid the energy losses will be minimize because of the diminishing of churning losses as well as fluid film shear losses. Whereas, at higher temperature both of the speed as the lubricant viscosity decrease. Nevertheless if the viscosity go down with some values which affects the protection against gear tooth failures like scuffing, micro-pitting, pitting and wear also limits the gear and axle bearing life [Law and Rowe, 1994].

Therefore, it is necessary to find a compromise between optimum contact friction which maintains lubricating film with minimum speed dependent losses, depending on the vehicle drive cycle (torque and speed) profile.

2.8. Full vehicle modelling

Since the last 25 years, the increase of fuel economy has a great importance especially for manufactures. There is a significantly amount of fuel economy can be saved with the reduction of axle losses. When the axle generates an excessive heat the operating temperature will be higher, and hence, a reduction in gear and bearing life [Bala et al., 2000a].

In the interest of increasing the vehicle efficiency with less heat generation, lubrication and gear are the most efficient systems which can after allow a better vehicle performance. That's why a good choice in the lubricant properties and gear and rolling bearing types can limit the generated heat and then the energy losses.

All the researchers in this field are unanimous in the fact that the improvement of the axle transmission efficiency requires a wide of experimental validation and not only in all full axle transmission, but also, and more important, in all its components: gears, rolling bearings and axle gear oils [Kolivand et al., 2010, Marques et al., 2014, Fernandes et al., 2013c, Fernandes et al., 2013d, Fernandes et al., 2013b, Fernandes et al., 2013a, Fernandes et al., 2014a, Fernandes et al., 2014b, Kolivand and Kahraman, 2009].

Several published studies well established experimental validation procedures are imposed to gear oils [Bala et al., 2000a, Bala et al., 2000b, Bjornen et al., 2003, Vinci et al., 2004, Warden et al., 2010, Evans, 2014], to rolling bearings [Evans, 2014, P.Nixon, 2006, Kolivand et al., 2010, Marques et al., 2014, Fernandes et al., 2013c, Fernandes et al., 2013d, Fernandes et al., 2013b, Fernandes et al., 2013a, Fernandes et al., 2014a, Fernandes et al., 2014b], to gears [Kolivand et al., 2010, Kolivand and Kahraman, 2009] and to axle transmissions [Bala et al., 2000a, Bala et al., 2000b, Bjornen et al., 2003, Vinci et al., 2004, Warden et al., 2010, Evans, 2014]. However, in order to reduce the cost of validation tests, significant improvement in torque loss models are needed [Kolivand et al., 2010, Kolekar et al., 2013, Marques et al., 2014, Fernandes et al., 2013d, Kolivand and Kahraman, 2009, Talbot et al., 2016].

Concerning the prediction of power loss of gear pairs, some methods can be categorized.

Some studies focus on measured the coefficient of friction using experimental test machines under conditions simulating a gear pair with the expectation that these measurement values can be used to predict the efficiency of gear pair [Misharin, 1958, Benedict and Kelley, 1961, O'donoghue and Cameron, 1966, Drozdov and Gavrikov, 1968, Plint, 1967, Ku et al., 1978, NARUSE and HAIZUKA, 1978].

Others proposed empirical formulae for coefficient of friction which is currently widely used in gear applications [Benedict and Kelley, 1961, O'donoghue and Cameron, 1966, Drozdov and Gavrikov, 1968]. These empirical formulae depend on number of parameters including lubricant viscosity, radii of curvature of the surfaces in contact, sliding and rolling velocities, contact pressure and surface roughness.

A number of spur gear efficiency models adopted a constant coefficient of friction along the tooth contact [Denny, 1998, Vaishya and Houser, 1999, Anderson and Loewenthal, 1982, Seetharaman and Kahraman, 2009]. The mechanical efficiency of spur gear pair was calculated using the tangential friction force in the sliding direction by using this constant of coefficient of friction and the involute geometry. Although these models, the understanding

to the role of geometry on mechanical efficiency of the spur gear pair still qualitatively because it is not accurate to use a constant coefficient of friction whatever the contacting point on the tooth surface. Other published experiments on contacts subjected to combined sliding and rolling indicate that many parameters might influence coefficient of friction [Benedict and Kelley, 1961, O'donoghue and Cameron, 1966, Drozdov and Gavrikov, 1968].

Another efficiency models considered spur [Vaishya and Houser, 1999, Anderson and Loewenthal, 1982] and helical [Heingartner and Mba, 2003] gear pairs. Where the parameters needed to define the empirical coefficient of friction are calculated in the interest of increasing the solution accuracy.

However, each empirical coefficient of friction formula typically characterizes a certain type of test conditions that might differ from those of the modelling gear pair which appears to be the key limitation of these models.

The last models are the more advanced because they use an elastohydronamic lubrication (EHL) to predict the coefficient of friction instead of using user-defined value or an empirical formula [Snidle and Evans, 1997, Dyson, 1970, Martin, 1981, Larsson, 1997, Mihailidis et al., 2002]. Dowson and Higginson [Dowson and Higginson, 1964] and Martin [Martin, 1981] used a smooth surface EHL model to determine the instantaneous friction coefficient at the contact using the surface shear stress distribution caused by the fluid film. Larsson [Larsson, 1997] used a transient thermal-EHL model for involute spur gear lubrication with smooth surfaces. Mihalidis *et al.* [Mihailidis et al., 2002] analysed the influence of the asperity contacts in calculating coefficient of friction, and hence, efficiency.

In these models [Dowson and Higginson, 1964, Martin, 1981, Larsson, 1997, Mihailidis et al., 2002] there is no need for a previous knowledge of the coefficient of friction but they demand significantly more computational effort.

Also their applications were limited to spur gears to predict the coefficient of friction using EHL theory. There are a few efficiency studies on helical gears [Pleguezuelos et al., 2010, Simon, 1988, Heingartner and Mba, 2003] and worm gears [Tan et al., 1991, Höhn and Steingröver, 1998].

Furthermore, literature is even scare in the modelling of hypoid gear efficiency [Krenzer, 1981, NARUSE et al., 1986, Buckingham, 1988, Coleman, 1975, Simon, 1981, Kolivand et al., 2010]. Krenzer [Krenzer, 1981] described a model for analysing tooth contact and motion transmission errors of spiral bevel and hypoid gears in the loaded state using standard tooth contact analysis programs (TCA) and blank dimensions. Naruse *et al.* [NARUSE and HAIZUKA, 1978] conducted several tests on limiting loads for scoring and frictional losses of hypoid gears. Buckingham [Buckingham, 1958] proposed an approximate formula for calculating the power losses of hypoid gears, which is the sum of the losses of equivalent spiral bevel and worm gear pairs. Coleman [Coleman, 1975] used a simple formula to calculate hypoid gear efficiency using a coefficient of friction with a very limited number of parameters. Simon [Simon, 1981] applied a smooth-surface EHL formulation of the hypoid gear efficiency problem.

Finally, Kolivand *et al.* [Kolivand et al., 2010] proposed a new spiral bevel and hypoid gear mechanical efficiency model which is a mixed EHL based surface traction model to predict friction power losses for both face-milling and face-hobbing type cutting methods.

2.8.1. Elastohydrodynamic lubrication (EHL)

Elastohydrodynamic lubrication (EHL) is a type of lubrication that occurs in lubricated contraformal contacts where the elastic deformation of lubricated surfaces has a substantial influence on the thickness of the lubricating film. Such contacts are found in rolling bearings, gears and cam-tappet systems. The cause of this elastic deformation is the high pressures in such contacts which lead to increase viscosity. These two effects have a positive influence on the film thickness of the lubricant [Lugt and Morales-Espejel, 2011].

The history of EHL starts from 1886, basis of the Navier–Stokes theory of fluid mechanics, Reynolds published his famous formulation where he derived the differential equation which describes the load-carrying capacity and pressure distribution of lubricating films for journal bearings [Reynolds, 1886, WILEY-VCH Verlag GmbH & Co. KGaA, 2007]. The EHL equation is simplified using the narrow gap assumption where is relates the geometry of this gap and the velocities of contacting surfaces with the pressure in the film.

All lubricant's viscosities decrease with temperature and increase with pressure. The moving of contact solid surfaces in different relative speeds and loads is the source of shear stresses. The lubrication regime can be lightly or heavily loaded which depends on the loading conditions, speed, material properties of contact surfaces, the contact size and the lubricant viscosity.

In lightly loaded contacts, the lubricant produces a much stronger separating film in the oil to separate the moving surfaces and the deformation of these surfaces is negligible. This type of lubrication is called hydrodynamic lubrication (HL) theory. Such lubrication regime is considered an ideal form of lubrication since it generates low friction and wears protection [WILEY-VCH Verlag GmbH & Co. KGaA, 2007, Hamrock and Dowson, 1981, 386].

In case of heavily loaded non-conforming contacts, the elastic deformation of contact faces (Hertzian pressure) as well as the oil pressure viscosity is relevant. These are generally defined by elastohydrodynamic lubrication (EHL).

In heavy loaded surface contacts, the formation of the lubricant film is important in the way to provide a correct functioning of gears and rolling bearings. Taking the example of gears when they are revolving, the tooth contact present both sliding and rolling motion under load which causes frictional power losses. The amount of sliding frictional loss depends on the normal tooth load, coefficient of friction and relative sliding velocity of the surfaces. Otherwise, for rolling bearings the rolling friction comes from resistance to rolling motion because of the deformation of the two contacting surfaces [Gohar, 2001, Hamrock et al., 2004, Dowson and Higginson, 1966].

In 1902, Stribeck [Stribeck and Schröter, 1903] provides a good overview of the states of friction occurring in different bearings. It translates the relation between the friction coefficient and film thickness as a function of the velocity of mating surfaces [Mang, 2014].

The friction or lubrication conditions between boundary to hydrodynamic lubrication are graphically illustrated by use of Stribeck diagram (see Figure 2.12).

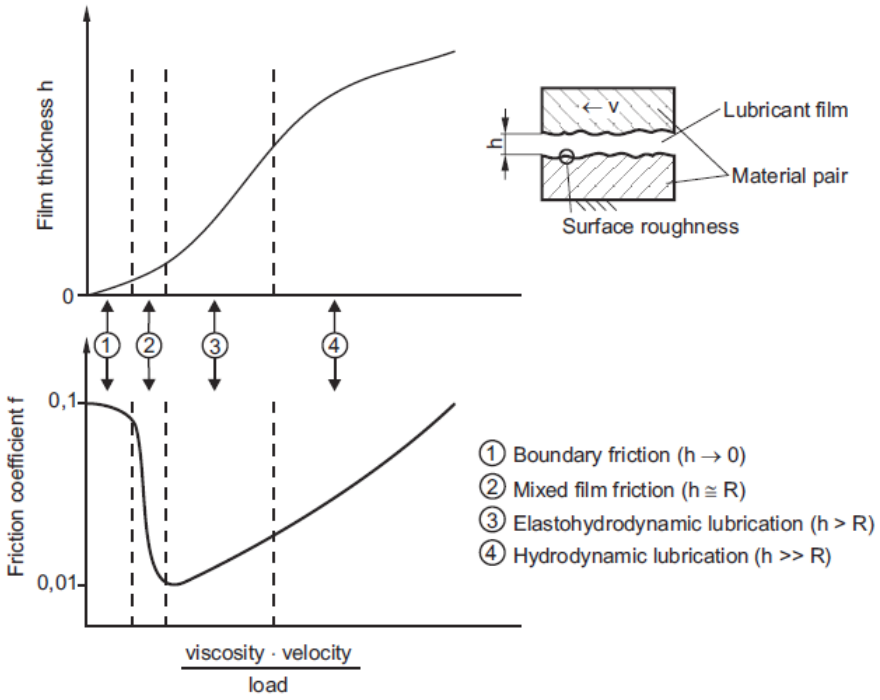

Figure 2.12: Stribeck graph [WILEY-VCH Verlag GmbH & Co. KGaA, 2007].

In boundary lubrication (BL), the contact surfaces are only separated by a boundary layer of chemical reaction products a few nanometres thick that's why the solid asperities dominates the contact. In boundary lubrication the load increases, speed or the fluid viscosity decreases and the coefficient of friction can increase sharply and approach high level (about 0.1 or much higher) [Bhushan, 2013].

With the increase of the entrainment speed the contact condition is modified into mixed lubrication (ML). This lubrication regime is the transition between boundary lubrication and elasdtohydrodynamic lubrication in which these two mechanisms may be functioning.

In fact, there is liquid friction and dry friction at the same time. The solid contacts lead to a cycle of adhesion, metal transfer, wear particle formation, and eventual seizure. However, in liquid lubricated bearings there is prevention from adhesion during most asperity encounters. At high speed, EHL or HL predominates when the asperities are completely separated from each other by a thicker lubricant film as hydrodynamic pressure increases. So the lubrication regime is basically affected with the amount of lubricant supplied in the contact. Other factor affect the lubrication is the temperature which is determined by, lubricant viscosity, applied load, thermal and elastic properties of the contacting solids, contact surface speeds, and lubricant thermal parameters. This temperature affects the friction in contact. Finally, coefficient of friction in the contact is one of the major parameters affecting pitting, wear and other fatigue occurrences.

2.8.2. The film thickness calculation

In 1976, Hamrock and Dowson [Hamrock and Dowson, 1976] were among the first to present numerical simulations assuming isothermal Newtonian fluid model and exponential piezo-viscosity to develop the most popular minimum film thickness formula to EHL contacts. From their results they derived a formula to predict the film thickness as a function of the operating conditions [Nijenbanning et al., 1994a, Fernandes et al., 2015].

The most important characteristic of the lubricant film thickness are the temperature and the pressure variation (see Figure 2.13) which are measured using experimental methods like thin film transducers [Stribeck and Schröter, 1903] and optical interferometry [Archard and Kirk, 1961].

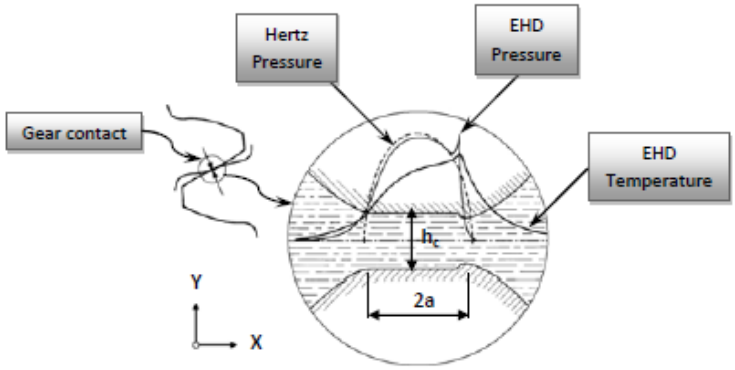

Figure 2.13: Film thickness calculation for EHD contact.

Since the introduction of computers and computational methods, theoretical studies often involve the numerical solution of surface stresses, the pressure profile in the contact and the lubricant film formed a set of differential and integral equations describing the lubricant flow, the lubricant behaviour and the surface deformation [Nijenbanning et al., 1994a].

A lot of factors effect on the film thickness and the most important among them are oil viscosity, temperature, speed and load between the two surfaces. Central and Minimum oil thickness's are theoretically investigated under sliding and rolling contact. In order to calculate the fluid film thickness there are two types of contacts performed when two simple non-conforming solids are in contact with no load:

1. Line contact, while the shape of the contact area is a straight or curved line like in gears and roller bearings.
2. Point contact, where the contact area is a single point like in ball bearings.

After the applied load, the line contact expands to a rectangle and the point contact to an ellipse or a circular. The loaded contact will be more detailed in the following paragraph.

2.8.2.1. Line contact

Over the last four decades for line contacts, the pioneering numerical work of EHL theories has been carried out considering isothermal and smooth contacts and Newtonian fluids [Par-

inam and Karan, 2014].

Using Reynolds equation Grubin (1949) [Grubin and Vinogradova, 1949] solved the pressure build-up in the oil film between two rollers, assuming them to have the same form as a dry Hertzian contact. This assumption allowed an accurate prediction of film thickness in the central region of the contact.

Later, Petrusevich (1951) [Petrusevich, 1951], Dowson and Higginson (1959) [Dowson and Higginson, 1959] and Dowson-Toyoda film thickness (1978) [Dowson and Toyoda, 1978] solved the elastohydrodynamic problem of EHL line-contact. But there are limitation in the applicable ranges of their formulations, the error increase in its limits. An accurate numerical formulation proposed by Zhang and Gou [Zhang and Gou, 1989] gives significant overestimations when the contact regime is outside a certain range. Zhang and Gou [Zhang and Gou, 1989] analysed the central and mean film thickness which are provided in multi-regime line contact formula for EHD contact using dimensionless regression equations.

The other models calculate the minimum film thickness and center film thickness for a line contact in elasto-hydrodynamic lubrication which is suitable for all regimes of contact are presented in the following equations:

Grubin film thickness formula [Grubin and Vinogradova, 1949]

$$h_0 = 1.95 \cdot R_x \cdot U^{8/11} \cdot G^{8/11} \cdot W^{-1/11} \tag{2.1}$$

Dowson and Higginson's equation for minimum film thickness [Dowson and Higginson, 1959]

$$h_m = 2.65 \cdot R_x \cdot U^{0.7} \cdot G^{0.54} \cdot W^{-0.13} \tag{2.2}$$

Dowson and Toyoda's equation for central film thickness [Dowson and Toyoda, 1978]

$$h_0 = 3.11 \cdot R_x \cdot U^{0.69} \cdot G^{0.56} \cdot W^{-0.1} \tag{2.3}$$

where, U the speed parameter, G the material parameter, W the load parameter and R_x the effective radius of curvature. All these parameters are calculated using the following equations.

$$U = \frac{\eta_0 \cdot U}{E^* \cdot R_x} \tag{2.4}$$

$$G = \alpha \cdot E^* \tag{2.5}$$

$$W = \frac{F_n}{E^* \cdot R_x \cdot l} \tag{2.6}$$

For line contact, the effective radius of curvature is given by Equation (2.7)

$$\frac{1}{R_x} = \frac{1}{R_{x1}} + \frac{1}{R_{x2}} \tag{2.7}$$

2.8.2.2. Point contact

The understanding of point contacts is less advanced comparing to line contacts. Therefore the line contact application of the approximations for film thickness calculation is simple. For point contact it is more complex, owing to side leakage effects and piezoviscous effect, where fluid viscosity in contact incurs the pressure spikes [Cameron and Gohar, 1966].

The authors understand that work in progress in order to solve the problems associated with these numerical methods [Hamrock and Dowson, 1981, Mostofi and Gohar, 1982, Evans and Snidle, 1983, Chittenden et al., 1985].

Hamrock and Dowson [Hamrock and Dowson, 1981] (1981) formulate expressions for an elliptical contact when the lubricant entraining velocity vector was parallel to the minor axis of the hertzian contact ellipse.

Then Mostofi and Gohar [Mostofi and Gohar, 1982] (1982), presented the numerical solutions for elastohydrodynamic point contacts, with an ellipticity ratio less than unity, which are only applicative for moderate loads and low materials parameter and such conditions are presented in the EHL between glass and steel. In addition, they discussed the EHL of a point contact under pure spin.

Snidle and Evans [Evans and Snidle, 1983] (1983), have also studied the elatohydrodynamic lubrication where the direction of lubricant entrainment was along the major axis of the Hertzian contact ellipse. The application was the tooth contacts that occur in the high conformity (Wilhaber-Novikov) and such high load solution is extremely expensive of computer time.

Chittenden et al. [Chittenden et al., 1985] (1984) produce a converged solution to EHL point contact problem where the velocity is along the long axis, so a considerable reduction in minimum film thickness and they obtained the same values of film thickness presented by the other workers when the rolling velocity vector is along the minor axis of static contact ellipse.

For entrainment along the long axis, Gohar [Gohar, 2001] presents a comparison for the results obtained by Mostofi and Gohar [Mostofi and Gohar, 1982], Snidle and Evans [Evans and Snidle, 1983], Chittenden *et al.* [Chittenden et al., 1985] and he showed that the Chittenden empirical equations are mainly accurate for a wide range of conditions and for lubricant entrainment and angle θ to the minor axis.

Hamrock and Dowson [Hamrock and Dowson, 1981] formula, the minimum film thickness and center film thickness are given by the following Equations (2.8) and (2.9), respectively.

$$h_m = 3.63 \cdot R^* \cdot U^{0.68} \cdot G^{0.49} \cdot W^{-0.073} \cdot (1 - e^{-0.68k}) \tag{2.8}$$

$$h_0 = 2.69 \cdot R^* \cdot U^{0.67} \cdot G^{0.53} \cdot W^{-0.067} \cdot (1 - 0.61e^{-0.73k}) \tag{2.9}$$

where the dimensionless speed (U), material (G) and load (W) parameters are calculated with Equations (2.10), (2.11) and (2.12), respectively.

$$U = \frac{\eta_0 \cdot U}{E^* \cdot R^*} \tag{2.10}$$

$$G = \alpha \cdot E^* \tag{2.11}$$

$$W = \frac{F_n}{E^* \cdot R^*} \tag{2.12}$$

For point contact, the curvature radius is given by Equation (2.13).

$$\frac{1}{R^*} = \frac{1}{R_x} + \frac{1}{R_y} \tag{2.13}$$

where

$$\frac{1}{R_x} = \frac{1}{R_{x1}} + \frac{1}{R_{x2}} \tag{2.14}$$

$$\frac{1}{R_y} = \frac{1}{R_{y1}} + \frac{1}{R_{y2}} \tag{2.15}$$

The ellipticity ratio k may be defined in terms of the principal axes of the Hertzian contact ellipse and presented in Equation (2.16).

$$k = \frac{a}{b} = \frac{semi-major\ \ axis}{semi-minor\ \ axis} \tag{2.16}$$

Chittenden *et al.* [Chittenden et al., 1985] formula

R_x / $R_y \leq 1$ (entrainment along major axis of the contact ellipse)

$$h_m = 3 \cdot U^{0.68} \cdot G^{0.49} \cdot W^{-0.073} \cdot (1 - e^{-0.96(\frac{R_x}{R_y})}) \tag{2.17}$$

$$h_0 = 3.06 \cdot U^{0.68} \cdot G^{0.49} \cdot W^{-0.073} \cdot (1 - e^{-3.36(\frac{R_x}{R_y})}) \tag{2.18}$$

(entrainment along minor axis of the contact ellipse)

$$h_m = 3.68 \cdot U^{0.68} \cdot G^{0.49} \cdot W^{-0.073} \cdot (1 - e^{-0.67(\frac{R_x}{R_y})^{2/3}}) \tag{2.19}$$

$$h_0 = 4.31 \cdot U^{0.68} \cdot G^{0.49} \cdot W^{-0.073} \cdot (1 - e^{-1.23(\frac{R_x}{R_y})^{2/3}}) \tag{2.20}$$

where the ellipticity ratio k is calculated using the equivalent radii of curvature in both directions (x,y) presented in Equation (2.21).

$$k = \frac{a}{b} = (\frac{R_y}{R_x})^{2/3} \tag{2.21}$$

2.8.3. Hypoid gear approximation

The topic of hypoid gear is discussed before in section 2.5.2.1. Hypoid gears are common found in automotive drive axles. Hypoid gear set is a type of the bevel gears where the axes of the pinion and gear do not intersect but have a distance in space [Stadtfeld, 2001].

The purpose of these gears to transmit motion and torque through ninety degrees. Hypoid gears are stronger but they have some sliding action along the teeth which reduces the mechanical efficiency. Hypoid gear combine the sliding action of worm gears with the rolling action and high tooth pressure of spiral bevel gears. The amount of the sliding is dependent on the amount of offset of the axes [Buckingham, 1988].

The shaft offset is the main difference between the spiral bevel and hypoid gears. When compare these two types, hypoid gears provide the following [Bhandari, 2010, Litvin, 1989]:

- Hypoid gears operate more quietly with higher contact ratio;
- They transmit higher torque with greater tooth contact area (better durability);
- The driving efficiency of an automotive hypoid gear is 85-97 % which is less than that of a spiral bevel gear which ia around 99 %.

Hypoid gears are generated using two different basic cutting methods namely face-milling (FM) and face-hobbing (FH). The first hypoid cutting method was FM for decades, then it was replaced by FH process due to its productivity caused by continuous indexing. The difference between face-milling and face-hobbing processes is shown in Figure 2.14.

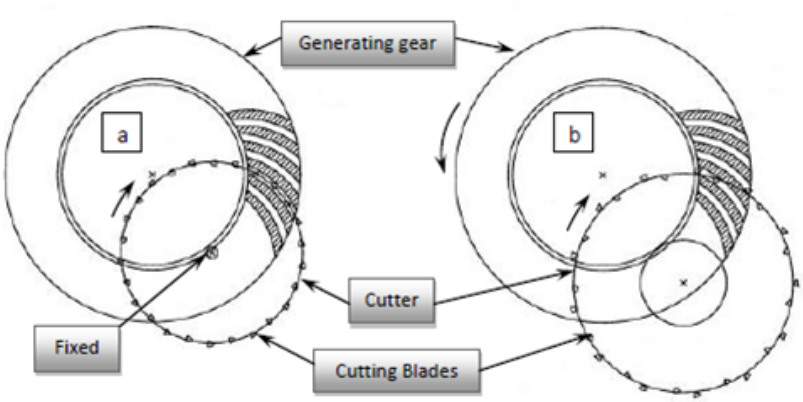

Figure 2.14: (a) Face-milling and (b) face-hobbing cutting processes [Kolivand and Kahraman, 2009].

The concept of the generating gear is a key to the basic understanding of hypoid gears [Kolivand and Kahraman, 2009]. In face-milling process, the generating gear is fixed while the cutting wheel interact with one tooth space and then it is indexed to the next location during the tooth generation process. The cutting process is performed using conical shape blades which are arranged inside and outside the cutter head. The outside blades (OB) cut concave side of tooth slot while inside blades (IB) cut convex side of the same slot. In the

face-hobbing method, the cutter blades are different from the first method. The gear is continuously cut indexing due to the rolling of the cutter head and the generating gear together. Kolivand et *al.* [Kolivand and Kahraman, 2009] developed a friction power losses for both face-milling and face-hobbing type cutting methods using a mechanical efficiency model.

In the following part Buckingham explains [Buckingham, 1988] the approach for hypoid gear in order to calculate the power loss. In a pair of non-parallel shafts that do not intersect, the action between the gear teeth is mainly sliding. The tooth action of hypoid gears is complex that's why Buckingham proposed an approximation for the tooth action of hypoid gears in the interest of determining sliding velocities. The gears are decomposed using the pitch line of hyperboloid surfaces into a worm gear and a spiral bevel gear. The tooth action of spiral bevel gears is similar to the equivalent helical gears.

Buckingham's approach developed the following assumptions:

- Hypoid gears have predominantly the same conjugate gear-tooth action as spiral bevel gears, and thus the power loss can be calculated using a spiral bevel gear analysis;
- The controlling factor of the worm gear action is the sliding of the pitch surfaces in the planes of rotation of the two members and as a results of this sliding are proportionate of the worm gear action. Therefore, the average sliding velocity is equal to the peripheral velocity of the radius to the pitch plane of the worm;
- The total power loss is equal to the sum of the spiral bevel gear loss and the worm gear loss.

The value of the helix angle is equated to the spiral angle of the ring gear of the hypoid system. The spiral angle changes across the face of the hypoid because of the varying contact condition but the value at the center of the ring gear face is expected to give a reasonable value. The arcs of approach and recess determined in the middle of the gear face are used to obtain the average velocity of the sliding action.

2.9. Need for current research

The efficiency prediction of automotive drive trains has become an increasingly critical research topic. This is basically due to government regulations in regards to fuel economy and carbon emissions which are becoming more stringent [Willermet and Dixon, 1977, Naunheimer, 2011]. Axle transmissions require very high reliability and so, the durability of the oil, of the gears and the rolling bearings must be guaranteed. Experimental work are validated through numerical models in order to diminish the expense and the length of the design cycle of lubricants, axles by testing the energy management strategies in such mechanical system.

2.10. Summary

The literature review presented above has elucidated the axle transmission as a complex mechanical system. The key component of this mechanical system basically are hypoid and bevel gears, tapered rolling bearings, seals, shafts and axle gear oil. In this chapter, each component is presented separately according to the bibliographic research. Then, the developed methodology will combine those components in the interest to know the more accurate and efficient combination. Therefore, the most previous axle efficiency models are concentrated on hypoid gear pair contacts or axle temperature experimentally measured. Consequently, this research will emphasize on the overall axle efficiency model using experimental and numerical studies on the influence of bearing type, gear design and oil formulations which are carried out and shown in the following Chapters.

3. Axle Gear Oils characterization

3.1. Introduction

The lubrication system in modern high-performance, heavily loaded gearboxes can now be decided upon and laid out in the initial stages along with the internal running gear which results in transmissions with much better efficiencies and longer lives [Stokes, 1992]. In automotive vehicles these gearboxes consist of the transmission and differential or combination transaxle.

For the automotive industry, improving efficiency of all components in a vehicle is a major challenge today. Although transmission systems show a high global efficiency, it is still possible to reduce energy losses by improving the lubricant formulation. The lubricant is directly related to churning losses, friction losses and traction losses. All OEM's struggle to recover each gram lost in the drive-line system and lubricants play a significant role in these losses. Therefore, new lubricant developments usually integrate an objective of fuel economy improvement [Alder da Costa D'Ambros and Tinguy, 2012].

Along with the strong drive towards better fuel economy consumers have been demanding higher performance, requiring automotive lubricants with improved durability protection and lower operating temperature [Evans, 2014].

One potential area for fuel consumption improvement is found in the lubricating fluids located throughout the drive-line. By varying the lubricating fluids used in automotive transmissions, a potential reduction in mechanical losses can be achieved [Warden et al., 2010].

A special challenge in recent years is predicting properties of fully formulated automotive oils because lubricants do not just lubricate but must fulfil some functions [Kerthe, 2012].

The following points cover some of the properties which lubricating oil must include [Stokes, 1992]:

- The lubricant must have good adhesive qualities, i.e. it must stay on the gear teeth, resisting centrifugal force and the pressures created by the tooth meshing forces;
- It must protect the gear tooth surfaces from all forms of corrosion, as this could reduce the gear life drastically;
- When operating over a wide temperature range, the oil must remain in a fairly constant form, not becoming too thin when hot and thus losing part of its lubricating power, nor too thick to pour or run freely when cold;

- It should remain unaffected chemically by heat, especially regarding oxidation.
- It must flow freely and be capable of dissipating any heat caused by friction or churning as quickly as possible;
- It must resist emulsification with water and yet still be capable of providing the necessary lubrication even with small quantities of water in suspension;
- It should not form stable foam within the gear casing while the transmission is in use.

During the last 50 years, the automotive industry developed a very significant effort to constantly monitor and improve lubricants and reduce friction losses in engines and transmissions.

Starting in the 1980s, synthetic lubricants have played a crucial role in power train lubrication, specifically in the heavy-duty over-the-road segment. Ongoing changes in the passenger car and light-duty truck gear oil requirements are presenting new opportunities for synthetics for these applications also. Worldwide, synthetic gear lubricants are being recognized as useful components in the area of low maintenance and long durability in transmissions and axles [Rudnick, 2013].

This chapter is totally dedicated to a complete description of the selected axle lubricants. Starting with a brief description of the multi-grade oils. Then, the mentioning of the axle gear oil performance requirements. Next, the depiction of the synthetic and mineral base oil usually found in automotive gear transmissions. After that, their performance packages are listed and explained. Afterwords, the selection of the axle gear lubricants. Additionally, the physical, rheological and chemical properties were performed in order to characterize the new axle oil formulations.

3.2. Axle gear oils description (Multi-grade oils)

Considerable effort has recently been devoted to improve the energy efficiency of cars. One approach has been to alter the properties of lubricants used in the engine and gears [Kubo et al., 1986]. The introduction of lower viscosity engine oils, SAE 5W20 [for, 2006] and 0W20 grades provides optimum fuel economy and durability performance meeting all requirements for vehicle's engine. Efforts have been extended to the rest of the power train including the effort to reduce losses in axles.

In the past, high viscosity of the oil used in engines during the summer made engine cranking difficult in winter, so different grades have been defined for the two seasons which is the same for axle gear oil. Low viscosity multi-grade oils are now widely used. A specific additives that reduce the change in oil's viscosity with temperature are often used and this has meant that the same grade can be used throughout the year. These oils are called multi-grade or cross-grade, or given trade names that suggest the viscosity remains constant. They can be recognized by the special SAE (Society of Automotive Engineers) rating; this has two numbers separated by the letter 'W'. A typical oil is 'SAE 75W90'. In this case the oil is equivalent to SAE 75W when tested at a sub-zero temperature, (the 'W' indicates

winter conditions) and has a viscosity of SAE 90 at the normal rated temperature [Hillier and Coombes, 2004, Corporation, 2014].

Lowering the viscosity of multi-grade gear oils is effective in improving shift-feeling performance at low temperature, noise-prevention at high temperature, and fuel economy. Multi-grade oils are used also to reduce fluid friction and to ensure easy supply of lubricant to bearings. In fact the use of such oil often gives rise to the axle efficiency.

3.3. Axle gear oil general performance requirements

3.3.1. Normative references

Nowadays, there are a lot of modifications affecting the automotive lubricant requirements. The aim of these changes are the increasing demand for improved efficiency, lower cost and lower weight for the vehicle [Rudnick, 2013].

The main defining category for the lubrication system can be defined as the viscosity. Its crucial role is to provide a sufficient oil film between the moving contact surfaces. The viscosity functions predominantly by providing protection in the hydrodynamic or elastohydrodynamic mode of lubrication. In these modes of lubrication, the metal surfaces are sufficiently separated so no metal to metal contact.

For that the automotive lubricants are defined using two viscosity classifications. The first one is the SAE J306 defines the 'Axle and Manual Transmission Lubricant Viscosity Classification' which contains the original mono-grades and winter grade classes (See Table A.1). This classification is based on the following criteria:

- Maximum temperature for a viscosity of 150,000 cP corresponding to one of the W grades.
- Maximum kinematic viscosities at 100 °C corresponding to one of the non W grades and a minimum kinematic viscosities at 100 °C for both the W and the non W grades.

The second classification is the MIL-PRF-2105E / SAE J2360 defines the minimum level of performance for use in the qualification of oils, lubricating gear in multi-purpose (Metric) Military use. It includes three viscosity grades combined with a channel point requirement (See Table A.2).

For the viscosity properties of the gear oil at the low-temperature are indicated in the SAE with winter classes (70W, 75W, 80W, 85W) and in the MIL-PRF-2105E with the channel points. Most synthetic gear lubricants have viscosity limited to 70W or 75W viscosity grades, whilst most petroleum based gear oils are of 80W or 85W viscosity grades.

3.3.2. API Classifications

After the viscosity grade has been defined, axle gear oils are classified according to the API (American Petroleum Institute). The API created a classification system for gear oils based

on application conditions and the type of gears most commonly used. API gear oil classifications are now internationally recognised and used. It designates service categories for automotive gear oils based on extreme pressure (EP) protection required and the level of anti-wear. These designations from GL-1 to GL-6 and MT-1 are dedicated to the lubricant used in typical automotive applications like manual transmissions, drive axles, steering axles, semi-automatic transmissions, automatic transmissions, and hydraulic systems. One lubricant can be appropriate to more than one service classification (see Table A.3).

The current service designations for automotive gear lubricants are API GL-4, API GL-5, and API MT-1. The API GL-4 oil is characterized with up to 4 % of extreme pressure (EP) additives for passenger car or moderately loaded hypoid axle gears while the API GL-5 lubricant contains up to 6.5 % of extreme pressure (EP) additives for moderately or heavily loaded hypoid gears in axles for passenger cars and trucks. The most recent classification is API MT-1, where lubricants contain active anti-wear or EP additives for heavy-duty manual transmissions [Rudnick, 2013, Totten, 2012].

3.4. Synthetic base oils

A typical automotive transmission or axle lubricant is composed of 80-90 percent base oil and with the remaining 10 to 20 percent additives to tailor performance to desired specifications. The base stocks can be either processed from mineral (petroleum), partial or full synthetic origin. Because the base oil selection is an economical decision, a careful cost/benefit analysis must be carried out. Synthetic oils such as polyalphalefins (PAOs), esters, or polyalkyleneglycols (PAGs) provide specific properties but are usually expensive than mineral-based fluids (Table 3.1). In contrast, synthetic base oils are characterized with a higher service life comparing to mineral oil where the PAO oil change intervals can be extended up to three times and for PAG up to five times the service life of an ordinary mineral oil [Mang, 2014] (Figure 3.1).

Table 3.1: Relative costs of synthetic base oils [Mang and Dresel, 2007].

	Mineral oils	PAOs	PAGs	Esters
Relative costs to mineral oils	1	4_15	6_15	10_20

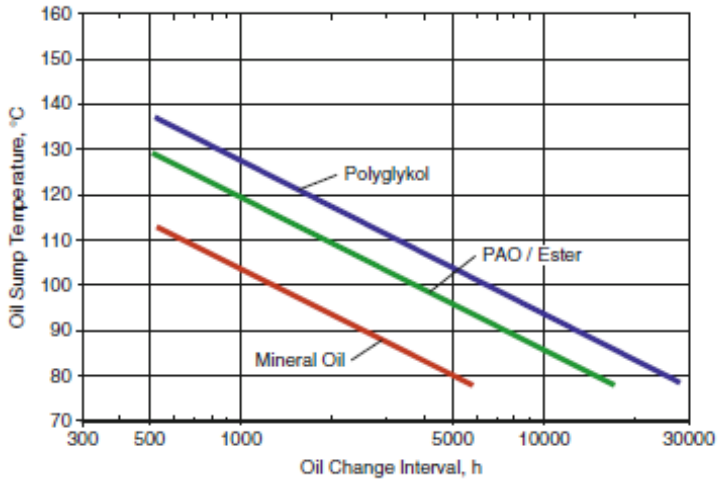

Figure 3.1: Oil service life: achievable oil change intervals [Mang, 2014].

The API established base oil guidelines, based on five categories according to the amount of saturates and sulfur level (Table 3.2).

Table 3.2: API 1509 Base Oil Guidelines [Rudnick, 2013].

Category	Sulfur (%)	Saturates (%)	Viscosity index
Group I	> 0.03	< 90 %	80 to 120
Group II	≤ 0.03	≥ 90%	80 to 120
Group III	≤ 0.03	≥ 90%	≥ 120
Group IV	All polyalphalefins (PAO's)		
Group V	All others not included in Groups I, II,II, or IV		

The ASTM defined the synthetic lubricant as a product which consists of stocks manufactured by chemical synthesis and containing necessary performance additives. The key word in this definition is synthesis which means to take small chemical building blocks and combine them in an ordered, predictable reaction to form precise large molecules (Figure 3.2).

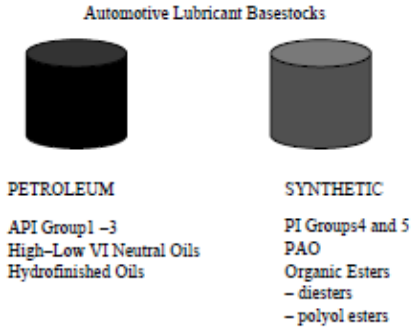

Figure 3.2: Automotive lubricant base stock types [Rudnick, 2013].

The lubricant base stocks widely used in automotive gear and transmission area are all PAO, all ester (diester or polyol ester), or a mixture of PAO and ester.

3.4.1. Polyalphaolefin (PAO)

Polyalphalefins (PAO) are considered a synthetic high performance base stocks. This term when used for lubricant base stocks refers to hydrogenated oligomers of an α-olefin [Mortier et al., 1992]. That means, they are manufactured by the catalytic oligomerisation of linear alphalefins. Polyalphalefins are formed by wax-free combination of molecules of predetermined chain length between 8 to 12 carbon molecules [Mang, 2014]. They are described in detail by Shubkin [Shubkin, 1992].

Polyalphalefins have many favourable properties which leads to their rapidly growing use for a variety of industrial applications like:

- Good viscosity index;
- Wide operating temperature range;
- Good thermal stability;
- Hydrolytically stable;
- Low toxicity;
- Low pour point;
- Low volatility;
- Chemical inertness;
- Good natural lubricity;
- Compatible with mineral oils and Esters.

3.5. Mineral base oils

Mineral lubricants are obtained from distillation and refining processes crude petroleum, which is separated into fractions of progressively decreasing volatility, with elimination of the unwanted ones. Mineral oils are made up of hydrocarbons, i.e.,compounds of hydrogen and carbon [Bassani and Piccigallo, 1992].

As presented in Figure 3.2, API has classified mineral base oils into three groups. The classification of petroleum base oils (Groups I, II, III) has considered three parameters: sulfur level, saturates content and Viscosity Index (VI).

According to Table 3.2, Group I oils are solvent-extracted with high VI, Group II oils are hydrogenated or hydrocraked oils (as the sulfur content of $\leq 0.03\%$), and Group III products are very high VI oils manufactured by severe hydrocracking and or wax isomerization (VI $>$ 120, sulfur $\leq 0.03\%$) [Mang et al., 2011].

Although the high number of the available lubricants in the marketplace today, mineral oil still be used due to their strengths which are improved additive solubility, natural oxidation resistance characteristics, better seal compatibility and lower base oil cost whereas their weaknesses which are the limitations in high and low temperature applications and certain atmospheres [Schwindaman, 2006].

3.6. Performance packages

An axle gear oil is required to afford performance that cannot be delivered by a simple mix of base oil and viscosity modifier. The performance packages used to improve the characteristics of the base oil are usually necessary in the axle gear oil. The main functions of lubricating oil are to carry away heat, to protect against rust, to reduce friction, to protect against wear and to remove contaminants.

So the role of additives is to enhance the natural properties of the lubricating oil and to prevent undesirable properties.

Thus, additives are chemical compounds added to the base oil to impart specific properties to the finished oils. However the additives do not act with same way; some additives impart new and useful properties to the lubricant, some enhance properties already present, whereas other additives act to reduce the rate at which undesirable changes take place in the product during the service life of the lubricating oil [Speight and Exall, 2014].

Each additive is selected for its ability to achieve one or more specific functions in combination with other additives. Selected additives are formulated into packages for use with a specific lubricant base stock and for a specified end-use application.

The major functional additive types containing in axle gear oil are [Totten, 2012]:

- Viscosity Index improvement
- Antiwear/extreme pressure additives

- Detergent and dispersant
- Corrosion inhibitors
- Oxidation inhibitors
- Antifoaming agents
- Friction modifiers

These additives are presented with detail in Appendix A.3.

3.7. Axle gear oils selection

In order to obtain an overview of the axle gear oils generally available for use, five multigrade oils applied in gearboxes and differentials were selected as they are available on the market and they cover a large range of kinematic viscosity.
All the lubricants are synthetic oils except for the 80W90-A product which is a semi synthetic oil. Three among them (75W90-A, 80W90-A and 75W140-A), are reference oils (A) and labelled as "Fuel Efficient", and the other two products (75W85-B and 75W90-B) are candidate oils (B), as presented in Table 3.3. The reference lubricants 75W90-A and 80W90-A meet the requirements of API GL-4 and/or GL-5 and/or MT-1 standards and reference oil 75W140-A meet the requirements of API GL-5 standard. The candidate lubricants, 75W90-B and 75W85-B have not yet been assessed in what concerns the API standards. Several experimental analysis were performed to characterize the chemical, physical and rheological properties of the selected axle oil formulations.

3.8. Physical properties

Before performing any test using the selected lubricants, their physical properties needed to be measured in order to verify the information provided by the manufacturer.

The physical characterization of the oils was based on density measurement (Densimeter), viscosity measurement (Engler viscometer, Vibrational viscometer), and rheometry measurement (rheometer).

The axle lubricant temperatures measured during an EPA (Environmental Protection Agency) city cycle, including both city and highway cycles, presented in Figure 3.3, are in the range between 20 °C and 80 °C, although higher temperatures can be reached under more severe operating conditions. Thus, the physical properties of the axle oil formulations were measured at three different temperatures, respectively 40 °C, 70 °C and 100 °C.

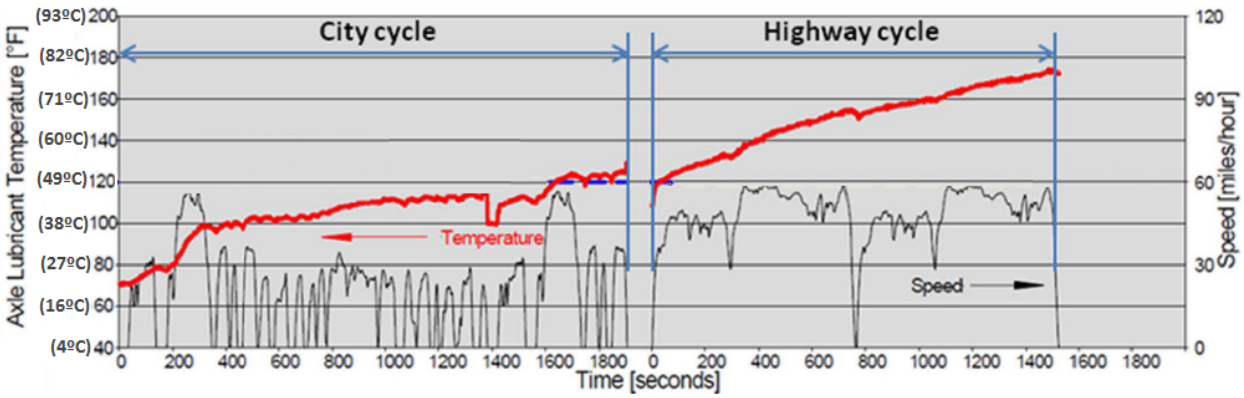

Figure 3.3: Axle oil temperature and vehicle speed during the EPA driving cycle [Xu et al., 2012]).

3.8.1. Density

It is well known that the density of a lubricant is the mass of a unit volume, generally calculated at 15 °C. To determine the density of an oil sample, an Antom Par densimeter is used (see Figure 3.4a).

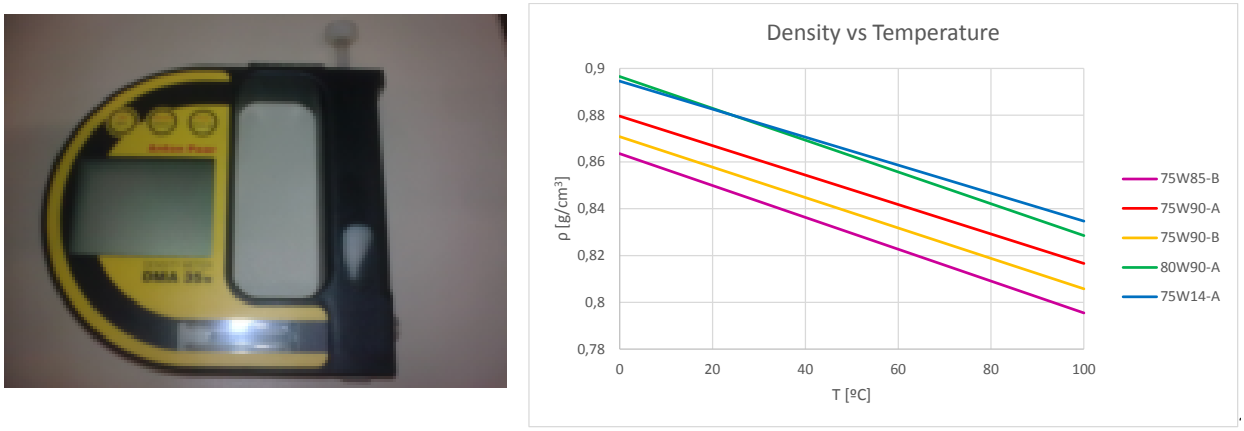

(a) (b)

Figure 3.4: Antom Par densimeter device (a) and density variation with the temperature of the tested oils (b).

The temperature of the sample should not be superior to 100 °C or inferior to 0 °C. Nevertheless the measuring device only effectively determines the density for temperatures until 40 °C which is enough to know the density of the fluid under ambient temperature conditions. At the reference temperature (15 °C), the density was determined for the five axle gear oils and the values are presented in Table 3.3.

Table 3.3: Density (ρ) at 15 °C and thermal expansion coefficient (α_t) for the axle gear oils.

Parameter	Unit	75W85-B	75W90-A	75W90-B	80W90-A	75W140-A
		candidate	reference	candidate	reference	reference
API/standard	[-]	-	GL-4/GL-5/MT-1	-	GL-4/GL-5/MT-1	GL-5
ρ @ 15 °C	[g/cm^3]	0.853	0.870	0.861	0.886	0.885
$\alpha_t \times 10^{-4}$	[/]	-8.1	-7.3	-7.6	-7.7	-6.8

Through the linearity of the lubricant density with temperature, the thermal expansion coefficient can be calculated (see Table 3.3). It is defined as the property of being changed in density with temperature and it is stated approximately by the Equation (3.1).

$$\rho = \rho_0 \cdot (1 + \alpha_t (T - T_0)) \tag{3.1}$$

where

- ρ_0 - Density at the temperature T_0;
- α_t - Thermal expansion coefficient;
- T_0 - Reference temperature (normally at 15 °C or in this case, at ambient temperature).

Analysing the results, it is possible to observe in Figure 3.4b that the 80W90-A oil and the 75W140-A oil have the highest and similar densities around 0.88 at 15 °C while the 75W85-B oil is the one that has the lowest density and the two other oils 75W90-A and 75W90-B present a density values in between.

3.8.2. Engler viscometry

Probably the most important property of a lubricant is its viscosity. It represents the fluid stiffness or internal friction. A distinction is made between dynamic viscosity and kinematic viscosity. The kinematic viscosity is almost always quoted and it is measured of different lubricant oils at several temperatures using an Engler viscometer (see Figure 3.5a).

This device is composed by a recipient where the oil to be evaluated is poured. There is a small calibrated hole at the bottom of that recipient where a wood pointer should be inserted or removed in order to stop or allow the oil to flow.

To keep the oil at a selected temperature, this recipient is inside another recipient with a fluid between them (oil or water) which is warm up through an electric resistance. These two recipients are supported by a tripod that allows adjustments in order to keep both recipients levelled. Two thermometers are used to control temperatures, one on the test oil, and the other one on the heat carrying fluid.

The measurement procedure used follows what is stated on the IP 212/62 standard. Through this instrument, the Engler viscosity of the sample is calculated by dividing the time taken

to flow of 200 ml of oil at selected temperature by a factor representing the time flow for an equal volume of water at 20 °C.

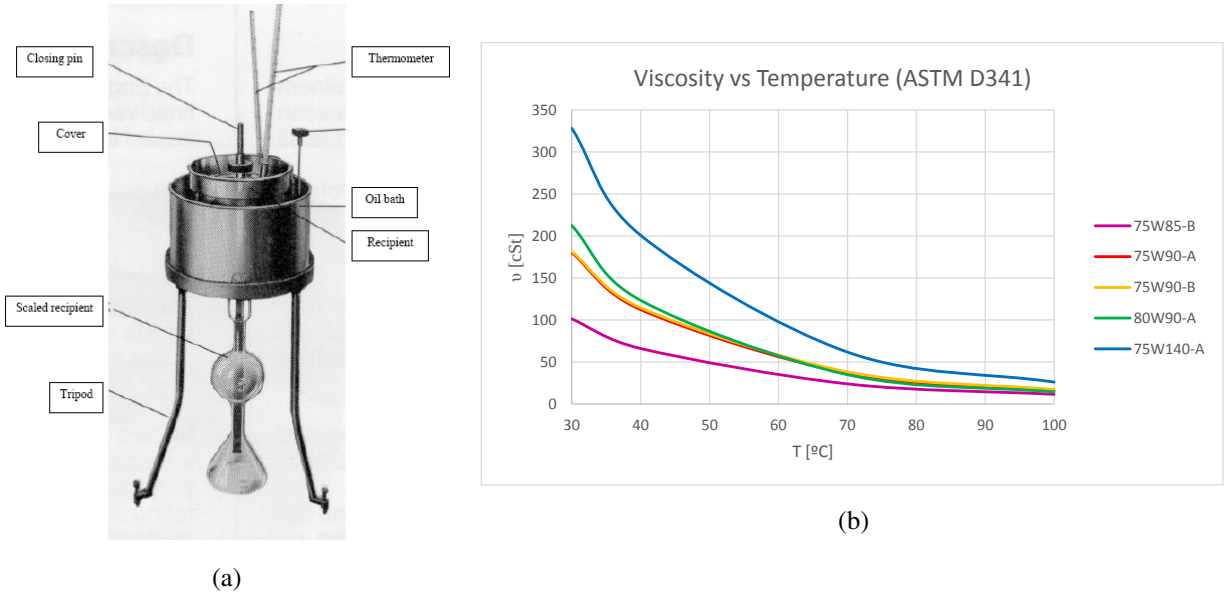

(a) (b)

Figure 3.5: Engler viscometer (DIN 51560/ASTM D 1665) (a) and viscosity variation with the temperature of the tested oils (b).

Then, the kinematic viscosity is calculated according to Equations (3.2) and (3.3).

$$^{\circ}Engler = \frac{flow\ time\ of\ fluid\ (200ml)}{flow\ time\ of\ water\ at\ 20^{\circ}C\ (200ml)} \tag{3.2}$$

$$cSt = K1 \cdot Engler + \frac{K2}{Engler + K3} \tag{3.3}$$

with,

- $^{\circ}Engler < 3 \rightarrow K1 = 14.867;\ \ k2 = 75.568;\ \ k3 = -6.198;$
- $^{\circ}Engler \geq 3 \rightarrow k1 = 7.624;\ \ k2 = -2.717;\ \ k3 = -1.522.$

In order to measure the kinematic viscosity, the tests were performed at 40, 70 and 100 °C for all the selected axle gear oils. Table 3.4 shows the measurements of the kinematic viscosity for all axle gear oils and the results are plotted in Figure 3.5b. The viscosity values obtained are within the limits specified by the norm SAE J306 Viscosity Grade at 100 °C [vis,]. The reference oil 75W140-A exibited the highest kinematic viscosity of 26.21 cSt at 100 °C while the candidate axle gear oil 75W85-B presented the lowest kinematic viscosity of 11.44 cSt at 100 °C.

Table 3.4: Kinematic viscosity (ν), ASTM conatants (n_A, m_A), Vogel constants (k_ν, b_ν, c_ν), Viscosity Index (VI) and thermoviscosity (β) for the axle gear oils.

Parameter	Unit	75W85-B	75W90-A	75W90-B	80W90-A	75W140-A
ν @ 40 °C	[cSt]	65.95	112.35	114.42	123.30	200.70
ν @ 70 °C	[cSt]	23.86	36.70	38.14	34.86	61.86
ν @ 100 °C	[cSt]	11.44	16.37	17.18	14.38	26.21
n_A	[/]	7.666	7.583	7.407	8.503	7.154
m_A	[/]	2.967	2.913	2.842	3.278	2.721
k_ν	[/]	0.098	0.330	0.168	0.044	0.049
b_ν	[/]	1060	711.008	955.78	1281.600	1544.500
c_ν	[/]	122.888	81.926	106.482	121.530	145.467
VI	[/]	162	147	163	118	169
Thermoviscosity @ 40 °C ($\beta \times 10^3$)	$[K^{-1}]$	40.20	44.3	43.3	50.7	46.3
Thermoviscosity @ 70 °C ($\beta \times 10^3$)	$[K^{-1}]$	28.50	31.30	30.9	34.80	33.2
Thermoviscosity @ 100 °C ($\beta \times 10^3$)	$[K^{-1}]$	21.10	23.10	22.9	25.0	24.70

According to ASTM D341 [sta, 2009], two ASTM constants m_A and n_A are calculated using Walther Equation (3.4) while keeping the normal value a_A=0.7 for all oils and they are presented in Table 3.4.

$$log\ log(\nu + a_A) = m_A - n_A log(T) \tag{3.4}$$

Vogel Equation (3.5) represents a second expression to calculate the constants for the kinematic viscosity variation with temperature. Three constants k_ν, b_ν and c_ν were determined and presented in Table 3.4.

$$\nu = k_\nu \cdot \exp(\frac{b_\nu}{\theta + c_\nu}) \tag{3.5}$$

According to ASTM D 2270 [sta, a], the Viscosity Index (VI) is a unit-less parameter that indicates the change in kinematic viscosity as function of temperature between 40 and 100 °C. The higher the VI, the lesser the viscosity of the oil changes as a function of temperature. This parameter is calculated using the empirical formula proposed by Dean and Davis [Dean et al., 1929]. In the case of VI greater than 100, the Viscosity Index formula is given by the following Equations (3.6) and (3.7).

$$VI = \frac{10^N - 1}{0.00715} + 100 \tag{3.6}$$

$$N = \frac{logH - logU}{logY} \tag{3.7}$$

where

- H is the kinematic viscosity at 100 °C of an oil of 100 viscosity index having the same kinematic viscosity at 100 °C as the oil whose Viscosity Index is to be calculated;
- U is the kinematic viscosity at 40°C of the oil whose Viscosity Index is to be calculated;
- Y is the kinematic viscosity at 100 °C of the oil whose kinematic viscosity is to be calculated.

The results presented in Table 3.4 show that the five lubricants are formulated with base oils of different viscosities and different Viscosity Indexes (VI's).

Axle oils 75W85-B, 75W90-B and 75W140-A have very high Viscosity Index (above 160). However, the mineral oil based formulation, 80W90-A, has the lowest Viscosity Index (VI=118) when compared with the other polyalphaolefin (PAO) based formulations. The 75W90-A oil has intermediate value of 147.

The kinematic viscosity was used to determine the thermoviscosity of the oils, using the following Equation (3.8). Thermoviscosity is a characteristic of the oil and represents how the viscosity decreases with temperatures (see Table 3.4).

$$\beta = \frac{m_A}{T} \times \frac{(\nu + a_A) log(\nu + a_A)}{\nu} \tag{3.8}$$

3.8.3. Vibro viscometry

The dynamic viscosity measurements were performed using the method of low vibrational frequency (30 Hz) using vibro viscometer (SV$-$10) (see Figure 3.6a). This device is used mainly for its high measurement accuracy. It has two gold sensor plates immersed in the sample. These plates are in a tuning fork arrangement so when stimulated by an electromagnetic drive the plates vibrate at a constant frequency. The amplitude of vibration is detected and sufficient current is applied to the electromagnetic drive to maintain a constant amplitude. The sample viscosity causes the vibration to be damped and the current required to maintain the vibration amplitude is measured continuously and converted into a viscosity on the display [sv1,].

Figure 3.6b shows the values displayed for the five axle gear oils using the SV-10 as they are without any modification. By dividing the dynamic viscosity with the measured density at a given temperature, it is possible to obtain the kinematic viscosity and compare the values with the ones provided by the manufacturer and the ones obtained using the Engler viscometer.

Observing the data obtained with the vibro viscometer (Figure 3.6b) and converting the dynamic viscosity values into kinematic viscosity, it is proved again that the axle gear oil formulations are in the range acceptable for the SAE Viscosity Grade and as it is expected by the standard SAE J 306 [vis,], the viscosities at 100 °C of the selected lubricants are comprised between the indicated minimum and the maximum viscosity (see Table A.1).

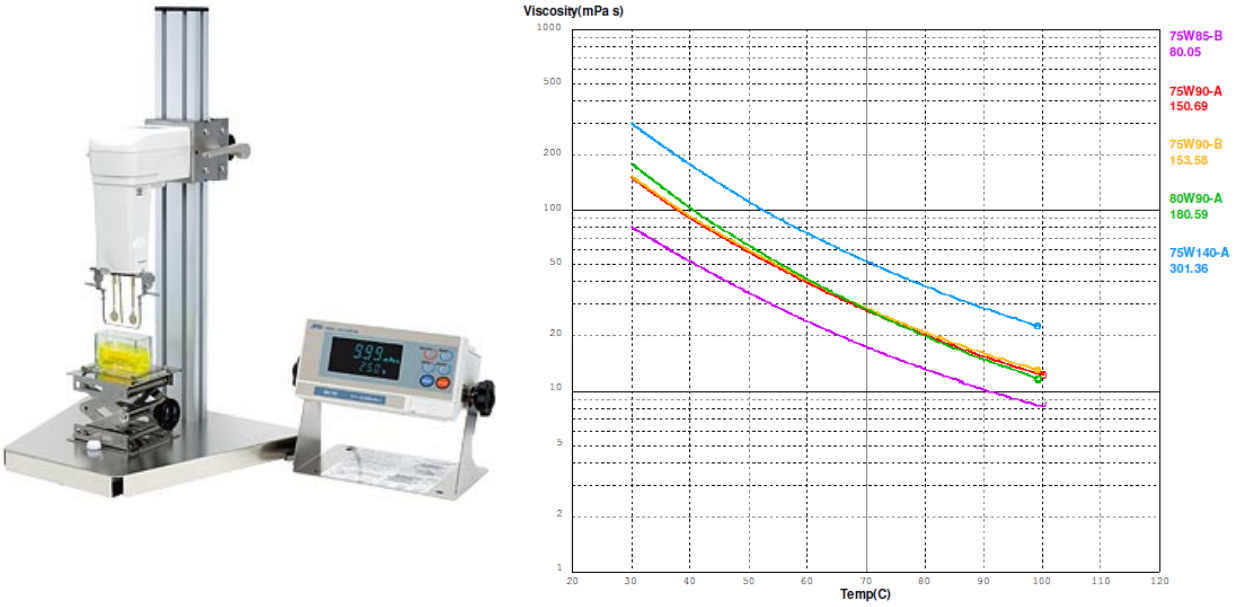

(a) (b)

Figure 3.6: SV-10 Vibro viscometer (a) and variation of the dynamic viscosity against temperature for the axle gear oils (b).

3.8.4. Pressure viscosity

In elastohydrodynamic lubrication, which generates very high pressures, an increase in lubricant viscosity is significant. Thus, the pressure viscosity coefficient is considered as an important factor in ensuring successful lubrication for gears and bearings [Kajdas et al., 1990]. It is also used in film thickness lubricant calculation and EHD analysis. The most commonly equation for the relation between viscosity and pressure is developed since 1893 by Barus in the following formula (3.9) [Hamrock et al., 2004].

$$\eta = \eta_0 \cdot e^{\alpha.P} \tag{3.9}$$

where η is the dynamic viscosity at pressure P, η_0 is the dynamic viscosity at atmospheric pressure, and α is a temperature-dependent and pressure-independent constant called the pressure viscosity coefficient.

Inasmuch as the kinematic viscosity of the five axle gear oils are calculated and presented in section 3.8.2, the pressure viscosity coefficient will be easily determined following Gold's Equation (3.10). The calculation can be accurate when using the correct base oil for each axle gear oil 80W90-A (mineral) and the other four lubricants are polyalphaolefin base oil.

$$\alpha = s \cdot \nu^t \tag{3.10}$$

where the constants s and t derived from the IME database at 0.2 GPa are presented in Table 3.5.

Table 3.5: Parameters of Gold equation valid for 0.2 GPa for the axle gear oils [Gold et al., 2001].

Parameter	75W85-B	75W90-A	75W90-B	80W90-A	75W140-A
s	0.7382	0.7382	0.7382	0.9904	0.7382
t	0.1335	0.1335	0.1335	0.1390	0.1335

When the Gold constants s and t are known for mineral and PAO base oils, the pressure viscosity coefficient can be calculated at different temperatures. Table 3.6 shows the values calculated of the pressure viscosity α for the tested axle gear oils at 40, 70 and 100 °C. It is possible to compare the pressure viscosities of the oils and prove the following behaviour. The mineral axle gear oil 80W90-A presents the highest piezoviscosity coefficient whatever the temperature considered while the candidate oil 75W85-B presents the lowest values at 40 and 100 °C. The 75W140-A, 75W90-B and 75W90-A axle gear oils have intermediate pressure viscosity coefficient values. The piezoviscosity has mainly a very significant influence on lubricant film thickness.

Table 3.6: Pressure viscosity coefficient (α) calculated at 40, 70, and 100 °C for the selected axle gear oils.

Oil	Unit	75W85-B	75W90-A	75W90-B	80W90-A	75W140-A
$\alpha \times 10^{-8}$ @ 40 °C	$[Pa^{-1}]$	1.291	1.387	1.390	1.934	1.498
$\alpha \times 10^{-8}$ @ 70 °C	$[Pa^{-1}]$	1.128	1.194	1.200	1.623	1.280
$\alpha \times 10^{-8}$ @ 100 °C	$[Pa^{-1}]$	1.022	1.072	1.079	1.435	1.142

3.8.5. Rheometry

Rheometry is defined as the study of flow behaviour. It is generally applied to fluid materials. Flow is typically measured using shear. The shear stress (τ) and the shear rate ($\dot{\gamma}$) are calculated from measurements of torque and flow rate. Viscosity (η) is defined as $\eta = \tau/\dot{\gamma}$ [Flick, 1989]. It is important to identify the lubricant behaviour through this way which is based on the correlation between shear stress and shear rate which is graphically displayed in a digram called 'Viscosity Curve' which is very common where the viscosity (η) is plotted versus shear rate ($\dot{\gamma}$).

In order to clarify the flow behaviour of the five automotive lubricants, a RHEOMAT 115 rotational viscometer operating according to Searle principle is used (see Figure 3.9a). It is a laboratory device that is composed of a measuring bob which rotates in the measuring substance driving by an electromotor. The braking torque thereby exerted on the bob by the substance is measured in the measuring head of RHEOMAT 115 and indicated in the control instrument. The shearing speed prevailing in the substance is a function of the bob's rotational speed, and the shear stress is a function of the braking torque. Then, the substance's viscosity, or it flow behaviour respectively can be deduced.

Figure 3.7 presents a popular bob design based on a German standard (DIN 53019). The DIN norm 53019 states some restrictions for the concentric cylinder geometry like the dimensions of the bob, the cup and the inner cylinder [Steffe and Daubert, 2006]. The following preferred dimensions are: $\alpha = \frac{R_c}{R_b} = 1.0847$; $\frac{h}{R_b} = 3$; $\frac{h'}{R_b} = 1$; $\frac{h''}{R_b} = 1$; $\frac{R_s}{R_b} \leq 0.3$; θ= 120 °±1 °.

Its rheological correct cylindrical geometry provides extremely accurate viscosity measurements and shear rate determinations.

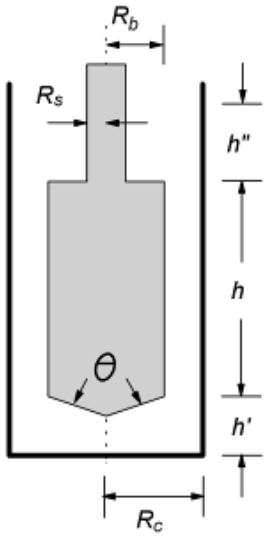

Figure 3.7: Concentric cylinder system based on the DIN 53019 standard [Steffe and Daubert, 2006].

Some equations are needed to calculate the rheological characteristic of the testing substance. The shear rate ($\dot{\gamma}$) of the fluid tested in a rotational viscometer is dependent on the velocity of the bob (U_{bob}) and the geometric parameters (Da= 48.8 mm and Di= 45 mm) as it is presented in Equation (3.11).

$$\dot{\gamma} = \frac{du}{dy} = \frac{U_{bob}}{(Da - Di)} \tag{3.11}$$

To facilitate calculation of the absolute viscosity a representative dynamic viscosity factor is calculated by the division of the representative shear stress by the shear rate as shown in Equation (3.12). The value of τ_{rep}=195.5 is determined from the Measuring System MS DIN 145.

$$\eta\% = \frac{\tau_{rep}}{\dot{\gamma}} \tag{3.12}$$

The Rheomat 115 viscometer measures a dimensionless value (T%) which allows to calculate the dynamic viscosity according to Equation (3.13).

$$\eta = \frac{\eta\%}{T\%} \tag{3.13}$$

Five axle lubricants presented in section 3.7 are rheologically characterized following the measurement procedure described before. The working temperatures are 40, 70 and 100 °C. The shear strain rate is ranged between the possible minimum value of the rheometer 6.38 s^{-1} and the maximum of 967 s^{-1}. These limitations are basically due to the motor performance that accelerates the bob cup (Figure 3.7). The results are graphically displayed in a diagram called 'Viscosity Curve' defined previously (see Figure 3.8b. The latter Figure shows that the ratio of all pairs of τ and $\dot{\gamma}$ values belonging to this graph is approximately constant. This means that the dynamic viscosity η is generally not affected by changes in shear strain rate and all the axle gear oils tested are proving the truth of this statement so they have a Newtonian behaviour which is expected for this range of shear strain rate and the decrease of the viscosity of 75W140-A oil at 40 °C with the increase of shear rate is explained with the difficulties faced by the instrument (RHEOMAT 115) in keeping the temperature constant when the speed or the shear strain rate increase.

(a)

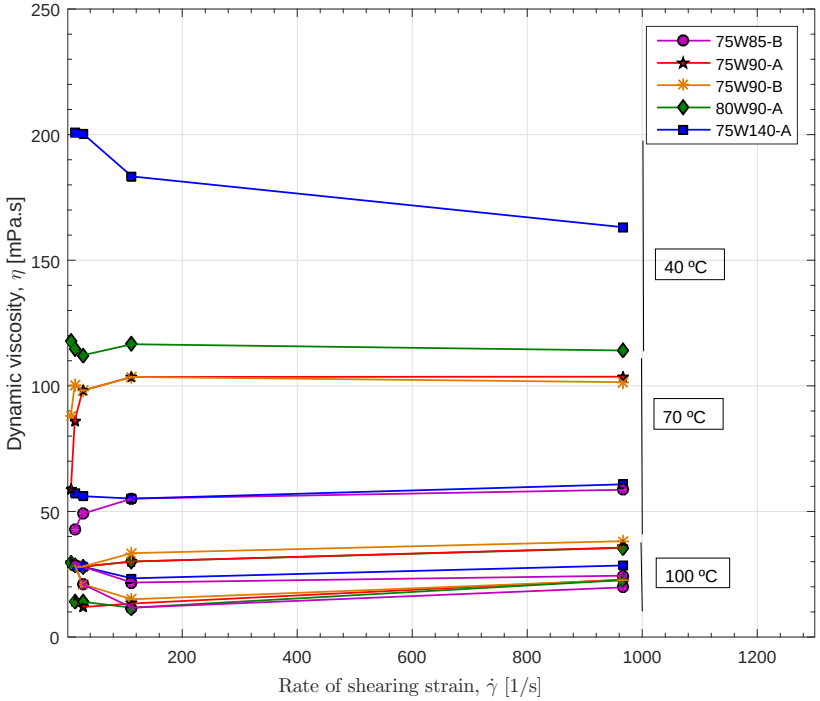

(b)

Figure 3.8: RHEOMAT 115 instrument (a) and Dynamic viscosity against shear strain rate at 40, 70, and 100 °C for automotive lubricants (b).

To obtain more precision and to show the behaviour of the axle oils under high shear rate, an MCR 301 rheometer from Anton Paar is used (see Figure 3.9a). A plate−plate geometry (PP50) was selected with a small gap of 0.1 mm is imposed between the two plates. This device is very known with its high shear rate. The shear rate is ranged between a minimum value of 10^0 s^{-1} and a maximum value of 10^5 s^{-1}, which is a significantly high shear rate. The measurements are performed at 70°C and 100 °C.

Figure 3.9b and Figure 3.9c show the variation of the dynamic viscosity η with increasing

shear rates $\dot{\gamma}$, at two different temperatures, 70 °C and 100 °C. The dynamic viscosity of all axle gear oils remains almost constant up to $10^4\ s^{-1}$, suggesting they behave like a Newtonian fluid (see Equation (3.12)) [Flick, 1989]. The small decrease in viscosity observed is only due to the slight increase of the temperature as the shear rate increases. For higher shear rates, up to $10^5\ s^{-1}$, the dynamic viscosity decreases slightly, indicating that these oils have a shear-thinning effect at very high shear rates. At both temperatures, whatever the shear rate, oil 75W140-A always presents the highest dynamic viscosity and oil 75W85-B the lowest one. Fluids 75W90-A, 75W90-B and 80W90-A are placed in between the previous two, showing very similar dynamic viscosities.

(a)

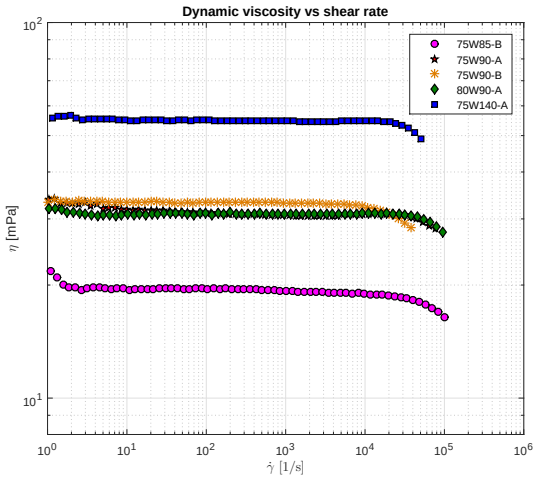

(b)

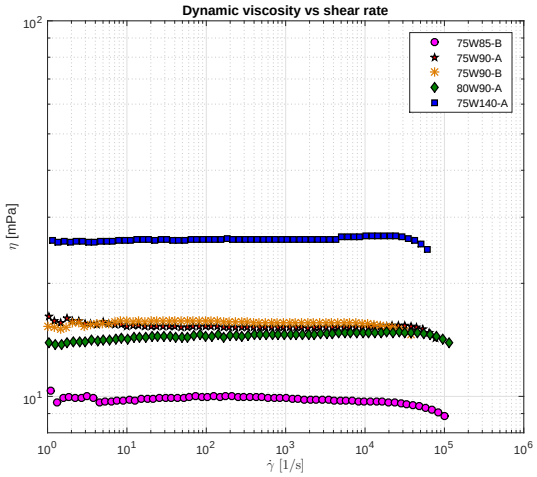

(c)

Figure 3.9: MCR 301 rheometer instrument (a) and Dynamic viscosity against shear rate at 70 °C (b) and at 100 °C for the five axle oils (c).

3.9. Chemical properties

3.9.1. Inductively coupled plasma atomic emission spectrometry (ICP-AES)

Inductively coupled plasma atomic emission spectrometry (ICP-AES) represents an effective technique for element analysis. This technique is to dissociate the sample into its constituent atoms or ions and show their chemical compositions, which, for the lubricants analysed, are mainly based on barium, boron, calcium, magnesium, phosphorus, silicon, sodium, tin, and zinc (see Table 3.7). This method is not effective to sort out the accurate trace elements of the formulated product but it is helpful to obtain a sweeping overview about the amount of certain oil additive elements, wear metals and contaminants. The additives usually used to enhance the lubricating properties of mineral and synthetic base oils in which they are blended are also put into evidence (see Appendix A.3.2).

The three reference oils (A) contain high amounts of sulphur and phosphorus based organic compounds, well known as extreme-pressure (EP) and anti-wear (AW) additives, as well as a large quantity of magnesium, related to detergent and dispersant additives. The two candidate oils (B) contain a large amount of zinc, known as a common anti-wear, anti-oxidant and corrosion inhibitor additive, as well as a high quantity of calcium, related to detergent and dispersant additives. They also exhibit significant amounts of sulphur and phosphorous. In the case of the 75W90-B candidate oil, boron based friction modifier additives are also present in the formulation, having an important role in reducing friction. Other additives such as barium, sodium, silicon, and tin are present in very small amounts in all formulations.

Table 3.7: Typical ICP-AES analysis of axle gear oils.

Parameter	Unit	75W85-B	75W90-A	75W90-B	80W90-A	75W140-A
Boron (B)	[ppm]	0	-	81	-	-
Barium (Ba)	[ppm]	0	< 5	0	< 5	< 5
Calcium (Ca)	[ppm]	1795	18	2891	97	33
Magnesium (Mg)	[ppm]	6	1087	17	936	1093
Sodium (Na)	[ppm]	0	5	0	< 5	< 5
Phosphorus (P)	[ppm]	783	1622	958	1436	1686
Silicon (Si)	[ppm]	4	-	5	-	-
Tin (Sn)	[ppm]	0	8	0	7	8
Sulphur (S)	[ppm]	2954	23262	3271	26947	22784
Zinc (Zn)	[ppm]	899	7	1120	23	12

3.9.2. Fourier Transform Infra Red spectroscopy (FTIR)

FTIR is an effective analytical instrument for detecting functional groups and identifying chemical bonds in a fresh or used oil sample by producing an infrared absorption spectrum.

FTIR analysis are performed using Agilent Cary 630 device presented in Figure 3.10.

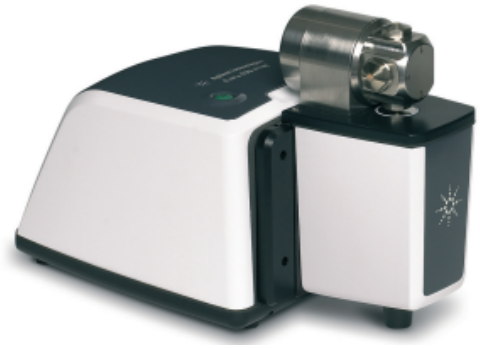

Figure 3.10: Dialpath Accessory.

FTIR Dialpath liquid sampling system is used for the analysis of the five axle gear oils and it is based on ASTM D7678-11. The technology of Agilent's Dialpath Accessory on the Cary 630 facilitates fast FTIR transmission measurements of liquids and it offers several advantages over classic transmission cells. The Dialpath features an optical head that can be rotated to select one of three factory-calibrated which is fixed to 0.05 mm. The accessory only requires a very small amount of liquid, with one drop on the crystal interface (crystal made of material with high refractive index) being sufficient for the measurement. It is also fast and sample to clean using a cheaper and safer solvent (Propanol). The measurements are exposed as spectra profiles which are derived from a MicroLab FTIR software and are directly shown without any changes.

The FTIR spectrum of a fresh oil is substantial to control the lubricant during its lifetime and to easily detect any oxidation, additive depletion or contamination when it is compared to the used oil. FTIR spectrum is divided in to parts. The first part is the fingerprint area for a wavenumber between 700 cm^{-1} and 1500 cm^{-1} and the second part is the functional groups for a wavenumber between 1500 cm^{-1} and 4000 cm^{-1}.

The fingerprint zone of the five fresh axle gear oils are overlaid in Figure 3.11. This main zone depicts the difference between the axle gear oil formulations in terms of additive packages. It is a daunting task to figure out which additive compounds are present in the formulations without a known spectra of the base oil.

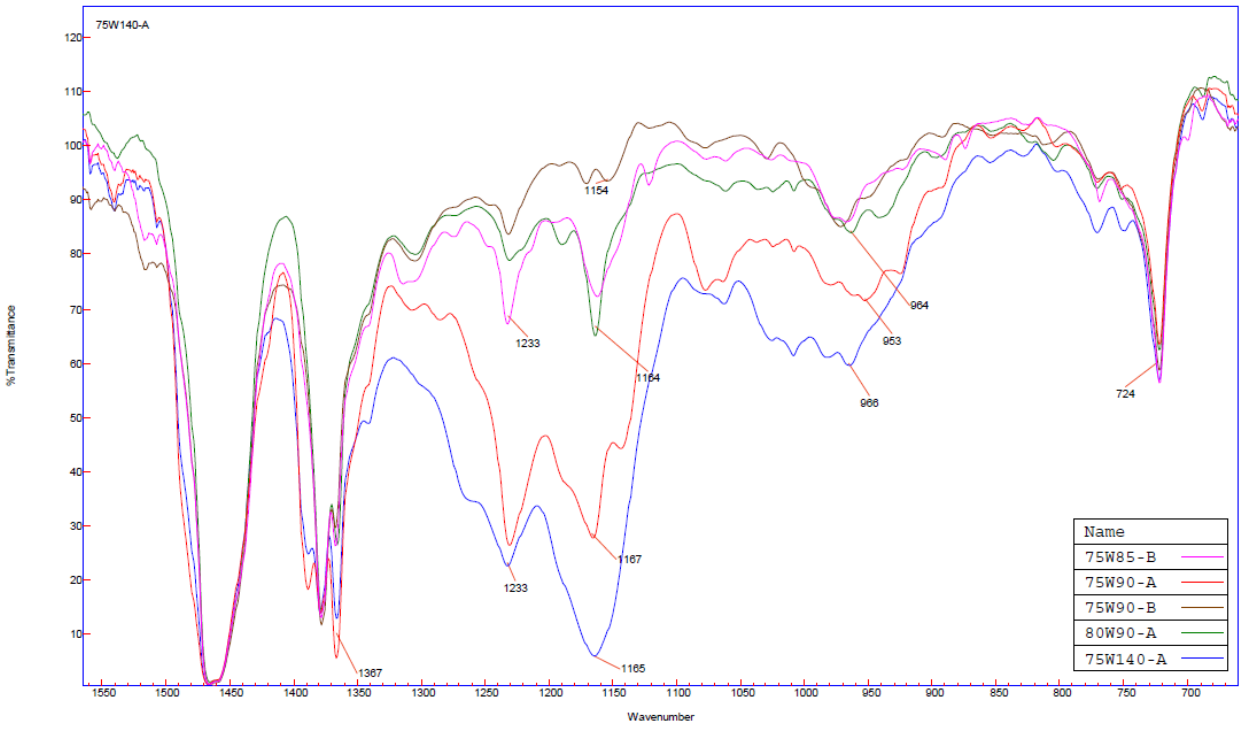

Figure 3.11: FTIR Spectra on fingerprint zone of the axle gear oils.

All FTIR spectra of fresh axle gear oils (see Figure 3.12) are illustrated under the wavelength area between 4000 to 700 cm^{-1} including the two parts.

Normally the base oil of the axle gear oil formulations should be known in advance which is not the case. The general shape of the spectra help us to identify the base oil types and prove that the 75W85-B, 75W90-A, 75W90-B and 75W140-A oils are polyalphaolefins while the 80W90-A oil presents a different behaviour which corresponds to a mineral base oil. Using this method, some information about specific chemical bonds and functional groups can be delivered.

The left part of the spectra in the five oils dominated by a large bands in the range 2800-3000 cm^{-1} caused by the large amount of carbon-hydrogen (C=H) asymmetric stretch of CH2 and CH3 molecules that are hydrocarbon structures, present on base oil of the lubricants. The same group is present at 1465 cm^{-1} where the five oils show exactly the same off-peak. A smaller off-peak seen at 724 cm^{-1} caused by (C-H) bonds. The ester bonds (C=O) seen around the range of 1700-1750 cm^{-1} in which the exact position depends on the type of carbonyl. Also another ester bonds (C-O) presented under a range of 1135-1175 cm^{-1}, which show that the 75W90-A and 75W140-A oils include ester in their formulations.

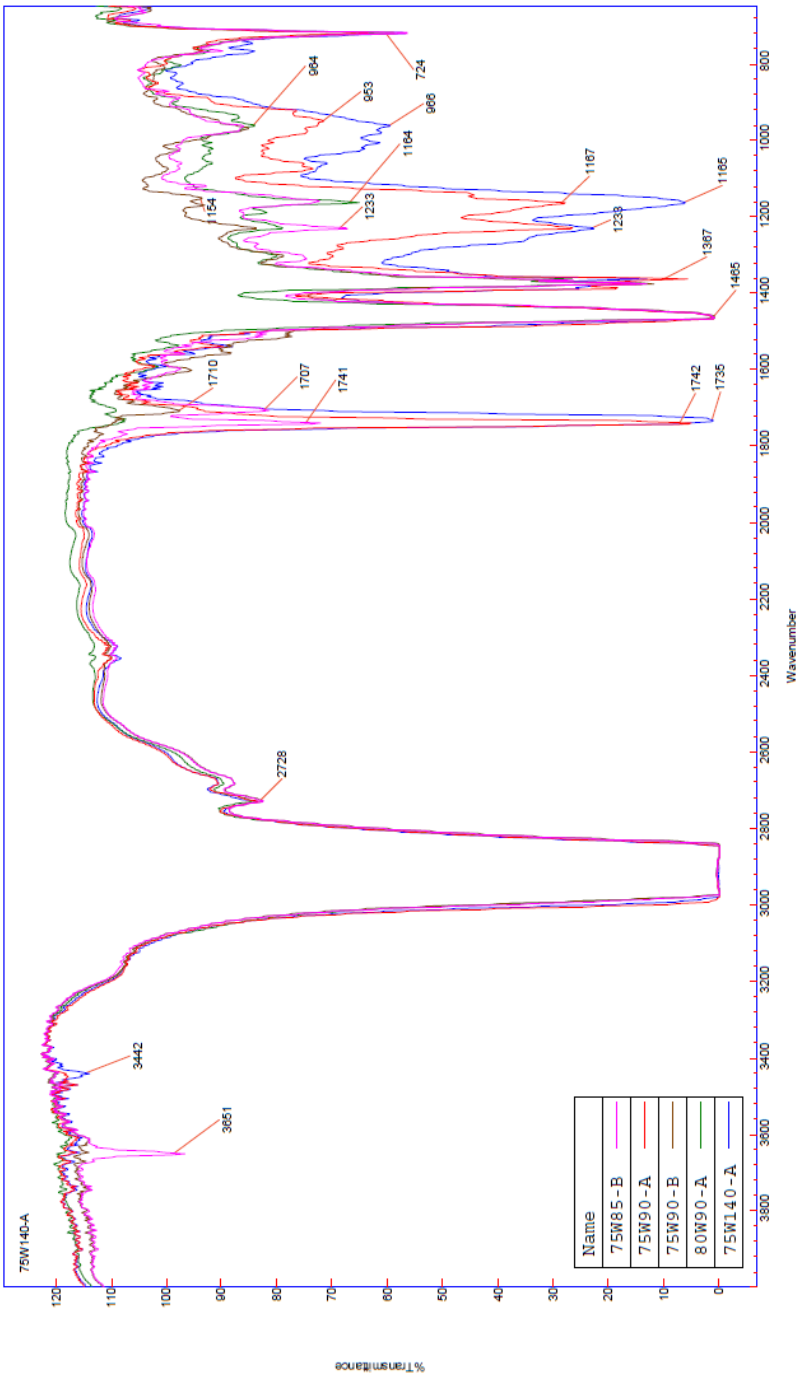

Figure 3.12: FTIR Spectra of the axle gear oils.

3.10. Summary

This chapter detailed and defined the selected multigrade oils through their performance requirements and their base oils. Axle oil formulations were classified with their performance packages and developed as a Fuel Efficiency. Overall five axle gear oil formulations are chemically characterized using the element analysis ICP and FTIR. The physical properties are extracted to find out the density, the viscosity and the piezoviscosity. A detailed presentation of those analysis and properties measured can be found in Table 3.8. The obtained results prove that the oils confirm the norms indicated by the SAE J306 Viscosity Grades. The behaviour of the tested lubricants is confirmed as a Newtonian behaviour under the condition of the rheological tests.

Table 3.8: Axle gear oils properties.

Parameter	Unit	75W85-B	75W90-A	75W90-B	80W90-A	75W140-A
		candidate	reference	candidate	reference	reference
Base oil	[-]	PAO	PAO	PAO	Mineral	PAO
API/standard	[-]	-	GL-4/GL-5 /MT-1	-	GL-4/GL-5 /MT-1	GL-5
Chemical composition						
Boron (B)	[ppm]	0	-	81	-	-
Calcium (Ca)	[ppm]	1795	18	2891	97	33
Magnesium (Mg)	[ppm]	6	1087	17	936	1093
Phosphorus (P)	[ppm]	783	1622	958	1436	1686
Sulphur (S)	[ppm]	2954	23262	3271	26947	22784
Zinc (Zn)	[ppm]	899	7	1120	23	12
Physical properties						
Density @ 15 °C	[g/cm ^{3}]	0.853	0.87	0.861	0.886	0.885
Thermal expansion coefficient ($\alpha_t \times 10^{-4}$)	[/]	-8.1	-7.3	-7.6	-7.7	-6.8
Viscosity @ 40 °C	[cSt]	68.95	112.35	114.42	123.3	200.7
Viscosity @ 70 °C	[cSt]	23.86	36.7	38.14	34.86	61.86
Viscosity @ 100 °C	[cSt]	11.44	16.37	17.18	14.38	26.21
a_A	[/]			0.7		
n_A	[/]	7.6655	7.5833	7.407	8.5027	7.1537
m_A	[/]	2.9663	2.9133	2.842	3.2783	2.7211
Thermoviscosity @ 40 °C ($\beta \times 10^3$)	[K^{-1}]	40.2	44.3	43.3	50.7	46.3
Thermoviscosity @ 70 °C ($\beta \times 10^3$)	[K^{-1}]	28.5	31.3	30.9	34.8	33.2
Thermoviscosity @ 100 °C ($\beta \times 10^3$)	[K^{-1}]	21.1	23.1	22.9	25	24.7
s @ 0,2 GPa [Gold et al., 2001]	[/]	0.7382	0.7382	0.7382	0.9904	0.7382
t @ 0,2 GPa [Gold et al., 2001]	[/]	0.1335	0.1335	0.1335	0.139	0.1335
Piezoviscosity @ 40 °C ($\alpha_{Gold} \times 10^{-8}$) [Gold et al., 2001]	[Pa^{-1}]	1.291	1.387	1.39	1.934	1.498
Piezoviscosity @ 70 °C ($\alpha_{Gold} \times 10^{-8}$) [Gold et al., 2001]	[Pa^{-1}]	1.128	1.194	1.2	1.623	1.28
Piezoviscosity @ 100 °C ($\alpha_{Gold} \times 10^{-8}$) [Gold et al., 2001]	[Pa^{-1}]	1.022	1.072	1.079	1.435	1.142
VI	[/]	162	147	163	118	169

4. Film thickness, tribofilm generation and friction behaviour of axle gear oils

4.1. Introduction

Lubricated contacts in automotive axles are often operate in the regime referred to as elastohydrodynamic lubrication (EHL) defined in section 2.8.1. These contacts are mainly between gear teeth, the rolling element and the inner or outer raceway in rolling element bearings [Nijenbanning et al., 1994a]. This type of lubrication has been studied intensively through the prediction of the film thickness with line contact (see section 2.8.2.1) and point contact (see section 2.8.2.2) and the friction behaviour in particular with traction and Stribeck curves.

Early numerical studies of the EHL problem adapt some simplifying assumptions such an isothermal Newtonian fluid model and exponential piezoviscosity in order to develop the most popular minimum film thickness [Anuradha and Kumar, 2011].

Lubricant traction coefficient (rolling/sliding friction coefficient) has a crucial role since it determines the power losses and stability of the rolling element. The traction properties of the lubricant are characterized by its limiting shear stress and its elastic shear modulus [Fang et al., 2000].

This part plans to evaluate axle gear oil formulations ability to generate a lubricating film, under full-film, mixed and boundary lubrication regimes with ball-on-disc contact configuration. The film thickness prediction is also discussed and related to experimental results. Also it intends to discuss the experimental results using the traction coefficient curves as well as Stribeck curves.

4.2. Film thickness

4.2.1. Test equipment and methods

The film thickness is probably the most important parameter in lubricated contacts and several methods [Johnston et al., 1991, Guangteng et al., 2000, Cann et al., 1996] have been used to measure it. One of the most used techniques is optical interferometry, due to its capacity to provide a high accuracy local measurement of the film thickness inside the contact

zone [Bassani and Ciulli, 1997]. An EHD2 Ball-on-Disc apparatus, from PCS Instruments was used for these measurements (see Figure 4.1).

Figure 4.1: EHD2 ball-on-disc test apparatus from PCS Instruments.

The point contact generated between the ball and the disc simulates a real contact between the components of a mechanical system such as a rolling bearing. The contacting bodies are a standard space layer disc and a 3/4" (19.05 mm) diameter drilled steel ball. The glass disc used in oil film thickness measurements has a semi-reflecting chrome layer and a silica space layer coated onto one side. The test ball has a highly polished surface finishing because it plays an important role in maintaining high levels of repeatability, and reduces disc wear. A light source, microscope assembly and spectrometer are used to measure the lubricant film thickness. The system analysis the light returned from the central plateau of the contact and then calculates the central film thickness [Fernandes et al., 2015]. Both the disc and the ball are driven by DC electric motors allowing continuous variation of each component rotating speed. Figure 4.2 shows the four steps defining the EHD2 method and they are described as follows.

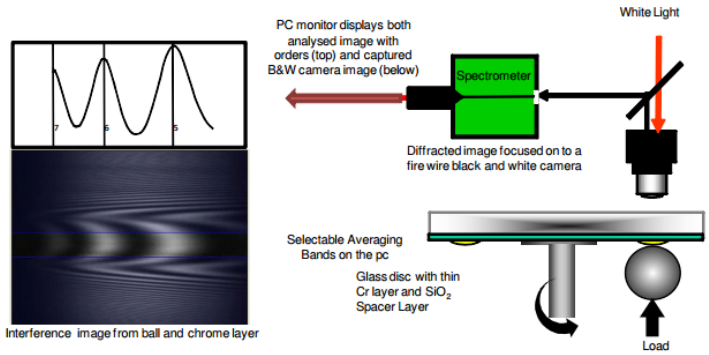

Figure 4.2: Optical interferance technique used on the EHD test rig.

1. The contact is illuminated by a white light source directed down a microscope through a glass disc on to the contact.
2. The light is divided into one part which is reflected from the Cr layer and another part penetrates through the SiO_2 layer and fluid film and is reflected back from the steel ball.

3. The two light paths are recombining and forms an interference image which is passed into a spectrometer and high resolution black and white CCD camera.

4. A video frame grabber captures the camera image which is analysed with a control software in order to determine the film thickness.

4.2.2. Test inputs

The specimen configuration consists of a standard ball made of carbon chrome steel, having high grade surface finish to ensure good reflectivity, and a glass disc coated first with 20 nm chromium and then with 500 nm "spacer-layer" of silica, the purpose of the latter being to act as an artificial film of oil and allow constructive interference to occur at any real value of the oil film thickness [Taylor et al., 1997]. The silica space layer is characterized with a refractive index of 1.4785 and the maximum contact pressure between steel ball and glass disc is 0.66 GPa.

The lubricant properties are detailed in Chapter 3 and the specimen properties between ball and disc are summarised in Table 4.13 [Taylor et al., 1997].

Table 4.1: Contact parameters for on the ball-on-disc apparatus (glass disc vs. steel ball).

Parameters	**Symbol**	**Unit**	**Glass disc**		**Steel ball**
Materials properties					
Elastic Modulus	E	[Gpa]	64		210
Poisson Coefficient	ν	[-]	0.2		0,29
Equivalent Young Modulus	E^*	[GPa]		51.6	
Specimen and contact geometry					
Radius	R	[mm]	50		9.525
Radius in X direction	R_x	[mm]	∞		9.525
Radius in Y direction	R_y	[mm]	∞		9.525
Surface roughness	R_a	[nm]	5		5
Space layer thickness	-	[nm]	500		-
Space layer refractive index	-	[-]	1.4785		-
Hertzian contact parameters					
Normal force	F_n	[N]		50	
Maximum Hertz pressure	p_0	[GPa]		0.66	
Medium pressure	p_m	[GPa]		0.44	
Radius of the contact circle	a	[mm]		0.19	
Penetration	δ	[μm]		3.809	

4.2.3. Test procedure

The oil reservoir of the ball-on-disc apparatus is filled with one of the axle gear oils presented in Section 3.7, up to the level of the center of ball drive shaft. The maximum oil volume is 0.012 litter which is heated up to the operating temperature, which is restricted to range between the ambient temperature up to 150 °C. The ball and disc are loaded together to produce a point contact and the applied load is kept constant at 50 N corresponding to the maximum Hertzian pressure of 0.66 GPa. The tests are performed under imposed values of 3% and 30% of the slide-to-roll ratio (*SRR*), defined by Equation (4.1).

$$SRR\ [\%] = \frac{U_{disc} - U_{ball}}{(\frac{U_{disc}+U_{ball}}{2})} \times 100 \tag{4.1}$$

The film thickness can only be measured up to 1000 nm due to the performance of the optical device. Such restriction limits the maximum entrainment speed used in the tests, mainly at low temperature or high viscosity. In order to confirm repeatability, the measurements are performed from the highest to lowest entrainment speed, and then backwards from the lowest up to the highest entrainment speed. Whatever the operating temperature used, the highest entrainment speed is always the same and equal to 2 m/s, however, the lowest entrainment speed depends on the temperature, 0.1 m/s at 40°C, 0.25 m/s at 70 °C and 0.5 m/s at 100 °C, in order to avoid the contact between the ball and the disc. During the film thickness measurements the traction force and the temperature are also recorded. This procedure is very important to obtain an accurate measurement of the film thickness.

4.2.4. Experimental results and comparison of the oils

The experimental measurements of the film thickness are plotted in Figure 4.3 and Figure 4.4, for the slide-to-roll ratios of 3 % and 30 %, respectively, a hertzian pressure of p_0 = 0.66 GPa, three temperatures, 40, 70 and 100 °C, and a wide range of the entrainment speed. All the axle gear oils are tested where the experimental film thickness measurements are represented with markers and the corresponding theoretical values predicted by Equation (4.3) are represented by the straight lines. For the same geometry and constant operating speeds (load, speed and lubricant temperature), the lubricant film thickness depends only on the oil's viscosity and piezoviscosity. The oil piezoviscosity coefficient can be calculated using Gold's equation (see Equation (3.10), [Gold et al., 2001]), whose s and t values are shown in Table 3.5 for each axle oil. The Lubricant Parameter (*LP*) proposed by Cheng [Gupta et al., 1992], defined by Equation (4.2) and presented in Table 4.2, can be used to understand the influence of those fluid parameters on the film thickness generation.

$$LP = \eta \times \alpha \tag{4.2}$$

Table 4.2: Lubricant parameter ($LP \times 10^{-10}$ [s]) for the axle gear oils tested.

	75W85-B	75W90-A	75W90-B	80W90-A	75W140-A
Lubricant Parameter @ 40 °C	7.12	13.31	13.44	20.73	26.18
Lubricant Parameter @ 70 °C	2.20	3.66	3.78	4.80	6.75
Lubricant Parameter @ 100 °C	0.93	1.43	1.49	1.71	2.50

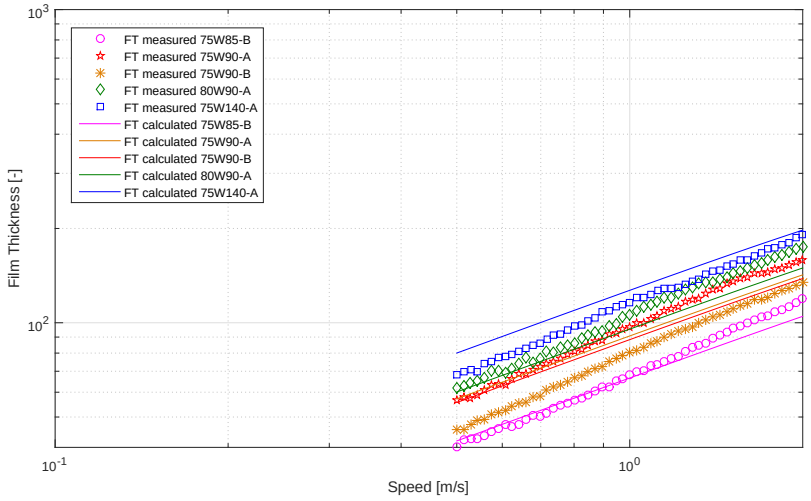

(a) $T = 40$ °C: $SRR = 3\%$

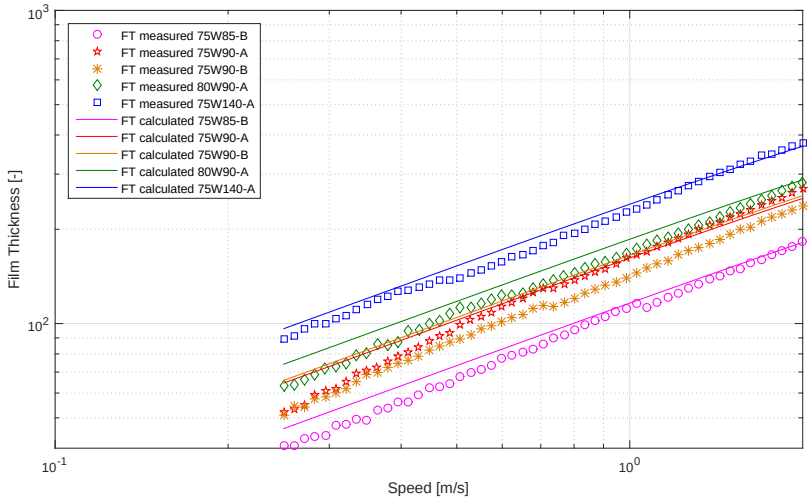

(b) $T = 70$ °C; $SRR = 3\%$

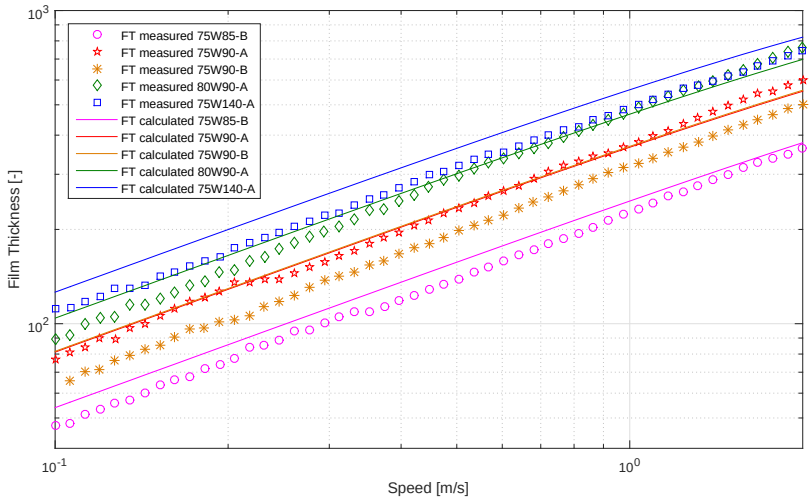

(c) $T = 100$ °C; $SRR = 3\%$

Figure 4.3: Comparison between measured and calculated film thickness (FT) with $SRR = 3\%$.

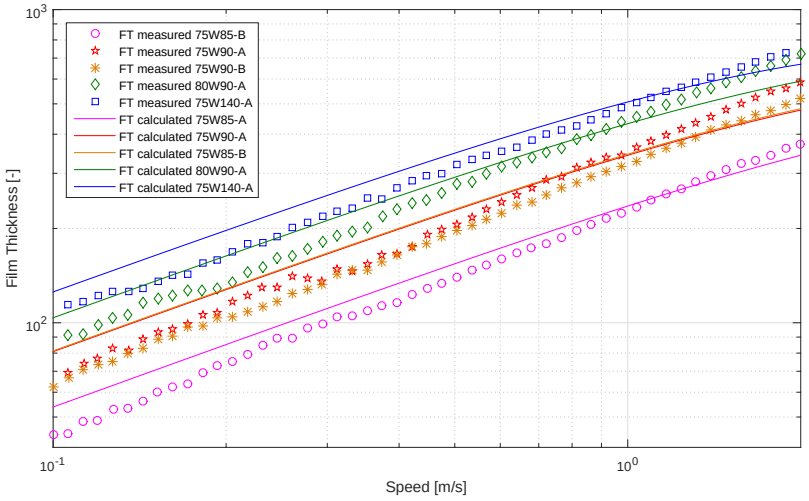

(a) $T = 40$ °C: $SRR = 30\%$

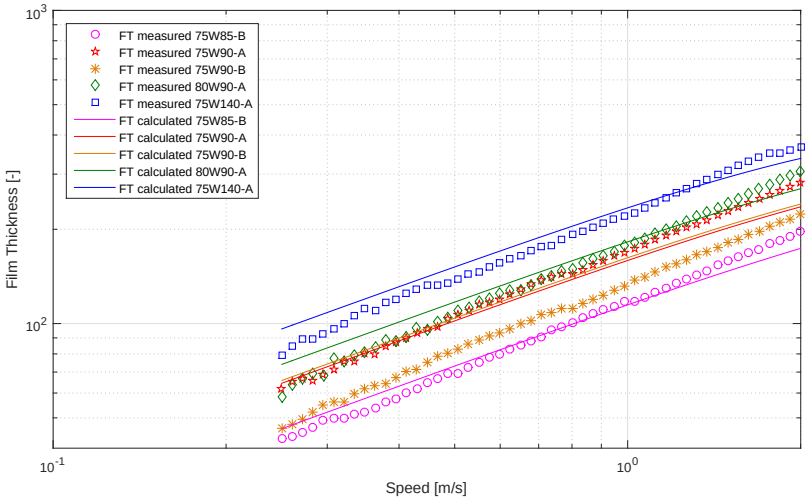

(b) $T = 70$ °C; $SRR = 30\%$

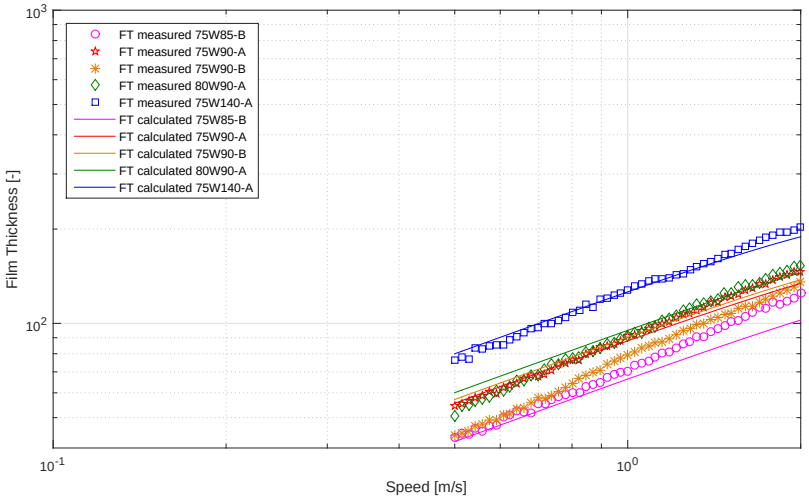

(c) $T = 100$ °C; $SRR = 30\%$

Figure 4.4: Comparison between measured and calculated film thickness (FT) with $SRR = 30\%$.

Whatever the operating temperature, the film thickness measurements always follow the same order: Higher *LP* generates a higher center film thickness, as shown in Figures 4.3 and 4.4. In fact, the 75W140-A oil has the highest Lubricant Parameter and generates the highest film thickness, while oil 75W85-B has the lowest Lubricant Parameter and generates the lowest film thickness. Oils 75W90-A, 75W90-B and 80W90-A, are placed in between the previous two, depending directly on their Lubricant Parameter value. The sorting of the lubricant confirms the relationship between film thickness and the Lubricant Parameter, since all tests were performed under the same operating conditions. The comparison between Figure 4.3 and 4.4 suggests that the slide-to-roll ratio does not have a significant impact on the measured film thickness, at least for the operating conditions used in these tests.

4.2.5. Theoretical film thickness - Point contact

The calculation of the theoretical film thickness is not a goal in itself, it is a first step towards the explanation of successful operation or failure of concentrated contacts. Despite the broad number of the numerical methods and the developed formulas for the film thickness in elliptical contacts (e.g. Hamrock & Dawson [Hamrock and Dowson, 1976], Mostofi & Gohar [Mostofi and Gohar, 1982], Evans & Snidle [Evans and Snidle, 1983], and Chittenden *et al.* [Chittenden et al., 1985]), one should be aware of the models limitations (see Chapter 2, section 2.8.2.2). In this work the center film thickness is calculated using the Hamrock and Dowson [Hamrock and Dowson, 1981, 386] formula (4.3) because it fits rather well the experimental data under the same operating conditions and for a known lubricant piezoviscosity coefficient (α).

$$h_0 = 2.69 \cdot R_x \cdot U^{0.67} \cdot G^{0.53} \cdot W^{-0.067} \cdot (1 - 0.61 exp(-0.752(\frac{R_y}{R_x})^{0.64})) \tag{4.3}$$

Equation (4.3) is useful since it takes the lubricant's viscosity variation with pressure through the material parameter G. The speed parameter, the material parameter and the load parameter, respectively U, G and W, are defined by Equations (2.10), (2.11), and (2.12), R_x is the effective radius of curvature of the contact, and the contact ellipticity, k, is equal to 1 since the Ball-on-Disc contact generates a circular contact area.

Then, the center film thickness, defined by Equation (4.3), is corrected by taking into account the inlet shear heating of the lubricant, as defined by Equation (4.4). This correction is proposed by Gupta *et al.* [Gupta et al., 1992] and corresponds to a thermal correction factor (ϕ_T), given by Equation (4.5).

$$h_{0C} = \phi_T \cdot h_0 \tag{4.4}$$

$$\phi_T = (1 + 0.1(1 + 14.8 \cdot Ve^{0.83}) \cdot L^{0.64})^{-1} \tag{4.5}$$

Parameters Ve and L are given by Equations (4.6) and (4.7), where β is the thermoviscosity coefficient and presented in Equation (3.8).

$$Ve = \frac{|U_1 - U_2|}{(U_1 + U_2)} \tag{4.6}$$

$$L = \frac{\beta \cdot \eta \cdot (U_{ball} + U_{disc})^2}{K_L} \tag{4.7}$$

Integrating Equations (4.3) to (2.6) in Equation (4.4), one gets Equation (4.8), which can be used to predict the center film thickness in a point contact.

The center film thickness with inlet shear heating correction can also be expressed as represented in Equation (4.8), where the exponent of piezoviscosity coefficient and the exponent of viscosity are clear. The piezoviscosity coefficient is determined according to Gold's expression (Equation (3.10)).

$$h_{0C} = h_0 \cdot \phi_T = 1.165 \cdot (1 - 061 \cdot e^{-0.752(\frac{R_y}{R_x})^{0.64}}) \cdot \frac{[\eta_0 (U_{disc} + U_{ball})]^{0.67} \cdot \alpha^{0.53} \cdot R_x^{0.464}}{F_n^{0.067} E^{*0.073}} \cdot \phi_T \tag{4.8}$$

4.2.6. Discussion on film thickness results

A good agreement is found between the measured and the predicted film thickness results, although slight differences are observed and, in most cases, the film thickness predictions overestimate the measurements. Equation (4.8) shows that the predicted film thickness depends on the modified Lubricant Parameter, defined by the product LP^*=$\eta^{0,67}.\alpha^{0,53}$. Thus, the differences between measured and predicted film thickness can be minimized by optimizing the modified lubricant parameter.

Table 4.3 shows the modified Lubricant Parameter LP^*, calculated using the piezoviscosity values proposed by Gold *et al.* $(\eta^{0,67}.\alpha^{0,53})_{Gold}$ and those obtained by the optimization procedure $(\eta^{0,67}.\alpha^{0,53})_{FTM}$, using the experimental film thickness measurements (FTM) obtained with the slide-to-roll ratios of 3 % and 30 %. The difference between calculated and optimized modified Lubricant Parameters never exceeds 24 % and, in most cases the optimized values are lower than the calculated ones.

The difference between these calculated and optimized values decreases as the temperature increases from 40 °C up to 100 °C. Nevertheless, calculated and optimized modified Lubricant Parameters always follow the same order: Higher LP^* generates higher center film thickness. In fact, the LP^* and the film thickness of oil 75W140-A are approximately twice those of oil 75W85-B, confirming there is a direct proportionality between the modified Lubricant Parameter and the center film thickness.

Table 4.3: Modified lubricant parameter ($\eta^{0,67} \cdot \alpha^{0,53}$) determined based on film thickness measurements (FTM) and Gold's equation.

		75W85-B	**75W90-A**	**75W90-B**	**80W90-A**	**75W140-A**
	$LP^* \times 10^{-6}$	PAO	PAO	PAO	MIN	PAO
40 °C	$\eta^{0,67} \cdot \alpha^{0,53}_{Gold}$	9.46	14.24	14.32	18.28	22.15
	$(\eta^{0,67} \cdot \alpha^{0,53})_{FTM}$ (SRR = 3%)	8.29	13.6	11.3	16.7	18
	$(\eta^{0,67} \cdot \alpha^{0,53})_{FTM}$ (SRR = 30%)	8.01	12.1	11	14.8	16.8
70 °C	$\eta^{0,67} \cdot \alpha^{0,53}_{Gold}$	4.39	6.126	6.25	7.035	9.129
	$(\eta^{0,67} \cdot \alpha^{0,53})_{FTM}$ (SRR = 3%)	4.02	5.98	5.24	6.38	8.5
	$(\eta^{0,67} \cdot \alpha^{0,53})_{FTM}$ (SRR = 30%)	4.2	6.06	4.87	6.5	8.16
100 °C	$\eta^{0,67} \cdot \alpha^{0,53}_{Gold}$	2.5	3.321	3.4	3.579	4.772
	$(\eta^{0,67} \cdot \alpha^{0,53})_{FTM}$ (SRR = 3%)	2.55	3.57	2.94	3.87	4.35
	$(\eta^{0,67} \cdot \alpha^{0,53})_{FTM}$ (SRR = 30%)	2.68	3.32	2.85	3.35	4.58

4.3. Tribofilms generation

4.3.1. Experimental friction torque measurements

4.3.1.1. Rolling bearing assembly

The total friction torque, generated by the rolling bearing lubricated with each axle gear oil, was measured on a modified Four-Ball machine (Cameron-Plint TE 82/7752), where the four-ball arrangement was replaced by a rolling bearing assembly, developed by Cousseau *et al.* [Cousseau et al., 2010], as shown in Figure 4.5. Additional details of this assembly can be found in [Cousseau et al., 2010]. This assembly allows to perform tests with several rolling bearing geometries and also to obtain a reliable friction torque and operating temperature measurements.

The rolling bearing assembly is composed mainly of two parts. The first part contains the bearing lower race (3) which is fitted in the spacer (2) and this set is fitted on the bearing house (1). These parts of the group (A) are tight clamped to ensure that there is no relative motion between them. The second part (B) consists of the bearing upper race (5) which is mounted on the shaft adapter (6). In operation, the load (P) is applied on the lower plate (13) and the rotational speed (n) is transmitted to the shaft adapter (6), which is connected to the drive shaft of the machine (see Figure 4.5). The upper race movement is transmitted to the rollers and cage assembly (4). Then, through the bearing housing (1) the internal bearing friction torque is transmitted to the torque cell (11). The friction torque was measured with a piezoelectric torque cell KISTLER 9339A, ensuring high accuracy measurements ($\pm$ 1 Nmm) even when the friction torque generated in the bearings was very small compared to the measurement range available (see Table 4.4).

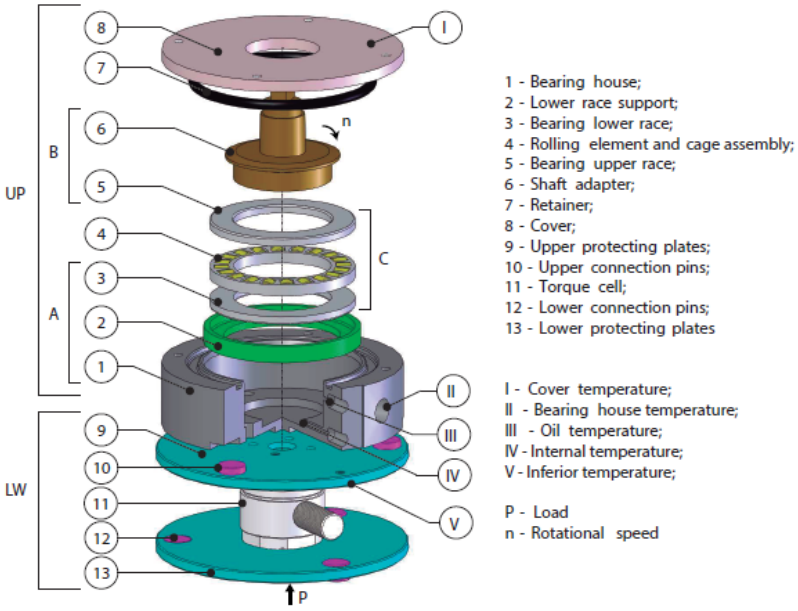

Figure 4.5: Schematic view of the rolling bearing assembly.

Table 4.4: Technical specifications of the torque cell.

Piezoelectric reaction torque sensor KISTLER (Type 9339A)	
Measuring range 100 % [Nm]	-10 to +10
Measuring range 10 % [Nm]	-1 to +1
Overload [Nm]	-12/12
Linearity [% FSO]	$\leq \mp 0.2$
Hysteresis [%FSO]	≤ 0.3
Accuracy [%]	0.01
Operating temperature range [°C]	-40 to +120
Temperature sensitivity [%/°C]	-0.02

During the test, the temperature at several different locations was recorded. Five thermocouples (I-V) were positioned in strategic locations in order to measure and control the lubricant and bearing housing temperatures (see Figure 4.5). Two other thermocouples were used to measure the temperatures of the room and of the air flow around the bearing housing. When assembled in the modified four-ball machine, the rolling bearing assembly was exposed to forced air convection to evacuate the heat generated during bearing operation using two 38 mm diameter fans running at 2000 rpm, cooling the chamber surrounding the bearing housing. In order to control the temperature during the tests, the bearing assembly was mounted with two heaters which were controlled with a PID control system with feedback given by thermocouple III (see Figure 4.6). The control system can assure a temperature variation always below than $\mp$ 1 °C.

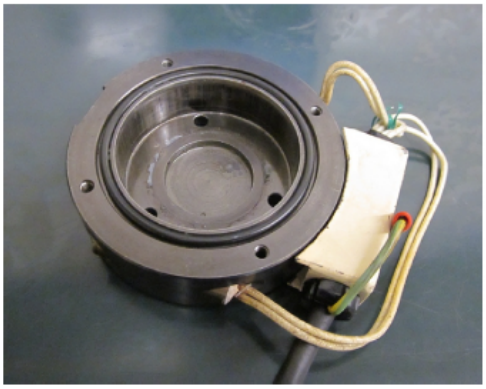

Figure 4.6: Bearing house with heaters controlled with a PID system.

4.3.1.2. Rolling bearing tested

A wide range of rolling bearing geometries might be used in axle differentials. Generally, the axle contains eight bearings. Four taper roller bearings are used in the differential assembly, where two support the input pinion and two more support the crown wheel. Other types of rolling bearings are used on the outboard end of each of the two half shafts [Kolekar et al., 2013].
According to Cousseau *et al.* [Cousseau et al., 2010], the rolling bearing test rig allows the friction torque measurements with specific types of rolling bearings, whose dimensions are limited by the bearing housing and the machine itself, i.e the test assembly only allows rolling bearings with a maximum outer diameter of 56 mm and a maximum width of 16 mm.
With such limitations, it is important to understand the lubrication capabilities of different axle gear oils inside the rolling bearing and to compare the measured friction torque, knowing the influence of several parameters such as speed, load, oil formulation and bearing geometry.
The torque measurement tests were performed using cylindrical roller thrust bearings (RTB) (SKF ref. 81107 TN) lubricated with the selected axle gear oils. The geometrical characteristics of the 81107 TN rolling bearing are displayed in Figure 4.7.

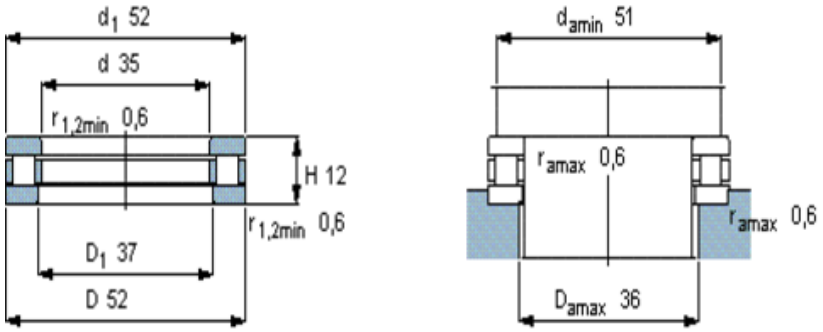

Figure 4.7: Cylindrical roller thrust bearing (RTB) 81107 TN geometry [SKF, 2013].

4.3.1.3. Operating conditions

A new rolling bearing was mounted for each tested oil in order to avoid the possible chemical interactions between oils and even to reduce the influence of the surface finishing. The roughness measurements of the raceways and the rollers on three different cylindrical roller thrust bearing samples, performed in previous work developed by Fernandes [Fernandes, 2015], showed identical surface finishing of the rolling bearings before use.

The asperities interactions and the chemical reactions between axle gear oil additives and rolling-element bearing contact surfaces led to the generation of tribochemical films (so-called tribofilms) [Martin et al., 2000, Bruce, 2012].

The operating conditions were selected to promote this tribofilm formation. Each cylindrical roller thrust bearing was tested continuously for 24 hours at 75 rpm, maximum allowable test rig load (7 kN) and high oil operating temperature (110 °C). High temperatures reduce the lubricant viscosity and consequently the film thickness in the contact decreases. Low operating speed affects directly the rolling speed between the roller and raceways decreasing the lubricant capacity to generate a film thick enough to separate both surfaces.

In order to increase the raceway-roller maximum contact pressure, 15 out of 20 rollers were removed (see Table 4.5). The estimated raceway-roller maximum contact pressure was 2 GPa for the cylindrical roller thrust bearing (RTB) with only 5 rollers. Under these operating conditions, the contact roller-raceway is characterized in Table 4.5.

Table 4.5: Roller-raceway contact parameters for RTB 81107 rolling bearing.

Parameter	Designation	Units	Number of rollers	
			5	20
Raceway radius of curvature	R_{x1}	[m]	∞	
Roller radius of curvature	R_{x2}	[m]	2.5×10^{-3}	
Equivalent radius of curvature	R_x	[m]	5×10^{-3}	
Roller length	l	[m]	5×10^{-3}	
Composite roughness	R_q	[μm]	0.161	
Normal load	F_n	[N]	7000	
Rolling bearing rotational speed	n	[rpm]	75	
Operating temperature	T	[°C]	110	
Maximum Hertz pressure	p_0	[GPa]	2.008	1.004
Hertzian contact width	a	[μm]	87	43.5
Surface contact area	A_c	[mm^2]	0.87	0.435

4.3.1.4. Test procedure

A new rolling bearing was assembled and 14 ml of fresh oil was added [Cousseau et al., 2010]. The oil level should reach the center of the lowest rolling element as indicated by the rolling bearing manufacturer [SKF, 2013].

Before starting each test, a running-in period is always required for each rolling bearing and it is carried under an axial load of 1000 N while increasing rotational speed from 75 to 1200 rpm for 10 minutes.

For each test with the selected axle gear oil, the (7 kN) load was applied, the rotational speed was set to 75 rpm and the operating temperature of 110 °C was imposed. After 60 min of operation, the machine reached the stabilized temperature of 110 °C (thermal equilibrium) due to the heaters, and the friction torque measurements can be made.

Two sets of four measurements were performed, after 1 hour and 24 hours of operation, respectively. Three values were kept and the most dispersed one was disregarded. The torque measurements should be made in short periods of time (less than 120 s) at stabilized temperatures ($\pm$ 2 °C) in order to avoid the "drift effect" of the piezoelectric torque cell [Cousseau et al., 2010]. The friction torque value displayed (for each rotational speed and load) is the average value of the three closest measurements.

4.3.2. Post test analysis

After each test, the used oil was collected from the axial rolling bearing test rig and analyzed by Direct Reading Ferrography (DRIII) and Analytical Ferrography (FMIII) techniques. The surface roughness of the raceways was measured and an X-ray photoelectron spectroscopy (XPS) was performed to chemically characterize the tribofilm formed in the rollers of the tested rolling bearing.

4.3.2.1. Surface roughness measurements

The surface topography measurements were performed on the lower (stationary) raceway of the roller bearing (see Figure 4.5). A 3D optical microscope (BRUKER^{TM} NPFLEX), equipped with a non-contacting optical vertical scanning interferometry (VSI) technique, was used. According to ISO 4288-1996 [for Standardization. Technical Committee ISO/TC 57, 1996], a filter cut-off value of λ_c=0.25 mm was selected, according to the texture of the rolling bearing raceway. The roughness analysis was performed using a Gaussian filter defined by ISO 11562-1992. The 2D roughness measurements, extracted from the 3D topographies, were measured across the raceway contact track, in the radial direction.

4.3.2.2. Oil sample analysis

Ferrography is a sensitive and successful monitoring and inspection technique on wear state of engineering systems. It is a method of particle separation based upon the interaction between an external magnetic field and the magnetic particles present in the used oil [Makhlouf and Aliofkhazraei, 2015]. Two basic types of ferrometric analysis were performed which are the Direct Reading Ferroghraphy (DR III) and Analytical Ferrography (FMIII).

The Direct Reading Ferroghraphy measures, directly, the amount of large and small wear particles contained in the lubricant sample, the 'D_L' and 'D_S' indexes, respectively. Knowing these values it is possible to determine several wear indexes: the Wear Particle Concentration

(*CPUC*), the Severity of Wear Particles (*ISUC*) and the Percentage of Large Particles (*PLP*), given by equations (4.9-4.11), respectively, where d is the dilution factor of the sample in cases of excessive contamination where dilution is required.

$$CPUC = \frac{D_L + D_S}{d} \tag{4.9}$$

$$ISUC = \frac{D_L^2 - D_S^2}{d^2} \tag{4.10}$$

$$PLP = \frac{100 \times (D_L - D_S)}{(D_L + D_S)} \tag{4.11}$$

The Analytical Ferrography (FMIII) was used to characterize the wear of the raceways and rollers, through detailed analysis of wear particles and contaminants contained in the lubricant samples.

4.3.2.3. Surface analysis by XPS

The X-ray photoelectron spectroscopy (XPS) also known as Electron Spectroscopy for Chemical Analysis (ESCA) represents a sophisticated analytical method to investigate the chemistry of a surface sample. It is widely used surface analysis technique, due to its relative simplicity in use and data interpretation. Based on photoelectric effect, the photo-emission is used as an analytical tool, where the acquired data is represented by an XPS spectra. Figure 4.8 shows a surface sample which is irradiated by low-energy X-ray photons provided by the photon source.

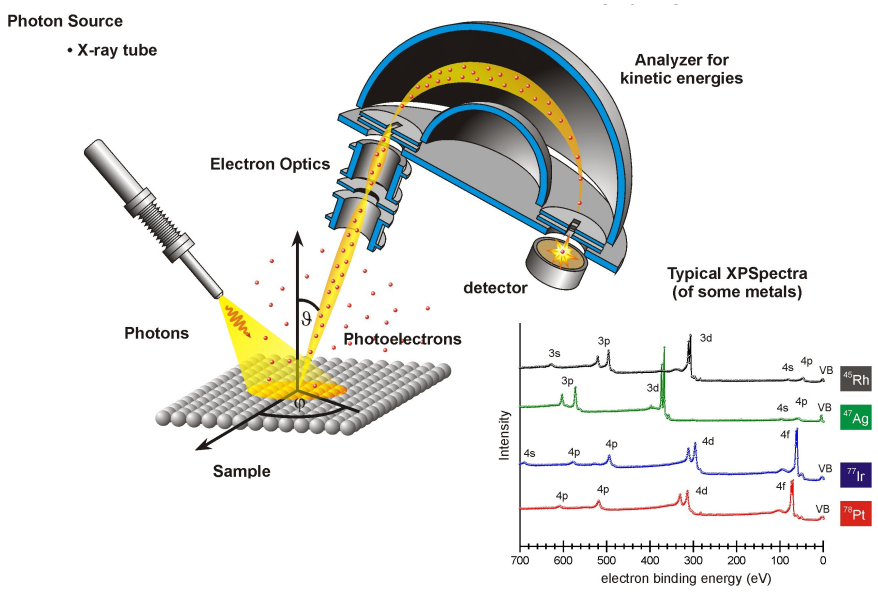

Figure 4.8: Scheme of basic components of XPS instrument [K.Jacobs,].

The interaction between the X-ray photons of a specific energy and the sample causes electron ejections from the chemical elements, located between 0 and 10 nm of depth. An electrostatic analyser detects the emitted electrons, according to their kinetic energy at the entrance of the detector, and by measuring their flux as a function of their kinetic energy, a spectra, representing the sample composition is obtained. In order to enable the emitted electrons to be analysed without interference from gas phase collisions, the entire process is performed under an ultra high vacuum (UHV) chamber ($< 10^{-7}$ Pa), which includes X-ray source, sample, electron analyser and detector equipments [Fairley, 2009].

Since XPS is a non-destructive technique, which allows to evaluate the surface element composition, it is an excellent method to acquire information about the tribofilm presence at the rollers of rolling bearings surfaces.

In this study, the surfaces were analysed with Kratos Axis Ultra HSA instrument (see Figure 4.9) incorporating a high power rotating anode and monochromatised AlKα X-ray source. All the spectra recorded were taken with an X-ray power source of 150 watts (15 kV) and were obtained using a slot aperture.

Figure 4.9: Kratos Axis Ultra HSA.

Like any typical XPS analysis, survey scans of the rollers were obtained, before and after the Roller Thrust Bearing (RTB) tests described previously. The survey spectra were recorded with a scan range from 0 up to 1350 eV binding energy, which is sufficient for the identification of all the detectable elements. An analyzer pass energy of 160 eV is recommended for survey scans in order to produce very high signal intensities, minimizing data acquisition time and maximizing elemental detectability. The analysis performed after the tests are designated by the suffix M (M=after mechanical work).

Then long scans of the selected peaks were obtained for better comprehension of the chemical composition. An analyzer pass energy of 80 eV is normally adequate for detail scans as it permits to determine the exact position of the peaks. A higher resolution is required and lower pass energies can be used with corresponding loss of signal intensity [Chastain et al., 1995]. The data collected was compared with the peaks curve fitting recorded on the surface of roller bearings raceways submerged in oil without any mechanical work.

4.3.3. Experimental results

The Cylindrical Roller Thrust Bearing tests were performed under a constant oil sump temperature of 110 °C, measured by thermocouple III (see Figure 4.5) and used to control the test temperature. Table 4.6 shows the temperature measured in each test as well as the physical properties of the oil (kinematic viscosity, dynamic viscosity, thermoviscosity, piezoviscosity and Lubricant Parameter) at the operating temperature, as well as the corresponding modified Stribeck parameter Sp and the roller/raceway lubricant center film thickness.

The Lubricant Parameter is defined by the product of the dynamic viscosity by the piezoviscosity of the lubricant, at the operating temperature, that is $LP{=}\eta\alpha$. The modified Stribeck parameter, Sp, is a non dimensional parameter defined by Equation (4.12).

$$Sp = \frac{U \cdot \eta \cdot \alpha^{1/2}}{F_n^{1/2}} \tag{4.12}$$

The center film thickness in the roller/raceway contact of the RTB can be determined using Dowson and Higginson [Dowson and Higginson, 1959] equation for an elastohydrodynamic line contact. The formulation of this model is delineated in section 2.8.2.1.

Table 4.6: Lubricant physical properties and film thickness at the operating temperature.

Parameter	Unit	Axle gear oil				
		75W85-B	75W90-A	75W90-B	80W90-A	75W140-A
Oil temperature (T)	[°C]	110	110	110	110	110
Kinematic viscosity (ν)	[cSt]	9.33	13.39	13.87	11.20	20.49
Dynamic viscosity (η)	[mPa.s]	7.4	10.6	11.0	9.3	17.2
Thermoviscosity ($\beta\times10^{-2}$)	[K^{-1}]	1.92	2.11	2.09	2.26	2.25
Piezoviscosity ($\alpha\times10^{-8}$)	[Pa^{-1}]	0.995	1.041	1.048	1.389	1.107
Lubricant Parameter ($LP\times10^{-10}$)	[s]	0.797	1.193	1.250	1.399	2.041
Stribeck parameter ($Sp\times10^{-9}$)	[-]	3.465	5.069	5.295	5.150	8.409
Lubricant film thickness ($h_{0C}\times10^{-3}$)	[μm]	5.51	7.39	7.65	8.30	10.92

Table 4.6 indicates that, as expected, the lubricant film thickness and the Stribeck parameter increase as the Lubricant Parameter ($LP{=}\eta\alpha\times10^{-10}$) also increases. Thus, oil 75W85-B presents the lowest values of film thickness and Stribeck parameter while oil 75W140-A has the highest ones.

4.3.3.1. Internal friction torque after 1 and 24 hours

The operating temperature of the RTB remains stable during the 24 hours of the test, and equal to 110 °C for all the gear oils tested. The internal friction torque of the RTB was measured and recorded, after running the test during one hour and at the end of the test (after 24 hours). Table 4.7 shows the values of the internal friction torque, as well as of the calculated specific film thickness of the roller/raceway contact.

The internal friction torque of the RTBs, M_t^{exp}, was always very high, as expected, since the RTBs were operating under high load, high temperature and low speed, generating boundary film lubrication conditions, as suggested by the Stribeck parameter values presented in Table 4.6 ($Sp < 10^{-8}$).

Under such operating conditions, significant asperity interaction between the roller-raceway surfaces and oil additives activation are expected, together with tribofilm generation.

Table 4.7: Friction torque and lubricant analysis after 1 and 24 hours. (* new surface).

Parameter	Unit	Axle gear oil				
		75W85-B	75W90-A	75W90-B	80W90-A	75W140-A
Results after 1 hour:						
Internal friction torque ($M_{t1}{}^{exp}$)	[Nmm]	1147	1056	974	986	994
Root mean square profile height (R_{q1})*	[μm]	0.161	0.161	0.161	0.161	0.161
Specific film thickness (Λ_1)	[-]	0.034	0.046	0.048	0.052	0.068
Results after 24 hours:						
Internal friction torque ($M_{t24}{}^{exp}$)	[Nmm]	1143	976	977	940	936
Root mean square profile height (R_{q24})	[μm]	0.210	0.150	0.173	0.147	0.119
Specific film thickness (Λ_{24})	[-]	0.026	0.049	0.044	0.056	0.092
Lubricant sample analysis after 24 hours:						
Large particles (D_L)	[-]	53.9	16.7	35	25.5	18.6
Small particles (D_S)	[-]	21.8	10.5	21.5	21	7.9
Dilution factor (d)	[-]	0.1	0.1	0.1	0.1	0.1
Wear Particle Concentration ($CPUC$)	[-]	757	272	565	465	265
Severity of Wear Particles ($ISUC$)	[-]	242997	19894	76275	20925	28355
Percentage of Large Particles (PLP)	[-]	42.4	22.8	23.9	9.7	40.4

After one hour, M_{t1}^{exp} reached 974 Nmm for 75W90-B oil, the lowest value, and 1147 Nmm for the 75W85-B oil, the highest value. After 24 hours the results were similar, since oil 75W140-A attained 936 Nmm, and oil 75W85-B attained 1143 Nmm, respectively the lowest and highest internal friction torques.
However, it is interesting to notice that the internal friction torque of the RTB, lubricated with the candidate (B) oils (75W85-B and 75W90-B), were identical after 1 hour and 24 hours ($\pm$ 0.003%). In the case of the reference (A) formulations, the internal friction torque at the end of the tests is always lower than after 1 hour, -7.6% for oil 75W90-A, -4.7% for oil 80W90-A and -5.8% for oil 75W140-A.
This different behaviour of the candidate (B) and of the reference (A) axle gear oils, can be clearly observed in Figure 4.10, where the internal friction torque is plotted for each axle gear oil formulation, after 1 hour and at the end of the test.

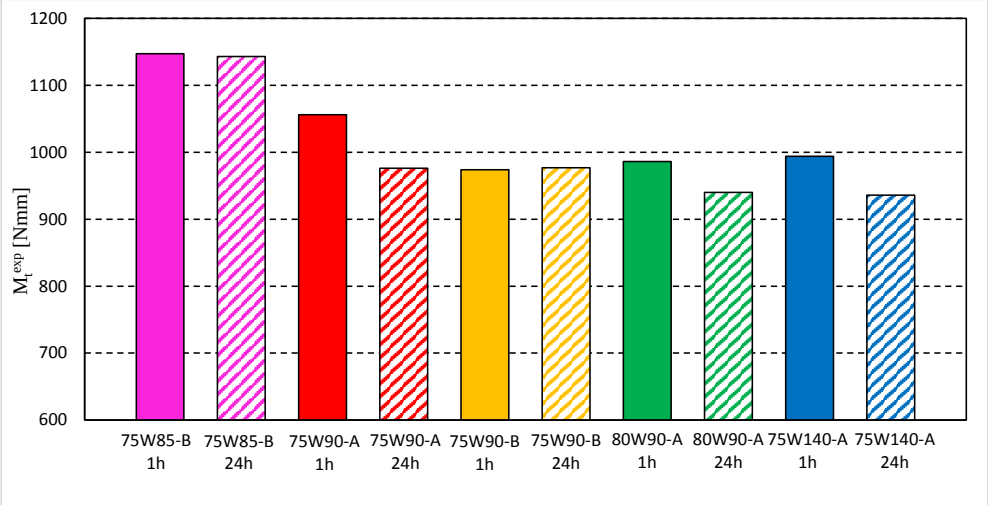

Figure 4.10: Internal friction torque after 1 hour and after 24 hours.

4.3.3.2. Surface roughness at the end of the test

The surface topographies of the lower (stationary) raceways, of the new and used RTB, were measured at the end of the tests. The 3D roughness parameters of the surface topographies and the 2D roughness parameters of the roughness profiles extracted from those surface topographies are presented in detail in Appendix B.

Table 4.7 presents the roughness parameter R_q (root mean square of the profile height) of the RTB raceways, as new and used (at the end of the tests). The R_q parameter of the raceways lubricated with the reference (A) axle gear oils (75W90-A, 80W90-A and 75W140-A) is smaller than the value of the new raceway ($R_q^A < R_q^{new}$) while the R_q parameter of the raceways lubricated with the candidate (B) oils (75W85-B and 75W90-B) is higher than the value of the new raceway ($R_q^B > R_q^{new}$). Such trend is also observed for other 2D roughness parameters (R_a, R_{max}, R_z and R_{pk}) and the 3D roughness parameters (S_a and S_q), as shown in Appendix B.

This trend suggests that the evolution of the surface roughness of the RTB raceways during the test is influenced by the oil formulation, under boundary film lubrication.

4.3.3.3. Specific film thickness

The center film thickness of the roller/raceway contact is presented in Table 4.6. It is only dependent on the dynamic viscosity, piezoviscosity and Lubricant Parameter of each gear oil.

Knowing the R_q roughness parameter, at the beginning and at the end of the tests, it is possible to calculate the specific film thickness (Λ, see Equation 4.13) of the roller/raceway contact, which are presented in Table 4.7.

$$\Lambda = \frac{h_{0C}}{\sigma_c} \tag{4.13}$$

with

$$\sigma_c = \sqrt{(\sigma_1)^2 + (\sigma_2)^2} \tag{4.14}$$

It is clear that Λ is very small in all cases (Λ<0.1), confirming that boundary film operating conditions prevails. Since R_q roughness parameter of the raceways, had opposite evolutions during tests, depending on the oil formulation, Λ also showed opposite trends for the reference (A) and candidate (B) formulations: $\Lambda_{24}^{A}>\Lambda_{1}^{A}$ and ($\Lambda_{24}^{B}<\Lambda_{1}^{B}$), as shown in Table 4.7.

In Figure 4.11, the internal friction torque of RTB $M_t{}^{exp}$ is presented in function of the specific film thickness Λ, at the beginning and at the end of the test. In the case of the reference oils (A) the specific film thickness increased ($\Lambda_{24}^{A}>\Lambda_{1}^{A}$) and the internal frictional torque decreased ($M_{t24}^{exp-A}<M_{t1}^{exp-A}$) while for the candidate oils (B) the specific film thickness decreased ($\Lambda_{24}^{B}<\Lambda_{1}^{B}$) and the internal friction torque remained constant ($M_{t24}^{exp-B}\approx M_{t1}^{exp-B}$).

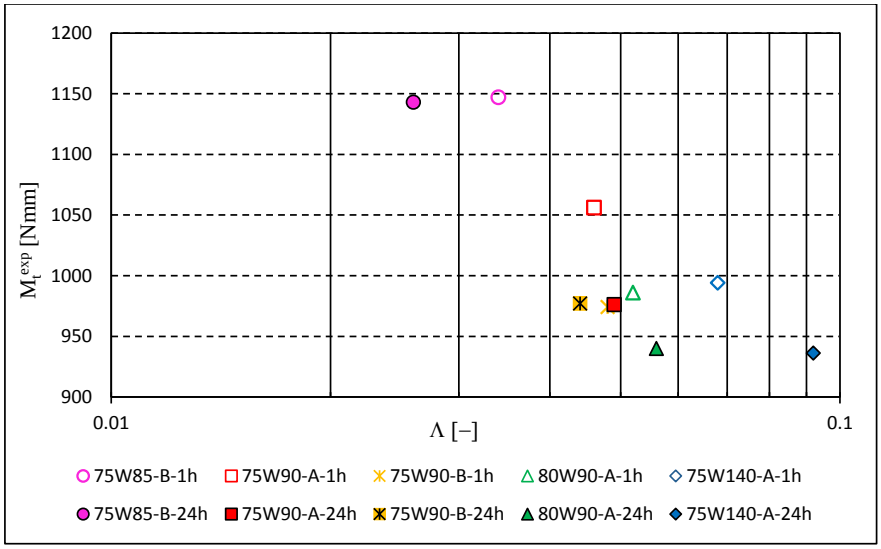

Figure 4.11: Variation of the internal friction torque of the RTB vs specific lubricant film thickness.

4.3.3.4. Lubricant sample analysis

At the end of the tests all the lubricants were collected in glass flasks. The oils were significantly charged with wear particles because the operating conditions were severe: high load, high temperature, low speed and very low specific film thickness (Λ). Thus, oil samples with a dilution factor of 0.1 (1 part of oil plus 9 parts of white oil) were produced. Those diluted samples were analyzed by Direct Reading Ferrography (DRIII) and Analytical Ferrography (FMIII) . The DRIII ferrography results for Large Particles (D_L), Small Particles (D_S), Concentration of Wear Particles ($CPUC$), Severity of Wear Particles ($ISUC$) and Percentage of Large Particles (PLP) are presented in Table 4.7.

The DRIII ferrography results are very clear. Reference (A) oils (75W90-A, 80W90-A and 75W140-A) generated wear indexes lower than the candidate (B) oils (75W85-B and 75W90-B), as presented in Table 4.7. That is, $D_L^A < D_L^B$, $D_S^A < D_S^B$, $CPUC^A < CPUC^B$ and $ISUC^A < ISUC^B$.

In Figure 4.12 (a) the *CPUC* results (Index for the Concentration of Wear Particles) are plotted as function of the specific film thickness Λ_{24}. Figure 4.12 (a) confirms that $CPUC^A < CPUC^B$, but it also shows that when Λ_{24} increased the *CPUC* decreased, for oils with the same type of base oil and similar additive package. Figure 4.12 (b) presents the *ISUC* results (Index for the Severity of the Wear Particles) vs Λ_{24} (specific lubricant film thickness after 24 hours) and shows a similar trend as Figure 4.12 (a).

In Figure 4.13, pictures of the ferrograms made for each oil sample by Analytical Ferrography (FMIII) are displayed. The ferrograms from the samples of the candidate (B) oils (75W85-B and 75W90-B, shown in Figures 4.13 (a), (b), (e) and (f)) are heavily loaded with wear particles (High D_L and high *CPUC*), followed by the ferrogram of oil sample 80W90-A (Figures 4.13 (g) and (h)). The ferrograms from the oil samples 75W90-A and 75W140-A (Figures 4.13 (c), (d), (i) and (j)) present significantly less wear particles than the other ferrograms.

The results from the analysis of the lubricant samples by Direct Reading Ferrography and Analytical Ferrography suggest that the specific lubricant film thickness and the oil formulation, in terms of the base oil type and additives, have a significant influence on the amount of wear particles generated by the RTB, when operating under boundary film lubrication conditions.

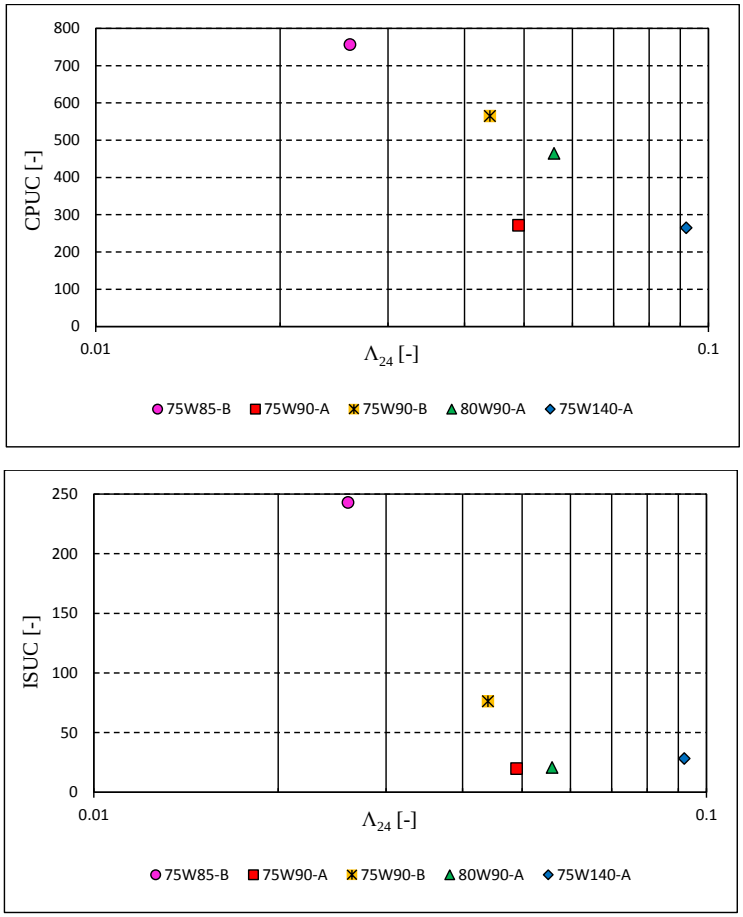

Figure 4.12: (a) Index for the Concentration of Wear Particles (*CPUC*) and (b) Index for the Severity of the Wear Particles (*ISUC*) against the specific film thickness (Λ).

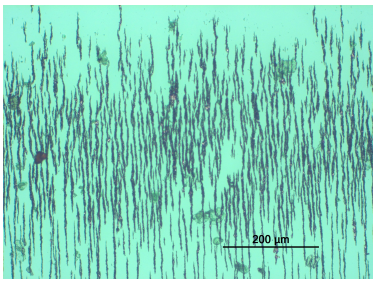

(a) 75W85-B oil (200×), *CPUC*=757

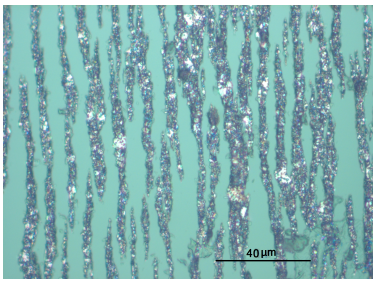

(b) 75W85-B oil (1000×), $ISUC$=243×10^3

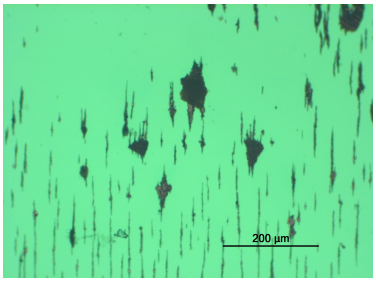

(c) 75W90-A oil (200×), *CPUC*=272

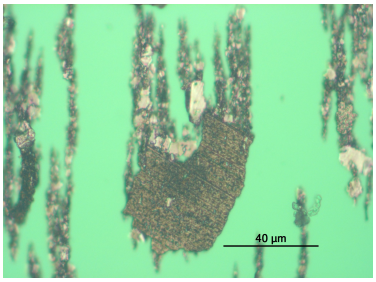

(d) 75W90-A oil (1000×), $ISUC$=19.8×10^3

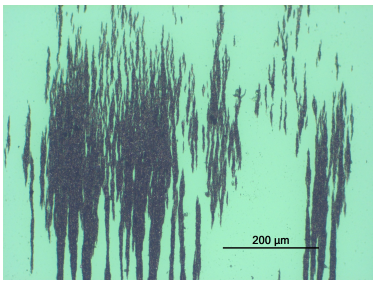

(e) 75W90-B oil (200×), *CPUC*=565

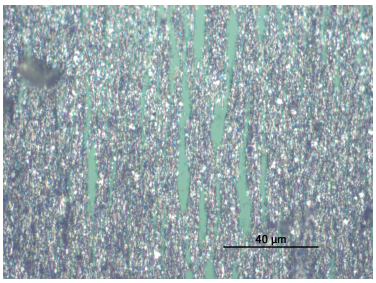

(f) 75W90-B oil (1000×), $ISUC$=76.3×10^3

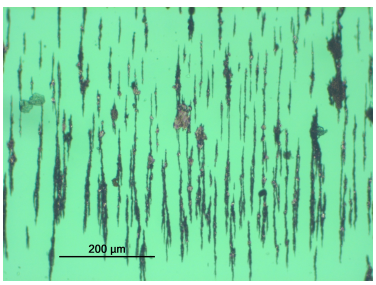

(g) 80W90-A oil (200×), *CPUC*=465

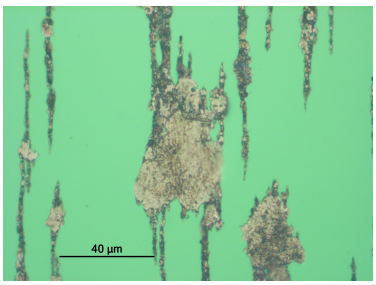

(h) 80W90-A oil (1000×), $ISUC$=20.9×10^3

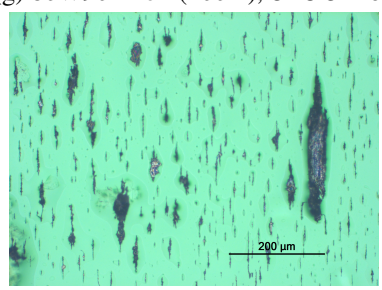

(i) 75W140-A oil (200×), *CPUC*=265

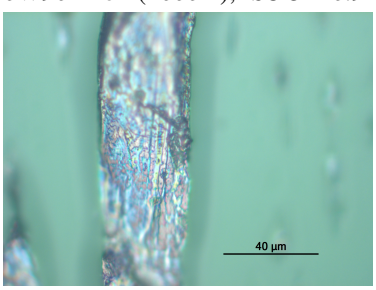

(j) 75W140-A oil (1000×), $ISUC$=28.4×10^3

Figure 4.13: Analytical Ferrography microphotographs magnified 200× and 1000×.

4.3.3.5. XPS surface analysis

As mentioned in section 4.3.1.3, 15 of the 20 rollers of RTB were removed and the RTB tests were performed with only 5 rollers inside the bearing, in order to increase the maximum contact pressure on each roller and mechanically promote the reaction of the oils additives with the steel surfaces.

Some of the remaining rollers were submerged in each axle gear oil and kept in an oven at 110 °C during 24h, in order to chemically promote the reaction of the oil additives with the steel surfaces.

The XPS analysis was performed on three different types of rollers: (i) a new roller that has not been in contact with any of the axle gear oils, designated as N (new), (ii) rollers that have been submerged in each oil during 24h at 110 °C, designated as S (submerged), and (iii) rollers that have been used in RTB tests, designated as M (mechanical testing). All the measurements were performed at the same location near the center of the rollers and the acquired data was restricted to a square sample area with 0.7 mm of side.

Figure 4.14 shows the survey scans of a new roller, of a roller submerged in oil 75W85-B, and of a roller from the RTB test with oil 75W85-B. Significant differences are observed among Figures 4.14 (a), 4.14 (b) and 4.14 (c).

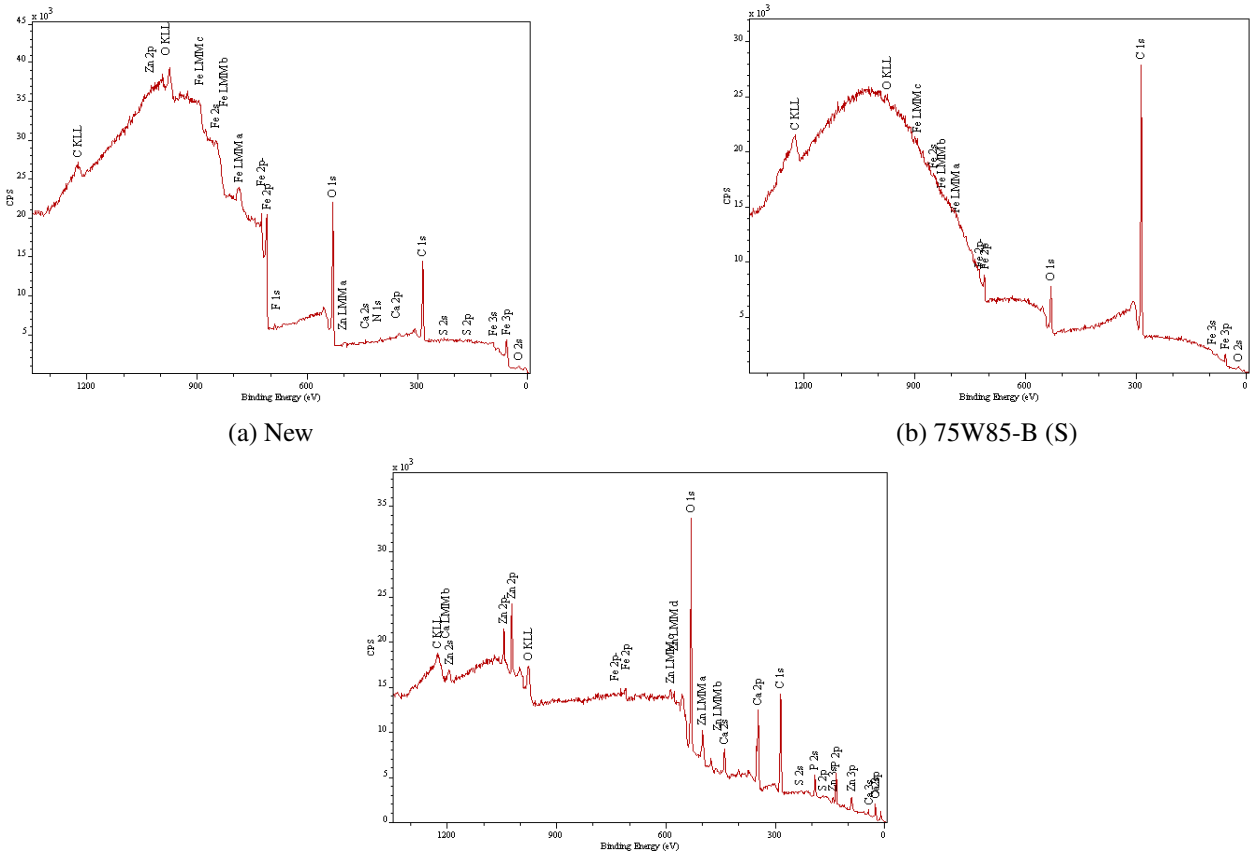

(a) New

(b) 75W85-B (S)

(c) 75W85-B (M)

Figure 4.14: XPS survey scans for the tribofilms on new RTB 81107 roller and on rollers lubricated with 75W85-B axle gear oils.

Figure 4.14 shows that there is no significant differences between the XPS scans of the new (N) and submerged (S) rollers and several chemical elements, present in the formulation of the 75W85-B oil, such as Calcium (Ca), Phosphorus (P), Sulful (S) and Zinc (Zn), only appear in the XPS scan of the rollers that were used in the RTB tests and that performed mechanical work (see Figure 4.14 (c)).

Furthermore, the Carbon (C), Iron (Fe) and Oxygen (O) chemical elements, related to the surface of steel, are very intense in the left part of the Figure 4.14 (a) and Figure 4.14 (b) (Binding Energy $\leq$ 600 eV) and are significantly less intense in Figure 4.14 (c).

These characteristics of the XPS scans, show that in the RTB tests a tribofilm was generated in the rollers surface, related to the formulation of each gear oil. The XPS survey scans of the rollers submerged in the oils (S) and the rollers used in the RTB tests (M), are presented in C.

Applying the curve fitting procedure, provided by a Gaussian-Lorentzian product function component line shape, along the scan results, clearly identifies the most relevant chemical elements: Calcium (Ca), Carbon (C), Iron (Fe), Magnesium (Mg), Oxygen (O), Phosphorus (P), Sulfur (S) and Zinc (Zn). The peaks curve fitting of these elements recorded in the surface of the rollers submerged (S) and tested (M) with gear oil 75W140-A, are shown in Appendix C.

Table 4.8 summarizes the peaks quantification obtained from the XPS analysis of the rollers submerged (S) and tested (M) for all the axle gear oils.

Table 4.8: XPS quantification in at % of the tribofilms formed on the roller surfaces before and after RTB tests.

	XPS quantification (at %)							
-	C 1s	Fe 2p	O 1s	Ca 2p	Mg 1s	P 2p	S 2p	Zn 2p3
Submerged in oil (S)								
75W85-B	87.97	1.75	9.7	0.44	-	ND	0.13	ND
75W90-A	59.69	5.04	31.85	ND	0.77	2.24	0.4	ND
75W90-B	72.65	5.69	21.02	0.49	-	ND	ND	ND
80W90-A	93.65	0.27	4.94	ND	0.15	0.48	0.51	ND
75W140-A	78.26	1.89	18.29	ND	ND	1.33	0.23	ND
-	C 1s	Fe 2p	O 1s	Ca 2p	Mg 1s	P 2p	S 2p	Zn 2p3
After RTB tests (M)								
75W85-B	38.87	0.83	40.37	7.68	-	8.75	1.21	2.3
75W90-A	48.83	0.52	40.47	ND	2.58	7.15	0.45	ND
75W90-B	35.01	1.29	44.24	10.23	-	5.91	2.01	1.32
80W90-A	39.11	0.39	47.41	0.39	3.88	7.58	0.6	0.07
75W140-A	53.79	ND	37.07	ND	2.24	6.38	0.5	ND

All XPS surface analysis and the corresponding tribofilms show a high amount of Carbon (C), related to the roller steel, and covering the other species underneath (rich phase), which is in agreement with the literature [Grossiord et al., 1999]. A higher concentration of Oxygen (O) was observed in the XPS surface analysis performed on the rollers (M) used in the RTB

tests, that were submitted to high contact pressures. The low concentration of Iron (Fe) in the mechanically tested rollers (M) is an indication of tribofilms covering the metallic surface .

Calcium (Ca) and Zinc (Zn) peaks were only detected in the rollers submerged (S) or tested (M) with candidate (B) oils (75W85-B and 75W90-B) being much more intense in the mechanically tested rollers (M).

On the opposite, the Magnesium (Mg) peaks were only detected in rollers submerged (S) or tested (M) with the reference (A) oils (75W90-A, 80W90-A and 75W140-A), being significantly more intense in the mechanically tested rollers (M).

The peaks of organic chemical elements Phosphorus (P) and Sulfur (S), are much more intense in the tested roller (M) than in the submerged (S) ones, reaching very high levels.

The results presented in Table 4.8, clearly demonstrate that the composition of the tribofilms generated on the rollers (M) used in RTB tests have a very close relation with the formulation of each gear oil tested.

4.3.3.6. Discussion on the experimental results

The Cylindrical Roller Thrust Bearings (RTB) were tested under severe operating conditions (high contact pressure, high temperature and low speed), generating low specific lubricant film thickness ($\Lambda < 0.1$) and leading to boundary film lubrication regime, for all the axle gear oils selected.

Under such lubrication conditions, tribofilms were generated on the surface of the RTB rollers, which were clearly identified by the XPS surface analysis and showed a close relation with the formulation and chemical composition of the axle gear oils used in RTB tests. In fact, the reference (A) oils and the tribofilms they generated, both contained Magnesium (Mg), and the candidate (B) oils and the tribofilms they generated, both contained Calcium (Ca) and Zinc (Zn).

The surface roughness measurements, at the end of the tests, showed that the raceways lubricated with the candidate (B) oils had higher or similar S_q and R_q roughness parameters than the new raceways, while the raceways lubricated with the reference (A) oils had the opposite trend, showing lower R_q values than the original raceways (see Table 4.6). All oil formulations (except 80W90-A) have the same type of base oil (PAO). A similar trend was observed with S_q and R_q parameters. The evolution of S_q and R_q are very important because they are used to establish the specific lubricant film thickness and, consequently, the lubrication regime.

The oil analysis results, at the end of the tests, indicated that the RTB lubricated with the candidate (B) oils had higher *CPUC* and *ISUC* wear indexes than the RTB lubricated with the reference (A) oils (see Table 4.7 and Figures 4.12 (a) and 4.12 (b)).

Comparing oils 75W90-A and 75W90-B, which had the same base oil (PAO), similar physical properties, similar Lubricant Parameter and generated almost the same film thickness at the beginning (see Table 4), it is clear that during the test oil 75W90-B promoted more wear and higher surface roughness than oil 75W90-A ($CPUC_{75W90-B}$=565 vs. $CPUC_{75W90-A}$=272, $R_{q75W90-B}$=0.173 μm vs. $R_{q75W90-A}$=0.150 μm and $S_{q75W90-B}$=0.190 μm vs. $S_{q75W90-A}$=0.125

μm, see Tables 4.7 and B.1 and Figures 4.12 (a) and 4.12 (b)). This can only be justified by the different additive package of each formulation.

Together, the surface roughness measurements and the oil analysis results, suggest that the additive package and the tribofilms generated by the candidate (B) oils promote more wear than the additive package and the tribofilms generated by the reference (A) oils.

The reference (A) oils showed a similar behaviour during the RTB tests. Oils 75W90-A and 75W140-A have a PAO base oil and a similar additive package but different Lubricant Parameters, promoting different center film thickness. The RTB lubricated with oil 75W140-A operates under higher specific lubricant film thickness than the one lubricated with oil 75W90-A and, consequently, generated slightly lower internal friction torque and S_q and R_q roughness parameters but similar wear particle indexes. The XPS surface analysis of the rollers from the two RTB exhibited the same results. Oil 80W90-A has a mineral base oil and an additive package similar to the other reference (A) lubricants. The behaviour of the RTB lubricated with this oil was similar to the previous ones, although it generates a higher *CPUC* wear index, which can only be related to the mineral base oil and its formulation. Oils 75W85-B and 75W90-B also have a PAO base oil, similar additive packages and the XPS surface analysis of the rollers from the RTB lubricated with these oils show very similar characteristics. However, the Lubricant Parameter and the specific lubricant film thickness generated by oil 75W85-B are significantly lower than those of oil 75W90-B, justifying its higher wear indexes, higher S_q and R_q roughness parameters and higher internal friction torque measured during the RTB tests. Generally, as shown in Figures 4.11 and 4.12, the internal friction torque of the RTB and the wear indexes decrease as the specific lubricant film thickness increases, whatever the axle gear oil considered.

4.3.4. Analytical results

The rolling and sliding friction torque inside the Cylindrical Roller Thrust Bearing (RTB) can be determined using Equations (5.36) - (5.39) which are only valid for a complete RTB, containing the 20 rollers (see Appendix E). The experimental friction torque results with a complete RTB 81107 TN lubricated with the same axle gear oils under the same operating conditions of temperature, load and rotational speed will be presented in Chapter 6.

Table 4.9 shows the internal friction torque of the 81107 TN Roller Thrust Bearing, with 5 and 20 rollers, under the same operating conditions defined in section 4.3.1.3.

Table 4.9: Experimental internal friction torque of the RTB with 5 and 20 rollers.

RTB Internal friction torque	Test duration	Axle gear oil				
		75W85-B	75W90-A	75W90-B	80W90-A	75W140-A
$M_t{}^{exp}$ (5 rollers) [Nmm]	1 hour	1147	1056	974	986	994
$M_t{}^{exp}$ (5 rollers) [Nmm]	24 hours	1143	976	977	940	936
$M_t{}^{exp}$ (20 rollers) [Nmm]	1 hour	924	993	835	893	916

4.3.4.1. Rolling and sliding friction torque

In order to relate the internal friction torque values presented in Table 4.9 and determine the rolling (M'_{rr}) and sliding (M_{sl}) torques of the RTB, the SKF model (see Appendix E) and equations (5.36-5.39) might be used.

The rolling torque (M'_{rr}) is defined by Equations (E.2) up to (E.5) and its values are presented in Table 4.10 for the RTB containing 20 rollers.

Table 4.10: Rolling friction torque for the RTB containing 20 rollers after 1 hour.

RTB Rolling torque	Test duration	Axle gear oil				
		75W85-B	75W90-A	75W90-B	80W90-A	75W140-A
M'_{rr} (20 rollers) [Nmm]	1 hour	14.3	17.4	18	16	22.7
$\frac{M'_{rr}}{M_t^{exp}} \times 100$ [%]		1.55	1.75	2.16	1.79	2.48

Table 4.10 shows that the rolling torque M'_{rr} is very small, representing only 1.5 % up to 2.5 % of the total internal frictional torque, which is expected due to the low rotational speed (75 rpm) and high temperature (110 °C) of the RTB tests.

In order to calculate the rolling torque and the sliding torque of RTB with 5 rollers, it is necessary to define the values of G_{sl} and G_{rr} (see Appendix E) for 5 and 20 rollers.

In the RTB the contact between the rollers and the raceways is a line contact. The maximum contact pressure is given by Equation (4.15).

$$p_{max} = \sqrt{\frac{2}{\pi} \cdot \frac{E^*}{R_x} \cdot \frac{F_n}{l}} \tag{4.15}$$

That is

$$p_{max} = \sqrt{\frac{F_n}{C_F}} \tag{4.16}$$

where

$$C_F = \frac{\pi}{2} \cdot \frac{R_x}{E^*} \cdot l \tag{4.17}$$

The load on each roller is given by:

$$F_n = \frac{F_a}{z} \tag{4.18}$$

where z is the number of rollers.

So,

$$\left(p_{max}^5\right)^2 = \frac{F_a/5}{C_F}, \;\; (p_{max}^{20})^2 = \frac{F_a/20}{C_F} \tag{4.19}$$

and

$$(\frac{p_{max}^5}{p_{max}^{20}})^2 = \frac{F_a/5}{F_a/20}, \quad \frac{p_{max}^5}{p_{max}^{20}} = 2.0 \tag{4.20}$$

The G_{sl} parameter is given by Equation (4.21).

$$G_{sl} = S_1 \cdot d_m^{0.62} \cdot F_a \tag{4.21}$$

and

$$\frac{G_{sl}^5}{G_{sl}^{20}} = \frac{S_1 \cdot d_m^{0.62} \cdot 5 \cdot C_F \cdot (p_{max}^5)^2}{S_1 \cdot d_m^{0.62} \cdot 20 \cdot C_F \cdot (p_{max}^{20})^2} = \frac{5}{20} \cdot \left(\frac{p_{max}^5}{p_{max}^{20}}\right)^2 = \frac{1}{4} \cdot 4 = 1.0 \tag{4.22}$$

The G_{rr} parameter is given by Equation (4.23).

$$G_{rr} = R_1 \cdot d_m^{2.38} \cdot F_a^{0.31} \tag{4.23}$$

$$\frac{G_{rr}^5}{G_{rr}^{20}} = \frac{R_1 \cdot d_m^{2.38} \cdot \left[5 \cdot C_F \cdot (p_{max}^5)^2\right]^{0.31}}{R_1 \cdot d_m^{2.38} \cdot [20 \cdot C_F \cdot (p_{max}^{20})^2]^{0.31}} = \left[\frac{5}{20} \cdot \left(\frac{p_{max}^5}{p_{max}^{20}}\right)^2\right]^{0.31} = \left(\frac{1}{4} \cdot 4\right)^{0.31} = 1.0 \tag{4.24}$$

Thus for the sake of simplicity, it will be considered that the G_{sl} and G_{rr} parameters of the rolling bearing friction torque model are equal for a RTB with 5 or 20 rollers. This hypothesis permits to consider that the rolling torque for 5 and 20 rollers is very similar, and the values presented in Table 4.10 are considered as the rolling torque for 5 rollers.

4.3.4.2. Sliding coefficient of friction

According to equation (6.15), the RTB sliding torque is given by Equation (4.25).

$$M_{sl}^5 = M_t^{exp5} - M_{rr}^{'5} \tag{4.25}$$

and the sliding coefficient of friction is given by Equation (4.26).

$$\mu_{sl}^5 = \frac{M_{sl}^5}{G_{sl}^5} \tag{4.26}$$

In Table 4.11, the values of M_{sl} and μ_{sl} are presented for each axle gear oil.

Table 4.11: Total, rolling and sliding torques and sliding coefficient of friction for RTB containing 5 rollers.

RTB Internal friction torque components	Test duration	Axle gear oil				
		75W85-B	75W90-A	75W90-B	80W90-A	75W140-A
$M_t{}^{exp5}$ [Nmm]	1h	1147	1056	974	986	994
	24h	1143	976	977	940	936
$M'_{rr}{}^{5}$ [Nmm]	1h	14.3	17.4	18	16	22.7
	24h					
$M_{sl}{}^{5}$ [Nmm]	1h	1132.7	1038.6	956	970	971.3
	24h	1128.7	958.6	959	924	913.3
$\mu_{sl}{}^{5}$ [-]	1h	0.101	0.093	0.085	0.087	0.087
	24h	0.101	0.086	0.086	0.083	0.0820

Since the rolling torque ($M'_{rr}{}^{5}$) is very small, the total ($M_t{}^{exp5}$) and the sliding torque ($M_{sl}{}^{5}$) show the same trends. The values of the sliding coefficient of friction are quite similar, and are in the range of $0.081 \leq \mu_{sl}{}^{5} \leq 0.101$.

In Figure 4.15, the sliding coefficient of friction is presented for each RTB, after 1 hour and at the end of the tests. In the case of the reference (A) oils, the specific lubricant film thickness increased ($\Lambda_{24}{}^{A} > \Lambda_1{}^{A}$) during the tests, and a small reduction of the sliding coefficient of friction is observed $\mu_{sl/24}{}^{A} < \mu_{sl/1}{}^{A}$, which is justified by the decrease in surface roughness that occured during the tests, as shown in Table 4.7 and in section 4.3.3.2.

In the case of the candidate (B) oils, the specific lubricant film thickness decreased ($\Lambda_{24}{}^{B} < \Lambda_1{}^{B}$) during the RTB tests and the sliding coefficient of friction remained constant $\mu_{sl/24}{}^{B} \approx \mu_{sl/1}{}^{B}$, which is coherent with the small increase in surface roughness that occurred during the tests.

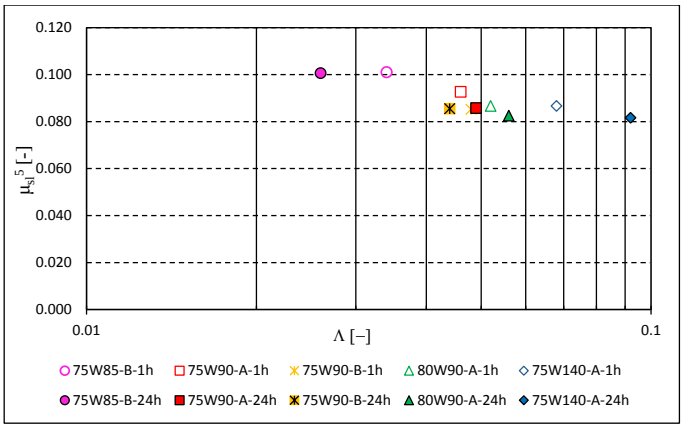

Figure 4.15: Variation of the sliding coefficient of friction of the RTB with 5 rollers vs specific film thickness parameter.

4.3.4.3. Boundary coefficient of friction

The RTB internal friction torque model (see section 5.3.2.2), states that the sliding coefficient of friction depends on the boundary film coefficient of friction (μ_{bl}) and on the full film coefficient of friction (μ_{EHL}), that is

$$\mu_{sl} = \phi_{bl} \cdot \mu_{bl} + (1 - \phi_{bl}) \cdot \mu_{EHL} \tag{4.27}$$

The influence of μ_{bl} and μ_{EHL} depends on the sliding friction torque weighting factor, ϕ_{bl}, given by Equation (4.28),

$$\phi_{bl} = \frac{1}{e^{2.6 \cdot 10^{-8} \cdot (n \cdot \nu)^{1.4} \cdot d_m}} \tag{4.28}$$

The values of ϕ_{bl} are presented in Table 4.12. In all RTB tests ϕ_{bl} is very close to 1.0 ($0.96 < \phi_{bl} < 1.0$), meaning that the coefficient of friction in full film conditions (μ_{EHL}) has got no influence on μ_{sl} under these operating condition, thus μ_{bl} might be considered equal to μ_{sl}. Furthermore, the values of ϕ_{bl} confirm that the RTB tests were performed under severe operating conditions, and that boundary film operating conditions prevail ($\phi_{bl} \approx 1.0$, $\Lambda < 0.1$ and $Sp < 10^{-8}$).

Table 4.12: Weighting factor (ϕ_{bl}) determined by set of performed measurement for each oil.

	Units	Test duration	Axle gear oil				
			75W85-B	75W90-A	75W90-B	75W140-A	80W90-A
ϕ_{bl}	[-]	1h	0.988	0.980	0.980	0.986	0.967
		24h	0.988	0.980	0.981	0.985	0.968

Since the sliding and the boundary coefficients of friction are equal ($\mu_{bl}=\mu_{sl}$), due to the operating conditions used in the RTB tests and to the corresponding ϕ_{bl} values, Figure 4.15 shows that the boundary coefficients of friction of the different axle gear oils present a linear decreasing trend with the logarithm of the specific lubricant film thickness ($\mu_{bl} \infty \log(\Lambda)$). Apparently, the type of additive package of each gear oil does have not influence significantly the boundary coefficient of friction.

4.4. Traction curves

4.4.1. Test equipment and methods

The traction behaviour of the axle gear oils are measured on the ball-on-disc apparatus (PCS Instruments), equipped with optical interferometry under controlled temperature. This type of measurement requires AISI 52100 steel disc instead of glass disc and a drilled ball which leads to an increase in the contact pressure until 1.11 GPa for a load of 50 N. A motor drives the disc while the drilled ball is driven by a another motor and is supported with a ball drive

adapter. The traction required to drive the ball is then measured. The profile used should contain a step where the slide /roll ratio (*SRR*) is not zero. Other conditions related to the capacities of the machine are described in Section 4.2.1.

4.4.2. Test specimens

The test specimens used to measure the traction coefficient of the lubricants are a steel disc that replaces the space layer disc with a diameter of 100 mm and a 3/4“ steel ball with a diameter of 19.05 mm. Two steel discs with different roughness are used. The average roughness of the discs and balls are measured with high repeatability, superior flexibility and accuracy using the NPFLEX optical interferometer (see Figure 4.16). Standard polished discs (smooth), non standard polished discs (rough) and balls are used, having an average roughness of R_a=2 nm, R_a=296 nm and R_a=5 nm, respectively (see Table 4.13 and see Figure 4.17), assuring that the traction measurements are performed under the three lubrication regimes. The test specimens properties are given in Table 4.13. Figure 4.17 shows the topographies (R_a) of the steel ball and the steel disc used for the measurements. The differences between the topographies are very significant. The smooth and rough discs clearly show some directionality in its roughness where the roughness marks are oriented in the rolling/sliding direction (see Figures 4.17 (a) and 4.17 (b)). The steel ball roughness, presented in Figure 4.17 (c), is isotropic.

The surface roughness of the ball-on-disc contact is similar to what might be found in rolling bearings [Nijenbanning et al., 1994b].

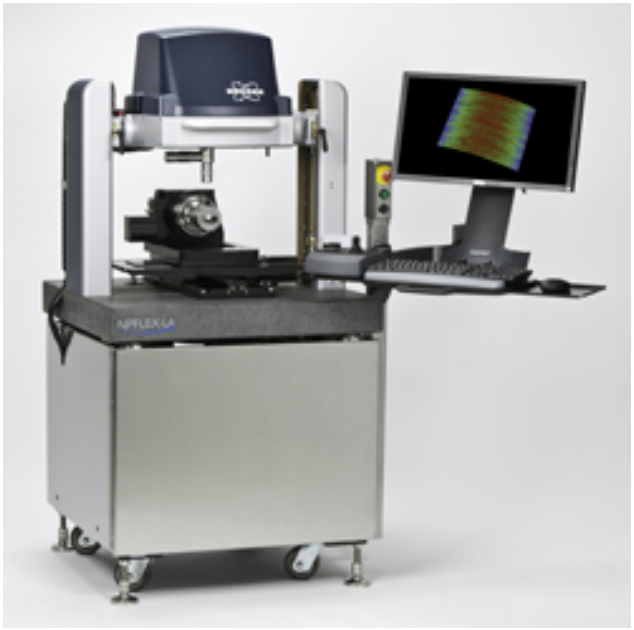

Figure 4.16: Bruker NPFLEX 3D instrument.

Table 4.13: Contact parameters for the ball-on-disc apparatus (smooth disc vs. steel ball and rough disc vs. steel ball).

Parameters	**Symbol**	**Unit**	**Smooth disc**	**Steel ball**	**Rough disc**
Materials properties					
Elastic Modulus	E	[Gpa]	210	210	210
Poisson Coefficient	ν	[-]	0.29	0.29	0.29
Equivalent Young Modulus	E^*	[GPa]		114.64	
Specimen and contact geometry					
Radius	R	[mm]	50	9.525	50
Radius in X direction	R_x	[mm]	∞	9.525	∞
Radius in Y direction	R_y	[mm]	∞	9.525	∞
Surface roughness	R_a	[nm]	2	5	296
Hertzian contact parameters					
Normal force	F_n	[N]		50	
Radius of the contact circle	a	[mm]		0.146	
Penetration	δ	[μm]		2.238	
Maximum Hertz pressure	p_0	[GPa]		1.11	
Medium pressure	p_m	[GPa]		0.745	

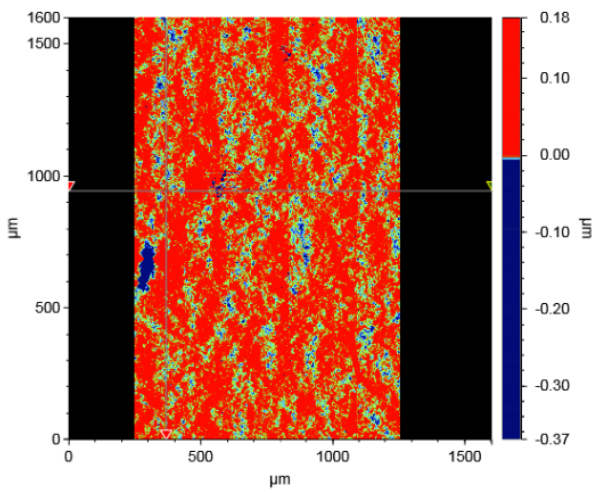

(a) The roughness profile of the smooth disc.

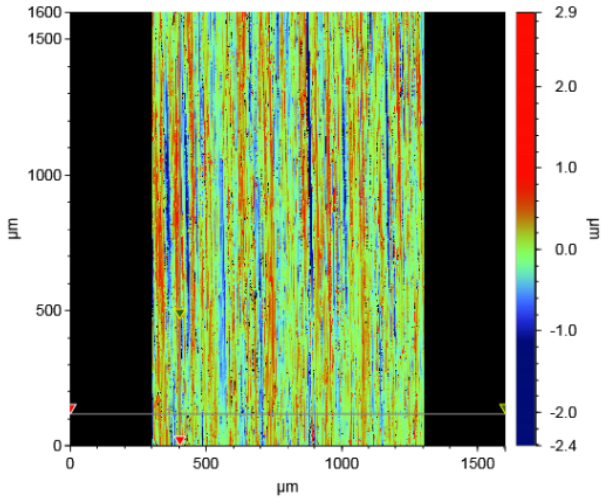

(b) The roughness profile of the rough disc.

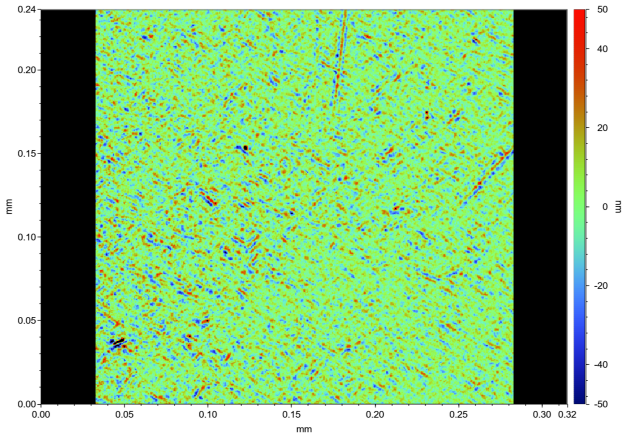

(c) The roughness profile of the ball.

Figure 4.17: Deviation of the surface roughness of the ball and the two discs made of carbon chrome steel.

4.4.3. Test procedure

The traction tests started by specifying the following set of parameters like slide-to-roll-ratio (*SRR*), contact load (F_n), oil bath temperature (T_0) and by fixing the entrainment speed (U). Each traction test is defined as one particular combination of those independent parameters.

The traction tests were performed with maximum contact pressure p_0=1.118 GPa between a rotating steel ball into a rotating steel disc which corresponds to an applied load equal to 50 N. The slide-to-roll ratio varied from 1 % to 50 %. The operating temperatures are the same used for the film thickness measurements: 40, 70 and 100 °C. Each test is divided into three steps and each step is characterized with a specific entrainment speed which can be equal to 0.5, 1 or 2 m/s.

The test cycle presents several loops where the *SRR* was increased from 1 to 50 % and then decreased to 1 % which allow again to verify the repeatability of the results. In the first loop the entrainment speed is held constant 2 m/s and then it decreased with 0.5 m/s for each loop. In all cases the ball rotated slower than the disc.

4.4.4. Traction coefficient results

4.4.4.1. Results of lubrication at point contact between ball and smooth disc

The experimental traction curves are shown in Figure 4.19 using the smooth disc and their values are displayed in Table 4.15 in order to compare the quantitative results with each other. Each sub-figure plots the coefficient of friction against the slide-to-roll ratio for all the five oils and for a precise combination of temperature and entrainment speed. The columns show the influence of the entrainment speed and the rows present the influence of the temperature on the traction behaviour of the axle gear lubricants. The first column presents the traction curves obtained at T = 40 °C and the second column those performed at T = 100 °C and for those at T = 70 °C are presented in Appendix D.1, being clear that when the temperature increases the traction coefficient decreases. The first row presents the traction curves measured at U = 0.5 m/s and the second row those measured at U = 1 m/s and the last one those at U = 2 m/s, showing that when the speed increases the traction coefficient decreases.

All the oils tested show the same behaviour, which is typical of full film lubrication conditions where no asperity interaction takes place, as suggested in the literature [Brandao et al., 2011]. The specific film thickness (Λ) [Brandao et al., 2011], given by ratio between the theoretical EHD film thickness and the combined RMS roughness of the specimen surfaces (R_q=σ), is determined for all testing conditions (see Equation (4.13). The calculations are reported in Table 4.15, confirming that in all cases and for all axle oils, the traction measurements were performed under a full film lubrication ($\Lambda >> 3$), since the specific film thickness values are always higher than 6.

All the sub-figures in Figure 4.19 show the same trends, and the mineral based oil 80W90-A oil always generated the highest traction coefficients. Among the PAO based formulations, the general trend is as follows: $COF_{75W90-A} > COF_{75W140} \approx COF_{75W90-B} > COF_{75W85-B}$. It is clear that the nature of the base oil, mineral or PAO, is determinant. This trend has already

been pointed out by Brandão [Brandao et al., 2011], and explains why the mineral based oil 80W90-A has the highest traction coefficient. In what concerns the PAO formulations the reference lubricants, 75W90-A and 75W140-A, showed higher traction coefficients than the candidate oils 75W90-B and 75W85-B, although the differences in traction coefficient between the PAO based oils are small.

The analysis of the traction curves does not show any clear or direct correlation between the traction coefficient and the physical properties of the gear oils (e.g. viscosity) or the ability to generate a lubricant film (e.g. modified Lubricant Parameter). However, a general trend is clear: oils with lower piezoviscosity or higher Viscosity Index generate lower traction coefficient, which as already been observed by Brandão [Brandao et al., 2011].

In Figure 4.18 the traction coefficients are plotted against the empirical parameter α/VI, being clear that when this parameter increases the traction coefficient also increases (see Table 4.14). This figure also distinguishes very clearly the PAO formulations and the mineral oil. Thus, the differences in the traction coefficient measurements of the different oil formulations can be fully justified by the relative differences in piezoviscosity and Viscosity Index, whatever the operating conditions considered.

Oil 80W90-A has the highest peiezoviscosity and the lowest VI, generating the highest traction coefficient. In fact, for the same viscosity grade mineral oils have higher piezoviscosity and lower VI than PAO's and, consequently, promote higher traction coefficients than PAO's. The comparison between oil 80W90-A and oil 75W90-A (e.g. at 70 °C (see Appendix D.1)) demonstrates this relation. Among the PAO formulations the influence of the piezoviscosity and of the Viscosity Index is also clear. Comparing oils 75W90-A and 75W90-B, which have similar piezoviscosities, it is clear that oil 75W90-B has a higher VI and generates a lower traction coefficient. Another interesting comparison is between oils 75W85-B, 75W90-B and 75W140-A, which have similar VI's (respectively, 162, 163 and 169). In this case, oils 75W140-A has the highest piezoviscosity and generates the highest traction coefficient, while oil 75W85-B has the lowest piezoviscosity and generates the lowest traction coefficient. Even at 100 °C, where the piezoviscosities of these oils are different, such trend is observed. So, under full film lubrication conditions, the oil formulation has an important influence on the traction coefficient through the type of base oil and its piezoviscosity and Viscosity Index. Of course, VI improvers are additives with a significant influence on such behaviour.

The comparison between the reference oil 75W90-A and the candidate oil 75W90-B is quite interesting. Despite their close values of kinematic viscosity and modified Lubricant Parameter, they have a different formulation (see section 3.9): the candidate lubricant 75W90-B contains Boron and Zinc, typically associated with friction modifiers and anti-wear additives, respectively, which might explain the lower traction coefficients generated by this candidate oil. Furthermore, oil 75W90-B has a VI higher then oil 75W90-A (163 and 147, respectively), which has already been identified has an influence parameter on the traction coefficient.

Table 4.14: Values of the coefficient of friction and the parameter α/VI for SRR = 30 % and U = 0.5m/s.

		75W85-B	75W90-A	75W90-B	80W90-A	75W140-A
40 °C	α/VI	0.0797	0.0944	0.0853	0.1639	0.0886
	COF	0.047	0.054	0.049	0.058	0.049
70 °C	α/VI	0.0696	0.0737	0.0741	0.1002	0.0790
	COF	0.034	0.04	0.035	0.045	0.036
100 °C	α/VI	0.0631	0.0662	0.0666	0.0886	0.0705
	COF	0.025	0.03	0.025	0.035	0.024

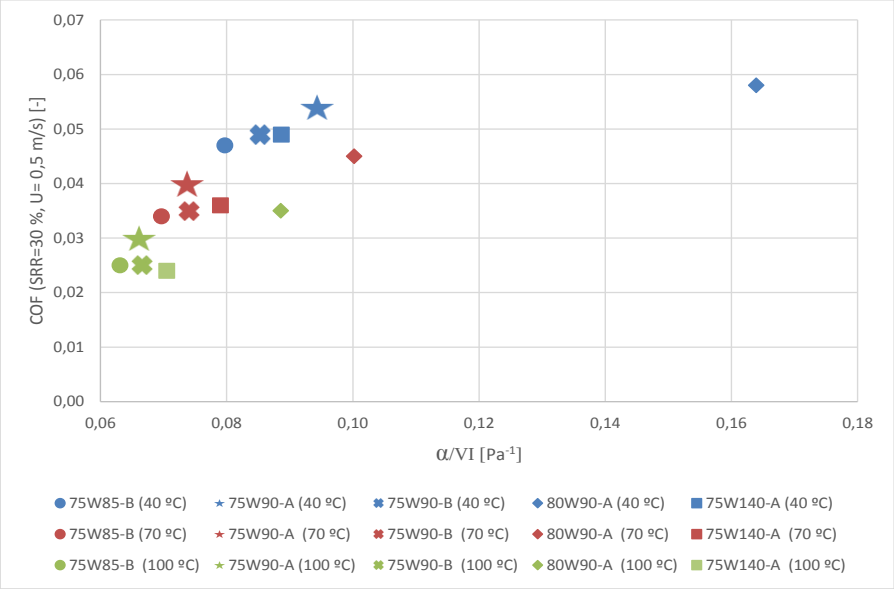

Figure 4.18: Variation of the traction coefficient against the empirical parameter α/VI.

Table 4.15: Specific film thickness of axle gear oils under different operating conditions.

		75W85-B	75W90-A	75W90-B	80W90-A	75W140-A
		PAO	PAO	PAO	MIN	PAO
T [°C]	u [m/s]	Λ [-]	Λ [-]	Λ [-]	Λ [-]	Λ [-]
40	0.5	23.5	35.3	35.5	45.2	54.6
40	1	37	55.2	55.6	70.6	84.8
40	2	57.5	84.7	85.3	107.6	127.7
70	0.5	10.9	15.3	15.6	17.5	22.7
70	1	17.3	24.1	24.6	27.7	35.9
70	2	27.3	37.9	38.6	43.4	55.8
100	0.5	6.2	8.3	8.5	8.9	11.9
100	1	9.9	13.1	13.5	14.2	18.9
100	2	15.7	20.8	21.3	22.4	29.7

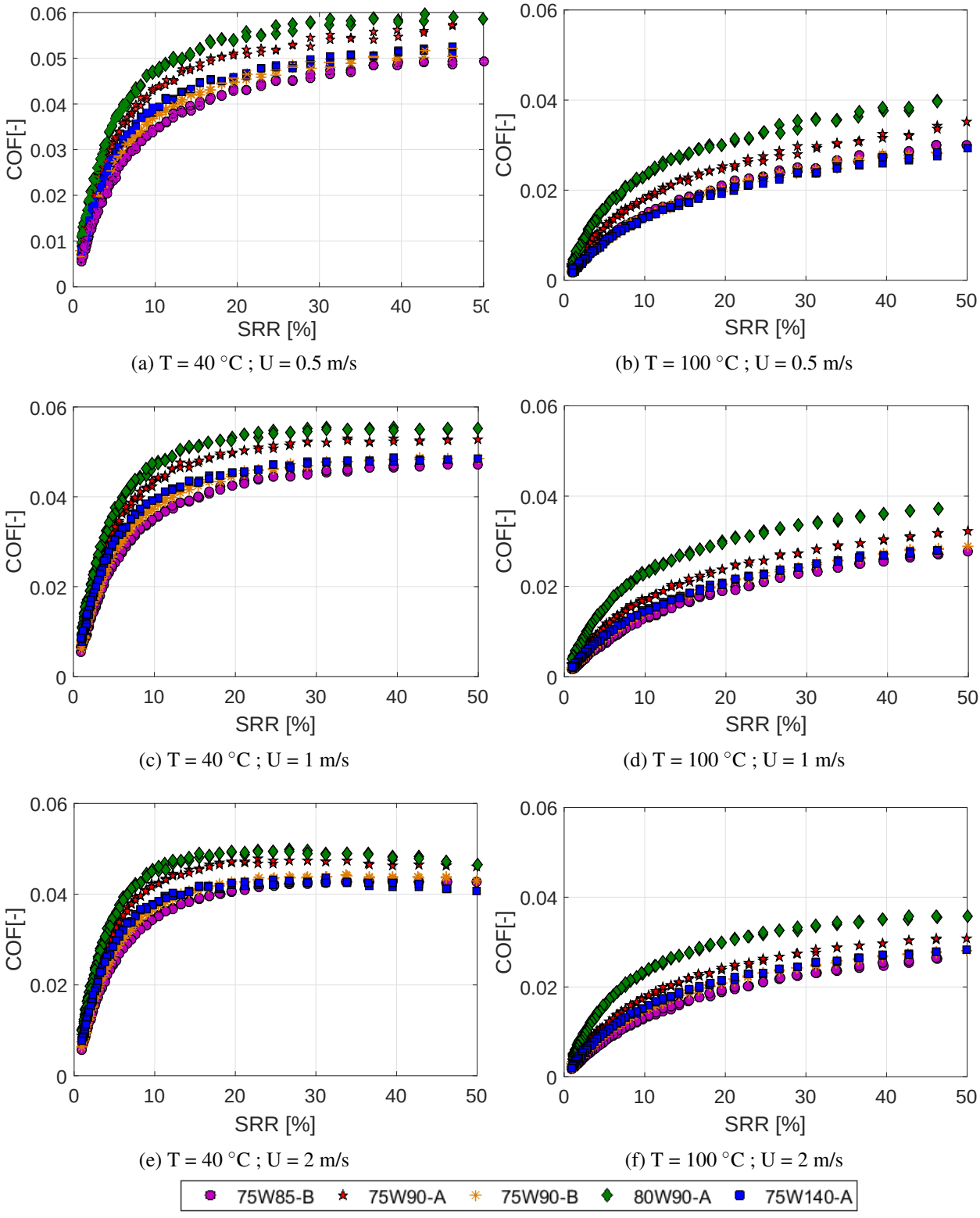

(a) T = 40 °C ; U = 0.5 m/s

(b) T = 100 °C ; U = 0.5 m/s

(c) T = 40 °C ; U = 1 m/s

(d) T = 100 °C ; U = 1 m/s

(e) T = 40 °C ; U = 2 m/s

(f) T = 100 °C ; U = 2 m/s

Figure 4.19: Traction curves for the five axle gear oils using smooth disc: (a), (c), and (e) at 40 °C , (b), (d), and (f) at 100 °C.

4.4.4.2. Results of lubrication at point contact between ball and rough disc

In this experiment the roughness of the specimen surfaces of the ball and the rough disc are indicated in Table 4.13.

The coefficient of friction results are shown in Figure 4.21 where the traction curves of each oil are plotted for several combinations of the operating conditions.

The corresponding experimental coefficients of friction are displayed in Table 4.16 in order to compare the quantitative results with each other.

It is clear that in most cases, the coefficients of friction measured with a rough disc are higher than those measured with smooth disc, due to the severity of the operating conditions (see Figure 4.22). In each subfigure, the traction coefficient of each oil is plotted against the slide-to-roll ratio for a given combination of the operating conditions, defined by a fixed value of the temperature and of the entrainment speed, making easier the comparison of the lubricants.

Figures 4.21 (a), 4.21 (c) and 4.21 (e) present the traction curves of the oils measured at T=40 °C and Figures 4.21 (b), 4.21 (d) and 4.21 (f) show those measured at T=100 °C. The comparison of these measurements indicates that the coefficients of friction increase when the temperature increases, which is typical of the mixed film lubrication regime and is due to the high surface roughness of the disc. Figures 4.21 (a) and 4.21 (b) present the traction curves at U=0.5 m/s, Figures 4.21 (c) and 4.21(d) present the traction curves at U=1 m/s and Figures 4.21 (e) and 4.21 (f) those at U=2 m/s, indicating that the coefficients of friction decrease when the entrainment speed increases. Additional results are given in Appendix D.2 for the operating temperature of T=70 °C under the three entrainment speeds.

Figure 4.21 (e) compares the coefficient of friction of the oils at 40 °C and U=2.0 m/s, where the specific lubricant film thickness is above $\Lambda \geq 1.0$. Under these conditions, and for a slide-to-roll ratio *SRR*=30%, the lubricants follow a clear trend: the oils that generate higher specific film thickness produce lower coefficient of friction, as shown in Figure 4.20 (Group I), which is typical of the mixed film regime. This means that in this case the physical properties of the gear oils (dynamic viscosity, piezoviscosity, Viscosity Index) are still important and the degree of interaction between surface asperities is crucial.

Figure 4.21 (b) compares the coefficient of friction of the oils at 100 °C and U=0.5 m/s , where the specific lubricant film thickness is very low $0.10 < \Lambda < 0.20$. Under these conditions, and for slide-to-roll ratio of 30%, the values of the coefficient of friction are very similar $0.103 \leq \text{COF} \leq 0.113$, and do not show any particular trend in relation to the specific film thickness, as shown in Figure 4.20 (Group II), which is typical of the boundary film lubrication regime. Here, the physical properties of the lubricants are no longer determinant and the additive package of each gear oil plays a fundamental role, reacting with the steel surfaces of the ball-on-disc and generating tribofilms.

The same trend was observed in the tests with Cylindrical Roller Thrust Bearing-RTB, shown in Figure 4.20 (Group III), although the roller-on-raceway line contact of the RTB (Group III) generates lower COF's than the ball-on-disc circular contact (Group II).

Gear oils 75W90-A and 75W90-B have the same base oil but they have different formulations in terms of additives (see Table 3.7). Figure 4.20 shows that they have very similar coefficient

of friction either in mixed film (Group I) or boundary film (Groups II and III) conditions, suggesting that both formulations (A and B) perform similarly well in terms of friction.

Lubricant 80W90-A is formulated with a mineral base oil and has an additive package similar to oil 75W90-A oil. In terms of physical properties it is not significantly different from the two oils mentioned above (see Table 3.4), and it generates similar coefficients of friction in boundary and mixed film lubrication, performing as well as oils 75W90-A and 75W90-B (see Figure 4.20).

Formulations, 75W85-B and 75W140-A behave differently from the previous ones in mixed lubrication conditions (Group I) because they have significantly different physical properties and generate different specific lubricant film thickness than oils 75W90-A, 75W90-B and 80W90-A.

Table 4.16: Ball-on-disc coefficients of friction using rough disc at 40 and 100 °C, for speeds of 0.5 m/s and 2.0 m/s.

T [°C]	Speed [m/s]	SRR (%)	75W85-B	75W90-A	75W90-B	80W90-A	75W140-A
40	0.5	10	0.083	0.078	0.081	0.073	0.076
		20	0.092	0.086	0.088	0.083	0.085
		30	0.095	0.090	0.092	0.086	0.089
		40	0.097	0.092	0.095	0.088	0.091
	2	10	0.065	0.058	0.061	0.052	0.051
		20	0.073	0.065	0.068	0.058	0.056
		30	0.075	0.065	0.070	0.059	0.057
		40	0.075	0.066	0.070	0.059	0.057
100	0.5	10	0.099	0.095	0.096	0.093	0.100
		20	0.105	0.103	0.103	0.101	0.110
		30	0.107	0.104	0.105	0.103	0.113
		40	0.107	0.104	0.106	0.105	0.115
	2	10	0.089	0.079	0.087	0.079	0.078
		20	0.097	0.088	0.095	0.088	0.085
		30	0.098	0.091	0.097	0.089	0.088
		40	0.099	0.093	0.097	0.092	0.090

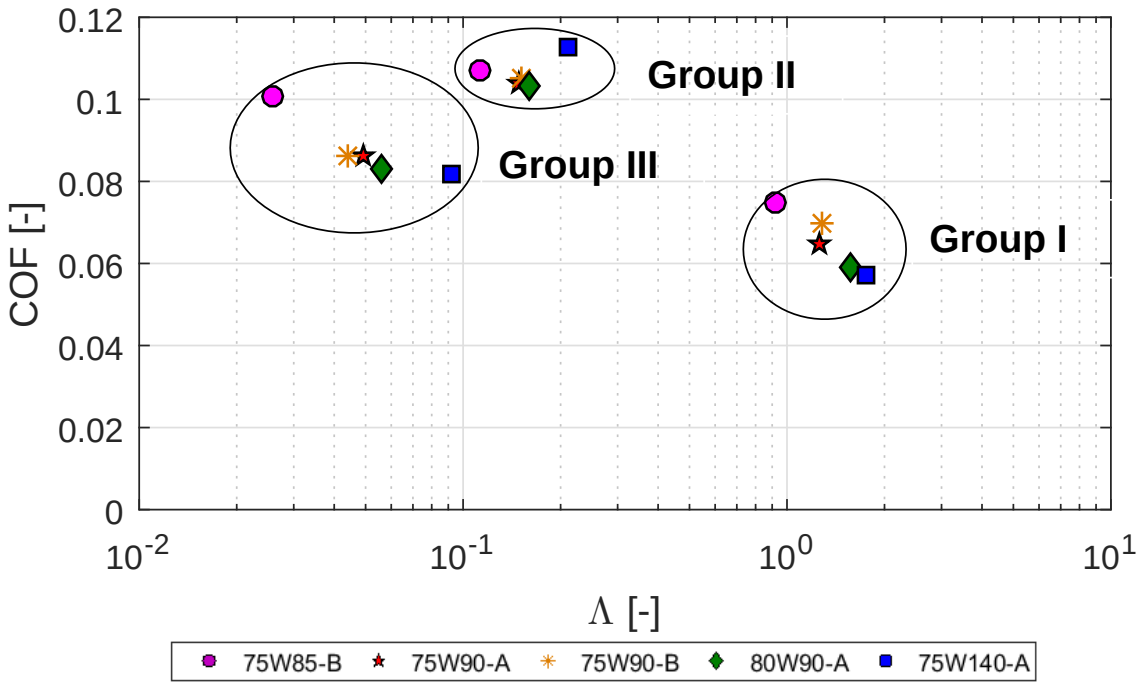

Figure 4.20: Coefficient of friction (COF) vs specific lubricant film thickness (Λ): Group I: ball-on disc, T=40 °C, U=2.0 m/s, SRR=30%; Group II: ball-on disc, T=100 °C, U=0.5 m/s, SRR=30%; Group III: RTB, T=110 °C, U=0.122 m/s.

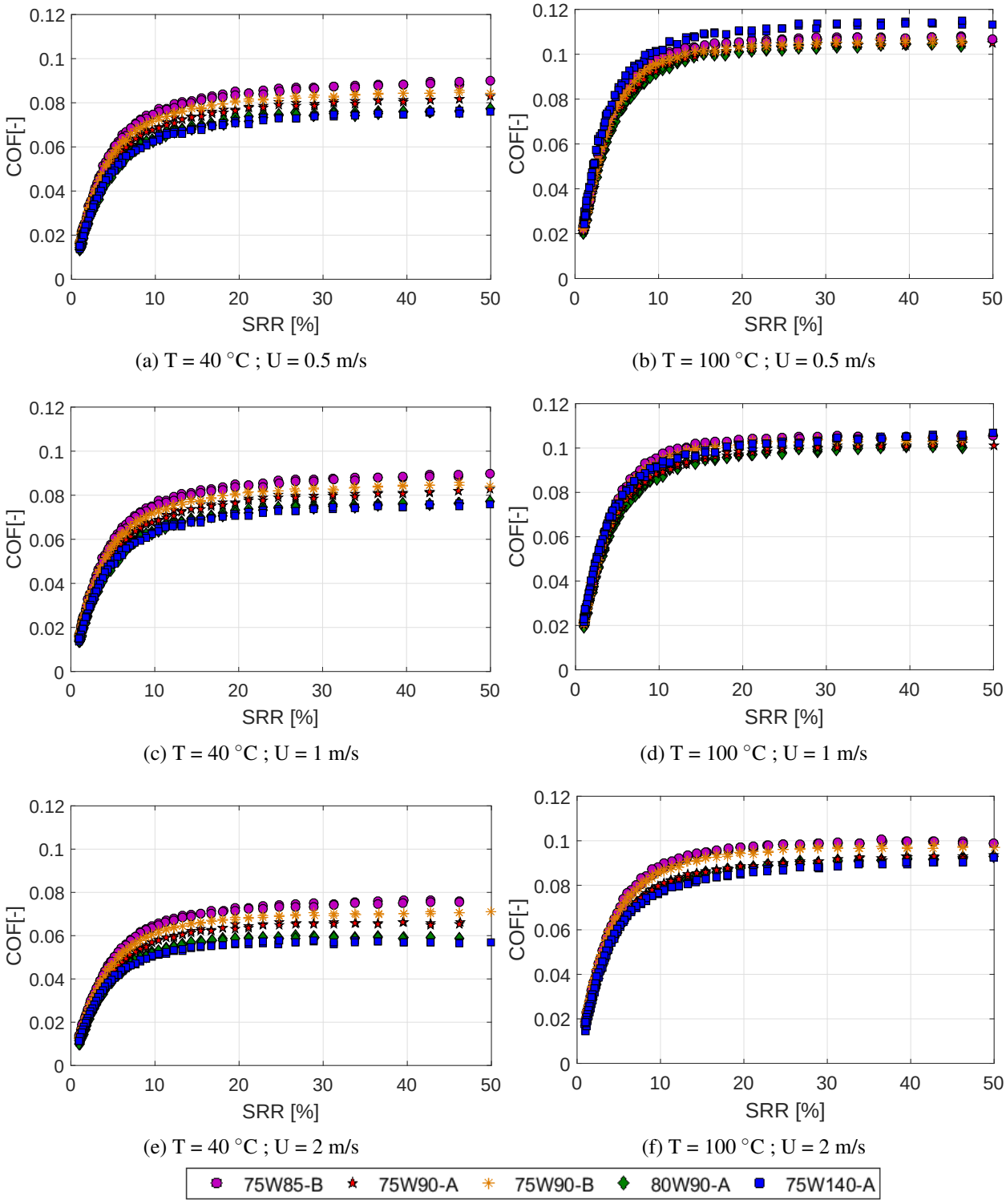

(a) T = 40 °C ; U = 0.5 m/s

(b) T = 100 °C ; U = 0.5 m/s

(c) T = 40 °C ; U = 1 m/s

(d) T = 100 °C ; U = 1 m/s

(e) T = 40 °C ; U = 2 m/s

(f) T = 100 °C ; U = 2 m/s

Figure 4.21: Traction curves for the five axle gear oils using rough disc: (a), (c), and (e) at 40 °C, (b), (d), and (f) at 100 °C.

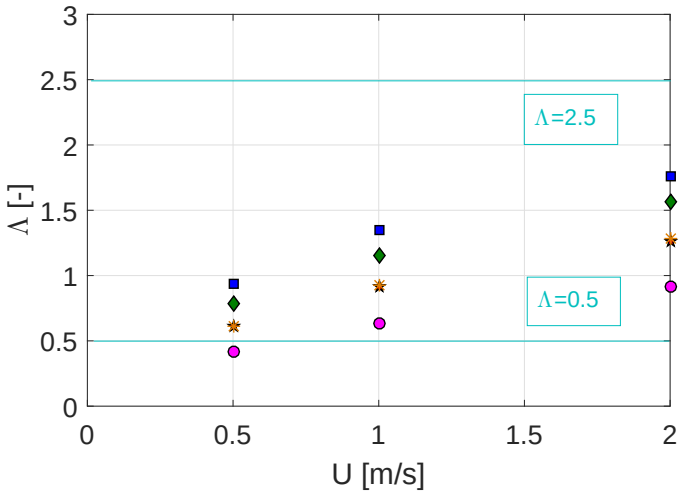

(a) Λ vs. U at 40 °C

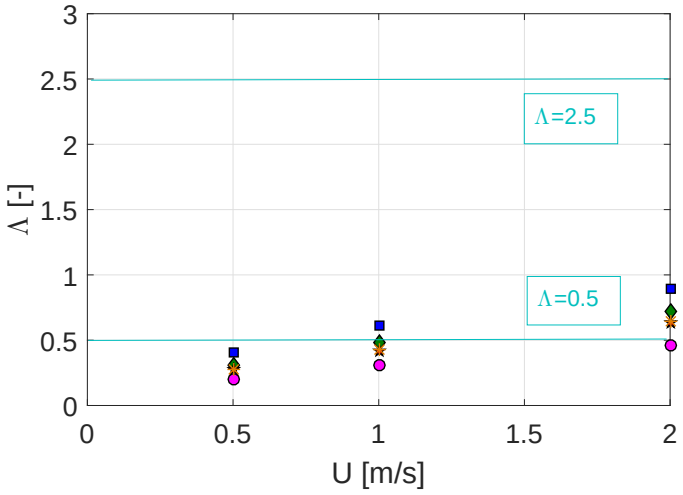

(b) Λ vs. U at 70 °C

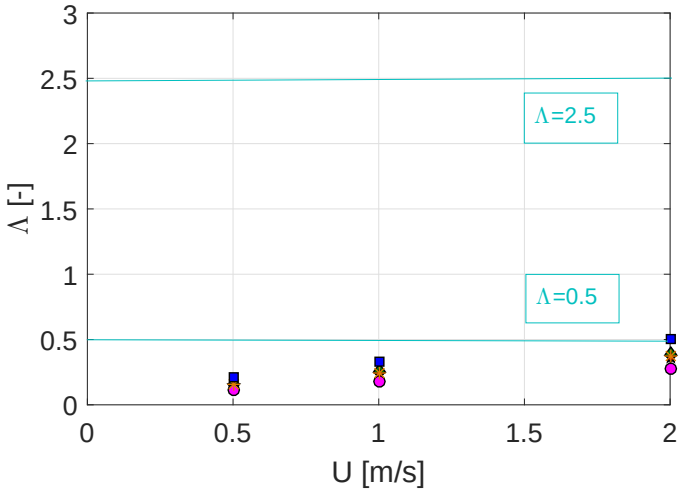

(c) Λ vs. U at 100 °C

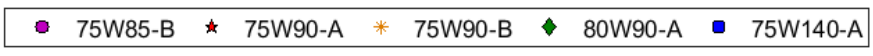

Figure 4.22: Specific film thickness of axle gear oils using rough disc.

4.5. Stribeck curves

The Stribeck curves of the axle gear oils are also measured on the ball-on-disc apparatus. The experimental procedure is similar to the one followed in the traction tests: the balls and the discs have the same characteristics, the same load and operating temperatures are used. In the case of the Stribeck curves the slide-to-roll ratio is kept constant at 30% and the rolling speed increases from 0.01 m/s up to 3 m/s and then it decreases back until 0.01 m/s, for repeatability considerations.

Figure 4.23 depicts the Stribeck curves of the axle gear oils at 40, 70 and 100 °C. The coefficient of friction (COF) is plotted against the specific film thickness in a logarithmic scale (Log Λ). The coefficient of friction is shown for the tests performed with a rough disc (R_q=384), on the left, and for the tests performed with a smooth disc (R_q=2 nm), on the right, of each subfigure (a), (b) and (c). The test performed with a rough disc, run at Λ<2.0, Λ<1.0 and Λ<0.7 for the temperatures of 40, 70 and 100 °C, respectively.

The modified Hersey number is given by Equation (4.29) [Brandao et al., 2009].

$$Hp = \frac{U_r \cdot \eta \cdot \alpha^{1/2}}{F_n^{1/2}} \tag{4.29}$$

where η is the dynamic viscosity of the oil, U_r is the rolling speed and F_n is the normal force. The rolling speed is defined as:

$$U_r = \frac{U_{ball} + U_{disc}}{2} \tag{4.30}$$

The modified Hersey number proposed by *Brandão et al.* [Brandao et al., 2009] includes the piezoviscosity of the oil, which is very interesting when oils with different base oils and additive packages are compared.

Figure 4.23 also shows the modified Hersey number of axle gear oil 75W90-A ($Hp^{75W90-A}$) in function of the Λ ratio, which is in the broad range of 10^{-9} and 10^{-5}, whatever the temperature. The Hersey number does not depend on the composite roughness of the ball-on-disc contact, and so $Hp^{75W90-A}$ is exactly the same for the tests performed with the smooth and rough discs.

Figure 4.23 clearly shows the difference between the coefficient of friction values when increasing the roughness of the disc and the transition from full film lubrication conditions to boundary lubrication conditions.

4.5.1. Stribeck curves measured with smooth discs

The experimental COF measurements obtained with the smooth disc where full-film lubrication conditions prevail (Λ>>3, mainly at 40 and 70 °C) were discussed in detail in Hammami *et al.* [Hammami et al., 2016] .

The corresponding Stribeck curves on the right side of Figures 4.23 (a), 4.23 (b) and 4.23 (c) have a common trend: oil 80W90-A always generated the highest COF while the candidate oil 75W85-B generated the lowest COF. The other formulations (75W90-B, 75W90-A and 75W140-A) showed very similar COF's at 70 °C. These measurements were done under full film lubrication and suggest that in these conditions the COF's are strongly dependent on the physical properties of the lubricant and oils with high Viscosity Index and low piezoviscosity generate lower coefficients of friction [Hammami et al., 2016].

This general trend is no longer observed for the Stribeck curves measured at 100 °C and a specific film thickness near to one ($\Lambda \approx 1.0$). In this condition the COF's show a significant increase, the influence of the disc roughness becomes significant and a typical mixed film lubrication behaviour starts to be observed.

4.5.2. Stribeck curves measured with rough discs

The Stribeck curves on the left side of figures 4.23 (a), 4.23 (b) and 4.23 (c), measured at 40, 70 and 100 °C, with the rough disc, are typical of boundary and mixed film lubrication. In the range $0.1 < \Lambda < 1.0$, the coefficient of friction increases significantly as Λ decreases (mixed film lubrication) and in the range $\Lambda < 0.1$ the coefficient of friction becomes almost constant (boundary film lubrication).

Under boundary film operating conditions, $\Lambda < 0.1$, the candidate oils (B) 75W85-B and 75W90-B generated similar COF's ($COF^{75W85-B} \approx COF^{75W90-B}$), always smaller than the COF's generated by the reference formulations (A). Among the reference (A) formulations, oils 75W90-A and 80W90-A generate similar COF's and oil 75W140-A always promoted the highest coefficients of friction.

This trend seems to indicate that the candidate (B) formulations containing Zinc ($900 \leq$ Zn/ppm ≤ 1120, see Table 3.7) and smaller amounts of phosphorus (P/ppm$<$1000) and Sulfur (S/ppm$<$ 3500) generate lower COF's than the reference (A) formulations containing large amounts of Phosphorus (P/ppm$>$1400) and Sulfur (S/ppm$>$20000).

Another interesting characteristic is that the COF's under boundary film lubrication, COF_{bl}, is that they are independent of the operating temperature, as shown in Table 4.17, and also independent of the physical characteristics of each axle gear oil, that is viscosity, piezoviscosity, Viscosity Index, or even the ability of each gear oil to generate a lubricant film. Under boundary film operating conditions, significant tribochemical activity occurs between the contacting surfaces and the gear oil additives (see section 4.3.3.5), as demonstrated for the same gear oil formulations, and the tribolayers generated prevail over the physical properties of the oils. The comparison of the formulations 75W90-A and 80W90-A for $\Lambda \leq 0.1$, seems to indicate that the base oil type (PAO or mineral, respectively) does not have a significant influence on the coefficient of friction (COF_{bl}).

Under mixed film lubrication conditions ($0.1 \leq \Lambda \leq 1.0$), the coefficients of friction (COF_{mix}) are strongly dependent on the specific lubricant film thickness (Λ) and they decrease very significantly as Λ increases. As expected, in mixed film lubrication the coefficient of friction depends on the COF's under boundary film and full-film lubrication (COF_{bl} and COF_{EHD}) of

Table 4.17: Boundary coefficient of friction for the axle gear oils at 40, 70 and 100 °C.

Λ=0.1	75W85-B	75W90-A	75W90-B	80W90-A	75W140-A
COF_{bl} @ 40, 70, 100 °C	0.105	0.115	0.105	0.115	0.120

each gear oil, and the transition from COF_{bl} to COF_{EHD} is controlled by the increase of the specific film thickness (Λ).

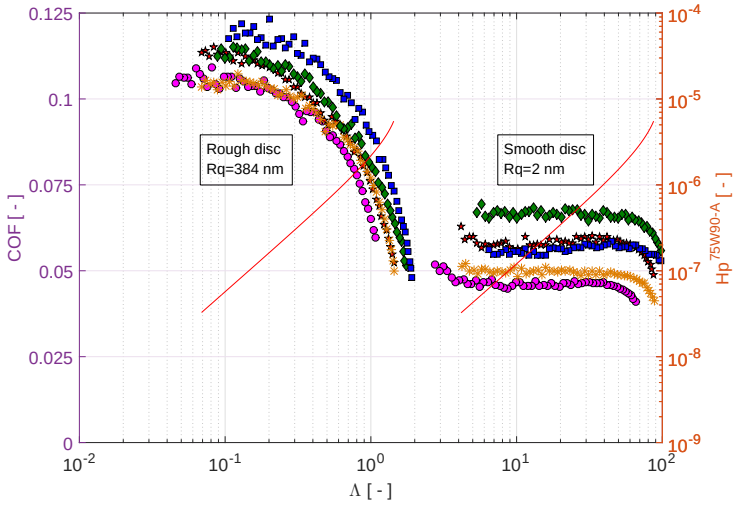

(a) T = 40 °C; SRR = 30%

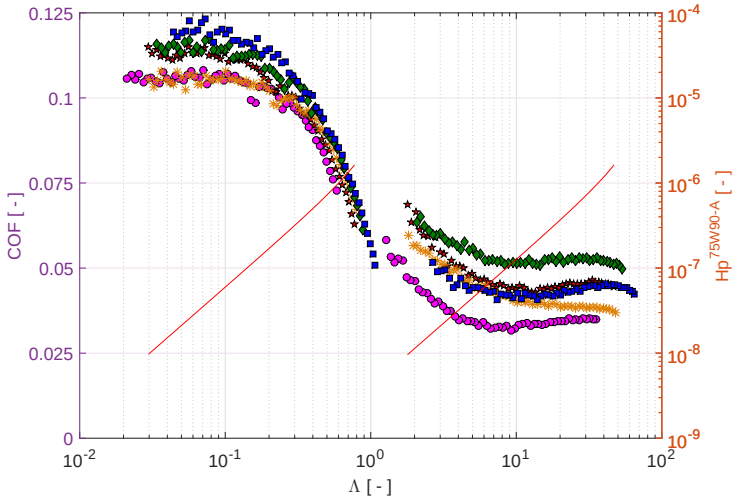

(b) T = 70 °C; SRR = 30%

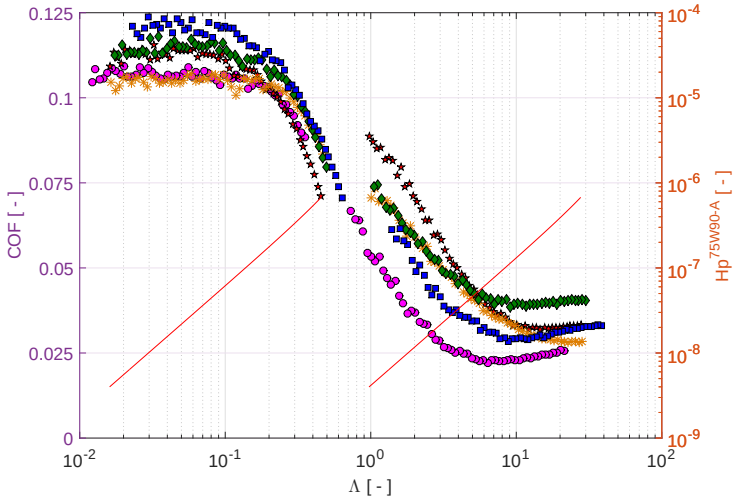

(c) T = 100 °C; SRR = 30%

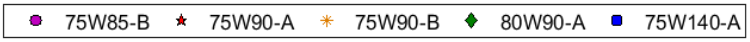

Figure 4.23: Stribeck curves for all axle gear oils under 30 % of SRR.

4.6. Summary

The ability to generate an EHD lubricant film can be evaluated through the modified Lubricant Parameter ($LP^* = \eta^{0,67}.\alpha^{0,53}$), which can be extracted from the film thickness measurements. At 100 °C the LP^* of reference oil 75W140-A is 38% larger then the corresponding values for oils 75W90-A and 80W90-A, and 70% and 60% larger then the LP^* of the candidate oils 75W85-B and 75W90-B, respectively. However, a larger capability to generate an EHD lubricant film does not have a significant influence on the friction behaviour of these lubricants, since oil 75W85-B always generated lower traction coefficients than 75W140-A oil, under full film and mixed film lubrication.

The Cylindrical Thrust Roller Bearing tests, using the 81107 TN rolling bearing with only 5 rollers instead of the standard 20 rollers, together with the high pressure, high temperature and low speed operating conditions, were able to generate a boundary film lubrication regime, where significant tribochemical activity occurs between the rollers, the raceways and the axle gear oil additives. The XPS surface analysis of the rollers surfaces clearly demonstrated the chemical modification of the contacting surfaces.

The comparison between axle gear oils 75W90-A and 75W90-B after 24 hours, under the same RTB tests and operating conditions, shows that, the Calcium-Zinc based additive package of the candidate (B) oil generated closer internal friction torque and boundary coefficient of friction than the additive package of the reference (A) oil. However, it promoted higher wear indexes and higher surface roughness at the end of the tests.

Under the severe boundary film lubrication operating conditions of the RTB tests, the behaviour of all axle gear oil formulations show a significant influence of the specific lubricant film thickness. When Λ increased all the parameters (internal friction torque, boundary coefficient of friction, wear indexes and surface roughness) decreased. The reference (A) oils generated lower internal friction torque, boundary coefficient of friction, wear indexes and surface roughness than those of candidate (B) oils.

Axle gear oil 75W85-B proved that it generated lower coefficient of friction than all other formulations under full-film conditions due to its lower operating viscosity. However, under severe boundary conditions, as used in these tests, it generated a boundary coefficient of friction which is at least 17 % higher than the other ones.

The traction curves and the Stribeck curves, performed under full film EHD lubrication regime ($\Lambda >> 3$), revealed consistent differences between the lubricating oils. The mineral based oil 80W90-A oil always generated the highest COF and, among the PAO based formulations, the sorting is $COF_{75W90-A} > COF_{75W140-A} > COF_{75W90-B} > COF_{75W85-B}$. The same measurements also indicate that a qualitative correlation can be established between the CoF and the thermal properties of the oils. In fact oils with high Viscosity Index and low piezoviscosity generate lower Coefficients of Friction.

The ball-on-disc tests performed under constant entrainment speed and a slide-to-roll ratio of 30 %, using a rough disc, showed that under boundary film lubrication (Λ<0.2), the coefficient of friction becomes almost constant and independent of the specific film thickness, of the physical properties of the lubricant, and of the base oil nature (PAO or Mineral).

The Stribeck curves, with smooth disc (R_q=2 nm), (see Figure 4.23), clearly indicate that the friction behaviours of the axle gear oil under full and mixed film lubricating regimes might be completely different. Nevertheless, the performance of an axle oil during the EPA driving cycle depends on its behaviour under full film and mixed film regimes, which are both important for the reduction of the spin losses and friction losses. Thus, the candidate axle oils (75W85-B and 75W90-B) have the best performance under full film conditions and have a very promising behaviour under mixed film lubrication and even under boundary lubrication.

The same tests performed with rough disc (R_q=384 nm) showed that under boundary film conditions, the candidate oils (B), formulated with an additive package containing Zinc (75W85-B and 75W90-B) generated lower friction coefficients than the reference oils (A).

The candidate axle gear oil 75W85-B always generated the lowest COF's, suggesting that reducing the dynamic viscosity, increasing the VI and formulating the oil with Zinc-based additives, allows an excellent friction behaviour in all lubricating regimes.

5. Automotive axle power loss model

5.1. Introduction

Power losses of automotive drive trains have become one of the major area of investigation in automotive industry [Joachim et al., 2011, Joachim et al., 2014, Xu et al., 2012, Katoh et al., 1983, Ko and Hosoi, 1984]. While the federal standards and the state government regulations in vehicle fuel economy combined with limits imposed by EPA rules on CO_2 emissions into the atmosphere have traditionally been the main reason for this focus in drive train power losses [Bala et al., 2000b, Bala et al., 2000a, Bjornen et al., 2003, Porrett et al., 1980]. The looming energy crisis and increasing fuel prices have also added to the motivation to reduce such losses.

It has been well settled that the automotive axle-differential is considered as a significant contributor to power loss in the drive line [Hurley, 2009]. Axle efficiency values were reported to be as low as 90 to 95 % depending on the type of vehicle and on the applied torque and speed [Joachim et al., 2014, Talbot et al., 2016, Kolivand et al., 2010]. Therefore, any tangible improvement to the axle efficiency has a significant impact on overall the carbon emissions and the energy consumption significantly [Xu et al., 2012, Talbot et al., 2016].

The axle transmission is a key component of the vehicle powertrain. It is a very compact mechanical system, consisting generally of a hypoid bevel geared transmission, tapered roller bearings, seals, shafts and an axle gear oil (see Figure 5.1)). The axle transmission requires a very high reliability, since failures are not accepted by consumers [Evans, 2014, Johnston et al., 1991, Guangteng et al., 2000].

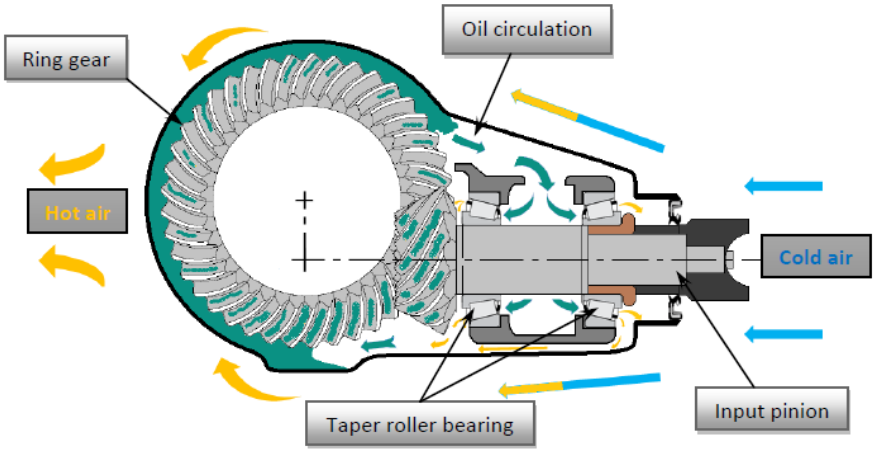

Figure 5.1: Oil circulation and heat flow in rear drive axle [Kolekar, 2013].

The axle transmission has three functions: the first one is to receive the power from the engine (via the gearbox and propeller shaft) and to transfer it to the driving wheels of the vehicle; the second one is to provide an overall reduction of the transmission ratio, avoiding to do it in the gearbox, thus keeping the gearbox much smaller; finally, the third one is to enable the wheels to travel at different speeds while cornering, without losing drive. So the main task of axle transmission is to accomplish these functions as efficiently as possible, minimizing the mechanical losses [Kolekar, 2013].

As any power transmission system, axle power losses are divided into several energy loss mechanisms as proposed in a number of papers by Hohn et al. [Hohn et al., 1996, Höhn et al., 2009, Seabra et al., 2011] as presented in Figure 5.2. The sources of the major axle power losses were dissipated mainly in friction loss between the meshing teeth of hypoid gears [Kolivand et al., 2010, Cheng and Lim, 2001, Cheng and Lim, 2003, Wang et al., 2007, Xu et al., 2007], friction loss in the bearings [Spindler and Von Petery, 2003, Matsuyama et al., 2004, Hosokawa et al., 2009], friction loss in the seals [Lin et al., 2005] and spin losses due to lubricant pumping and churning, and windage [Ko and Hosoi, 1984, Kolekar et al., 2013].

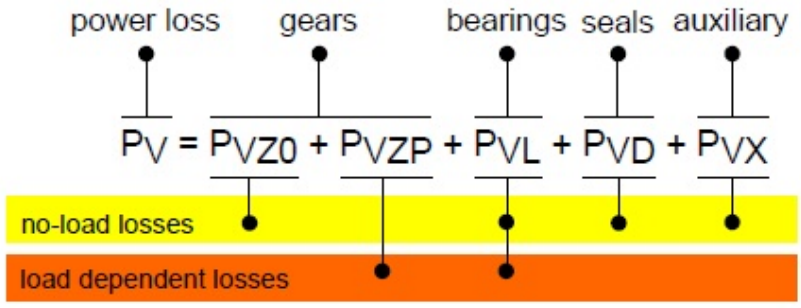

Figure 5.2: No-load and load dependent power losses in a vehicle axle [Höhn et al., 2009].

Axle power losses are originated in two type of losses. No-load losses which occur even without power transmission are generated by gears (P_{VZ0}), rolling bearings (P_{VL}) and seals (P_{VD}). They occur by the motion of the parts inside oil, or the relative motion between

surfaces separated by a lubricant film. The load independent mechanisms are affected by the rotational speed, the operating conditions, the lubricant properties such as viscosity and density of the oil as well the oil level [Bala et al., 2000a, Bala et al., 2000b, Bjornen et al., 2003, Johnston et al., 1991, Andersson, 2014]. The major contributors to no-load losses namely, bearings and gears are considered.

No-load bearing losses depend on its type and size, bearing arrangement, lubricant viscosity and supply [Seabra et al., 2011]. Besides, the no-load gear losses depend on lubricant viscosity as well as on immersion depth in sump lubricated axle [Changenet and Velex, 2008, Höhn et al., 2011].

When the speed is high and dip lubrication is adopted, high no-load losses dominate the total losses.

Load dependent losses generated by the contact between surface of the power transmitting components, gears (P_{VZP}) and rolling bearings (P_{VL}). These losses are related to the transmitted torque, coefficient of friction and sliding velocity in the contact area of the components. Load dependent rolling bearing losses also dependent on type and size, rolling and sliding conditions and lubricant type. In order to have a good predictions of the power losses of the system, each component should be tested separately.

To minimize the torque loss in the axle transmission, car manufactures act simultaneously on load depend and load independent losses, through design and material modifications as well as through improvements in lubrication. In fact during the operation of the axle system, the gear oil provides the important function of lubricating the sliding rolling contacts. The oil also acts as a coolant and removes the heat generated due to efficiency losses. Figure 5.1 shows oil and heat flow in a rear axle.

Chapter 5 outlines the overall power loss sources in automotive axle adopted in this study for the prediction of the mechanical efficiency of the axle and delineates the axle power loss model, to be calibrated and validated experimentally.

5.2. Gear losses

5.2.1. Load dependent gear losses P_{VZP}

Load-dependent losses are those from gears and bearings when torque is transferred. The mechanical power loss at the gear mesh surfaces is expressed with both components sliding and rolling losses.

5.2.1.1. Sliding losses

The sliding friction is a direct product of the relative sliding between the two contacting surfaces. The contact between meshing teeth is the most dominant portion of power loss in gear transmission system mainly in the cases of low speed or/and high torque applications which is the case of my current application of automotive axles.

Ohlendorf, 1958 [Ohlendorf, 1958] introduced an approach for the load dependent losses of spur gears based on the local parameters as shown in Figure 5.3. The low mesh losses can be achieved when the gear contact is around the pitch point C with zero sliding and pure rolling occurs and low value of the coefficient of gear friction. Equation (5.1) is used to calculate the power loss for each point of contact. This local power loss is integrated along the path of contact in order to give the mean value for the gear mesh loss as described in Equation (5.2).

$$P_{VZP}(x) = F_R(x) \cdot v_g(x) = F_N(x) \cdot \mu(x) \cdot v_g(x) \tag{5.1}$$

$$P_{VZP} = \frac{1}{p_{bt}} \int_A^E P_{VZP}(x) dx \tag{5.2}$$

The power loss generated between gear tooth contact can be calculated using Equation (5.3).

$$P_{VZP} = \mu_{mz} \cdot P_{IN} \cdot H_V \tag{5.3}$$

where, μ_{mz} is the mean coefficient of friction in mesh, P_{IN} is the transmitted power and H_V is the gear loss factor.

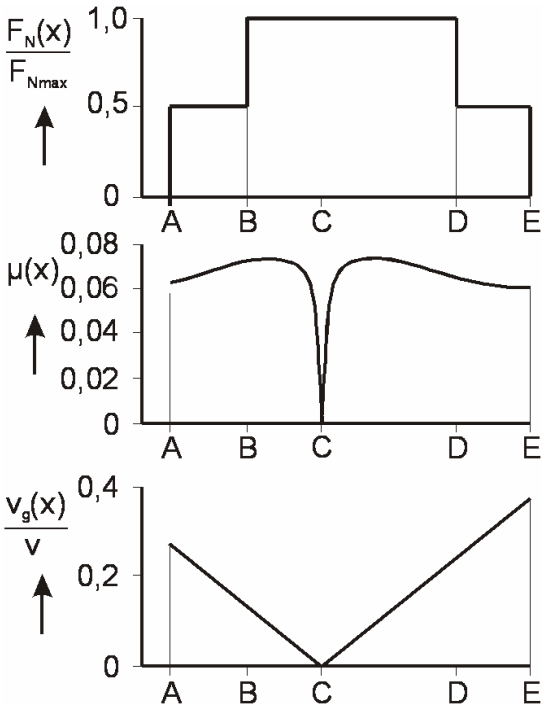

Figure 5.3: The distribution of local relative parameters of load, coefficient of friction and sliding speed along the path of contact [Höhn et al., 2009].

Ohlendorf solved Equation (5.4) in order to obtain the gear loss factor for spur gear, given in Equation (5.5) which it is only valid under the following conditions: $1 \leq \varepsilon_\alpha \leq 2$, $\varepsilon_1 \leq p_{bt}$ and $\varepsilon_2 \leq p_{bt}$.

$$H_V^{Ohlendorf} = \frac{1}{p_{bt}} \cdot \int_A^E \frac{F_N(x)}{F_{bt}} \cdot \frac{v_g(x)}{v_{tb}} dx \tag{5.4}$$

$$H_V = \frac{\pi \cdot (u+1)}{z_1 \cdot u \cdot cos\beta_b} (1 - \varepsilon_\alpha + \varepsilon_1^2 + \varepsilon_2^2) \tag{5.5}$$

where, ε_α is the transverse contact ratio and ε_1 and ε_2 are the pinion and gear addendum contact ratio, respectively.

The Ohlendorf approach is not proved for spur gears with profile shift corrections and even for helical gears.

Wimmer *et al.* [Höhn et al., June 2007] solve the problem of such limitations using the sophisticated calculation method which is the FVA-program RIKOR proven by experimental investigations.

A local gear loss factor H_{VL} with the more realistic load distribution given in Equation (5.7) is solved using such method. The software solved load distribution problem (F_N(x,y), see Equation (5.6)) along the path of contact considering elastic effects.

$$F_N(x,y) = F_{bn} \cdot \frac{1}{\sum_{i=1}^{n} l^i(x,y)} \tag{5.6}$$

where (l^i) is the length of contacting lines along the plane of action.

$$H_{VL}^{Ohlendorf} = \frac{1}{p_{bt}} \int_0^b \int_A^E \frac{F_N(x,y)}{F_{bt}} \cdot \frac{v_g(x,y)}{v_{tb}} dxdy \tag{5.7}$$

where, p_{bt} is the transverse base pitch, F_N is the normal force, F_{bt} is the transverse force to tooth flank, v_g is the sliding velocity and v_{tb} is the absolute tangential speed on the base plane.

Thus, a gear loss factor obtained for almost every gear geometry, with or without profile shift correction, spur or helical gears. Profile modifications are among the ways to reduce the power loss in the meshing gears [Höhn et al., June 2007].

Gears very often operated under mixed film lubrication and a large number of empirical formulae for coefficient of friction (in mixed regime mainly) has been published in the literature [Xu and Kahraman, 2007]. Most of these formulae were obtained by curve fitting of measured data collected from twin-disk type tests. They are based on the following general form [Xu, 2005]:

$$\mu = f(\nu, \eta, v_g, v_r, \rho_{redc}, F_{bt}/b, p_0, R_a) \tag{5.8}$$

Many researchers have attempted to derive a formula for estimating the coefficient of gear tooth friction which are quite different in terms of the parameters that are included. The

empirical formulas can be classified into two types. The first type takes into consideration surface roughness and the other type does not.

Authors [Buckingham, 1958], [Misharin, 1958], [Benedict and Kelley, 1961], [Kelley and Lemanski, 1967], [Drozdov and Gavrikov, 1968] and [Trachman et al., 1977] proposed a coefficient of friction formula based on experimental results which did not take into account the surface roughness parameter. For an accurate estimating gear mesh friction under a mixed lubrication condition where an interaction between surface roughness asperities occur, it is meaningless to do not include such important parameter.

Other works, developed by [O'donoghue and Cameron, 1966], [Drozdov, 1972], [NARUSE and HAIZUKA, 1978] and [Xu et al., 2007], consider the surface roughness with the other external parameters (load, speed, viscosity, radius) in their formulas.

To go further, Schlenk [Schlenk, 1994] proposed Equation (5.9) for the average coefficient of friction along path of contact which is recently introduced in the ISO standard 14179-2 [sta, b]. This formula is the most used as it takes into account not only the oil viscosity but also the influence of the oil formulation also it includes the applied load, the gear geometry, the velocity and the surface finishing. Schlenk's approach is given by Equation (5.9).

$$\mu_{mZ} = 0.048 \cdot \left(\frac{F_{bt}/b}{\nu_{\sum C} \cdot \rho_{redC}} \right)^{0.2} \cdot \eta^{-0.05} \cdot R_a^{0.25} \cdot X_L \tag{5.9}$$

where X_L is the lubricant parameter which allows the correlation of the friction coefficient for each lubricant. Since each lubricant parameter has different values depending on its base oil and additive packages blended on it.

Two other formulas proposed by [Höhn et al., 2001] and [Matsumoto and Morikawa, 2014] not only include the roughness parameter but also include a term for the lubrication condition such as the ratio of surface roughness to the oil film thickness under elastohydrodynamic lubrication (EHL).

Doleschel [Höhn et al., 2001] stated that the coefficient of friction in a gear mesh can be calculated as a combination of a boundary coefficient of friction, μ_{bl}, and of a full-film coefficient of friction μ_{EHD}. Equation (5.10) defines the coefficient of friction μ_{mZ} in mixed lubrication and ζ represents the portion of fluid friction.

$$\mu_{mZ} = (1-\zeta) \cdot \mu_{bl} + \zeta \cdot \mu_{EHD} \tag{5.10}$$

This coefficient of friction was derived from FZG-FVA gear efficiency tests. The portion ζ of fluid and solid friction depends on the relative film thickness Λ as presented in Equation (5.11) and displayed in Figure 5.4 [Höhn et al., 2009].

$$\zeta = \begin{cases} 1-(1-0.5\Lambda)^2, & for\ \ \Lambda \geq 2 \\ 1, & for\ \ \Lambda < 2 \end{cases} \tag{5.11}$$

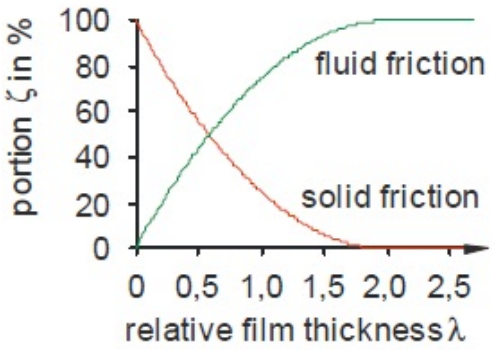

Figure 5.4: Fluid and solid friction in an EHD contact according to Doleschel.

The specific film thickness (or relative film thickness) is presented in Equation (5.12) [Tallian, 1967].

$$\Lambda = \frac{h_{0C}}{\sqrt{R_{a1}^2 + R_{a2}^2}} \tag{5.12}$$

where h_{0C} is the center film thickness and R_a is the arithmetic average surface roughness.

Recently, Matsumoto [Matsumoto and Morikawa, 2014] showed that the equation proposed by Doleschel can correlate very well with experimental results. But in order to estimate the coefficient of friction with high accuracy (see Equation (5.13)), he inserted the sum value of maximum height (R_Z) (peak-to-valley) of the surface roughness of both surfaces in the portion of solid/liquid coefficient of friction. It was found that the boundary load ratio can be expressed with a simple equation defined in (5.14) and (5.15).

$$\mu_{mZ} = (1 - \zeta) \cdot \mu_{EHD} + \zeta \cdot \mu_{bl} \tag{5.13}$$

$$\zeta = 0.5 \cdot logD \tag{5.14}$$

$$D = \frac{R_{Z1} + R_{Z2}}{h_0} \tag{5.15}$$

Figure (5.5) presents the comparison of the load sharing functions of Doleschel and Matsumoto. Matsumoto equation predicts higher coefficients of (μ_{mZ}) higher than Doleschel equation, for the same lubrication regime.

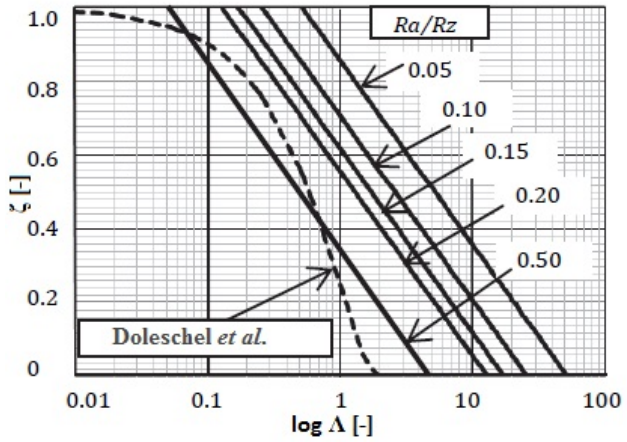

Figure 5.5: Comparison of the boundary lubrication part ratio of Doleschel and Matsumoto for an ISO VG 32 mineral oil without additives with a Type C gear.

5.2.1.2. Rolling losses

Rolling losses represent a small portion of the mesh gear losses. This term is generally neglected in the calculations [Croes and (K.U.Leuven),]. There is no rolling loses when the involute gear has a perfect shape without tooth flexibility. However, these losses can be originated from the tooth deformation and the resistance of the lubricant film. Anderson and Loewenthal [Anderson and Loewenthal, 1980] proposed Equations (5.16) and (5.17) to calculate the rolling losses in a gear mesh.

$$P_{VZP,rolling} = F_R \cdot v_r \tag{5.16}$$

$$F_R = C_R \cdot h_0 \cdot \phi_T \cdot b \tag{5.17}$$

The constant C_R is equal to 9×10^7 and the gear contact film thickness is calculated by Hamrock and Dowson method [Hamrock and Dowson, 1976].

5.2.2. Load independent gear losses P_{VZ0}

The no-load losses (spin losses) occur without any load being transmitted. Due to the rotation of shafts, gears dragged the lubricant. The energy consumed by this process is called the churning losses [Kakavas et al., 2016]. Gear churning losses can be a major contributor of energy dissipation in a gearbox.

They are mainly affected by lubricant viscosity and density as well as immersion depth of the components of a sump lubricated gearbox [Höhn et al., 2011, Seetharaman et al., 2009].

This type of power loss is directly related to the type of lubrication method used. Dip lubrication is often used in low to medium speed automotive gearbox or industrial transmission

applications. When the operating gear speeds are relatively high, jet lubrication is preferred over dip lubrication.

Under dip lubrication, oil churning losses are divided into two categories: losses associated with the interactions between the rotating gears with the fluid and losses due to interaction of the gear at the gear mesh interface with squeezing and pocketing losses being the most relevant mode of power loss. The interaction of the rotating gears can be both with oil (churning) or air (windage) [Seetharaman and Kahraman, 2009, Croes and (K.U.Leuven),]. In automotive applications, for instance, front or rear axles, might rotate at reasonably high speeds (gear pitch-line velocity in excess of 20-30 m/s) to cause important amount of spin losses.

Looking to an alternative of dip lubrication which is jet lubrication. Under jet lubrication, power losses are attributed to windage between the interaction of air/oil-air mixture environments and the rotating gears. The windage losses for gears are due to squeezing of compressible air/oil-air mixture on the meshing gears and to the drag power losses due to air drag along the teeth and sides of rotating gears [Diab et al., 2003].

Both types of spin losses (dip or jet) involve an intrinsic complex hydrodynamic phenomena which are very difficult to describe in analytical formulations. When the majority of the contributing factors are taken into account (gearbox and gears design, rotational speed, oil properties, oil level, etc), the nature of the environment surrounding the gears results in a difficult task to formulate a fluid mechanics based model. Therefore, the most of the published works are empirical or semi-empirical analysis. This means that such models will only be valid in very limited boundary conditions [Croes and (K.U.Leuven), , Changenet and Velex, 2008].

The number of published works about no-load power losses under dip lubrication is much higher than those published about oil jet lubrication.

5.2.2.1. Dip lubrication

In a typical application of automotive gears, splash lubrication appears as the most appropriate solution. However, this lubrication process can be the main dissipation source of churning losses leading to a significant rise in bulk temperatures [Changenet et al., 2006].

A number of studies have been conducted in an effort to try to quantify the power loss due to the churning of the gears in an oil bath. As it is still some debate on which are the parameters which have the most effect on churning losses, different empiric formulations validated with experimental results can be found in literature. The well-known authors with their representative scientific contributions in this field, are [Terekhov, 1975, Walter, 1982, Lauster and Boos, 1983, Mauz, 1987a, Boness, 1989, Michaelis and Höhn, 1994, Hohn et al., 1996, Luke and Olver, 1999, Höhn et al., 2008, Petry-Johnson et al., 2008, Seetharaman et al., 2009].

Terekhov [Terekhov, 1975] and Lauster and Boos [Lauster and Boos, 1983] developed empirical formulas for a dimensionless toque needed in the churning torque calculation from numerous experiments on gears rotating under bath lubrication. Both equations are independent of gear tooth geometry.

Mauz [Mauz, 1987a] showed that with increasing viscosity, churning losses increase for low speeds and decrease churning losses for high speeds (see Figure 5.6).

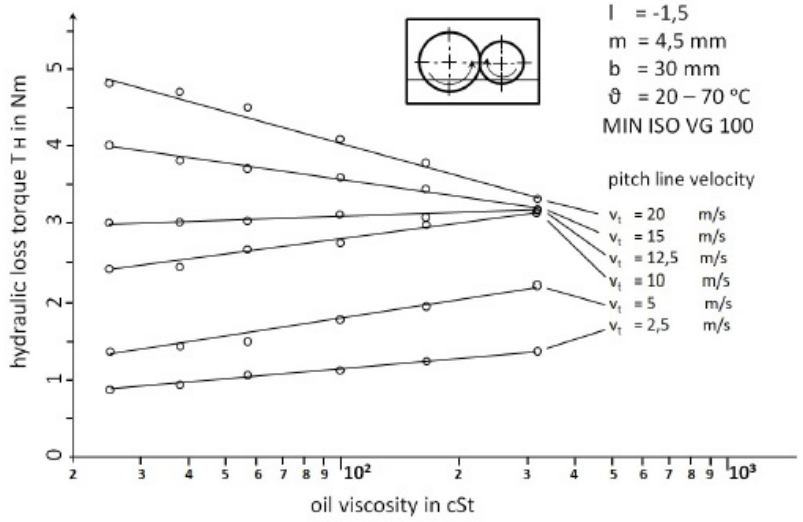

Figure 5.6: Influence of oil viscosity on gear churning losses [Seabra et al., 2011].

Boness [Boness, 1989] carried out friction torque tests using a range of smooth discs of various diameters and widths partially submerged in high-viscosity oil and compared these results to results with a gear. He developed a similar but more simple equation than the empirical formulas proposed by Terekhov [Terekhov, 1975] and Lauster and Boos [Lauster and Boos, 1983].

More recent efforts using similar methods are present in the works of [Hohn et al., 1996,Luke and Olver, 1999, Changenet and Velex, 2007].

The dependence of the spin power loss on viscosity, observed in Mauz and Seetharman *et al.* works, is rather limited or even contradicts the experiments of Luke and Olver [Luke and Olver, 1999] and Changenet and Velex [Changenet and Velex, 2007].

The investigations of H*ö*hn *et al.* [Höhn et al., 2008] showed that gear speed has the largest effect on gear churning losses. The power Losses decrease with decreasing immersion depth. The strong link between high power losses and increasing rotational speed and immersion depth of the gears was also reported by Seetharaman *et al.* [Seetharaman et al., 2009] and Petry-Johnson *et al.* [Petry-Johnson et al., 2008].

Later on, Stavytsky [Stavytskyy et al., 2010] made a review of load independent power loss models and reported that researchers agree that the speed has an important role on the churning losses and the tooth module has little effect on it. Most models take into account the flow regime which is not necessary according to Lauster and Boos [Lauster and Boos, 1983].

Changenet and Velex [Changenet and Velex, 2007] published a comparison between their measurement of churning losses and the predictions using Terekhov [Terekhov, 1975], Lauster and Boos [Lauster and Boos, 1983] and Boness [Boness, 1989] equations.

They concluded that none of the models gives satisfactory correlations over the parameter

range of variation which justify the development of more reliable formulas. The Changenet's gear churning loss model is expressed in Equation (5.18).

$$C_{ch} = \frac{1}{2} \cdot \rho \cdot \omega^2 \cdot r_1^3 \cdot S_m \cdot C_m \tag{5.18}$$

The churning loss depends on the following parameters: the density of the lubricant ρ, the angular frequency ω, the pinion pitch radius r_1, the immersed surface of the pinion S_m (see Figure 5.7) and the dimensionless drag torque C_m.

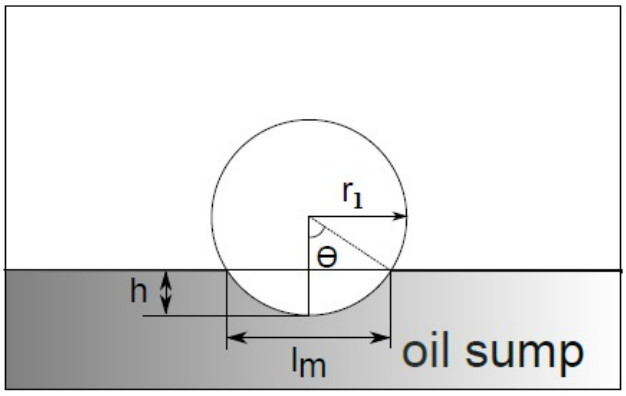

Figure 5.7: Geometrical data of the pinion immersed surface [Changenet and Velex, 2007].

The dimensionless drag group (C_m) was determined from dimensional analysis using the Vashy-Buckingham theorem and is given by Equation (5.19).

$$C_m = \psi_1 \cdot (\frac{m}{d_1})^{\psi_2} \cdot (\frac{b}{d_1})^{\psi_3} \cdot (\frac{h}{d_1})^{\psi_4} \cdot (\frac{V_0}{d_1^3})^{\psi_5} \cdot Re_c^{\psi_6} \cdot Fr^{\psi_7} \tag{5.19}$$

where ψ_i for i=(1..7) are constant coefficients which are derived from experimental results. The Froude number Fr, and the critical Reynolds number Re_c are defined in Equations (5.20) and (5.21), respectively.

$$Fr = \frac{r_1 \cdot \omega^2}{g} \tag{5.20}$$

$$Re_c = \frac{r_1 \cdot b \cdot \omega}{\nu} \tag{5.21}$$

The C_m parameter depends on the flow conditions through the critical Reynolds number (see Equation (5.21)) as defined in the following equations:

For laminar flow, Re_c>6000

$$C_m = 1.36 \cdot (\frac{h}{d_1})^{0.45} \cdot (\frac{V_0}{d_1^3})^{0.1} \cdot Re_c^{-0.21} \cdot Fr^{-0.6} \tag{5.22}$$

For turbulent flow, Re_c>9000

$$C_m = 3.644 \cdot (\frac{h}{d_1})^{0.1} \cdot (\frac{b}{d_1})^{0.85} \cdot (\frac{V_0}{d_1^3})^{-0.35} \cdot Re_c^{-0.21} \cdot Fr^{-0.88} \tag{5.23}$$

In 2009, Seetharaman and Kahraman [Seetharaman and Kahraman, 2009] developed a physics-based fluid mechanics model to predict the no-load losses of gear pairs due to oil churning and windage and presented very promising results.

5.2.2.2. Jet lubrication

The load-independent power loss include windage losses for the case of jet lubrication. Several models have been developed to quantify this type of power loss and the most popular among them are the works of [Ariura et al., 1973, Anderson and Loewenthal, 1982, Mauz, 1987b, Dawson, 1984, Handschuh and Kilmain, 2003, Diab et al., 2003].

Ariura et *al.* [Ariura et al., 1973] is one of the pioneers in the field of churning loss under oil-jet lubrication. They developed the first model for the windage losses based on experimental results. The windage loss is the sum of three terms the oil squeeze by the displacement of the oil in the contact area between the teeth, the ventilation and the acceleration of the oil by gear teeth. These contributions are built up by dimensional analysis and experimental results and resumed in Equation (5.24).

$$P_{VZ0} = P_{VZ0,squeeze} + P_{VZ0,ventilation} + P_{VZ0,acceleration} \tag{5.24}$$

Mauz [Mauz, 1987b] derived the squeeze loss $P_{VZ0,squeeze}$, given by Equation (5.25), by taking into account the usual parameters besides the oil volume flow $\dot{Q}_e$ and nozzle position (see Figure 5.8).

$$P_{VZ0,squeeze} = \omega \cdot 4.12 \cdot C_1 \cdot \rho \cdot \dot{Q}_e^{0.75} \cdot r \cdot (v_t \cdot b \cdot m \cdot \frac{v}{v_0})^{0.25} \cdot (\frac{h_t}{h_{t0}})^{0.5} \tag{5.25}$$

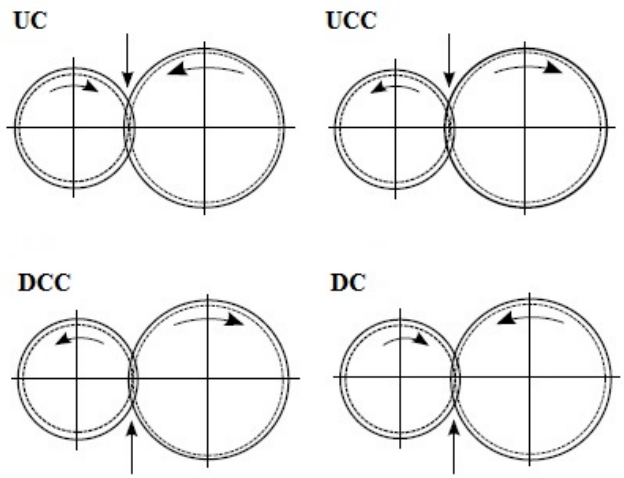

Figure 5.8: Different cases of jet lubrication.

Ariura et *al.* [Ariura et al., 1973] defined the acceleration power loss $P_{VZ0,acceleration}$ as follows:

$$P_{VZ0,acceleration} = \omega \cdot C_x \cdot \rho \cdot \dot{Q}_e \cdot (|v_t| - v_0) \tag{5.26}$$

with C_x coefficient to account for gravity, is equal to 1 for UC and UCC and to 0.9 for DC and DCC.

According to Maurer [Maurer, 1994], the ventilation power loss is composed of two sources, the individual gear (ID) and the mating contact area (CA) as presented in Equation (5.27).

$$P_{VZ0,ventilation} = P_{VZ0,ventilation,ID} + P_{VZ0,ventilation,CA} \tag{5.27}$$

with,

$$P_{VZ0,ventilation,ID} = 1.37 \times 10^{-9} \cdot v_t^{1.9} \cdot d^{1.5} \cdot b^{0.52} \cdot m^{0.69} \cdot \lambda_{wand} \tag{5.28}$$

$$P_{VZ0,ventilation,CA} = 1.17 \times 10^{-6} \cdot v_t^{1.95} \cdot u^{0.73} \cdot b^{1.37} \cdot \lambda_{wand} \tag{5.29}$$

with, λ_{wand} is the factor to take into account the influence of the gearbox geometry.

The previous model is compiled by Clemens *et al.* to calculate the no-load losses under oil jet lubrication.

Other authors like [Anderson and Loewenthal, 1982,Mauz, 1987b,Dawson, 1984,Handschuh and Kilmain, 2003, Diab et al., 2003, Petry-Johnson et al., 2008] proposed unique equations to calculate the windage losses. All of these empirical models can be found in literature [Stavytskyy et al., 2010].

In recent years, CFD (Computational Fluid Dynamics) is becoming more and more attractive approach to estimate the windage losses. Recently, Marchesse *et al.* [Marchesse et al., 2011,

Marchesse et al., 2014] and Fondelli *et al.* [Fondelli et al., 2015] have been studied the oil injection losses by means of CFD simulations, with promising results.

5.3. Rolling bearing losses P_{VL}

Recently, the automotive manufacturers and the rolling bearings manufacturers are trying to improve rolling bearing designs in order to reduce the power loss generated, the energy consumption and the operating temperatures and also to improve the lubrication conditions. At the same time, they claim the lubricant manufacturers to provide new products that increase rolling bearing life, while reducing the energy dissipated [Matsuyama et al., 2004, Hosokawa et al., 2009].

Only a limited number of studies focused on developing the axle rolling bearings friction torque [Spindler and Von Petery, 2003, Matsuyama et al., 2004, von Petery, 2004, Hosokawa et al., 2009].

In order to predict the power loss in rolling bearings, there is many models based on large number of experimental measurements have been developed by bearing manufacturers such as Timken [] (began the manufacture of tapered roller bearings in 1899), SKF [Catalogue, 2005] (founded in 1907), NSK [NSK, CAT. No. E728g] (founded in 1916), FAG [Group, 2011] and NTN [NTN, (CAT. No. 9012/E)].

5.3.1. Sources of friction losses in rolling bearings

Rolling element bearing losses originate from various sources [Xu, 2005]: (i) rolling friction due to deformation and elastic hysteresis at raceway contacts, (ii) sliding friction from unequal curvatures in contact areas, sliding contact of cage with rolling elements and guiding surfaces, sliding between the ends of the rollers and ring flanges, and seal friction, (iii) lubricant friction due to viscous shearing on rolling element, cage and raceway surfaces, and (iv) churning and working of lubricant dispersed within the bearing cavity.

5.3.1.1. Rolling friction

The rolling friction losses in rolling bearings are divided in literature in two main effects: deformation and elastic hysteresis [Harris, 1966, Harris and Kotzalas, 2006].

In rolling bearing, the balls or rollers are the components that exposed to normal loads to the contact area. These normal loads lead to a deformation of the rolling elements and raceways at each contact. As consequence of this deformation and the rolling motion of the roller over the raceway, which requires a tangential force to overcome rolling resistance, the raceway material is squeezed up to form a bulge in the forward portion of the contact, as presented in Figure 5.9a. After that a depression is formed in the rear of the contact area. Thus, an additional tangential force is required to overcome the resisting force of the bulge.

A rolling element under compressive load travels over a raceway, the material in the forward portion of the contact in the direction of rolling undergoes compression while the material in

the rear of the contact is relieved of stress. It is known that as load increases, a given stress corresponds to a smaller deflection than when load decreases, as shown in Figure 5.9b. The area comprised between the curves is called the hysteresis loop, and represents an energy loss (friction power loss). The friction due to elastic hysteresis is generally very small compared with other types of friction presenting in rolling bearing [Harris and Kotzalas, 2006].

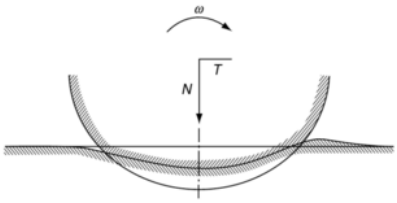

(a) Roller-raceway contact showing bulge due to rolling deformation.

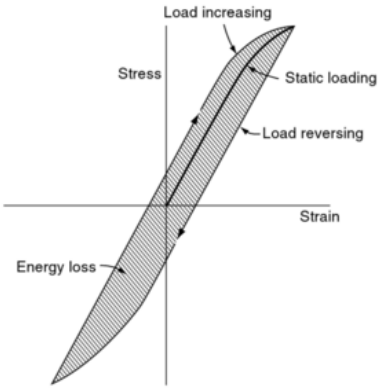

(b) Hysteresis loop for elastic material subjected to reversing stresses.

Figure 5.9: Rolling friction losses in a rolling bearing effects.

5.3.1.2. Sliding friction

The major source of friction during the operation of rolling bearings is sliding. This type of friction occurs mainly due to microslip and rolling motion [Harris and Kotzalas, 2006]. If the rolling bearing operates without misalignment under moderate speed, the gross sliding in the roller–raceway contacts would not occur. Depending on the elastic properties of the contacting bodies and the coefficient of friction between the contacting surfaces, microslip could occur and energy loss is produced.

A rolling bearing under simple radial load, a single contact pure rolling can only occur at two points, designated 'A' (see Figure 5.10a). For all other points along the contact, sliding must occur in a direction parallel to rolling motion. Outside of points A, sliding is oriented in one direction and between points A sliding occurs in opposite direction. It assumes that the coefficient of friction is not sufficiently great to cause the possibility of a locked region as shown in Figure 5.10b. In the case of lubricated bearings this never happens because the coefficient of friction is not very high.

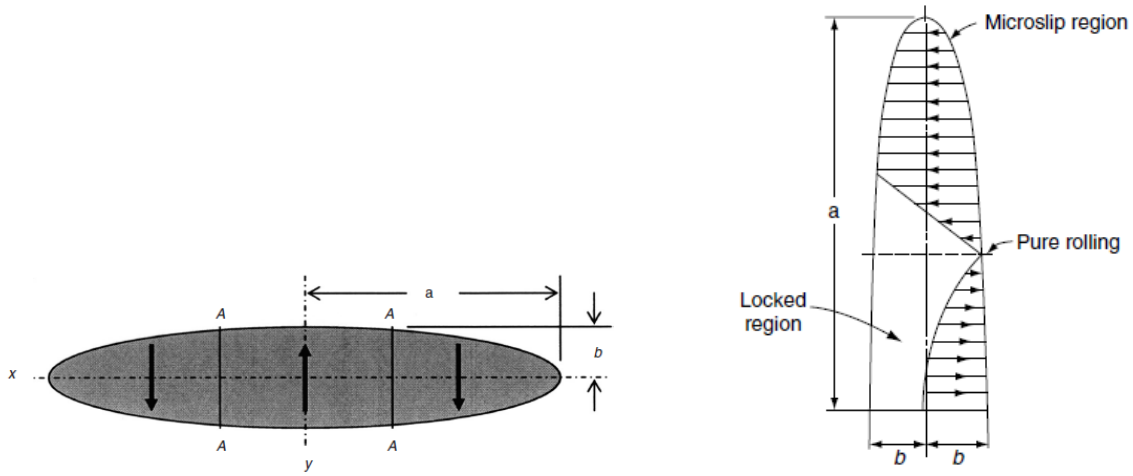

(a) Sliding directions.

(b) Locked region.

Figure 5.10: The sliding direction for ball–raceway elliptical contact area in a radially loaded, radial bearing.

5.3.1.3. Drag friction

The drag friction in oil bath lubrication considers resistance of the rolling elements when moving through the oil. The lubricant builds up a film between the raceway and the rolling elements. Usually, from the oil provided to cool and lubricate the contact, only a small portion is used to build up the fluid film. The excess of oil acts as a friction force contrary to the rotational speed of the rolling elements. The power loss due to drag friction includes the effects of the viscosity of the lubricant and the speed.

5.3.1.4. Rolling bearing seals friction

Seals are used to prevent the bearing to become contaminated with moisture, corrosive media or any other material. Additionally the seal retains the lubricant in the housing. The contact between the rubber of the seal and the shaft generates friction and must be considered as a source of power loss. The loss due to seals friction is mainly dependent on the rotational speed [Fernandes, 2015].

5.3.2. Rolling bearing friction torque models

5.3.2.1. Avrid Palmgren model (1959)

Harris [Harris, 1966] reported that the most widely accepted bearing efficiency formulation which is based on the original formulations of Palmgren.

Palmgren [Palmgren, 1959] empirically evaluated bearing friction torque due to all mechanical friction phenomena.

A reasonable estimate of the bearing friction moment of a rolling bearing element without taking account for friction torque due to seals can be written as the sum of load independent (M_0) and load dependent (M_1) losses (see Equation (5.30)). Since M_0 and M_1 are based on empirical formulas, the cage friction in rolling element pockets, the cage guiding surfaces and the viscous friction are included.

$$M_t = M_0 + M_1 \tag{5.30}$$

The load independent fiction torque M_0 is given by Equation (5.31) and it depends on the lubricant kinematic viscosity (ν), on the bearing speed (n) and the factor (f_0) which depends upon the rolling bearing geometry and method of lubrication.

$$M_0 = 10^{-7} \cdot f_0 \cdot (\nu \cdot n)^{2/3} \cdot d_m^3 \tag{5.31}$$

The second component is the load dependent moment M_1 which is the result of rolling and sliding friction in loaded rolling contacts. It depends on the function of the bearing type (f_1) and on the equivalent bearing load (P_1).

$$M_1 = f_1 \cdot P_1 \cdot d_m \tag{5.32}$$

Through experimental tests using different bearing sizes and types, Palmgren evaluated the rolling bearing friction torque. The values of the parameters f_0 and f_1 were determined for each type of rolling bearing [Palmgren, 1959].

5.3.2.2. New SKF friction torque model (2004)

In order to calculate the total friction torque generated in rolling bearings, SKF presented a detailed model [Catalogue, 2005] where the total friction torque is the sum of four different physical sources of torque loss, presented by Equation (6.12).

$$M_t = M'_{rr} + M_{sl} + M_{seal} + M_{drag} \tag{5.33}$$

where

- M_t - Total frictional torque [Nmm];
- M'_{rr} - Rolling frictional torque [Nmm];
- M_{sl} - Sliding frictional torque [Nmm];
- M_{seal} - Frictional torque of the seals [Nmm];
- M_{drag} - Frictional torque of drag losses, churning, splashing, etc, [Nmm].

Then, the power loss in the rolling bearings can be calculated when the rotational speed n of the bearing is known, as given in Equation (5.34):

$$P_{VL} = M \times n \times \frac{\pi}{30} \times 10^{-3} \tag{5.34}$$

Figure 5.11 displays the variation of the frictional moment of the bearing with speed or lubricant viscosity. It is observed that in the first zone, as speed or viscosity increases, the frictional moment decreases as the film is still being formed. As speed or viscosity continue to increase and the bearings enters a full elasto-hydrodynamic lubrication (EHL) and the film thickness increases which leads to increase the friction torque. In the case when the speed and viscosity continue to increase the friction torque eventually remains constant or even decrease due to the inlet shear heating and kinematic starvation.

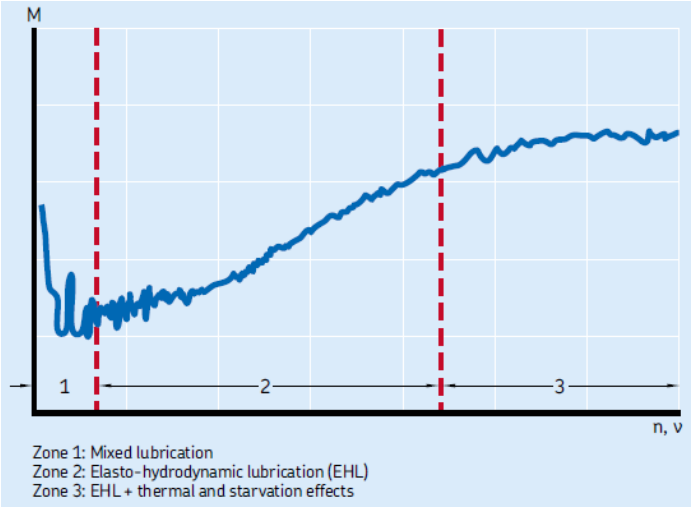

Figure 5.11: Bearing frictional moment as function of speed or viscosity [SKF, 2013].

To accurately calculate the total frictional moment in rolling bearing, their different sources and their tribological effects must be taken into account.

As the SKF model closely follows the real behaviour of the bearing, it details very well the different sources of the total friction torque are presented in the following items.

• Rolling Friction Torque - M_{rr}

The rolling frictional moment is calculated using Equation (5.35).

$$M_{rr} = G_{rr} \cdot (\nu \cdot n)^{0.6} \tag{5.35}$$

where ν is the kinematic viscosity of the lubricant at operating temperature in mm^2/s, n is the rotational speed in $\mathrm{r/min}$ and G_{rr} represents the load distribution in rolling contacts and it depends mainly on the bearing type, the bearing mean diameter (d_m) and the radial (F_r) and axial (F_a) loads.

Including the inlet shear heating (ϕ_{ish}) and the kinematic replenishment/starvation effects (ϕ_{rs}), the rolling frictional moment can be expressed by the following equation.

$$M'_{rr} = \phi_{ish} \cdot \phi_{rs} \cdot [G_{rr} \cdot (\nu \cdot n)^{0.6}] \tag{5.36}$$

Figure 5.12 shows the typical behaviour of the rolling torque including (M'_{rr}) and not including (M_{rr}) the reduction factors.

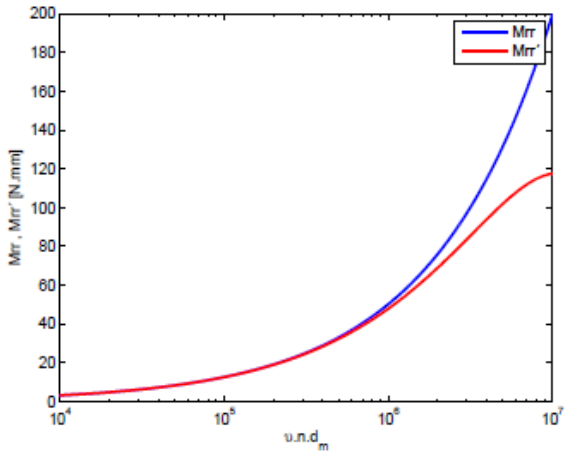

Figure 5.12: Variation of the rolling torque M_{rr} and M'_{rr} with the operating parameter ν.n.dm [Fernandes, 2015].

• Sliding Friction Torque - M_{sl}

The sliding friction torque is calculated using Equation (5.37).

$$M_{sl} = G_{sl} \cdot \mu_{sl} \tag{5.37}$$

where G_{sl} represents the influence of the bearing load on the sliding friction and depends on the bearing type, the bearing mean diameter (d_m) and the radial load (F_r) and axial load (F_a).

Also to calculate the sliding friction torque another term should be calculated which is the sliding friction coefficient μ_{sl}. It strongly depends on the lubrication regime, which is defined here by ϕ_{bl}. For full film lubrication μ_{sl} mostly depends on lubricant shearing (film thickness thick enough to completely separate the surfaces in contact) and for boundary lubrication on asperity contacts (film thickness not thick enough to completely separate the surfaces in contact). It is given by Equation (5.38).

$$\mu_{sl} = \phi_{bl} \cdot \mu_{bl} + (1 - \phi_{bl}) \cdot \mu_{EHL} \tag{5.38}$$

where μ_{bl} is the coefficient of friction in boundary lubrication and it depends mainly on the additive package in the lubricant, and μ_{EHL} is the coefficient of friction in full-film conditions and it depends strongly on the lubricant rheology and the contact area, then ϕ_{bl} is the weighting factor for the sliding friction coefficient and is determined by Equation (5.39).

$$\phi_{bl} = \frac{1}{e^{2.6 \cdot 10^{-8} \cdot (n \cdot \nu)^{1.4} \cdot d_m}} \tag{5.39}$$

Figure 5.13 presents the typical curve of ϕ_{bl} for the same inputs of speed, viscosity and bearing geometry. This Figure show that the full-film lubrication occurs when the weighting factor tends to zero and the transition to mixed lubrication can occur when the weighting factor is between zero and 1 ($0 < \phi_{bl} < 1$).

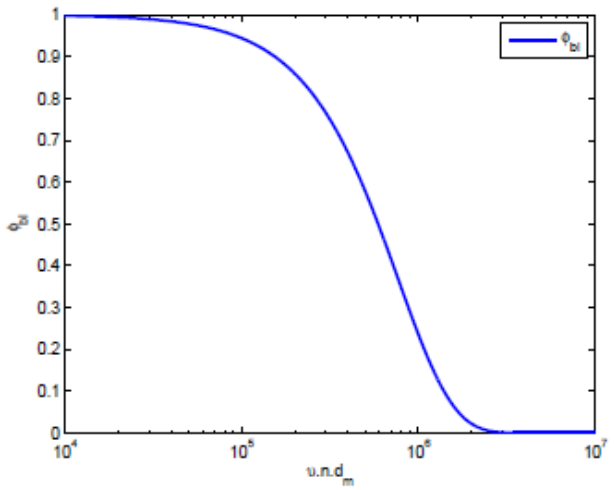

Figure 5.13: Variation of the weighting factor ϕ_{bl} with the operating parameter $\nu.n.d_m$ [Fernandes, 2015].

SKF recommends μ_{bl} = 0.15 and μ_{EHL} = 0.002 for tapered roller bearings (TRB), μ_{EHL} = 0.05 for mineral oils and μ_{EHL} = 0.04 for synthetic oils.

• Seals Friction Torque - M_{seal}

The seals friction torque for bearings that are sealed on both sides can be calculated using Equation (5.40).

$$M_{seal} = K_{S1} \cdot d_s^{\beta_R} + K_{S2} \tag{5.40}$$

where the constants K_{S1}, d_s, β_R and K_{S2} are dependent on the seal type and the bearing type and size.

• Drag Friction Torque - M_{drag}

The drag losses occur when the bearing is rotating in oil bath lubrication. Drag losses are influenced by bearing speed, oil viscosity and oil level and also by the size and geometry of the oil reservoir.

The rolling bearing drag losses are given by equation (5.41) for ball bearings or by Equation (5.42) for roller bearings.

$$M_{drag} = 0.4 \cdot V_M . K_{ball} . d_m^5 . n^2 + 1.093 \times 10^{-7} \cdot n^2 \cdot d_m^3 \cdot \left(\frac{n \cdot d_m^2 \cdot f_t}{\nu} \right)^{-1.379} \cdot R_s \tag{5.41}$$

$$M_{drag} = 4 \cdot V_M \cdot K_{roll} \cdot C_w \cdot B \cdot d_m^4 \cdot n^2 + 1.093 \times 10^{-7} \cdot n^2 \cdot d_m^3 \cdot \left(\frac{n \cdot d_m^2 \cdot f_t}{\nu} \right)^{-1.379} \cdot R_s \quad (5.42)$$

A detailed description of the new SKF rolling bearing friction torque model is given in Appendix E.

5.3.2.3. Comparison between the friction torque models presented

The first detailed approach to friction torque calculation of rolling contact bearings was published by Palmgren [Palmgren, 1959]. He proposed to split the friction torque into a load dependent torque and a load independent torque parts. The investigations by Harris [Harris, 1966] and INA/FAG [IIN,] are based on [Palmgren, 1959] and have been used for a long time. The relatively new approach by SKF [Catalogue, 2005] allows more detailed investigations because the losses are affected to the places where they occur in the bearing [Schlegel et al., 2009].

To evolve more difference between these models, a simulation was performed using Palmgren and New SKF model for Cylindrical Roller Thrust Bearing 81107 under a constant temperature of 90 °C and under different rotational speeds. The factors used for Palmgren simulation are $f_0 = 3$ and $f_1 = 0.0015$ and for the New SKF simulation are $\mu_{bl} = 0.15$ and $\mu_{EHL} = 0.04$ for the selected type of rolling bearing.

Figure 5.14 shows the results of the simulation for two tests performed under constant temperature conditions and two applied loads with cylindrical roller thrust bearing lubricated with 75W90-A axle gear oil.

It is clear that the prediction of the New SKF model is more or less good at higher speed as it gives a closer value to the experimental results under 4000 N of load (see Figure 5.14a). For low speeds, the New SKF model predicts a friction torque very different from the measured one. While at higher load, this model gives different values of friction torque from the experimental results but it follows the behaviour of the experimental friction torque with rotational speed. The Palmgren model is independent of the rotational speed and the friction torque calculated is not close to the experimental results. This model show worst correlation with experimental results. As any friction torque model, it is possible to calibrate the model according to the experimental data. Palmgren model takes into account the influence of the temperature and the the rotational speed through the oil viscosity. An adjustment for the factors of the Palmgren model for different rolling bearing geometry is required to obtain an accurate prediction. The New SKF model simulates the influence of the lubricant temperature, the rotational speed and also the lubrication conditions. For constant temperature and when the speed increases, the lubrication regime evolves from boundary to full-film conditions, consequently, the parameter ϕ_{bl} decreases from 1 to 0. This reveals that μ_{bl} has a strong influence at low speeds. In order to predict the rolling bearing friction torque effectively using this type of model, a new values for μ_{bl} and μ_{EHL} should be determined for each oil, independently of the rolling bearing geometry. This is the major advantage of the new SKF rolling bearing friction torque model.

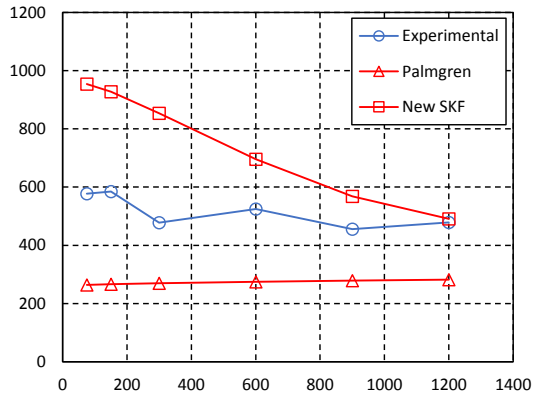

(a) 4000 N; T = 90 °C.

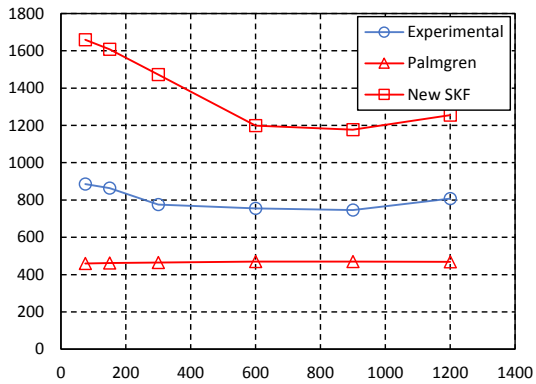

(b) 7000 N; T = 90 °C.

Figure 5.14: Experimental results of 75W90-A oil against different friction torque models.

5.4. *Shaft seal losses P_{VD}*

The seal losses as one of the contributor to the rolling bearing power loss were discussed in the prior section. However, the use of seals in the shafts are very usual in axles and should be taken into account in the total power loss. Due to the friction between the sealing lip and the rotating shaft, seals may contribute approximately 5 % to 15 % of the total power loss of the axle [Lin et al., 2005]. The seal component was used on the shaft to avoid air and oil leakage along with minimum friction losses. In most case the seals losses are less than 0.01 % of the nominal transmitted power, a very small value when compared to the other losses in the axle (valid for low tangential speeds).

The power losses in seals were estimated by Linke [Linke, 1996] and by Kettler [Kettler, 2002] and their approaches have been in used due to their simplicity compared with other approaches. Linke defined the power losses in seals as follows:

$$P_{VD} = [145 - 1.6 \cdot T_{oil} + 350 loglog(\upsilon_{40} + 0.8)] \cdot d_{sh}^2 \cdot n \times 10^{-7} \tag{5.43}$$

Keller gives a different formulation for the seals friction torque:

$$P_{VD} = 7.9163 \times 10^{-6} \cdot F_{D,\rho} \cdot d_{sh}^2 \cdot n \tag{5.44}$$

The factor $F_{D,\rho}$ represents the effect of the temperature dependent viscosity change. This method to calculate seal losses can be found in Andersson [Andersson, 2014], Martins, Moura and Seabra [Martins et al., 2006b].

The seal manufacturers as e.g Freudenberg [kat, 1976] proposed a simple equation for prediction of seal losses that only considers the shaft diameter d_{sh} and the rotational speed n.

After a large number of measurements, Freudenberg Simrit observed that the seal losses are function of seal diameter and rotational speed.

The experimental work of Freudenberg summarized in Equation (5.45) to predict seal losses. The formula only takes into account the shaft diameter and the rotational speed while the oil effect is not considered.

$$P_{VD} = 7.69 \times 10^{-6} \cdot d_{sh}^2 \cdot n \tag{5.45}$$

Using the following formula, the same shaft seal losses for all lubricants are obtained. P_{VD} increases with tangential speed at the seal lip as shown in Figure 5.15. When the seal diameter increases the seal losses become very significant and cannot be disregarded and when the seal diameter is low, the torque loss or power loss is usually very small.

The shaft seal torque loss was quite substantially influenced with different pressure at the seal lip which is designed into the seal and also with different seal materials.

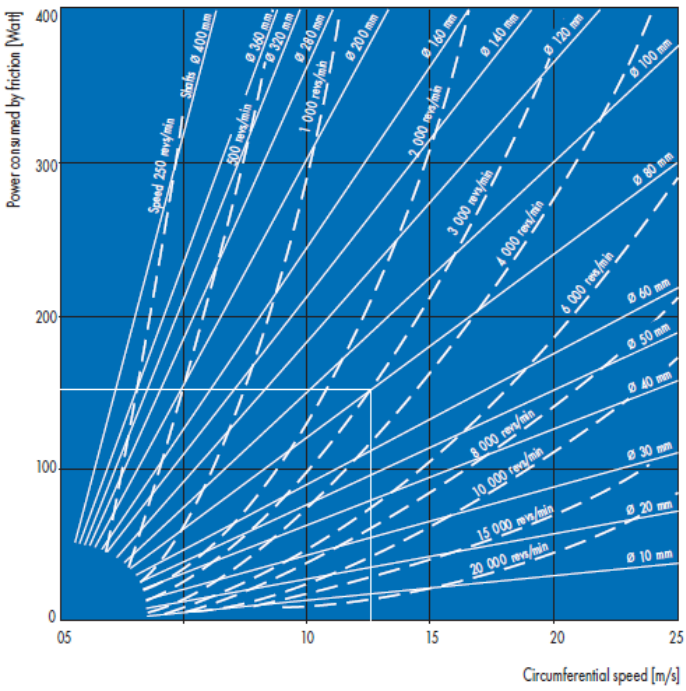

Figure 5.15: Recommended values for the friction loss on a Simmerring in engine oil SAE 20, at T=100 °C [Simmerrings and Seals,].

5.5. *Auxiliary losses* P_{VX}

The auxiliary losses represent other dissipative sources that are not generated by gears, bearings or seals e.g oil pumps have to be taken into consideration.

5.6. Experimental determination of gear power loss

A gearbox cannot be considered as a single entity but it is in fact a complete subsystem. The power loss occurring in a gearbox are generated by different mechanisms. To model the losses of such a gearbox, it should be taken into account the seal losses which are the less important source of power loss and will be determined using the Freudenberg equation plus the rolling bearing power loss which will be determined using the new SKF friction. Both seals and bearings losses add a considerable amount to the total power loss in gearboxes [Lin et al., 2005].

For this work the experimental results are used mainly to predict the most important source of power loss which is dissipated in gears. As the no-load gear power losses are difficult to predict (section 5.2.2), they were experimentally measured for each gear oil formulation and operating speed, using a special test procedure.

For all combinations of the operating conditions (input torque (load stage *i*), speed and operating temperature), the overall torque loss in an FZG gearbox can be calculated using Equation (5.46).

$$P_V^i = P_{VZ0}^i + P_{VZP}^i + P_{VL}^i + P_{VD}^i \tag{5.46}$$

Under the same speed and temperature, the power loss under the load stage 1 (low input speed, T_{IN} = 3.3 Nm) is expressed in the following Equation (5.47).

$$P_V^1 = P_{VZ0}^1 + P_{VZP}^1 + P_{VL}^1 + P_{VD}^1 \tag{5.47}$$

It is assumed that the P_V^1 term is determined experimentally at load stage K1. The no-load gear losses are independent of the torque which results in Equation (5.48).

$$P_{VZ0}^i = P_{VZ0}^1 = P_{VZ0}, \forall \ i \tag{5.48}$$

Assuming also for load stage K1, the friction power loss in the meshing gears is equal to zero.

$$P_{VZP}^1 \approx 0 \tag{5.49}$$

For this load stage, the rolling bearing power losses P_{VL}^1 are calculated using new SKF model. The seal power losses are calculated using Equation (5.45), which are independent of the applied load resulting in Equation (5.50).

$$P_{VD}^i = P_{VD}^1 = P_{VD}, \forall \ i \tag{5.50}$$

Finally, Equation (5.51) gives the equation of the total power loss at K1 load stage.

$$P_V^1 = P_{VZ0} + P_{VL}^1 + P_{VD} \tag{5.51}$$

After that, it is possible to determine the no-load gear loss (P_{VZ0}) using Equation (5.52).

$$P_{VZ0} = P_V^{1\ exp} - P_{VL}^1 - P_{VD} \tag{5.52}$$

The load dependent gear losses for any load stage (i) and input speed are calculated, according to Equation (5.53), by subtracting of the total experimental power loss by the rolling bearings losses, the seal losses and the no-load losses previously calculated in Equation (5.52).

$$P_{VZP}^i = P_V^{i\ exp} - P_{VL}^i - P_{VD} - P_{VZ0} \tag{5.53}$$

5.7. Coupling gearbox power loss model with a thermal balance model

Power loss sources presented in the previous sections showed that most of the parameters depend on oil temperature and that the oil temperature influences the overall power loss of the gearbox.

Höhn *et al.* [Hohn et al., 1996] introduced an energetic model of the FZG gearbox where it is integrated both mechanisms of power dissipation and heat evacuation in order to determine its operating equilibrium temperature, as given in Equation (5.54). The model was calibrated using power loss and wall and oil temperatures measured in a FZG machine.

$$P_{VZ0} + P_{VZP} + P_{VL} + P_{VD} = Q_{conv} + Q_{rad} + Q_{cond} \tag{5.54}$$

Different load stages and temperatures on FZG machine cause different pressure and friction values due to the teeth meshing, generating a heat dissipation source in between the pinion and wheel teeth [Prakash del Valle, 2014].

After correlation between experimental and model results, the lubricant friction coefficient on the meshing gears can be optimized for different oil formulations.

The friction coefficient between gear teeth for mineral and ester base oils were optimized in the works developed by Martins *et al.* [Martins et al., 2004, Martins et al., 2005, Martins et al., 2006a, Oliveira et al., 2006, Martins et al., 2008b].

Figure 5.16 shows the different mechanisms of power dissipation and heat evacuation as Martins *et al.* [Martins et al., 2006a] proposed.

Equations (5.55) and (5.56) allow to calculate the heat evacuated by radiation based on Stefan Boltzmann law.

$$Q_{rad} = \alpha_{rad} \cdot A_{rad} \cdot (\theta_{oil} - \theta_a) \tag{5.55}$$

$$\alpha_{rad} = 0.23 \times 10^{-6} \cdot \varepsilon \cdot \left(\frac{\theta_{oil} + \theta_a}{2} \right)^3 \tag{5.56}$$

The heat dissipation by convection is defined in Equation (5.57).

$$Q_{conv} = (\alpha_{conv,v} \cdot A_v + \alpha_{conv,h} \cdot A_h) \cdot (\theta_{oil} - \theta_a) \tag{5.57}$$

The vertical and horizontal coefficients of natural convection ($\alpha_{conv,v}$ and $\alpha_{conv,h}$) are given in Equations (5.58) and (5.59), respectively.

$$\alpha_{conv,v} = 11.06 \cdot h_{ca}^{-0.1} \cdot \left(\frac{\theta_{oil} - \theta_a}{\theta_a} \right)^{0.3} \tag{5.58}$$

$$\alpha_{conv,h} = 12.87 \cdot L_{ca}^{-0.04} \cdot \left(\frac{\theta_{oil} - \theta_a}{\theta_a} \right)^{0.32} \tag{5.59}$$

The heat conduction is the most complex form of heat in FZG gearbox. For that, it is estimated in Equation (5.60) as function of the radiation and convection heat.

$$Q_{cond} = (Q_{rad} + Q_{conv}) \cdot c_f \cdot \frac{A_{base}}{A_{ca}} \tag{5.60}$$

with the conduction factor (c_f) is equal to 1.5.

So, the total heat evacuated in FZG gearbox is expressed in Equation (5.61).

$$Q_T = Q_{rad} + Q_{conv} + Q_{cond} \tag{5.61}$$

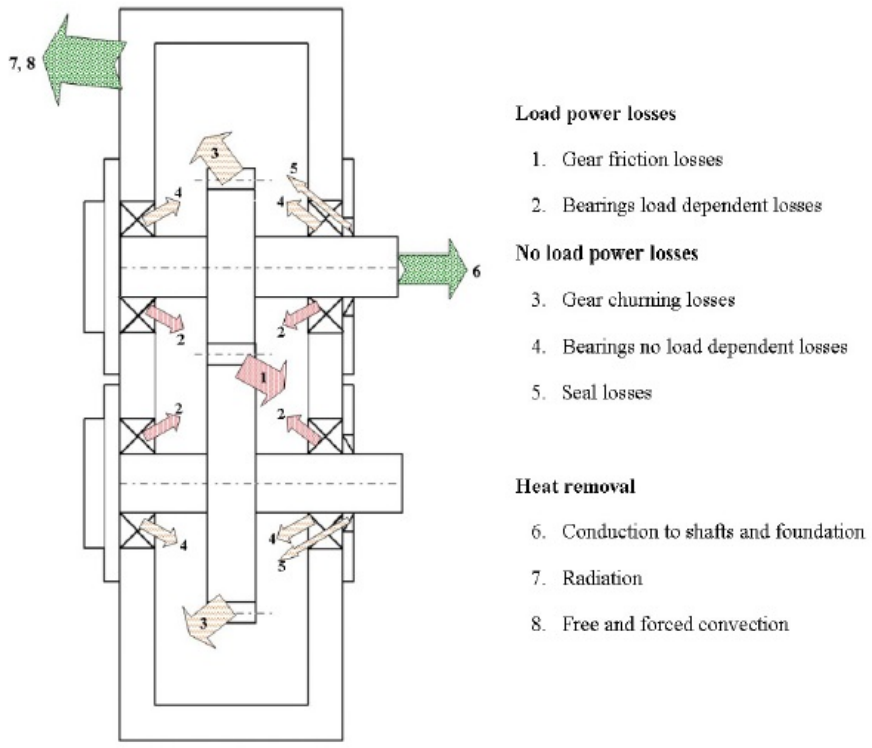

Figure 5.16: Schematic view of the different power loss sources and heat evacuation mechanisms [Martins et al., 2006a].

Recently, a second model, different from the model used by Höhn *et al.* [Hohn et al., 1996] and Martins *et al.* [Martins et al., 2006a], is set up. Changenet *et al.* [Changenet et al., 2006, De Gevigney et al., 2012] proved that isothermal approaches based on the oil sump temperature underestimate gearbox efficiency and he suggested a thermal network method based on different nodal temperatures locations along the gearbox. The advantages of this model is to provide a more detailed thermal mapping in the gearbox through the prediction of bulk temperature of the oil in each contact. The thermal network follows the electrical network laws (see Figure 5.17).

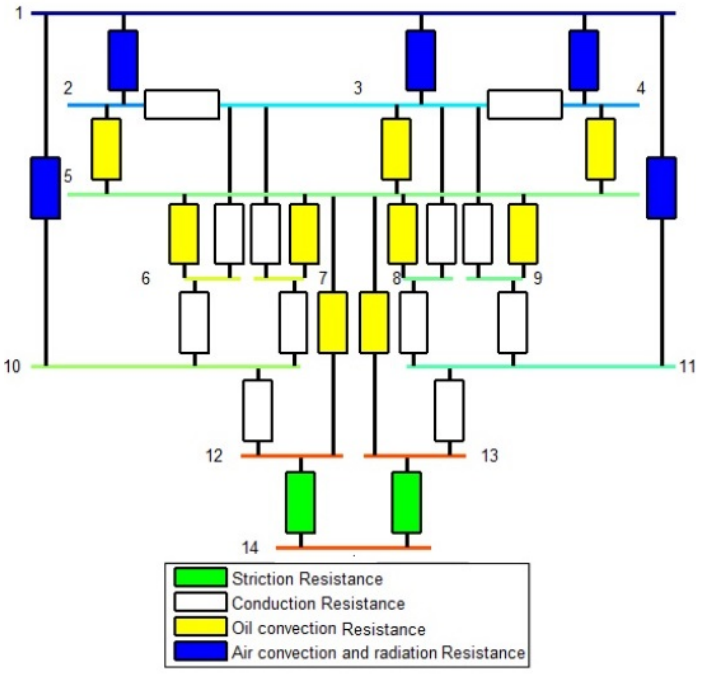

Node	Element
1	Ambient air
2	Lower part of the casing
3	Lateral part of the casing
4	Top part of the casing
5	Oil sump
6	Pinion shaft bearing
7	Pinion shaft bearing
8	Gear shaft bearing
9	Gear shaft bearing
10	Pinion shaft
11	Gear shaft
12	Pinion
13	Gear
14	Meshing of gear teeth

Figure 5.17: Thermal network of FZG machine [Prakash del Valle, 2014].

5.8. Summary

This chapter gives an overview of the the different power loss mechanisms in a gearbox and the corresponding models used in literature. A detailed description is restricted to gears, bearings and seals losses.

The load independent gear losses were measured and not predicted due to the difficulties to quantify it under several gearbox designs, operating conditions and lubrication methods (dip or oil-jet lubrication). The load dependent losses were defined and several approaches were compared. To compute this type of power loss, different coefficient of friction formulas and gear loss factor equations were presented.

Several models of rolling bearing power loss were discussed and compared. The new SKF model seems to represent very well the influences of the rolling bearing type and geometry, of the oil formulation and of the lubrication regime.

Finally, the gearbox power loss model prediction is given in Equation (5.62) and to correlate between model prediction and experimental results Equation (5.63) is used.

$$P_V^i = \underbrace{P_{VZ0}}_{P_V^{1\ exp}-P_{VL}^1-P_{VD}} - \underbrace{P_{VZP}^i}_{\mu_{mz}\cdot P_{IN}\cdot H_V} - \underbrace{P_{VL}^i}_{NewSKFModel} - \underbrace{P_{VD}}_{SimritEquation} \tag{5.62}$$

$$P_V^i = \underbrace{P_{VZ0}}_{P_V^{1\ exp}-P_{VL}^1-P_{VD}} - \underbrace{P_{VZP}^i}_{P_V^{i\ exp}-P_{VL}^i-P_{VD}-P_{VZ0}} - \underbrace{P_{VL}^i}_{NewSKFModel} - \underbrace{P_{VD}}_{SimritEquation} \tag{5.63}$$

6. Rolling bearings experimental results

6.1. Introduction

The main function of rolling bearings in axles is to support the pinion and the differential gear under high load carrying capacity and high stiffness. However, the rolling bearings are a major contributor to axle system power loss [Matsuyama et al., 2004].

To achieve high efficiency in axle differentials, the reduction of internal friction torque in rolling bearings is of major concern. Thus, the importance of understanding internal friction in rolling bearings becomes relevant. The energy saving and the bearings performance optimization are required [Cousseau et al., 2010].

The energy consumption due to rolling bearing power loss is becoming more and more important when taking into account the focus of science and industry on this issue.

Recently, the automotive manufacturers and the rolling bearings manufacturers are trying to improve rolling bearing designs in order to reduce the power loss generated, reduce the energy consumption, reduce the operating temperatures and improve the lubrication conditions. At the same time, they claim the lubricant manufacturers to provide new products that increase rolling bearing life, while reducing the energy dissipated [Matsuyama et al., 2004, Hosokawa et al., 2009].

Several authors have studied the rolling bearings friction torque. Spindler [Spindler and Von Petery, 2003] developed a new bearing design, where the tapered roller bearings used previously have been replaced by angular contact ball bearing, that meets the requirements for high rigidity, long life and no preload loss during operation. Matsuyama *et al.* [Matsuyama et al., 2004] developed a super-low friction torque tapered roller bearing (80 % torque reduction from that of a standard bearing). Hoshokawa *et al.* [Hosokawa et al., 2009] developed a new bearing concept which is the double row angular contact ball bearing -so-called Tandem Ball Bearings for rear axle drives. This bearing concept not only increases the service life but also make significant contribution to lower fuel consumption.

This chapter provide more new knowledge about rolling bearings lubricated with axle gear oils. Extensive tests were performed and a considerable amount of experimental results of power loss in rolling bearings, difficult to find in literature, were obtained. The SKF rolling bearing friction torque model defined in section 5.3 will be calibrated with the experimental results. The model allows a better understanding of the behaviour of different rolling bearing geometries and of the influence of oil formulation. The rolling bearing power loss model will be relevant for the global axle differential power loss model predictions.

6.2. Test equipment and methods

6.2.1. Rolling bearing assembly

The rolling bearing assembly was presented with detail in section 4.3.1.1.

The modified Four-Ball machine permits the measurements with different types of rolling bearings including thrust ball bearings (SKF ref.51103, ref.51107), cylindrical roller thrust bearings (SKF ref.81102 TN and ref.81107 TN), angular contact ball bearings (SKF ref.7203 and ref.7204) and tapered roller bearings (SKF ref.30302 J2, ref.30203 J2 and ref.320/28 X/Q) whose dimensions are limited by the bearing housing and the machine it self.

6.2.2. Rolling bearings tested

A wide range of rolling bearing geometries might be used. The axle contains eight bearings, four rolling bearings in the differential assembly where two are used to support the input pinion and two more to support the crown wheel. Two other type of rolling bearings on the outboard end of each of the two half shafts. But these outer bearings are physically remote from the main drive unit they are considered thermally distinct and their contribution was neglected [Kolekar et al., 2013].

The modified Four-Ball Machine permits the friction torque measurements with specific types of rolling bearings whose dimensions are limited by a maximum outer diameter of 56 mm and a maximum width of 16 mm.

With such limitations, it is crucial to understand the behaviour of different rolling element bearings, understand the lubrication capabilities of different axle gear oils and try to reduce the power loss in rolling bearings, knowing the influence of several parameters such as speed, load, oil formulation and bearing geometry.

The experimental tests were performed with three type of rolling bearing geometries lubricated with the selected axle gear oils. The geometries selected were the Thrust Ball Bearing SKF ref. 51107 (TBB), Cylindrical Roller Thrust Bearing SKF ref. 81107 (RTB) and Tapered Roller Bearings (TRB) ref. 320/28 X/Q. The dimensions and characteristics of the selected geometries are reported in Table 6.1 and Figure 6.1.

Table 6.1: Characteristics of TBB 51107, RTB 81107 TN and TRB 320/28 X/Q.

			TBB 51107	RTB 81107 TN	TRB 320/28 X/Q
Principal dimensions	d	mm	35		28
	H	mm	12		16
	D	mm		52	
Basic load ratings	Dynamic C	kN	19.9	29	31.9
	Static C_0	kN	51	93	38
Speed ratings	Reference speed	rpm	5600	2800	9500
	Limiting speed	rpm	7500	5600	13000

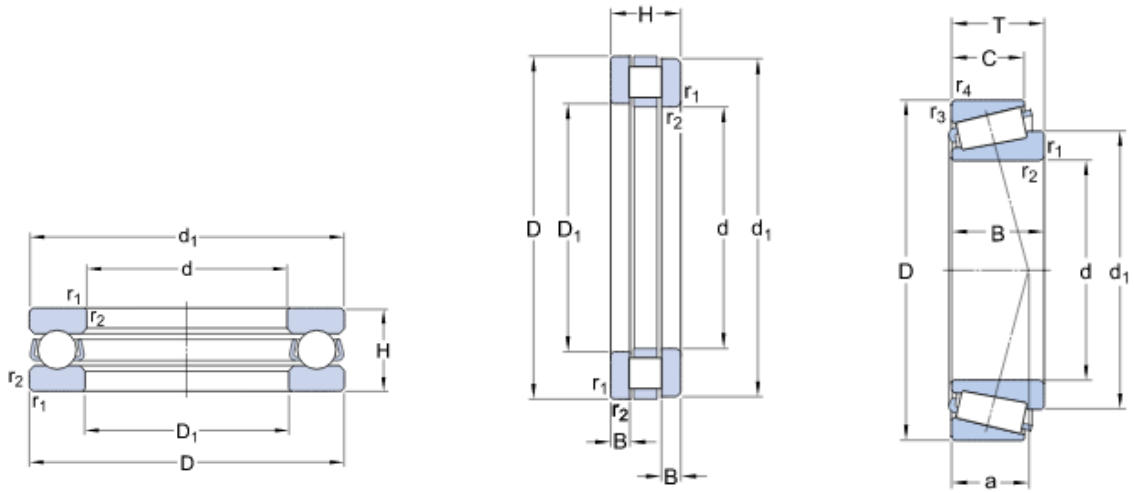

(a) TBB 51107. (b) RTB 81107 TN. (c) TRB 320/28 X/Q.

Figure 6.1: TBB 51107, RTB 81107 TN and TRB 320/28 X/Q geometries.

6.2.3. Operating conditions

The oil level should reach the center of the lowest rolling element as indicated by the manufacturer [SKF, 2013] and the oil volume required is approximately 14 ml for TBB and RTB and 8 ml for TRB as indicted by Cousseau [Cousseau et al., 2010]. A new rolling bearing is mounted for each tested oil in order to avoid the possible chemical interactions between oils and even to reduce the influence of the surface finish (similar finishing on the rolling bearings [Fernandes, 2015]).

The friction torque was measured for different rotational speeds between 75 and 1200 rpm. This speed range is within the limits of the test machine, allowing to cover all lubrication regimes, from boundary to full-film lubrication.

As presented in the previous Chapter 5, the SKF friction torque model proposed for the calculation of the sliding friction torque which is depending on the weighting factor ϕ_{bl}.

This parameter indicates the lubrication regime inside the contact, when ϕ_{bl} = 0 the rolling bearing is under full-film lubrication and when ϕ_{bl} = 1 the rolling bearing is under boundary lubrication. Equation (6.1) shows that the weighting factor depends mainly on the rotational speed (n), the viscosity of the lubricant (ν) and the average diameter d_m.

$$\phi_{bl} = \frac{1}{e^{2.6 \cdot 10^{-8} \cdot (n \cdot \nu)^{1.4} \cdot d_m}} = f((n \cdot \nu)^{1.4} \cdot d_m) \tag{6.1}$$

Under a constant temperature and with different rolling bearing geometry, the Lubrication Quality factor (LQ) has a great importance and it is given in Equation (6.2).

$$LQ = (n \cdot \nu)^{1.4} \cdot d_m \tag{6.2}$$

This factor is very useful in order to perform laboratory tests under the same LQ presented in real applications (see Equation (6.3)).

$$LQ_{real} = LQ_{test} \;\; or \;\; (n_{real} \cdot \nu_{real})^{1.4} \cdot d_{m\,real} = (n_{test} \cdot \nu_{test})^{1.4} \cdot d_{m\,test} \tag{6.3}$$

In typical automotive rear drive axle, the pinion speed levels are between 300 and 3000 rpm [Xu et al., 2012] and the mean diameter of the rolling bearing is about 51 mm [Matsuyama et al., 2004]. Using Equation (6.2), the minimum value of the Lubrication Quality is LQ_{real} = 149 809 and the maximum value is LQ_{real} = 3 763 049. It is necessary to have LQ_{real} = LQ_{test} to calculate the rotational speed of the tests with an average diameter of d_m = 43.5 mm (see Section 6.2.2).

$$n_{min} = (\frac{LQ_{min}}{d_m})^{1/1.4} = (\frac{149809}{43.5})^{1/1.4} = 336\ rpm \tag{6.4}$$

$$n_{max} = (\frac{LQ_{max}}{d_m})^{1/1.4} = (\frac{3763049}{43.5})^{1/1.4} = 3360\ rpm \tag{6.5}$$

From the calculations presented in Equations (6.4) and (6.5), the rotational speeds of the test were defined. As the maximum rotational speed of the machine is 1500 rpm, it is not possible to reach the specified maximum rotational speed of 3360 rpm. But it is not a problem because with a rotational speed of 1200 rpm, the full film lubrication regime is reached. So the tests were performed for different rotational speed between 75 and 1200 rpm, allowing to cover all lubrication regimes, from boundary to full-film lubrication.

Three operating temperatures (70, 90 and 110 °C) were specified after a study of oil temperature variations obtained in the EPA driving cycle (includes both city and highway cycles) shown in Figure 3.3. All rolling bearings were submitted to an axial load of 4000 and 7000 N, assuring a sufficiently high bearing rigidity [Spindler and Von Petery, 2003].

The characteristics of the contact between the rolling elements (ball or roller) and the raceway were displayed in Tables 6.2 and 6.3 for TBB and RTB, respectively. For TBB and RTB the normal load load is equal to the applied axial load.

Table 6.2: Ball-raceway contact parameters for TBB 51107 rolling bearing.

	Unit	Raceway	Ball
R_{Xi}	[m]	∞	3×10^{-3}
R_{Yi}	[m]	-3.38×10^{-3}	3×10^{-3}
R_X	[m]	6×10^{-3}	
R_Y	[m]	53.4×10^{-3}	
σ_c	[μm]	0.18	
Axial load	[N]	4000	7000
a	[μm]	102.8	123
A_c	[mm^2]	0.14	0.198
p_0	[GPa]	2.06	2.47
δ	[μm]	5.22	7.48

Table 6.3: Roller-raceway contact parameters for RTB 81107 TN rolling bearing.

	Unit	Raceway	Roller
R_{Xi}	[m]	∞	2.5×10^{-3}
R_X	[m]	5×10^{-3}	
l	[m]	5×10^{-3}	
σ_c	[μm]	0.14	
Axial load	[N]	4000	7000
a	[μm]	33.22	43.5
A_c	[mm^2]	0.332	0.435
p_0	[GPa]	0.766	1.004

6.2.4. Test procedure

A new rolling bearing is assembled and lubricated with 14 ml or 8 ml of fresh oil depending on the rolling bearing type. The rolling bearing assembly is submitted to a continuous air flow, forced by two 38 mm diameter fans, running at 2000 rpm, cooling the chamber surrounding the bearing house.

Before starting each test, a running-in period is always required for each rolling bearing and is carried under an axial load of 1000 N and increasing rotational speed from 75 to 1200 rpm during 10 minutes.

For each test with the selected rolling bearing, the axial load is applied and the rotational speed set to the required value and the operating temperature is imposed. When the machine reaches the stabilized temperature (thermal equilibrium) due to the heaters, four friction torque measurements were performed. Three values were kept and the most dispersed one

was disregarded. The torque measurement should be made in short periods of time (120 s) at stabilized temperatures (± 2 °C) in order to avoid the drift effect of the torque cell [Cousseau et al., 2010]. So, the friction torque value (for each rotational speed and load) is the average value of the three closest measurements.

6.2.5. Taper Rolling Bearings - Assembly, operating conditions and test procedure

Several modifications were introduced into the test assembly, the operating conditions and the test procedure in order to measure the internal friction torque in Taper Rolling Bearings (TRB). A different shaft adapter (see Figure 6.2), minimizing the misalignment of the TRB, and a lower race support were manufactured. Instead of a cone Morse connection, the superior part of the shaft adapter is a hollow shaft design to assemble on the machine input shaft. Furthermore, both pieces have a hole across their sections and perpendicular to their rotational axles with a screw applied to prevent the sliding effect among the two parts.

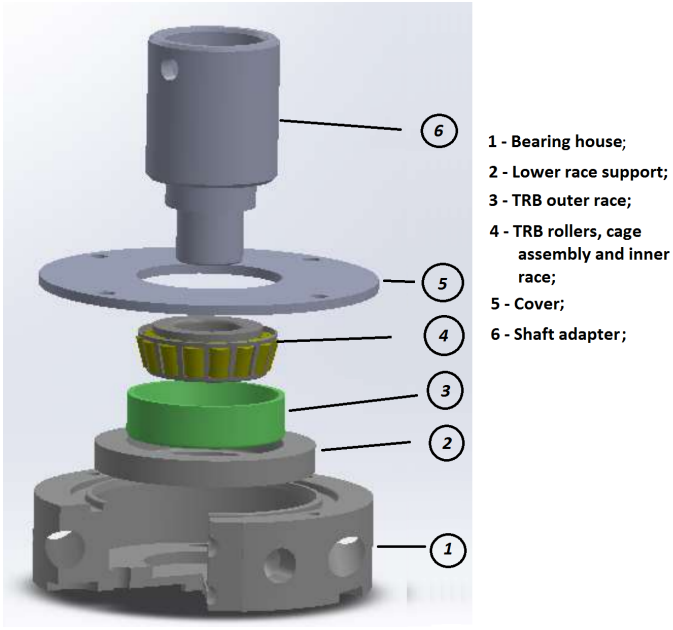

Figure 6.2: Schematic view of the TRB assembly.

The characteristics of the contact between the rollers and the raceway are displayed in Table 6.4 for TRB 320/28 X/Q. For the TRB the normal contact load between the roller and raceway is given by Equation (6.6) according to Eschamann [Eschmann, 1985] (see Figure 6.3).

$$F_n = \frac{F_a / \sin(\psi)}{z} \tag{6.6}$$

Table 6.4: Roller-raceway contact parameters for TRB 320/28 X/Q rolling bearing.

	Unit	Raceway	Roller
R_{Xi}	[m]	17.26×10^{-3}	2.95×10^{-3}
R_X	[m]	5.9×10^{-3}	
l	[m]	12.16×10^{-3}	
σ_c	[μm]	0,25	
Axial load [N]		4000	7000
a	[μm]	41.79	55.28
A_c	[mm^2]	1.016	1.345
p_0	[GPa]	0.957	1.266

where

$$\psi = \arctan\frac{e}{1.5} \tag{6.7}$$

It was necessary to take into account that tapered roller bearings should have a long running-in period, which is characterized by a significant amount of friction between the rolling elements and the raceways, and it can be identified by the temperature spike shown in Figure 6.4. After reaching the maximum operating temperature, a gradual decrease of the temperature is observed until a stabilized value is achieved. The time necessary to reach the stabilization temperature depends on the lubricant formulation and, consequently, the running-in time is not pre-defined. Instead, the running-in period is complete when the temperature variation is lower than one Celsius degree per hour.

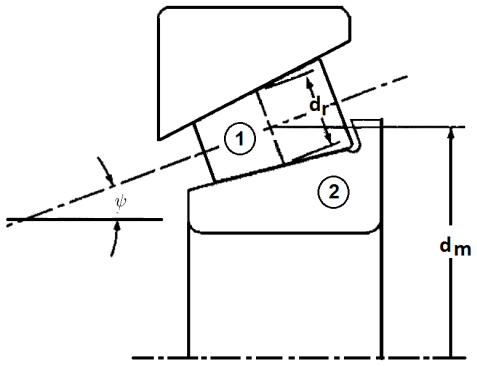

Figure 6.3: Simplified inter geometry for TRB [Hamrock et al., 2004].

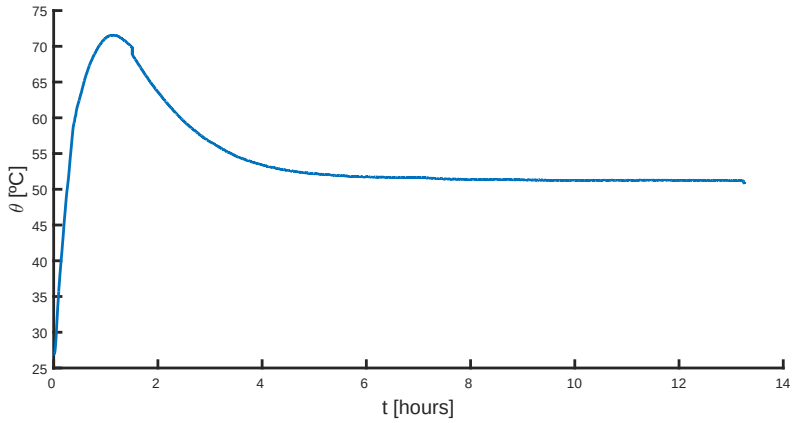

Figure 6.4: Temperature variation (θ) of tapered roller bearings during the running-in period (t).

6.3. Film thickness inside rolling bearings

The film thickness (h_0) of the rolling element/raceway contacts is calculated using the Hamrock and Dowson [Hamrock and Dowson, 1981, 386] equation (see section 2.8.2.2) for elliptical contacts (TBB) and Dowson and Higginson [Dowson, 1977] equation (see section 2.8.2.1) for line contacts (RTB and TRB).

The corrected film thickness (h_{0C}) is given in Equation 4.4 which is the product of the center film thickness with the thermal correction factor (ϕ_T), as shown in Equation (4.5).

The concept of specific film thickness (Λ) is usually used to determine the lubrication regime. The specific film thickness is calculated with Equation (6.8).

$$\Lambda = \frac{h_{0C}}{\sigma_c} \tag{6.8}$$

The composite roughness σ_c is calculated the roughness of the rolling element ($\sigma_{element}$, ball or roller depending on bearing geometry) and the roughness of the race (σ_{race}), according to Equation (6.9). The roughness values for each rolling bearing tested are presented in Tables 6.2, 6.3 and 6.4.

$$\sigma_c = \sqrt{(\sigma_{element})^2 + (\sigma_{race})^2} \tag{6.9}$$

To evaluate the film thickness and lubrication regime in rolling bearings, the concept of viscosity ratio may also be used to evaluate lubricant's effectiveness in forming sufficient lubricant film to separate the surfaces in contact. The viscosity ratio is calculated using Equation (6.10).

$$k = \frac{\nu}{\nu 1} \tag{6.10}$$

This parameter depends essentially on the mean diameter d_m of the rolling bearing without selecting the type of rolling bearing. For that reason, the viscosity ratio can be related to the specific film thickness, as it is shown in Equation (6.11).

$$k = \Lambda^{1.3} \tag{6.11}$$

Figure 6.5a presents the viscosity ratio, calculated using the SKF abacus [SKF, 2013], for TBB rolling bearing under constant temperature of 70 °C and 7000 N load. Using this concept it is possible to observe that the viscosity ratio increases when the speed increases. The five axle oils are classified according to their viscosity at the operating temperature. The 75W140-A oil has the highest viscosity generating the highest viscosity ratio while 75W85-B oil has the lowest viscosity and promotes the lowest viscosity ratio. The viscosity ratio values of the oils 75W90-B, 75W90-A and 80W90-A are placed between the previous two, depending directly on their viscosity.

In general [SKF, 2013], a rolling bearing operates under mixed-film lubrication for k higher than 1 and under full-film lubrication for k higher than 2. According to the literature [SKF, 2013], the rolling bearing reaches the boundary film conditions for a viscosity ratio lower than 0.4. Under these range of rotational speeds and for all the oil formulations, boundary and mixed-film lubrication are the dominant lubrication regimes except at 1200 rpm the full-film lubrication regime is achieved for all lubricants except the 75W85-B oil.

Figure 6.5b shows the variation of viscosity ratio in roller-raceway contact of RTB with the rotational speed under the applied loads of 7000 N and at 70 °C. It is possible to observe that the viscosity ratio increases when the speed increases up to 600 rpm. Axle gear oils share a similar behaviour as TBB tests for the speed range before 600 rpm since the temperature is maintained constant. The 75W85-B oil with the lowest viscosity and piezo-viscosity had an opposite behaviour of the 75W140-A oil, promoting the lowest viscosity ratio. The viscosity ratio values of the oils 75W90-B, 75W90-A and 80W90-A are placed between the previous two, depending directly on their kinematic viscosity (see Table 6.5).

Figure 6.5c displays the viscosity ratio values for TRB under the same operating conditions. It was observed that the lubricants were ranked with a similar trend as the viscosity ratio values in TBB tests. Generally the viscosity ratio values in TRB are slightly lower than the viscosity ratio values in TBB.

Under these range of rotational speeds and for all the axle oil formulations, boundary and mixed-film lubrication are the dominant lubrication regimes ($k \leq 2$) except at 1200 rpm.

Table 6.5: Kinematic viscosity and piezo-viscosity of the axle gear oils at 70 °C.

Axle gear oils	75W85-B	75W90-A	75W90-B	80W90-A	75W140-A
Kinematic viscosity (cSt)	23.86	36.7	38.14	34.86	61.86
Piezo-viscosity ($\alpha \times 10^{-8}$) [Pa^{-1}]	1.128	1.194	1.2	1.623	1.28

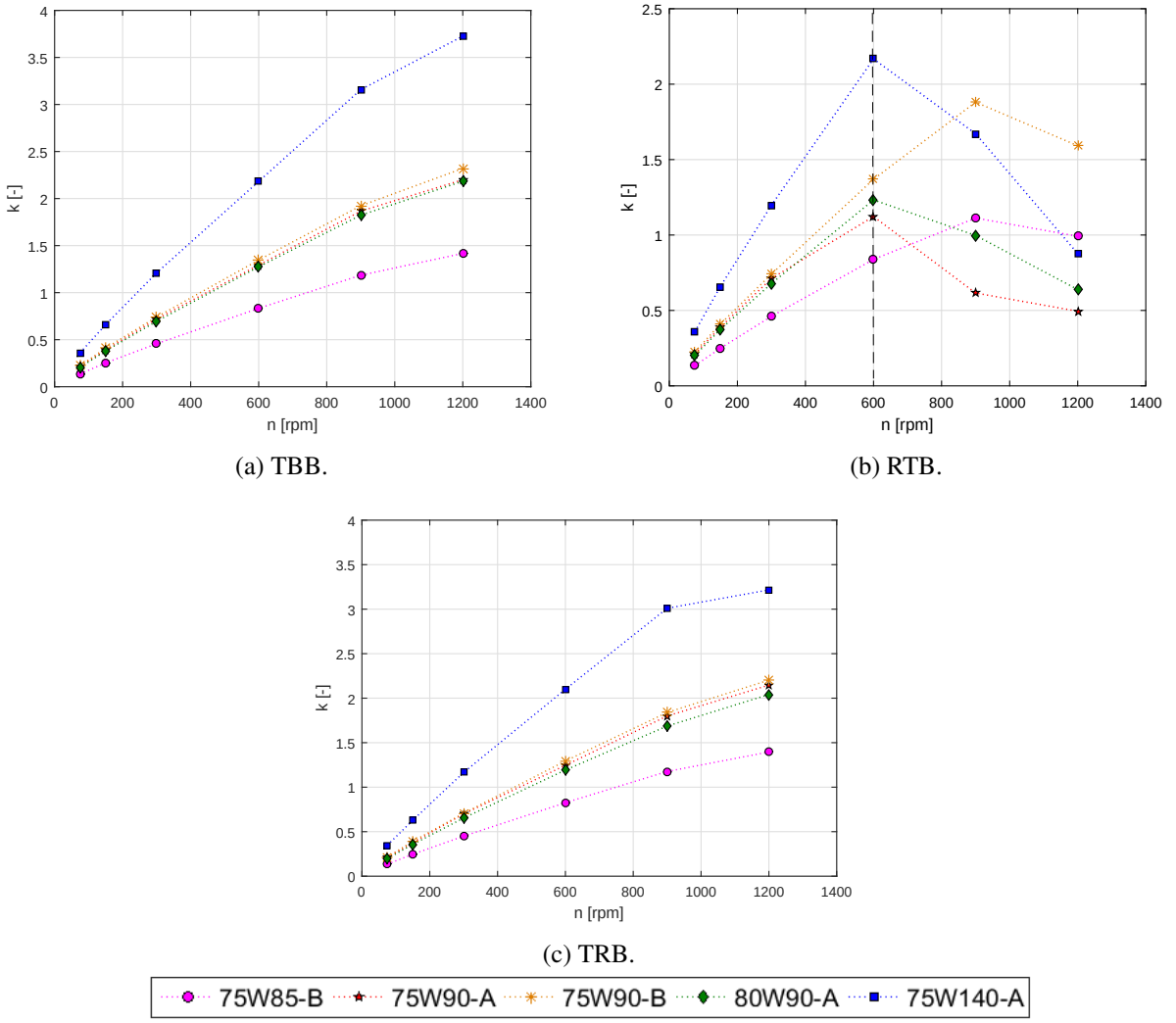

(a) TBB.

(b) RTB.

(c) TRB.

Figure 6.5: Viscosity ratio for TBB, RTB and TRB under 70 °C and 7000 N operating conditions.

6.4. Determination of the sliding coefficient of friction

The torque loss model proposed by SKF [SKF, 2013] considers that the total friction torque is the sum of four different physical sources of torque loss represented by Equation (6.12).

$$M_t = M'_{rr} + M_{sl} + M_{seal} + M_{drag} \tag{6.12}$$

Since the rolling bearings tested do not have seals, the M_{seal} component was disregarded in the calculation.

The drag losses are very small because the operating speeds and the mean diameter of the rolling bearings are also small (d_m = 43.5 mm for TBB and RTB and d_m = 40 mm for TRB), consequently, the drag torque loss term was also disregarded.

Therefore, the total friction torque of the rolling bearings have only two contributions: the rolling and sliding torques, respectively, M'_{rr} and M_{sl}, as presented in Equation (6.13).

$$M_t = M'_{rr} + M_{sl} \tag{6.13}$$

Assuming that the friction torque obtained from experimental measurements was equal to the total torque loss predicted by the SKF model ($M_t = M_t^{exp}$), it is possible to obtain such Equation (6.14).

$$M_t = M_t^{exp} = M'_{rr} + M_{sl} \tag{6.14}$$

The rolling torque was easily calculated according to the SKF model (Equations (5.35) to (5.36), presented in section 5.3). Assuming that the rolling torque was accurately calculated, the sliding torque is obtained using Equation (6.15).

$$M_{sl} = M_t^{exp} - M'_{rr} \tag{6.15}$$

Knowing the value of the sliding friction torque, it is possible to calculate the sliding coefficient of friction with Equation (6.16). The sliding coefficient of friction (μ_{sl}^{exp}) is now considered as an experimental coefficient of friction.

$$\mu_{sl}^{exp} = \frac{M_{sl}}{G_{sl}} = \frac{M_t^{exp} - M'_{rr}}{G_{sl}} \tag{6.16}$$

As mentioned before in section 5.3, it is possible to predict the values of the coefficient of friction using Equation (6.17), where the coefficient of friction is dependent on two coefficients: μ_{bl} that is related to the additive package in the lubricant and it is advisable by SKF model to be equal to 0.15 and μ_{EHL} that is related to the base oil and the bearing type.

$$\mu_{sl} = \phi_{bl} \cdot \mu_{bl} + (1 - \phi_{bl}) \cdot \mu_{EHL} \tag{6.17}$$

Using the provided values from the SKF model, the coefficient of friction obtained is slightly different from the experimental value. To minimize the difference between μ_{sl}^{exp} and μ_{sl}, the two coefficients μ_{bl} and μ_{EHL} should be calculated for each operating temperature and for each type of rolling bearing. They are clearly dependent on the speed range used in the rolling bearing tests, as will be shown later on.

6.5. Tests performed at 70 °C and 7000 N

6.5.1. Thrust Ball bearings experimental results (TBB 51107)

The TBB lubricated with axle gear oils tests were carried out under constant temperature of 70 °C and an axial load of 7000 N. Figure 6.6a shows that, in general, the measured total friction torque of the TBB decreases when the operating speed increases from 75 rpm to 1200 rpm, except in the case of oil 75W140-A, for which the friction torque increased as the speed increases.

It is clear that,for low rotational speeds, the two candidate (B) oils generated higher values of the total friction torque than the reference (A) oils (see Figure 6.6a) due do the significant differences between them in terms of the additive packages present in their formulations.

Figure 6.6b shows that when the speed increased the specific film thickness inside the TBB increased from 0.22/0.46 up to 1.30/2.75, depending on the tested oil, meaning that boundary and mixed lubrication regimes prevail under these operating conditions as indicated by Figure 6.6f as well.

The results of the rolling friction torque inside the thrust ball bearing are displayed in Figure 6.6c. As expected, at constant temperature (70 °C) the rolling torque increases when the speed increases ($M'_{rr} \propto (n \cdot \upsilon)^{0.6}$). Comparing the behaviour of the different oil formulations, the 75W140-A oil, with the highest operating viscosity, generated the highest rolling torques, while 75W85-B oil, with the lowest viscosity, generated the lowest rolling torques. The rolling torques of the other three oil formulations follow the trend of their viscosities. So the main parameter that differentiates the lubricants in the calculation of the rolling torque is the viscosity at the operating temperature.

As expected the sliding torque, presented in Figure 6.6d, are higher than those calculated for the rolling torque and they show the same trend of the total friction torque curves. In general, the results indicate that the sliding torque decreases with the increase of the rotational speeds. Such behaviour was anticipated since for a constant operating temperature the specific film thickness increases with increasing rotational speed, as shown in Figure 6.6b.

The experimental sliding torques can be used to determine the experimental sliding coefficient of friction, using Equation (6.16), as presented in Figure 6.6e. The sliding coefficient

of friction μ_{sl} follows the trend of the sliding torque.

Figure 6.6f shows the weighting factor ϕ_{bl}, which is always comprised between 0 and 1. This parameter decreases when the speed increases. The 75W85-B presents the highest values while the 75W140-A presents the lowest values. Other formulations show a similar values in between. This behaviour is explained that the weighting factor values are inversely proportional to the viscosities of the lubricants. The weighting factor presents a direct influence on the sliding coefficient of friction μ_{sl} presented in Figure 6.6e. It should also be noticed that the values of ϕ_{bl} for each oil formulation almost covers all the range of values ($0 \leq \phi_{bl} \leq 1$), meaning that the operating conditions represent all the lubrication regimes, from boundary to full-film lubrication.

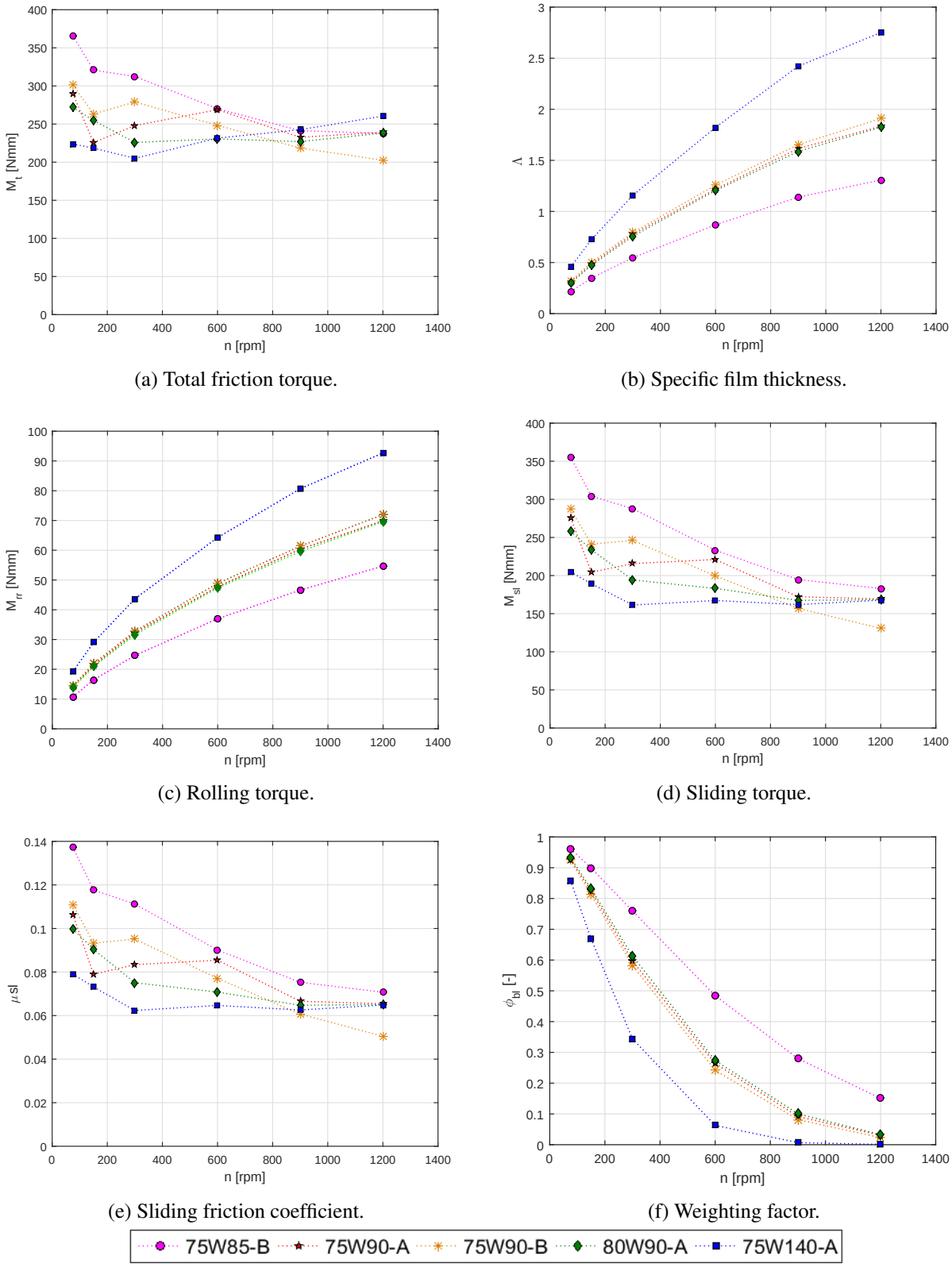

(a) Total friction torque.

(b) Specific film thickness.

(c) Rolling torque.

(d) Sliding torque.

(e) Sliding friction coefficient.

(f) Weighting factor.

Figure 6.6: Results of TBB 51107 lubricated with axle gear oils at constant temperature of 70 °C with an axial load of 7000 N.

6.5.2. Cylindrical roller bearings experimental results (RTB 81107)

The experimental tests with cylindrical roller thrust bearings, lubricated with axle gear oils, were carried out under the same constant operating temperature (70 °C) and a high axial load (7000 N). However, it was not possible to keep a constant operating temperature of 70 °C above 600 rpm, as shown in Figure 6.7. In those cases, it was necessary to cool the bearing housing, and that was not achieved. At 1200 rpm, the maximum temperature reached 135 °C with 75W90-A oil.

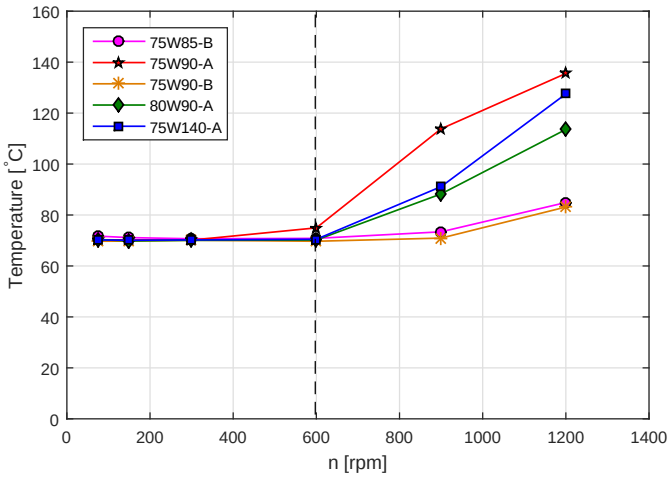

Figure 6.7: Temperature evolution under constant temperature measurements of 70 °C for RTB 81107.

Figure 6.8a displays the total friction torque measured for RTB in all operating conditions. The total friction torque decreases with increasing speed, up to 600 rpm and T=70 °C. Above 600 rpm, it is interesting to notice that the reference (A) oils generated significantly higher operating temperatures than the candidate (B) oils, whose operating temperature remained constant (70 °C) at 900 rpm and reached 85 °C at 1200 rpm.

Up to 600 rpm, 80W90-A oil generally produced the lowest values of the total friction torque while 75W90-A oil usually generated the highest corresponding values. Oils 75W140-A, 75W85-B and 75W90-B presented intermediate values. Above 600 rpm the candidate (B) oils generated the lowest friction torques.

Figure 6.8b shows that when the operating speed increases from 75 rpm to 600 rpm the specific film thickness inside the RTB increases from 0.21-0.45 up to 0.87-1.81, meaning that mixed film lubrication prevails. All axle gear oils share the same trend, where 75W140-A oil produced the highest Λ because of its high viscosity at 70 °C and 75W85-B oil generated the lowest Λ because of its low viscosity. Above 600 rpm the specific film thickness is exotic and strongly dependent on the test temperature.

The rolling torque calculated for RTB under the operating conditions is presented in Figure 6.8c. It is observed that when the speed increases the rolling torque increases. This figure also shows that the oils 75W90-B, 75W90-A and 80W90-A generated very similar rolling torques, because they have similar viscosities values at 70 °C.

Equation (6.15) was used to obtain the sliding friction torque (see Figure 6.8d). This figure shows that the sliding torque decreases with the increase of speed for all operating conditions. The lubricant behaviour presents the same trend of their total friction torque. However, it is not possible to compare the sliding torques of the different axle gear oils, below and above 600 rpm, because of the large differences in operating temperatures.

The sliding coefficients of friction are presented in Figure 6.8e, showing that reference (A) oils 80W90-A and 75W140-A have the lowest sliding torques below 600 rpm.

The weighting factor ϕ_{bl}, shown in Figure 6.8f, does explain the behaviour of the sliding coefficient of friction μ_{sl} up to 600 rpm. Above 600 rpm, the ϕ_{bl} values are not comparable.

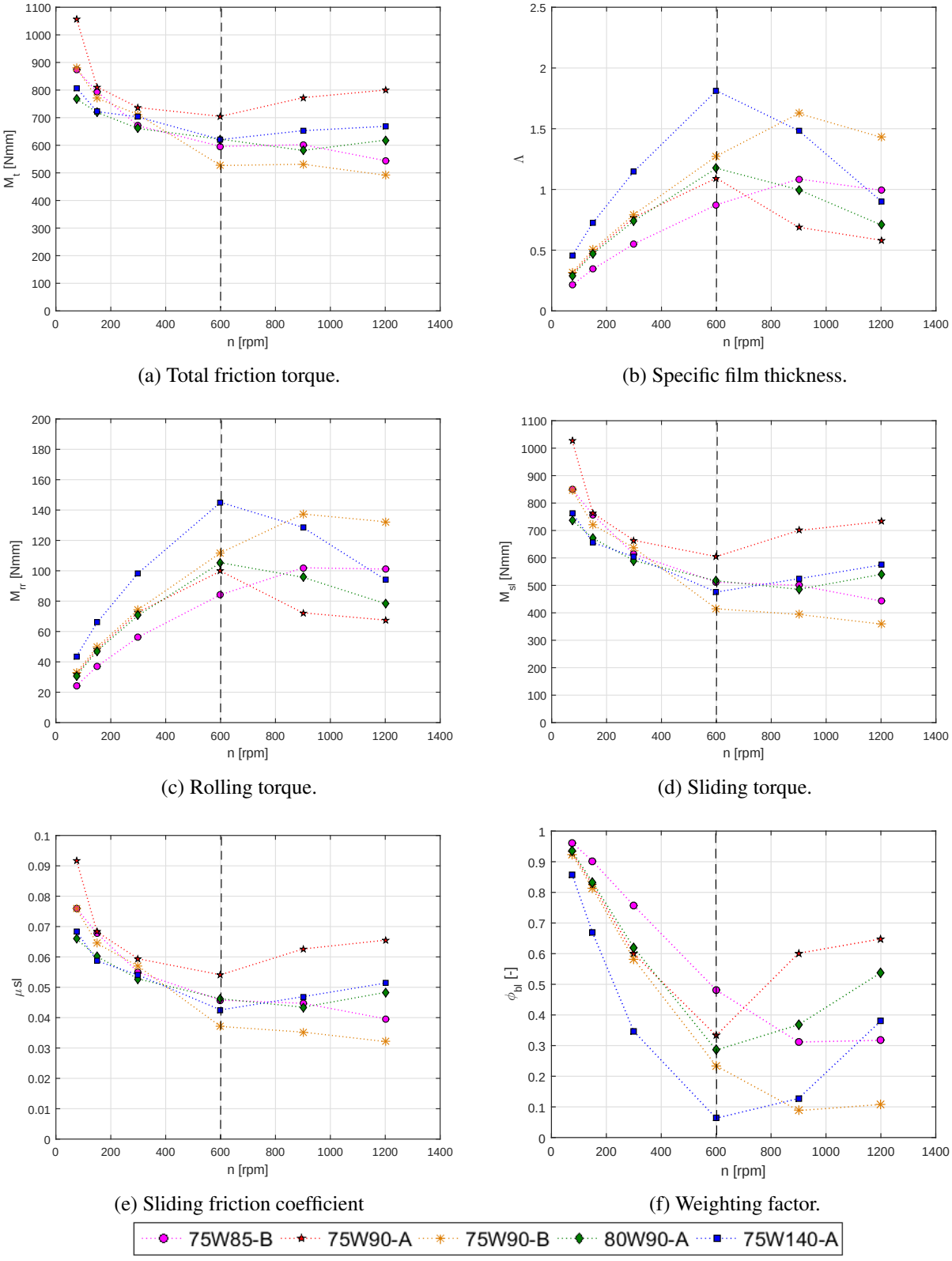

(a) Total friction torque.

(b) Specific film thickness.

(c) Rolling torque.

(d) Sliding torque.

(e) Sliding friction coefficient

(f) Weighting factor.

Figure 6.8: Results of RTB 81107 lubricated with axle gear oils at constant temperature of 70 °C with an axial load of 7000 N.

6.5.3. Comparison between TBB and RTB

It is interesting to compare the friction behaviours of the TBB and RTB rolling bearings. Under constant temperature (70 °C) and constant load (7000 N), the total friction torque decreases when the speed increases, both for TBB and RTB. However, the maximum torques measured for each type of bearing at 75 rpm are 370 N.mm and 1060 N.mm for TBB and RTB, respectively, showing the major role and influence of the rolling bearing type and geometry on the total friction torque M_t.

When the speed increases the rolling torque, M_{rr}, shows a small increase in the case of TBB and a large increase in the case of RTB (see Figures 6.6c and 6.8c). The maximum rolling torques calculated for each type of bearing are 92 N.mm for TBB and 142 N.mm for RTB, showing again the influence of the rolling bearing geometry on the rolling torque.

The reduction of the sliding torque, M_{sl}, with increasing speeds, is much more significant in a RTB than in a TBB, as may be noticed comparing Figures 6.6d and 6.8d.

These differences in the internal friction torque (M_t, M_{rr} and M_{sl}) between TBB and RTB are related to the geometry of the contact area, an elliptical contact in the case of TBB and a line (rectangular) contact in the case of the RTB, and to the sliding speed inside the contact, which is higher in the case of the RTB. These differences are reflected also on the values of G_{rr} and G_{sl}), which are significantly higher in the case of RTB.

As mentioned in section 6.4, the minimization of the difference between experimental and model values of the sliding coefficient of friction allows the calculation of the μ_{bl} and μ_{EHL} values. In this case, the values of μ_{bl} and μ_{EHL} were determined for each type of rolling bearing (TBB and RTB) and for each type of axle gear oil formulation according to three groups (group I: 75W85-B and 75W90-B, group II: 75W90-A and 80W90-A and group III: 75W140-A), as presented in Table 6.6.

The boundary coefficient of friction, μ_{bl}, depends on the gear oil formulation and rolling bearing type, as shown in Table 6.6. For all the lubricant formulations (A and B), the bound-

Table 6.6: Values of the coefficients μ_{bl} and μ_{EHL} for TBB 51107 and RTB 81107, under 7 kN and at 70 °C .

Valid for $3262.5 < n \cdot d_m < 52200$			
		Bearing type	
Lubricant	Parameter	TBB	RTB
75W85-B and 75W90-B	μ_{bl}	0.124	0.073
	μ_{EHL}	0.056	0.032
75W90-A and 80W90-A	μ_{bl}	0.097	0.071
	μ_{EHL}	0.064	0.036
75W140-A	μ_{bl}	0.078	0.073
	μ_{EHL}	0.063	0.040

ary coefficient of friction μ_{bl}^{TBB} is larger than μ_{bl}^{RTB}. In the case of the TBB, the values of μ_{bl} for the candidate (B) oils reached a high values (μ_{bl}^{TBB} = 0.124), meaning that the formulations containing Zinc generate very high sliding torque under boundary film lubrication. This behaviour was not observed with RTB.

The full-film coefficient of friction, μ_{EHL}, also depends on the gear oil formulation and rolling bearing type. The reference and the candidate oils have similar behaviours when lubricating the two rolling bearing types ($\mu_{EHL}^{TBB} > \mu_{EHL}^{RTB}$). In general, the candidate (B) oils, which have lower viscosities also generated lower μ_{EHL} coefficients.

The Stribeck curves of the five axle gear oils lubricating the two rolling bearing types are presented in Figures 6.9 and 6.10, for TBB and RTB, respectively. Those figures present the experimental results with the error bar for each value shown with markers and the model simulations shown by the continuous lines, in function of the modified Hersey parameter $Sp = Ur.\eta.\alpha^{0.5}.Fn^{-0.5}$. Figure 6.11 presents the same coefficient experimental and simulation for all the axle oil formulations in the same graph.

In general, the approximation of the sliding coefficient of friction μ_{sl}, predicted by the model, is quite good, whatever the axle gear oil formulation and rolling bearing type. It is also clear that there is a better approximation at high speeds and high viscosities (larger values of Sp). At low speed, under boundary film lubrication conditions, the scatter of the μ_{sl} values is larger.

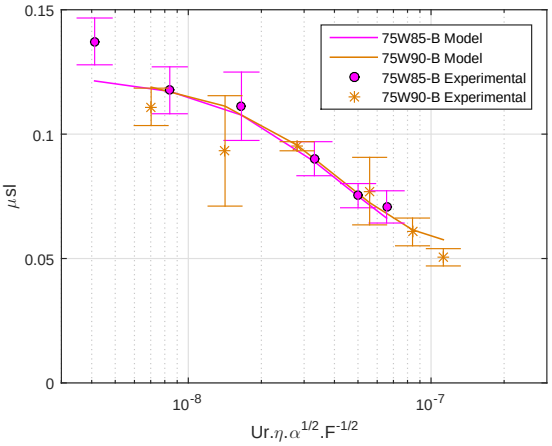

(a) TBB-75W85-B/75W90-B.

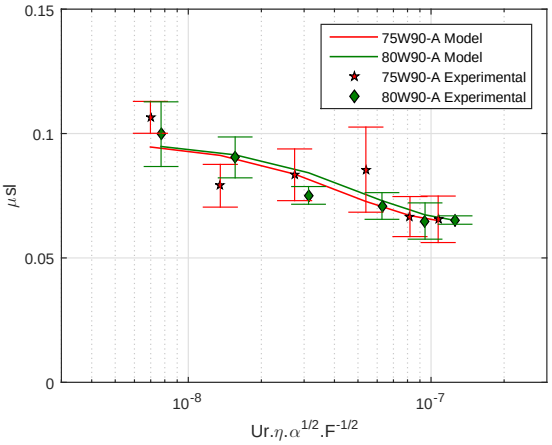

(b) TBB-75W90-A/80W90-A.

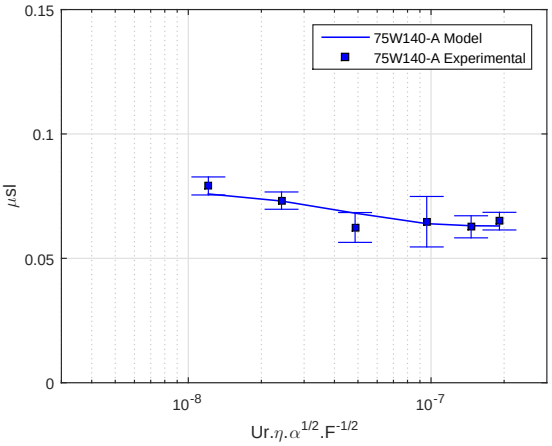

(c) TBB-75W140-A

Figure 6.9: Model simulations for sliding coefficient of friction against modified Hersey parameter for the TBB 51107 lubricated with axle gear oils at constant temperature of 70 °C with an axial load of 7000 N.

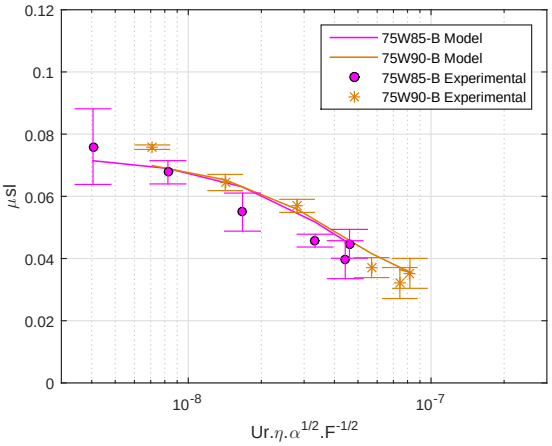

(a) RTB-75W85-B/75W90-B.

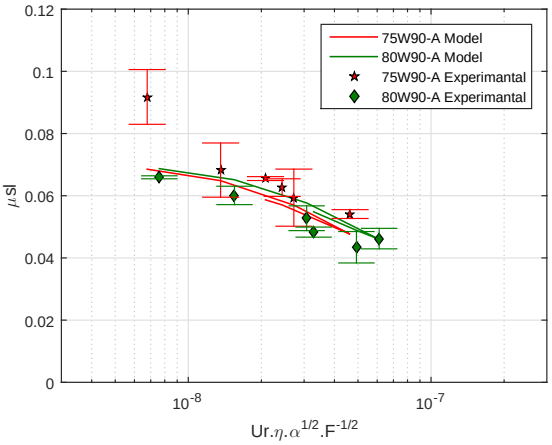

(b) RTB-75W90-A/80W90-A.

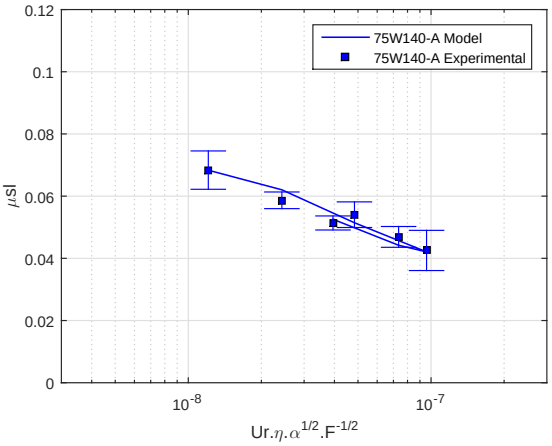

(c) RTB-75W140-A.

Figure 6.10: Model simulations for sliding coefficient of friction against modified Hersey parameter for the RTB 81107 lubricated with axle gear oils at constant temperature of 70 °C with an axial load of 7000 N.

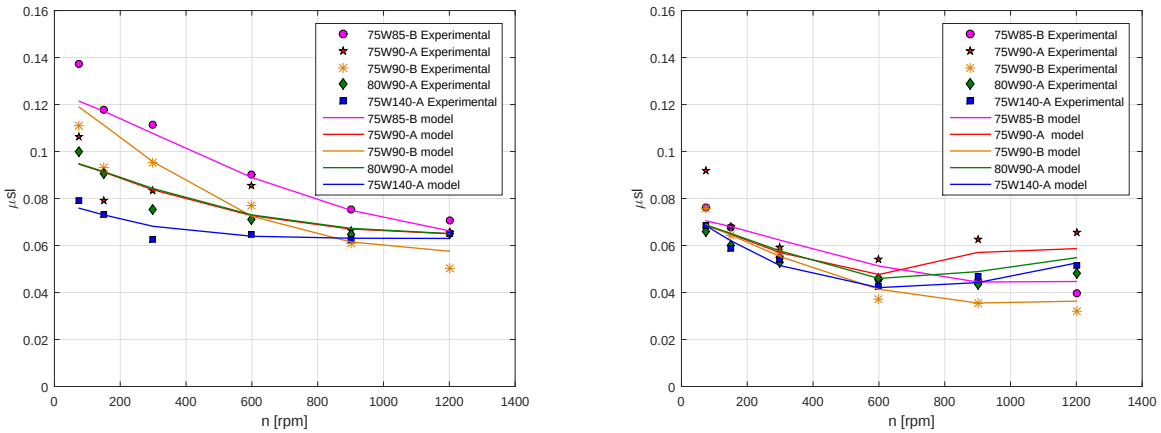

(a) TBB. (b) RTB.

Figure 6.11: Sliding coefficient of friction against rotational speed for a TBB 51107 and RTB 81107 and corresponding model simulations values lubricated with five axle gear oils under 70 °C and 7000 N operating conditions.

6.5.4. Tapered roller bearings experimental results (TRB 320/28 X/Q)

The results of the total friction torque measurements carried out on TRB, under a 7 kN axial load and at 70 °C, are presented in Figure 6.12. M_t decreases with the increase of the rotational speed, while the corresponding specific film thickness increased from 0.22-0.45 up to 1.29-2.46, that is from boundary film lubrication up to mixed film lubrication, (see Figure 6.12b).

At low speeds (n <= 300 rpm) the candidate (B) formulations generated higher friction torques than the standard (A) formulations. In fact, $M_t^{75W90-B}$ is 1800 N.mm while $M_t^{75W140-A}$ reaches 760 N.mm, that is 2.4 times higher. At 600 rpm and above, all axle gear oils generated very similar friction torques.

Figure 6.12a shows that the internal friction torque of the TRB M_t^{TRB} decreases drastically between 75 and 300 rpm, and above 300 rpm remains almost constant and very similar for all axle gear oil formulations. In fact, above 300 rpm M_t^{TRB} is significantly lower than M_t^{RTB}. This behaviour and the corresponding measurements of the internal friction torque for the TRB are probably related to the fact that the axial load applied generates a very small normal load between the rollers and the raceways, due to the internal geometry of the 320/28 X/Q tapered roller bearing. Unfortunately, the modified Four-Ball Machine is not prepared for axial loads above 7kN. Furthermore, it is possible that the friction torque model used (see section 6.4) is not prepared nor calibrated to deal with this type of loading (pure axial load and low normal load).

These measurements of the total friction torque carried out on TRB, are only indicative and eventually as a first approximation of the friction torque behaviour of the different axle gear

oil formulations in a TRB.

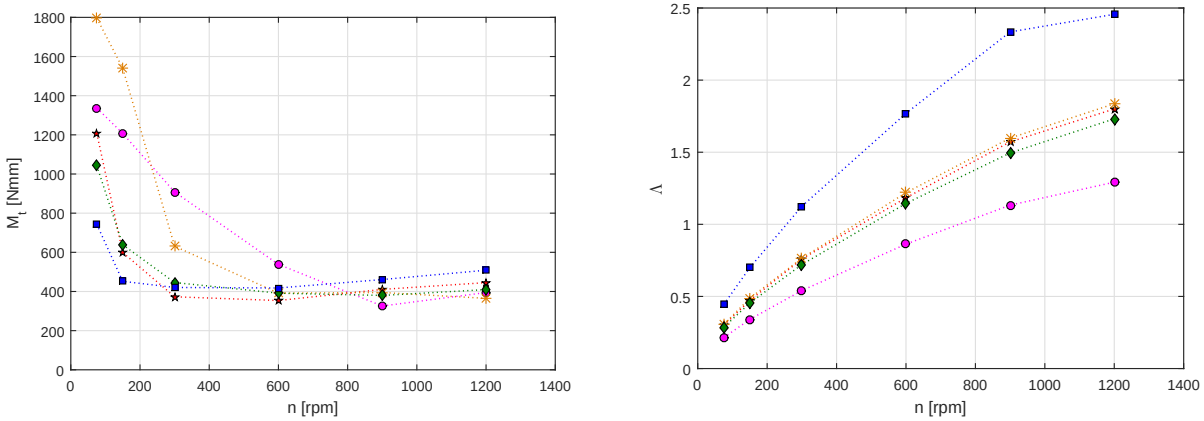

(a) Total friction torque.

(b) Specific film thickness.

Figure 6.12: Results of TRB 320/28 X/Q lubricated with axle gear oils at constant temperature of 70 °C with an axial load of 7000 N.

6.6. *Tests performed at 70 °C, 90 °C and 110 °C under 4000 N and 7000 N*

Additional battery of rolling bearing tests were performed, under significant ranges of operating speeds, loads [Spindler and Von Petery, 2003] and temperatures and using different types of rolling bearings, TBB 51107, RTB 81107 and TRB 320/28 X/Q. Table 6.7 summarizes the operating conditions used in these rolling bearing tests.

Table 6.7: Operating conditions of rolling bearing tests.

Operating conditions	TBB 21107	RTB 81107	TRB 320/28 X/Q
Rotational speed [rpm]	75, 150, 300, 600, 900, 1200		
Temperature [°C]	70, 90, 110		
Axial load [N]	4000, 7000		

The tests were performed in order to understand the behaviour of the lubricants with variation of load or temperature or even both and to determine the influence of the rolling bearing geometry.

The results were not detailed in this section. Tables 6.8 and 6.9 show the values of the coefficients μ_{bl} and μ_{EHL} determined for TBB and RTB, respectively under these operating conditions.

The values of the coefficients μ_{bl} and μ_{EHL} for TRB were not determined through the measurements of the total friction torque as the SKF model is not applicable in this case

It is observed that in almost cases (TBB and RTB), both coefficients μ_{bl} and μ_{EHL} generally decrease with an increase of load.

When comparing tests with different temperatures and the same load for each oil, in almost all cases a close values of μ_{bl} were verified. So, it is possible to conclude that under equal load conditions, the value of μ_{bl} is mainly influenced by each oil's composition and not its thermal properties. It is almost temperature independent. It is also important to notice again that for the tested conditions, the values of μ_{bl} and μ_{EHL} are very different of the values proposed by SKF model.

Table 6.8: Values of the coefficients μ_{bl} and μ_{EHL} for for TBB 51107 under three temperatures and two loads.

	75W85-B and 75W90-B		75W90-A and 80W90-A		75W140-A	
	μ_{bl}	μ_{EHL}	μ_{bl}	μ_{EHL}	μ_{bl}	μ_{EHL}
4000N/70 °C	0.149	0.076	0.095	0.086	0.076	0.079
4000N/90 °C	0.173	0.058	0.107	0.059	0.096	0.063
4000N/110 °C	0.152	0.033	0.121	0.036	0.104	0.059
7000N/70 °C	0.124	0.056	0.097	0.064	0.078	0.063
7000N/90 °C	0.125	0.050	0.101	0.048	0.092	0.047
7000N/110 °C	0.127	0.015	0.099	0.019	0.098	0.030

Table 6.9: Values of the coefficients μ_{bl} and μ_{EHL} for RTB 81107 under three temperatures and two loads.

	75W85-B and 75W90-B		75W90-A and 80W90-A		75W140-A	
	μ_{bl}	μ_{EHL}	μ_{bl}	μ_{EHL}	μ_{bl}	μ_{EHL}
4000N/70 °C	0.097	0.040	0.085	0.047	0.093	0.049
4000N/90 °C	0.098	0.031	0.087	0.053	0.086	0.050
4000N/110 °C	0.089	0.034	0.089	0.050	0.093	0.057
7000N/70 °C	0.073	0.032	0.071	0.036	0.073	0.040
7000N/90 °C	0.070	0.019	0.078	0.037	0.073	0.049
7000N/110 °C	0.073	0.002	0.079	0.026	0.080	0.041

6.7. Prediction of rolling bearings friction torque losses in a FZG gearbox

The sliding coefficient of friction can be calculated for any type of rolling bearing by using Equation (6.18) and with a known values of μ_{bl} and μ_{EHL} (see Tables 6.8 and 6.9).

$$\mu_{sl} = \phi_{bl} \cdot \mu_{bl} + (1 - \phi_{bl}) \cdot \mu_{EHL} \tag{6.18}$$

When the type of rolling bearing generates an elliptical contact, the values presented for TBB can be be used for this case. If the type of contact is linear, the values for RTB are adopted.

For that, the torque loss model can be applied to any type of bearing operating in any type of gearbox. Let's take the example of the test gearbox in the FZG machine. Both spur and helical gear geometries can be tested with FZG machine.

The slave gearbox is mounted with spur gears and cylindrical roller bearings (CRB) and they are only prepared to support radial loads.

The test gearbox, where both spur and helical gears can be tested, has both cylindrical roller bearings (CRB) and four-point contact ball bearings (FPCB) to balance the axial loads, as presented in Table 6.10.

Table 6.10: Rolling bearings assembled on the slave and test FZG gearboxes.

Gearbox	Rolling bearings
Slave	4 NJ 406 cylindrical roller bearings
Test	2 NJ 406 cylindrical roller bearings + 2 QJ 308 four-point contact ball bearings

Using the torque loss model and the corresponding sliding coefficient of friction determined in section 6.6 at 70 °C (see Tables 6.8 and 6.9), a simulation was performed for the cylindrical roller bearing and for the four-point contact ball bearing lubricated with each axle gear oil formulation. The equations related to the geometry of the bearings are used as presented in Appendix E. This simulation was performed considering the load stage K11 of the FZG machine (load arm length of 0.35 m) corresponding to an applied torque on the wheel of 479 Nm, and oil bath lubrication at 70 °C. In these conditions, the radial load on both rolling bearings (CRB and FPCB) are the same and equal to 3601 N and the axial load on the FPCB is equal to zero.

Under these operating conditions and for speeds between 250 rpm and 1750 rpm, the torque loss model together with the μ_{bl} and μ_{EHL} values from Tables 6.8 and 6.9, can be used to evaluate the rolling bearing friction torque in each bearing and in the test gearbox, as shown in Figure 6.13.

The cylindrical roller bearing (CRB) generated lower torque loss (M_t) than the four-point contact ball bearing (FPCB) for all the speed range. The rolling torque (M_{rr}) of the CRB is always higher than the rolling torque generated by the FPCB. The main differences are observed on the sliding torque (M_{sl}), since the FPCB generates a sliding torque loss that can be up to 10 times higher than the sliding torque generated by CRB.

For a constant operating temperature, the 80W90-A oil generated the lowest rolling torque for both geometries due to having the lowest Viscosity Index. At low speed, the four-point contact ball bearing promoted higher torque loss due to the sliding torque contribution, i.e. the sliding torque of that geometry is ten times higher than for a cylindrical roller bearing. Considering the sliding torque at high rotational speed, dependent on the coefficient of friction

of each oil, the results show a lower value for 75W90-B oil while the 75W140-A promoted the highest sliding torque loss.

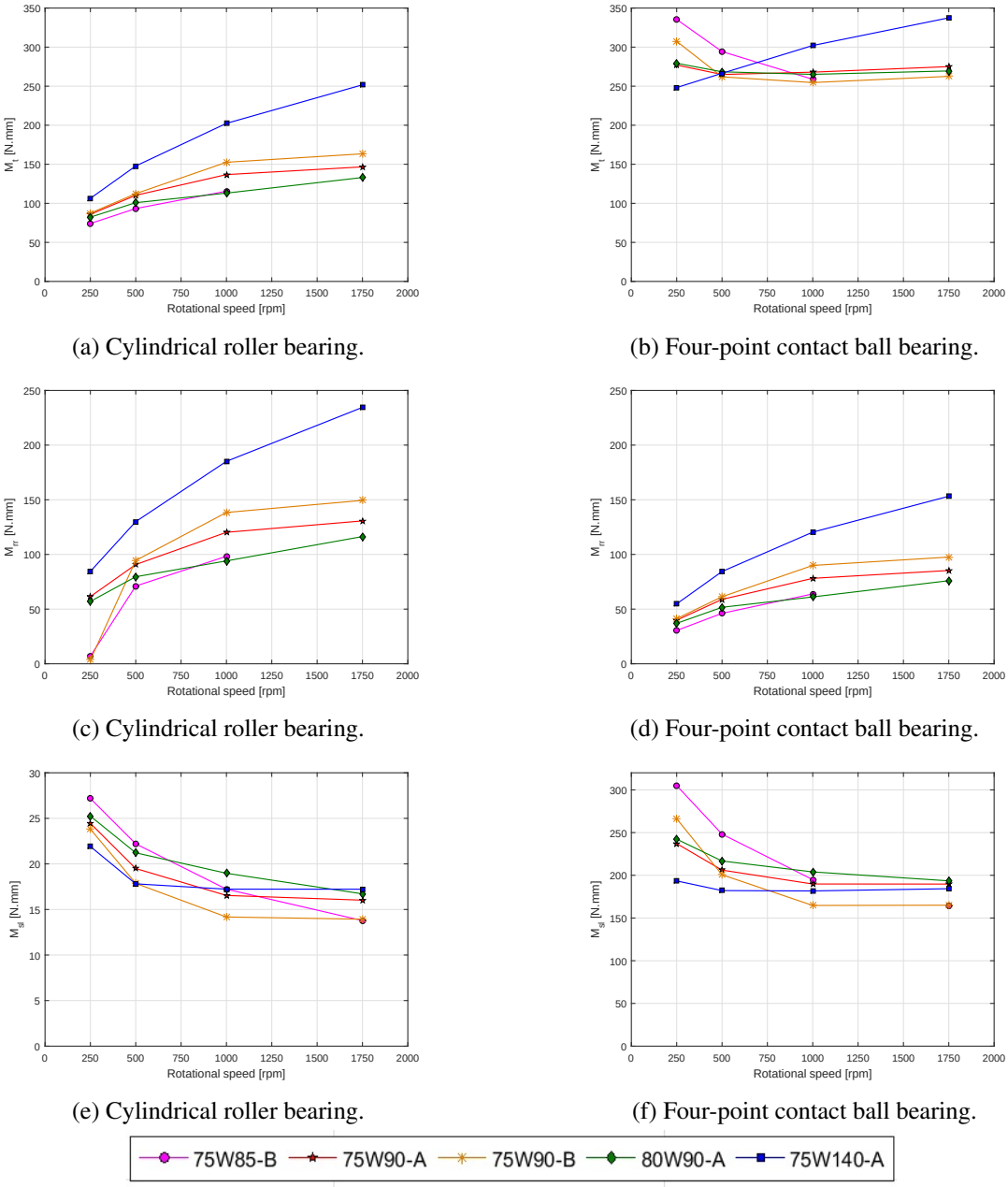

(a) Cylindrical roller bearing.

(b) Four-point contact ball bearing.

(c) Cylindrical roller bearing.

(d) Four-point contact ball bearing.

(e) Cylindrical roller bearing.

(f) Four-point contact ball bearing.

Figure 6.13: Simulation for torque loss of a rolling bearing of a FZG test gearbox for a load stage K11 (479 Nm) with bath lubrication at 70 °C.

6.8. Summary

Three rolling bearing types (TBB, RTB and TRB) were tested in a modified Four-Ball Machine, using five different axle gear oil formulations. The internal friction torque was measured for operating speeds between 75 and 1200 rpm. The friction torque measurements were correlated using a rolling bearing friction torque model.

- The experimental results show that the rolling bearing geometry has a prominent influence on the internal friction torque of the rolling bearings and on the corresponding torque and power loss. Among the three types of rolling bearings, TBB presented the lowest friction torque loss, followed by RTB and TRB ($M_t^{TBB}<M_t^{RTB}<M_t^{TRB}$). At low speed (75 rpm) and for a reference axle gear oil formulation (75W90-A), the torque loss on TBB, RTB and TRB are 290, 1060 and 1200 N.mm, respectively. This means that the elliptical contacts inside the TBB generate significantly less torque loss than the line contacts of the RTB and TRB, and that substantial gains in efficiency might be obtained replacing roller bearings by ball bearings. In fact, it was not possible to run the RTB tests at constant temperature above 600 rpm, because the corresponding torque and power loss was too high, which did not occur in the case of the TBB.
- The five axle gear oils tested showed substantial differences in torque loss, mainly under boundary to mixed film lubrication (specific film thickness Λ below 1.0 and weighting factor ϕ_{bl} greater than 0.5). Under these conditions, the low viscosity candidate (B) oils (75W85-B and 75W90-B) generated higher torque loss than the reference (A) oils (75W90-A, 80W90-a and 75W140-A), for all types of rolling bearings, although these differences were smaller in the case of the Cylindrical Roller Thrust Bearings (RTB). Under full-film lubrication (specific film thickness Λ above 1.0 and weighting factor ϕ_{bl} smaller than 0.5), the differences in torque loss among the five axle gear oils are small and they only reflect the differences in viscosity and in rolling torque of these oil formulations.
- It is assumed that the rolling torque M_{rr} only depends on the operating speed and kinematic viscosity, besides the rolling bearing geometry. Thus, oils 75W85-B and 75W140-A, generated the lowest and highest rolling torques, respectively, because they also have the lowest and the highest kinematic viscosities. The other axle gear oil formulations (75W90-A, 75W90-B and 80W90-A) have very similar viscosities and generated very similar rolling torques (in between the other two formulations), which is consistent with the experimental measurements of the torque loss.
- The sliding torque M_{sl} was determined using Equation (6.15). The analysis of Figures 6.6d and 6.8d show that, with increasing speeds the differences in torque loss among the five axle oil formulations decrease, becoming almost null for the TBB tested at 1200 rpm. This is not so clear in the case of the RTB, because above 600 rpm it was not possible to keep the operating temperature constant (70 °C). The sliding torque loss (M_{sl}) results confirm that, under boundary to mixed film lubrication (λ below 1.0 and ϕ_{bl} greater than 0.5), the low viscosity candidate (B) oils (75W85-B and 75W90-B) generated higher sliding torque loss than the reference (A) oils (75W90-A, 80W90-a and 75W140-A).

- The analysis of Figures 6.6f and 6.8f show that the range of operating speeds allowed to cover the full range of the weighting factor ϕ_{bl}, almost from 1.0 down to 0.0. This means that all lubrication regimes were considered, from boundary film lubrication, through mixed film regime, till full-film lubrication, for all oil formulations and both rolling bearing types. Thus, the calculation of the sliding coefficient of friction also covers all lubrication regimes and the values of μ_{bl} and μ_{EHL}, shown in Table 6.6, can be considered as representative of the axle gear oils tested. It is clear that the candidate (B) formulations have higher values of the boundary coefficient of friction than the standard (A) formulations ($\mu_{sl}^{B} > \mu_{sl}^{A}$), thus generating higher torque loss values at low speed. It is also clear that the candidate (B) formulations have lower values of the full-film coefficient of friction than the standard (A) formulations ($\mu_{EHL}^{B} < \mu_{EHL}^{A}$), thus generating lower torque loss values at high speed, mainly because they have lower kinematic viscosities.
- Three comparisons deserve special attention. Formulations 75W90-A and 75W90-B have very similar physical properties, but have different additive packages and generate different tribo-films [Hammami et al., 2017]. However, the differences in friction torque loss between these two formulations are not very significant, both for TBB and RTB, although in favor of the 75W90-A. Formulations 75W90-A and 80W90-A, have the same additive package but different base oils, PAO vs Mineral, respectively. However, they generate almost the same friction torque loss, whatever the operating conditions, justifying the pertinence of the mineral oil formulation for some applications. In fact, these two formulations have exactly the same values for the boundary and full-film coefficients of friction, that is $\mu_{bl}^{75W90-A} = \mu_{bl}^{80W90-A}$ and $\mu_{EHL}^{75W90-A} = \mu_{EHL}^{80W90-A}$. Finally, as expected, the heavy duty formulation 75W140-A exhibits a quite low friction torque loss under boundary film lubrication conditions.

The new SKF model was applied in order to determine a full-film coefficient of friction (μ_{EHL}) and a boundary film coefficient of friction (μ_{bl}) for a known operating conditions (temperature, load and axle gear oil). The friction torque model predicts with high accuracy the friction torque for the different type of rolling bearing geometries under some operating conditions and for each oil formulation. When the coefficient of frictions are known for each lubricant, the bearing torque loss of cylindrical roller bearings (CRB) and four-point contact ball bearings (FPCB) in test gearbox of FZG machine was calculated by applying the SKF model.

7. Power loss in FZG gearboxes

7.1. Introduction

It is well known that automotive axle is one of the major sources of power loss in the driveline. Thus, any power loss reduction can have the potential to impact in overall vehicle fuel economy. The power loss in axles are mainly due to friction induced mechanical losses at loaded hypoid gear mesh, bearings and seals also due to spin losses associated with lubricant pumping and churning and bearing pre-load [Xu et al., 2011]. Since 1970s, only limited number of experimental studies have been focused on the measurement of axle efficiency or power loss. Most of these works were published in Society of Automotive Engineers (SAE) publications [Hobson, 1979, Porrett et al., 1980, Katoh et al., 1983, Ko and Hosoi, 1984, Winter and Wech, 1988, Anderson and Maddock, 2008, Hurley, 2009, Xu et al., 2011].

Hobson [Hobson, 1979] proposed a laboratory procedure testing variety of axles efficiency as apart of the initial work for SAE required practice. The tests were applicable to full range of drive axles with several lubricants and gears ratio. The tests result demonstrated a significant sensitivity to lubrication conditions and variations in load, speed, and temperature in computing efficiency. Porret *et al.* [Porrett et al., 1980] developed a laboratory axle efficiency test using a torque sweep method. The test axle differential gears are locked to allow all power to be transferred to one axle shaft. The axle power loss was calculated through input and output signals delivered by the torque sensors. The axle efficiency and lubricant temperature were recorded simultaneously. Katoh *et al.* [Katoh et al., 1983] operated with different measurement technology where the tested axle is closed and immersed in the water tank. Assuming that the power loss of the test component is converted into heat rejection, the axle power loss can be measured through the measurement of the inlet and the outlet water stream temperatures and the flow rate.

Ko and Hosoi [Ko and Hosoi, 1984] developed a method for measuring the axle churning loss from the rise in lubricant temperature.

Winter and Wech [Winter and Wech, 1988] investigated the axle efficiency using a standardized efficiency tests using FZG hypoid back-to-back test rig. These tests have illustrated that axle offset and lubricant substantially influences the efficiency. They also reported that synthetic lubricants can increase the axle efficiency at high torque.

Recently, Anderson and Maddock [Anderson and Maddock, 2008], developed an improved methodology for axle power loss and efficiency tests. They proposed a loaded efficiency

block cycle which was repeated 15 times to break in the axle after three additional cycles were run as the actual efficiency test cycles.

Hurley [Hurley, 2009] and Xu *et al.* [Xu et al., 2011] investigated the thermal behaviour and the power losses of an instrumented automotive rear axle as an extension of the previous work defined in [Anderson and Maddock, 2008] except that the lubricant temperature is not constant but allowed to rise until reached steady state conditions.

Kolekar [Kolekar et al., 2013] provided an axle power loss prediction over a representative driving cycle relying heavily on empirical relations.

Talbot *et al.* [Talbot et al., 2016] used a methodology to predict total power loss of an automotive axle including both load dependent and load independent losses. This methodology was used to simulate the axle efficiency experiments of Xu *et al.* [Xu et al., 2012] under several operating and pre-load conditions in order to quantify its accuracy in predicting the total axle power losses.

The experimental results found in literature are usually interested on the general problem of axle power loss, without any particular discussion on meshing gear power loss lubricated with commercial available lubricants. This current chapter deals with the measurement of the torque loss in the FZG test gearbox, lubricated with different axle gear oils. A type A10 cylindrical gearing will be tested in FZG machine. This test method is useful for understanding the influence of each axle lubricant, used typically in hypoid gearing applications, on gear efficiency. The power loss model presented in Chapter 5 will be applied and calibrated for different axle lubricants, type A10 gear geometry and test conditions. The results allowed to characterize the coefficient of friction in meshing gear and to calculate the power loss in the meshing gear.

7.2. Materials and methods

7.2.1. Test rig

The FZG gear test rig schematic view is shown in Figure 7.1 (a). This was the main apparatus used while conducting the experimental tests. The FZG four square test machine is used in wide range of standardized gear tests like scuffing [Michaelis, 1986, iso, , iso, 2004, iso, 2005, Martins et al., 2008a], micropitting [Forschungsvereinigung Antriebstechnik, 1993, DGM, 2002] and pitting [Winter and Oster, 1987]. This machine utilizes a recirculating power loop principle to provide a fixed torque load to a pair of precision test gears. The slave (drive) gearbox (3) and the test gearbox are connected through two torsional shafts. The shaft connected to test pinion (1) contains a load clutch used to apply the torque through the use of known weights hung on the loading arm. The load clutch divides this shaft in two parts. One part of the clutch can be fixed with locking pin (5) and the other part can be twisted using the load lever (6) and different weights.

The test machine is powered by an AC-motor of maximum 7,4 kW at a speed of approximately 3000 r/min. The direction of rotation is presented in Figure 7.2. For dip lubrication, the test gearbox contains electrical heaters to increase the temperature of the oil. The heater and

the cooling coil allow to maintain the temperature constant as required by the test operating conditions. A temperature sensor (8) located in the side of the test gearbox is used to measure the temperature required. For jet lubrication, the slave gearbox receives the oil from the reservoir with heaters that helps to increase the oil temperature up to the desired value. Then the temperature is controlled by the feedback of the temperature sensor in the tube reservoir. The reservoir contains an oil pump which helps the oil to circulate in the slave gearbox with a selected oil flow.

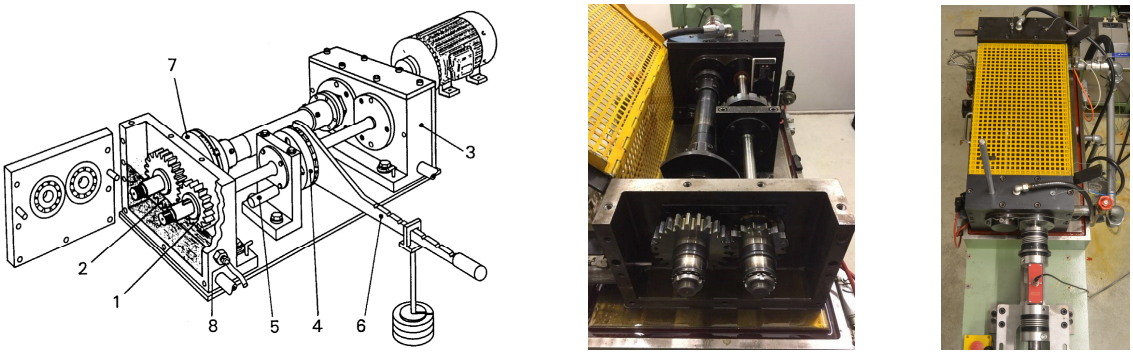

(a) Schematic view. (b) A10 gears detail. (c) Torque cell.

Figure 7.1: FZG gear test rig.

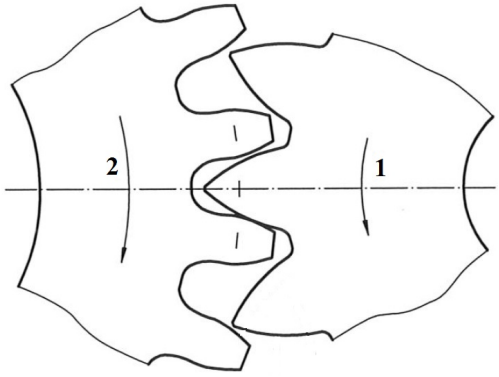

Figure 7.2: Mounting the FZG test gears of type A.

During the tests, the operating temperatures and torque loss were measured. The operating temperatures at specific points of the assembly were measured using type K thermocouples, as shown in Figure 7.3.

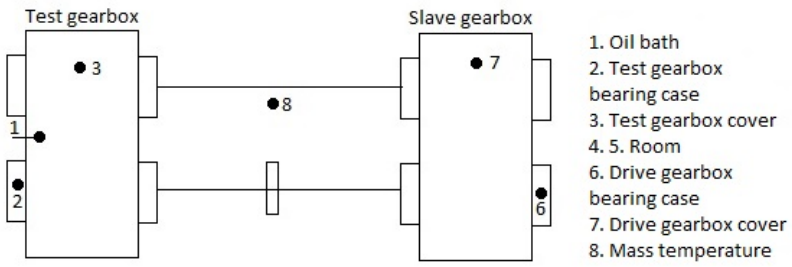

Figure 7.3: Thermocouples location in FZG machine.

The torque loss (T_L) was measured using EHT Messtechnik DRDL II torque transducer assembled on the FZG test rig between the drive gearbox and the DC motor, as presented in Figures 7.1 (c) and 7.4. The static torque is applied on the pinion (T_{IN}) which results in a static torque on the wheel according to Equation (7.1).

$$T_W = i \cdot T_{IN} \tag{7.1}$$

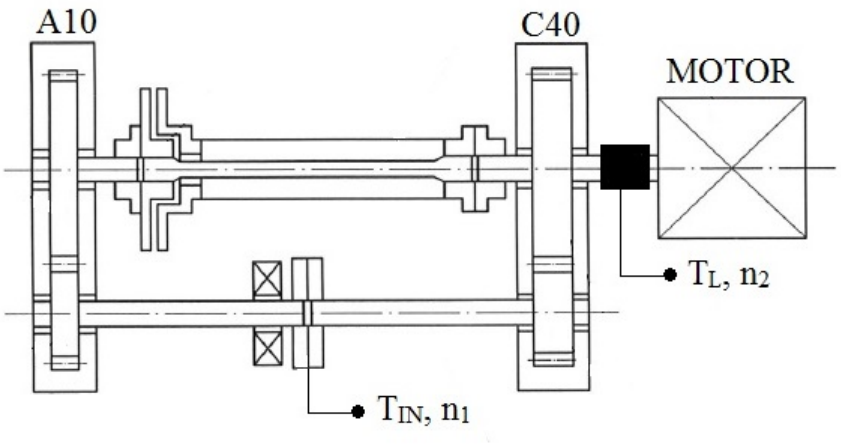

Figure 7.4: Schematic view of the FZG gear test rig with the torque measuring system.

To acquire data, the system uses a sensor interface (Value Master V. 2.43), communicating with a PC via Ethernet. The technical characteristic of the sensor are exhibited in Table 7.1. The integration of the torque cell with the software allows to record the torque values with an adjustable sampling rate (from 1 to 1000 Hz).

Table 7.1: Technical specifications of the ETH DRDL torque cell.

Torque transducer Type DRDL-II	
Nominal torque [Nm]	50
Measurement range [Nm]	10\50
Non -linearity[%]	<0.1
Hysteresis [%]	<0.1
Accuracy [%]	0.01
Temperature sensitivity [%/K]	0.01
Torque Measuring Module Type Value Master Base	
Accuracy [%]	0.02
Non -linearity[%]	0.1
AD converter resolution	11bit+1bit for leading sign

7.2.2. Gears

Torque loss tests were performed on FZG machine with different gearboxes configurations.

On the drive or slave gearbox, the type C gears with a face width of 40 mm were usually assembled (see Figure 7.5 (a)). The C40 gear was run-in under jet lubrication lubricated with PAO ISO VG 150 gear oil. This oil is usually used to lubricate the slave gearbox in micropitting and scuffing tests.

On the test gearbox, type A10 gears (see Figure 7.5 (b)) are dip lubricated with each axle gear oil. This type of gears was selected since it provides high Hertzian pressure and high tangential speed simulating the hypoid gears.

The main properties of each gear geometry, shown in Figure 7.5, are listed in Table 7.2.

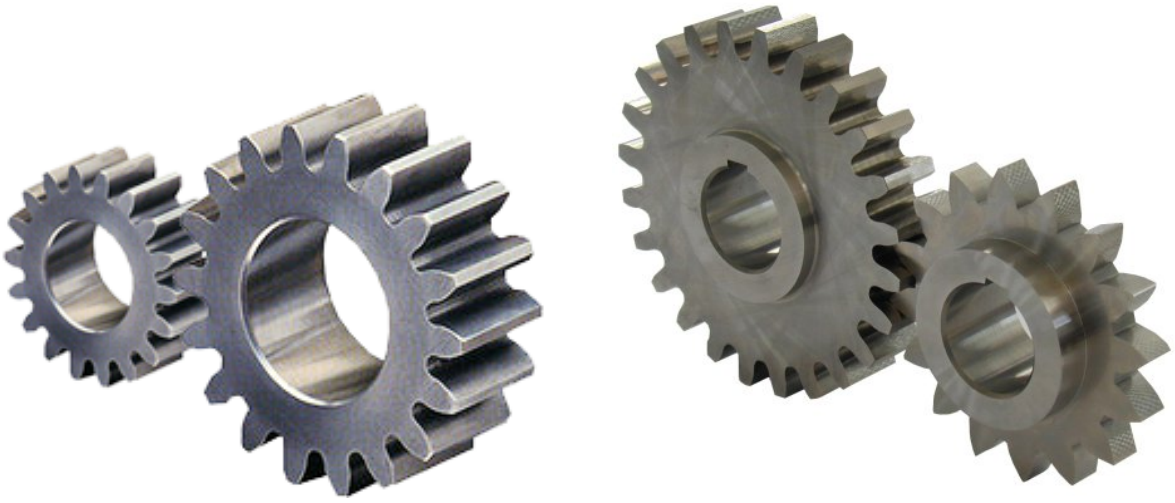

(a) C40. (b) A10.

Figure 7.5: (a) C40 and (b) A10 gears design.

Table 7.2: Geometric properties of the C40 and the A10 gears.

Property	Symbol	Units	C40		A10	
			Pinion	Wheel	Pinion	Wheel
Number of teeth	z	[-]	16	24	16	24
Module	m	[mm]	4.5			
Axis distance	a	[mm]	91.5			
Pressure angle	α_z	[°]	20			
Working pressure angle	α_w	[°]	22.44			
Face width	b	[mm]	40		10	20
Addendum modification coefficients	x	[-]	0.1817	0.1715	0.8532	-0.5
Reference diameter	d	[mm]	72	108	72	108
Working pitch diameter	d'	[mm]	82.64	118.54	73.2	109.8
Tip diameter	d_a	[mm]	82.46	118.36	88.5	112.32
Base diameter	d_b	[mm]	67.66	101.49	67.66	101.49
Total contact ratio	ε_γ	[-]	1.44		1.33	
Length of path of contact	g_α	[-]	19.099		17.665	
Material		[-]	20MnCr5			
Gear loss factor	H_{VL}	[-]	0.1995		0.3044	
Plane of action area	$\overline{AE}.b$	[mm^2]	763.9		176.6	

Since it is of major importance to compare the behaviour of each axle oil formulation, as well as calibrate the FZG slave gearbox and the power loss model, the surface roughness of A10 gear was evaluated before and after the end of the test with each selected axle gear oil under all the operating conditions.

Figure 7.6 displays the wheel tooth flank profiles measured before and after the end of the test in radial direction. The surface roughness of A10 pinions was measured between oil change in both directions and before and after the tests performed with the selected oil. The results were presented in Table 7.3. The surface roughness in radial direction is generally close to the roughness in axial direction due to the grinding procedure for type A10 gear.

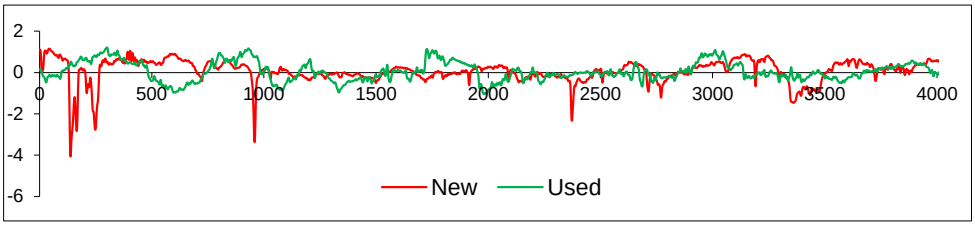

Figure 7.6: A10 wheel absolute average roughness (R_a) in radial direction.

Table 7.3: Roughness parameters of the A10 pinions before (New) and after (Used) the end of the test for each axle gear oil.

Lubricant	Condition	Direction	R_a	R_q	R_z	R_{max}
75W85-B	New	Radial	0.34	0.44	2.45	2.99
		Axial	0.36	0.47	2.93	3.52
	Used	Radial	0.20	0.28	1.80	2.40
		Axial	0.48	0.71	2.76	3.59
75W90-A	New	Radial	0.39	0.51	3.13	3.81
		Axial	0.36	0.47	2.60	3.34
	Used	Radial	0.25	0.34	2.38	2.82
		Axial	0.23	0.31	1.88	2.32
75W90-B	New	Radial	0.45	0.60	3.04	4.06
		Axial	0.45	0.59	3.81	5.35
	Used	Radial	0.27	0.37	2.21	2.98
		Axial	0.28	0.39	2.89	3.80
80W90-A	New	Radial	0.35	0.47	2.58	3.43
		Axial	0.37	0.48	3.10	4.13
	Used	Radial	0.18	0.27	1.78	2.63
		Axial	0.29	0.40	2.68	4.38
75W140-A	New	Radial	0.29	0.40	2.40	3.25
		Axial	0.33	0.44	3.00	3.87
	Used	Radial	0.14	0.21	1.51	2.07
		Axial	0.22	0.32	2.50	3.79

The load distribution and the corresponding local Hertzian pressure along the plane of action of A10 gear geometry were displayed in Figure 7.7 for an input torque on the wheel equal to 479 Nm, which corresponds to the standard FZG K11 load stage.

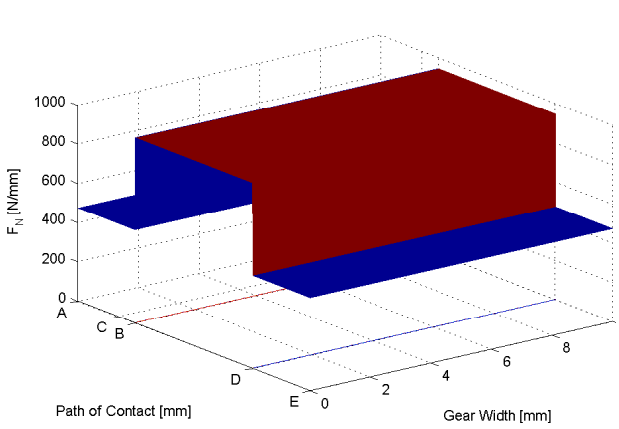

(a) The load distribution (F_N) for A10 gear.

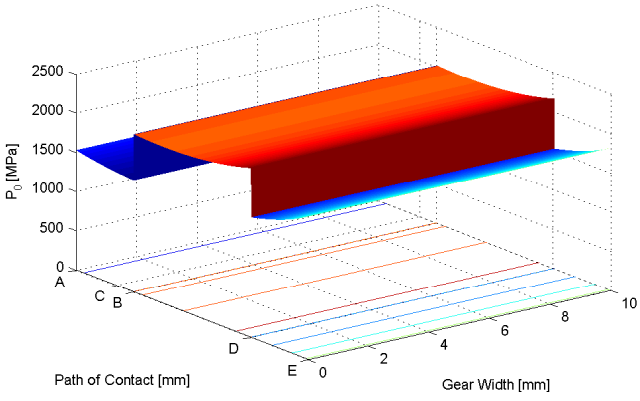

(b) The local Hertzian pressure (P_0) along the path of contact for A10 gear.

Figure 7.7: (a) The load distribution (F_N) and (b) the corresponding local Hertzian pressure (P_0) along the path of contact for A10 gear geometries.

It is clear that the maximum Hertzian pressure is very high for type A gear similar to hypoid gears used in axles (see Figure 7.9). The load transition for A10 gear (Figure 7.7 (c)) is not smoother. The number of teeth simultaneously in contact for A10 gear is not constant. The type A10 gear results in higher average load per unit length and higher Hertzian pressure and consequently lower flank safety factor (S_F = 0.8).

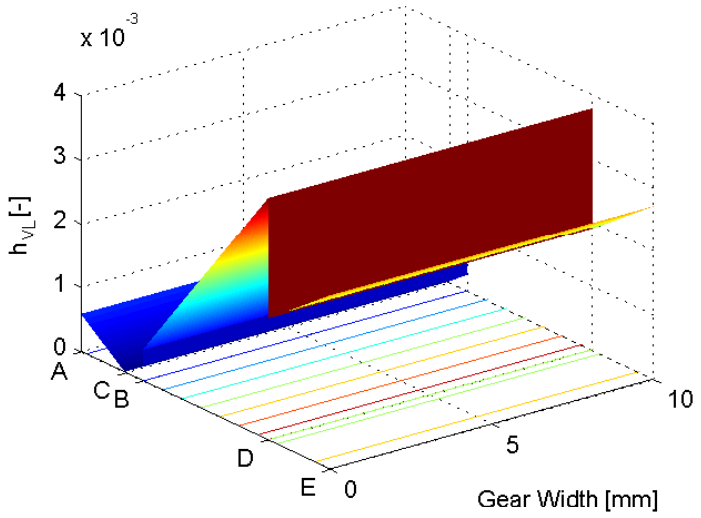

Figure 7.8: Dimensionless parameter h_{VL} representative of the instantaneous product of force and sliding velocity along the path of contact for A10 gear.

The gear loss factor was calculated using Equation (5.7). Figure 7.8 shows the evolution of the dimensionless parameter given by Equation (7.2), along the plane of action for A10 gear geometry. At the point D, the A10 gear show a maximum of the h_{VL} parameter.

By knowing that the volume below each surface is the actual gear loss factor H_{VL}, it is clear that A10 gear geometry promotes high gear loss factor. Table 7.2 presents the gear loss factor and the plane of action of area for each gear geometry.

$$h_{VL} = \frac{1}{p_{bt}} \cdot \frac{F_N(x,y)}{F_{bt}} \cdot \frac{v_g(x,y)}{v_{tb}} \tag{7.2}$$

7.2.3. Rolling bearings and seals

The shafts on the slave gearbox are supported with 4 cylindrical roller bearings (NJ 406 MA) and the shafts of the test gearbox are also supported with 4 cylindrical roller bearings (NJ 406 MA). The test gearbox rolling bearings are different from the configuration presented in Table 6.10 because A10 gears create high radial load. For that the 2 QJ 308 four-point contact ball bearings that support axial load were replaced with 2 NJ 406 cylindrical roller bearings that support radial load.

The cylindrical roller bearings has a dynamic load capacity of C=60.5 kN and a static load capacity of C_0=53 kN .

The gearboxes are sealed with four Viton lip seals with an internal diameter of d_{sh}=30 mm. A Viton lip seal is also assembled on the drive gearbox motor shaft (d_{sh}=26 mm).

7.3. Test conditions

The type A10 gears (see Table 7.4) were selected as they provide a high Hertzian pressure and high tangential speed simulating the hypoid gears found in axles (see Figure 7.9).

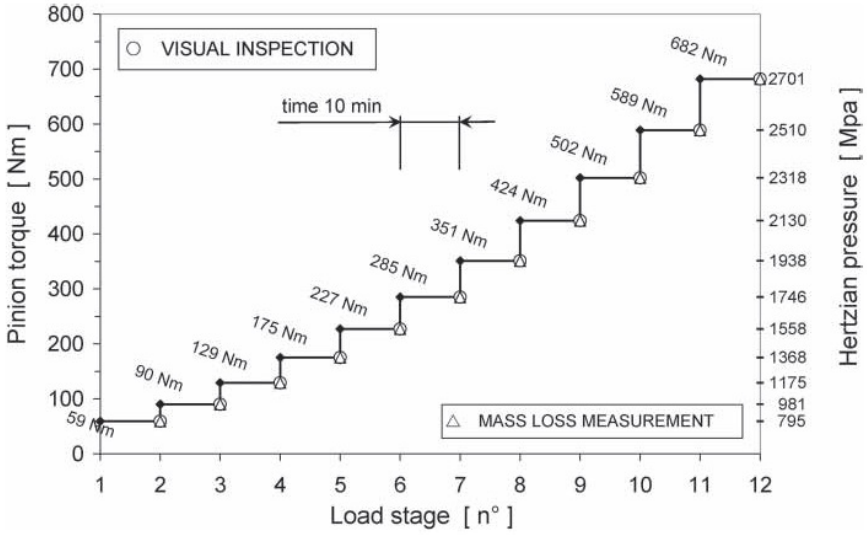

Figure 7.9: Experimental tests with hypoid gears [Conrado et al., 2007].

The gear load and speed were selected in order to mimic more realistic axle operating conditions. The test procedure is based on running the input shaft (pinion) at fixed load and speed condition. Figure 7.10 shows the bench test speed and torque obtained in road test.

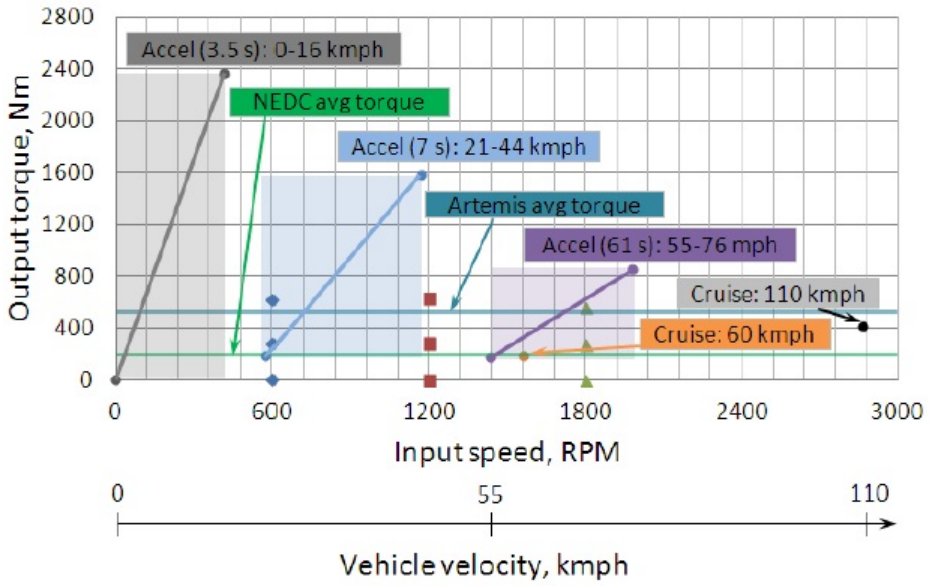

Figure 7.10: Comparison between rig test range to road test range [Kolekar, 2013].

Due to limitations of the input motor, the torque applied was not large enough to simulate maximum acceleration of the road test but was good enough to show intermediate cruise acceleration. For example, 1750 rpm represents 67 kmph speed on the road for a Ford F150 pickup truck. For that the input shaft speed range were selected from 250 rpm up to 1750 rpm. Figure 7.10 also presented the average torque applied in NEDC and Artemis drive cycles with a maximum out put torque of 200 Nm and 500 Nm, respectively.

The operating conditions of the real axle were used as reference for the test conditions selected for the FZG gear tests, presented in Table 7.4 (load arm of 0.35 m). The experimental tests were conducted at for load stages (K1, K5, K8 and K11).

Table 7.4: Applied loads in torque loss tests with a load lever arm of 0.35 m.

	Gears			Rolling bearings
K_{FZG}	T_W [Nm]	F_{bn} [N]	p_H [MPa]	F_r [N]
K1	4.95	97.5	217.8	49.5
K5	104.97	2068.6	1002.9	1049.1
K8	257.38	5072.1	1570.4	2572.2
K11	478.72	9434.1	2141.8	4784.3

7.4. Test procedure

Table 7.4 displays the operating conditions used in the torque loss tests. The tangential force transmitted by the gears, the Hertz pressure in the gears and the radial forces on the rolling bearings are also included.

Dipped lubrication is a way of distributing lubricants to the intended destination in enclosed mechanical systems using a rotating component, such as axle. Low oil sump level in dip lubricated gear pairs is used to reduce the no-load losses. The oil volume in the test gearbox was set to 1.1 l (see Figure 7.11). For the slave gearbox the jet oil temperature was kept at 80 °C with the oil injection flow of 3l/min.

The tests were run under hot start conditions where the starting sump lubricant temperature is equal to 70 °C.

The test procedure used in the torque loss tests can be summarized as follows:

1. Run load stage K_i at each rotational speed (see Table 7.4) during 2 hours;
   - Recording the working temperatures (see Figure 7.3);
   - Register torque measurement with a sample rate of 1 measurement per second;
2. Repeat the process until the highest load stage is reached.

The oil circulation system was operating continuously during the night at constant temperature to assure a faster stabilization temperature from one day to the next. The test room has a ventilation system in order to maintain a stabilized environment temperature.

The values presented for torque loss and temperature are the average of the last 30 minutes of operation because only the steady state operating conditions are considered for the average calculation. Between each oil tested, the test gearbox was flushed with solvent. The oil reservoir and the injection system lubricated with PAO 150 were kept for all the axle gear oils. The axle gear oils were tested in the following order: 75W90-A, 75W85-B, 80W90-A, 75W90-B and 75W140-A.

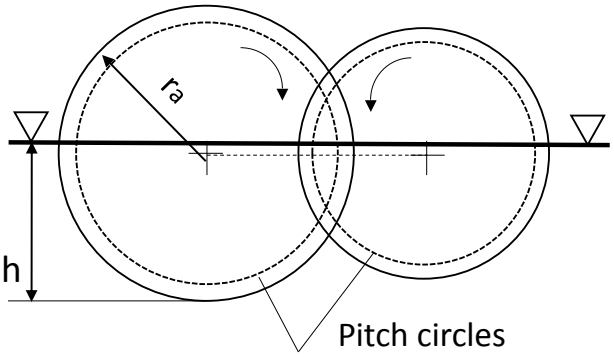

Figure 7.11: Oil level during tests.

7.5. Film thickness on meshing gears

Dowson and Higginson's equation for linear contacts [Dowson and Higginson, 1959] was used to determine the central film thickness in the gears contact (7.3).

$$h_0 = 1.95 \cdot R_x \cdot U^{0.727} \cdot G^{0.727} \cdot W^{-0.091} \tag{7.3}$$

The parameters U, G and W are detailed in Equations (2.4), (2.5), (2.6) and (2.7). Figure 7.12 displayed the average value of the specific film thickness along the path of contact for A10 gears at each test condition with an oil bath temperature equal to 70 °C. The differences between axle gear oils are due to the differences in the operating viscosity, but those differences are not enough to promote a different lubrication regime.

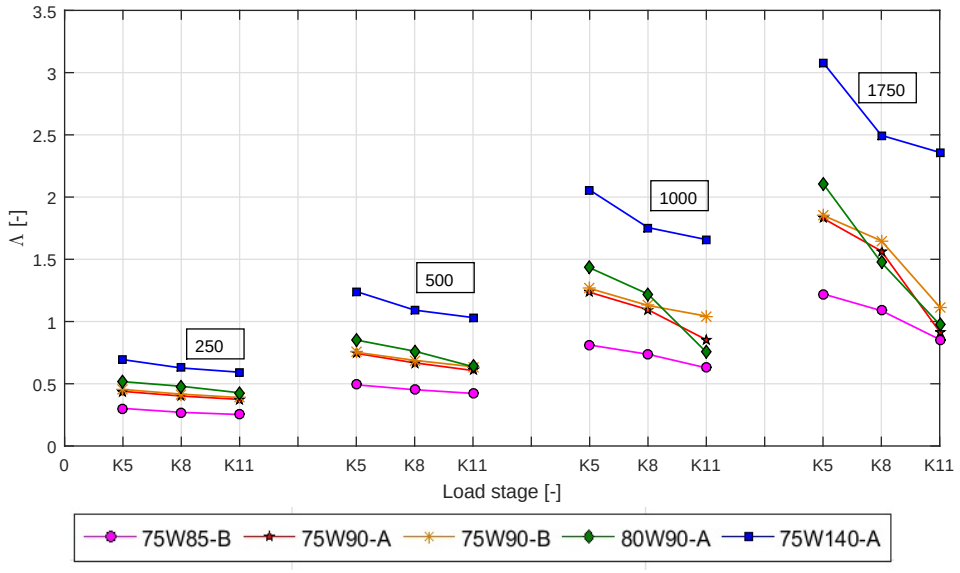

Figure 7.12: Average specific film thickness prediction for A10 gears at each test condition.

At 250 rpm, A10 gear geometry operates under boundary film lubrication because $\Lambda \leq 0.7$ except for 75W140-A oil where A10 gear operates under mixed lubrication condition. It is interesting to note that the majority of the tests at 500, 1000 and 1750 rpm were performed under mixed lubrication conditions except the test using 75W85-B oil at 500 rpm was performed under boundary lubrication condition. Another exception at 1750 rpm where Λ is greater than 2 for 75W140-A oil and for 80W90-A oil with K5 load stage, full film lubricating condition occurs.

7.6. Results and discussion

7.6.1. Temperatures

The temperature of the oil bath in the test gearbox is presented in Table 7.5 for all axle gear oils and test conditions. The tests were performed under constant operating temperature conditions. However, for higher loads and speeds, the temperature is higher than 70 °C .

It is also interesting to observe the stabilization temperature of the test rig base plate ($\theta_{stab,base}$), that is calculated using Equation (7.4). It was verified that for the same operating conditions, the difference between the maximum and the minimum stabilization temperature is quite smaller, usually smaller that 2 °C whatever the lubricating oil considered.

$$\theta_{stab,base} = \theta_{base} - \theta_{room} \tag{7.4}$$

Table 7.5: Temperature of oil bath in the test gearbox [°C].

n_2	K_{FZG}	75W85-B	75W90-A	75W90-B	80W90-A	75W140-A
250	K1	70.1	70.3	69.5	69.7	70.0
	K5	70.5	70.4	70.0	71.5	70.0
	K8	71.8	70.7	70.2	71.3	70.7
	K11	72.2	71.3	70.7	73.4	70.7
500	K1	69.5	68.4	69.8	70.4	67.2
	K5	71.3	69.5	69.9	71.7	67.2
	K8	71.3	70.5	70.3	72.7	68.8
	K11	71.8	72.1	71.1	77.1	68.8
1000	K1	70.2	68.5	68.7	71.2	67.2
	K5	71.4	69.4	69.3	71.2	67.2
	K8	72.0	70.9	70.6	73.9	69.9
	K11	76.5	78.6	71.5	90.4	69.9
1750	K1	69.8	68.6	68.9	70.4	67.2
	K5	71.3	70.0	70.3	71.8	67.2
	K8	72.8	72.8	71.7	82.0	71.9
	K11	79.5	93.5	85.7	97.0	71.9

7.6.2. Mass loss results

For all lubricants tested, the pinion was weighted before and after performing the FZG tests for all the load stages in order to calculate the mass loss. The mass loss is directly related to the oil level used. Since the reduction of oil level in the sump corresponds to a sensible decreasing of the scuffing load-capacity of gears for all lubricants tested [Conrado et al.,

2007]. Figure 7.13 shows the mass loss at the end of K11 load stage for each axle gear oil. These tests data refer to the tests performed with an immersion depth presented in Figure 7.11. It is known that the scuffing load stage can be defined with visual inspection and also it can be determined with mass loss measurement. Through visual inspection during performing the tests, it is observed a high wear rate on the contact surfaces of the tooth gears which means that the K11 load stage at 1750 rpm is the failure load stage for 75W85-B oil and that this oil has the lower load carrying capacity than other axle gear oil formulations. The results show that the 75W90-B oil presents the highest pinion mass loss followed by the 75W90-A oil and then the 75W85-B oil. The lowest pinion mass loss was presented for both 80W90-A and 75W140-A oils.

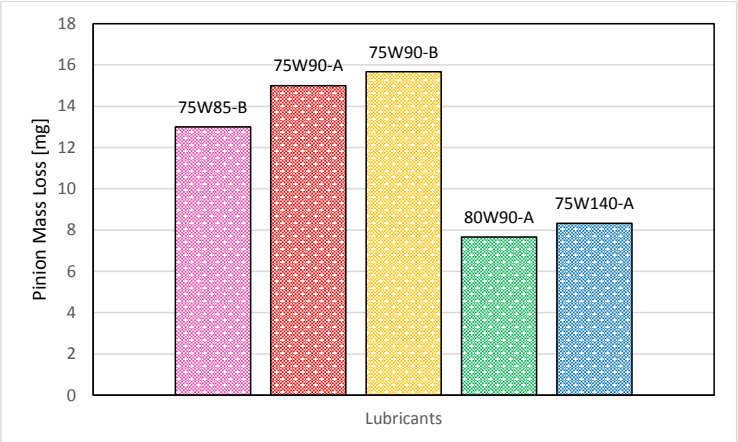

Figure 7.13: Pinion mass loss measurement after each axle gear oil.

7.6.3. Total torque loss

The total torque loss (T_L) measurements of both test and slave gearboxes, for all the lubricants and test conditions are displayed in Table 7.6.

Since the torque loss tests were performed with different gearboxes, different gears and different operating conditions, it is interesting to study separately the two gearboxes.

Table 7.6: Total torque loss (C40+A10) [Nm] for each tests condition.

n_2	K_{FZG}	75W85-B	75W90-A	75W90-B	80W90-A	75W140-A
250	K1	0.82	0.85	0.81	0.87	0.81
	K5	3.69	3.44	4.01	3.71	3.50
	K8	7.76	7.48	8.05	8.13	7.58
	K11	14.14	14.76	13.88	12.30	13.08
500	K1	1.04	1.06	1.03	1.04	1.14
	K5	3.66	3.33	3.83	3.68	3.48
	K8	7.25	6.86	7.41	7.87	7.04
	K11	12.76	13.13	12.52	11.28	11.88
1000	K1	1.30	1.29	1.33	1.36	1.41
	K5	3.83	3.41	3.91	3.89	3.71
	K8	7.04	6.59	7.12	7.74	6.88
	K11	11.29	12.07	11.47	11.04	11.04
1750	K1	1.49	1.67	1.64	1.69	2.10
	K5	4.14	3.75	4.27	4.15	4.22
	K8	6.88	6.71	7.13	7.55	6.95
	K11	–	10.75	10.49	9.99	10.48

7.6.3.1. Slave gearbox

The results from the slave gearbox where C40 gears were only tested with PAO ISO VG 150 oil are calculated using earlier experimental results [Fernandes et al., 2014b]. Fernandes *et al.* presented the results for an FZG tests assembled with a C40 gear set and 4 cylindrical roller bearings (NJ 406 MA) in both slave and test gearboxes (see Table 7.7). Both gearboxes were jet lubricated with PAO 150 gear oil. The oil jet input temperature was kept constant (80±1 °C). Tests were performed for different FZG standard load stages: K1, K5, K7 and K9 (arm lever=0.35m) and at three rotational speed: 200, 400 and 1200 rpm.

Table 7.7: Configuration of FZG geraboxes tested.

Gearbox	Slave	Test
Gears	C40	C40
Rolling bearings	4 NJ 406 MA	4 NJ 406 MA
Seals	2 viton seals (d=30mm)+1 viton seals (d=26mm)	2 viton seals (d=30mm)

The total power losses (C40+C40) dissipated in the slave and the test gearboxes were experimentally measured.

Since each type of power losses can be calculated as presented in Equation (5.62) and details in Chapter 5, it is possible to calculate the no-load losses P_{VZ0}.

For this case, it is possible to do an interpolation for the churning losses and presents the following Equation:

$$P_{VZ0} = 0.136 \times \omega_2^{1.2831} \tag{7.5}$$

Using Equation (7.5), it is possible to calculate the churning losses at 250, 500, 1000 and 1750 rpm.

Knowing the configuration of both gearboxes, the load depend gear losses P_{VZP} can be calculated using Ohlendorf Equation (5.3) under different FZG standard load stages: K1, K5, K8 and K11 (arm lever=0.35m (see Table 7.4)) and at four rotational speed: 250, 500, 1000 and 1750 rpm. The rolling bearing losses P_{VL} can be calculated using SKF model (see section 5.3.2.2) as the sum of the power losses of the 8 rolling bearings also the seals losses P_{VD} were calculated using Simrit Equation (5.45) as the sum of the power losses of the five viton seals.

So, applying the model presented in chapter 5, the experimental total power losses under K1, K5, K8 and K11 load stages and 250, 500, 1000 and 1750 rpm were determined (see Equation (7.6)).

$$P_V^i = \underbrace{P_{VZ0}}_{0.136\times\omega_2^{1.2831}} - \underbrace{P_{VZP}^i}_{\mu_{mz}\cdot P_{IN}\cdot H_V} - \underbrace{P_{VL}^i}_{NewSKFModel} - \underbrace{P_{VD}}_{SimritEquation} \tag{7.6}$$

In order to calculate the power loss in the slave gearbox P_{VS} Equation (7.7) was used.

$$P_{VS}(C40) = P_V(model(C40+C40))/2 \tag{7.7}$$

The experimental torque loss results of the slave gearbox are presented in Figure 7.14 for C40 gears for all load stages (K1, K5, K8, K11).

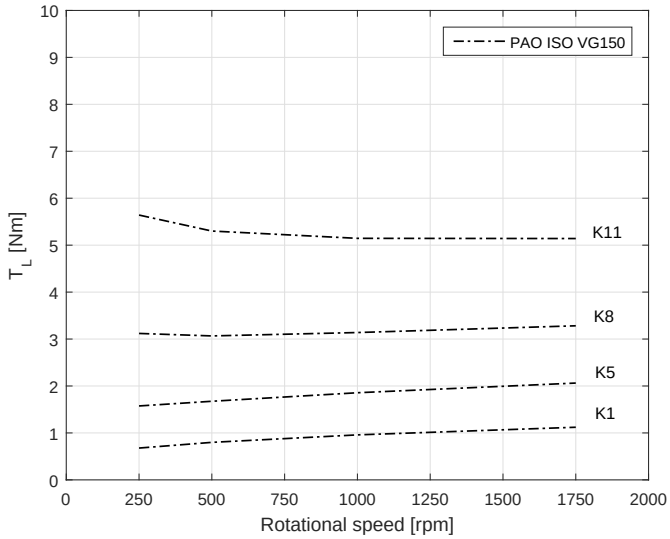

Figure 7.14: Experimental torque loss for the slave gearbox (C40 gears).

7.6.3.2. Test gearbox

For the test gearbox, the experimental torque loss results P_{VT}, calculated using Equation (7.8), for A10 gear, for all load stages (K1, K5, K8 and K11) at the input speeds of 250, 500, 1000 and 1750 rpm and for different axle gear oil formulations are presented in Figure 7.15.

$$P_{VT}(A10) = P_V^{exp} - P_{VS}(C40) \tag{7.8}$$

The torque loss measured for K1 load stage were performed to quantify the load independent losses of the gears. It is observed that the torque loss of the slave gearbox is higher than the torque loss of the test gearbox. This was expected since the tooth width of A10 gear is smaller than in C40 gear.

It is clear that 75W140-A oil with the highest operating viscosity, always generated the highest torque loss under load stage K1. It is observed also that 75W85-B oil with the lowest operating viscosity promoted the lowest torque loss. Other formulations presented similar torque losses for all speed range. This behaviour was expected since the lubricant viscosity is one of the factors that influence the no-load losses, as stated in section 5.2.2.

Under K5 load stage, 75W90-B oil generated the highest torque loss while 75W90-A generated lowest torque loss, no matter the rotational speed. The difference between them reached at least 23 %. The 75W140-A oil presented the highest increase of the torque loss values which is expected with the high rolling bearing losses at high speed (Figure 6.13). Both oils 80W90-A and 75W85-B shown similar behaviour whatever the rotational speed.

When load stage K8 was applied (see Figure 7.15) the highest torque loss is achieved using mineral oil (80W90-A). No matter the rotational speed, the 75W90-A keeps lower torque loss than other oil formulations. The other two candidate oils and 75W140-A oil generated a torque loss values in between the previous two oils.

For the tests performed at load stage K11, the 80W90-A oil generated much lower torque loss than other formulations: 36 % at 250 rpm and 15 % at 1750 rpm less than 75W90-A oil. The differences between the axle gear oils become smaller when the speed increases.

The influence of the rotational speed on the oil behaviour is changed according to the load stage applied. For K1 and K5 load stages, the no-load losses are still very important in total torque loss measured, resulting in an increased torque loss when the rotational speed increased. For K8 and K11 load stages, the torque loss start to decrease or remains constant with increasing rotational speed and the behaviour of the lubricant is expected to be influenced mainly with the coefficient of friction of each oil. The film thickness predictions clearly show that increasing from 250 rpm to 1750 rpm promotes lubrication regime transition which affects the meshing gears torque loss mainly when high loads are applied.

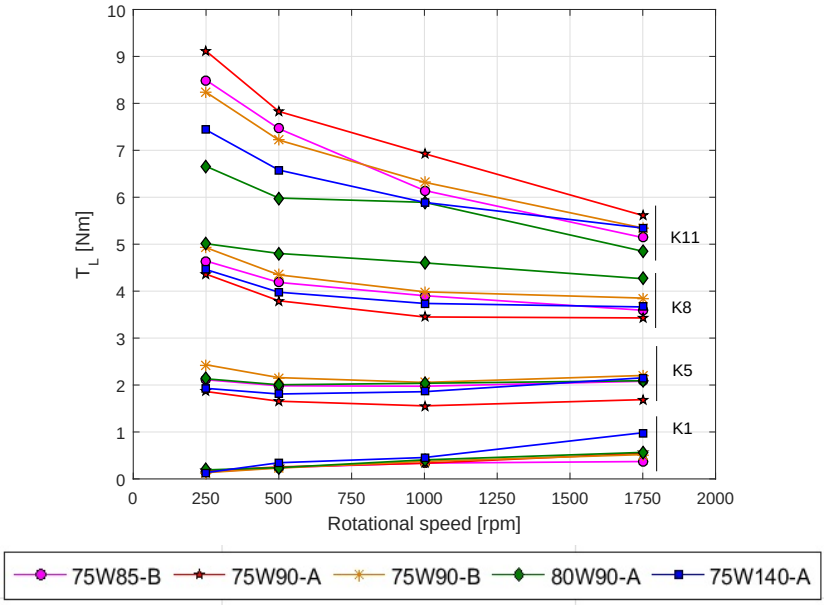

Figure 7.15: Experimental torque loss for the test gearbox (A10 gears).

7.6.4. Power loss model

The experimental results presented in section 7.6.3 were used in the power loss model in order to predict the power loss generated by each FZG gearboxes components. The gearbox power loss model detailed in Chapter 5, can be summarised in Equation (7.9).

$$P_V^{i\ exp} = \underbrace{P_{VZ0}}_{P_V^{1\ exp}-P_{VL}^1-P_{VD}} - \underbrace{P_{VZP}^i}_{\mu_{mz}\cdot P_{IN}\cdot H_V} - \underbrace{P_{VL}^i}_{NewSKFModel} - \underbrace{P_{VD}}_{SimritEquation} \tag{7.9}$$

For each load stage i the experimental power loss is calculated using Equation (7.10).

$$P_V^{i\ exp} = T_L^i \cdot \omega \tag{7.10}$$

As mentioned in section 5.6 under K1 load stage, the no-load gear losses can be calculated based on the experimental results. Different rolling bearing models were discussed in Chapter 5 and the New SKF friction torque model was calibrated in Chapter 6 for each axle gear oil used. The corresponding boundary (μ_{bl}) and full-film (μ_{EHL}) coefficients of friction are known for roller bearings. The seal losses were calculated using the Simrit equation, also discussed in Chapter 5.

7.6.5. No-load gear power loss

To understand the no-load behaviour of the each axle gear oils in the FZG gearboxes, the K1 load stage tests were performed. Under K1 load stage (low input torque, T_W = 4.95 Nm) Equation (7.9) becomes Equation (7.11).

$$P_V^{1\ exp} = P_{VZ0}^1 + P_{VZP}^1 + P_{VL}^1 + P_{VD}^1 \tag{7.11}$$

The no-load gears loss (P_{VZ0}) is determined through Equation (7.12), since P_{VZP}^1=0.

$$P_{VZ0} = P_V^{1\ exp} - P_{VL}^1 - P_{VD} \tag{7.12}$$

As presented in Figure (5.2), the no-load losses included the power loss generated by the gears, by the rolling bearings assembled in the clutch shaft (see Figure 7.1 (a)) and by the seal which is assembled on the drive gearbox motor shaft. Under no-load conditions, the new SKF rolling bearing friction torque model only considers the drag loss mechanism as a source of power dissipation.

As mentioned in Chapter 6, the predicted drag loss values are sometimes disregarded. To be more accurate in the quantification of the other power loss sources, the FZG rolling bearing losses under no-load conditions are taken into account in the term P_{VZ0}, given by Equation (7.12).

Figure 7.16 displays the results of T_{VZ0} (=P_{VZ0}/ω) for each rotational speed and axle gear oil formulation. The 80W90-A oil generated the highest no-load gear losses except at 500 and 1750 rpm, the 75W140-A oil promoted the highest no-load torque loss.

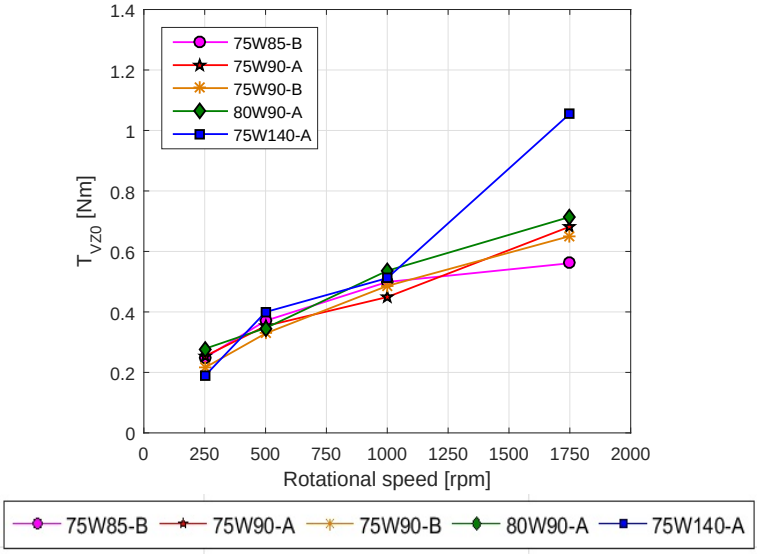

Figure 7.16: Load independent torque loss at K1 (T_{VZ0}) for A10 gears.

7.6.6. Meshing gear power loss

The load dependent gear losses can be calculated using Equation (7.13) by subtracting from the total experimental power loss ($P_V^{i\ exp}$) the rolling bearing losses (P_{VL}^i), the seal losses (P_{VD}) and the no-load losses (P_{VZ0}) previously calculated.

$$P_{VZP}^i = P_V^{i\ exp} - P_{VL}^i - P_{VD} - P_{VZ0} \tag{7.13}$$

Figure 7.17 presented the meshing gear torque loss T_{VZP}^i (=P_{VZP}^i/ω). The meshing gears torque loss decreases with increasing rotational speed which is expected since the tests were performed mainly under mixed film lubrication (see Figure 7.12). Considering the influence of the axle oil formulation, at low speed, all the lubricants behaviour was similar to what observed for the torque loss of A10 gears. At high speed, the 75W140-A oil always promoted the lowest meshing gear torque loss, for all the load stages, since its higher viscosity index seems to affect high speed behaviour, i.e higher speed promoted a reduction of the effect of the coefficient of friction.

The oils 75W90-B, 80W90-A and 75W90-A generated the highest value for K5, K8 and K11 load stages, respectively, no matter the rotational speed. In load stage K11, the meshing gear torque loss generated by 75W140-A oil is at least 15% lower than the one generated by 75W90-A oil, whatever the rotational speed.

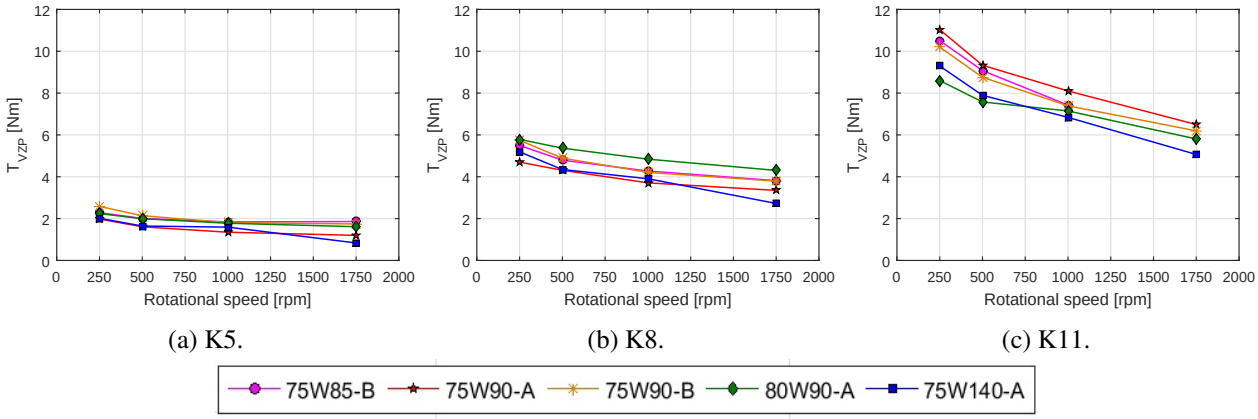

(a) K5. (b) K8. (c) K11.

Figure 7.17: Load dependent torque gear losses (T_{VZP}) for A10 gears.

7.6.7. Experimental coefficient of friction on meshing gears

The average coefficient of friction along the path of contact can be calculated based on the meshing gear power loss as given in Equation (7.14).

$$\mu_{mz}^{exp} = \frac{P_{VZP}}{P_{IN} \cdot H_V} \tag{7.14}$$

The gear loss factor of A10 gear was previously calculated (see Table 7.2). The average coefficient of friction for each load stage and rotational speed is presented in Figures 7.18 and 7.19.

It is observed that the average coefficient of friction decreases with increasing the rotational speed which is expected under mixed lubrication conditions. It was also observed this behaviour for the sliding coefficient of friction in rolling bearings (see Chapter 6).

The 80W90-A oil generally promoted the highest coefficient of friction for K5 load stage, confirming the previous results (see Figure 6.11a). For k11 load stage, the 75W90-A presented the highest coefficient of friction no matter the rotational speed confirming the prior results (see Figure 6.11b). The average coefficient of friction of the oil formulations became closer under K11 load stage. Figure 7.19 shows that the 75W140-A oil promoted the lowest coefficient of friction mainly at high speeds. It is clear that increasing the speed leads to a decrease of the average coefficient of friction of the oil formulations, no matter the load applied. This Figure also shows that the average coefficient of friction increases with increasing torque or remains constant except for 80W90-A oil. However, the influence of load seems to be less important than the influence of speed.

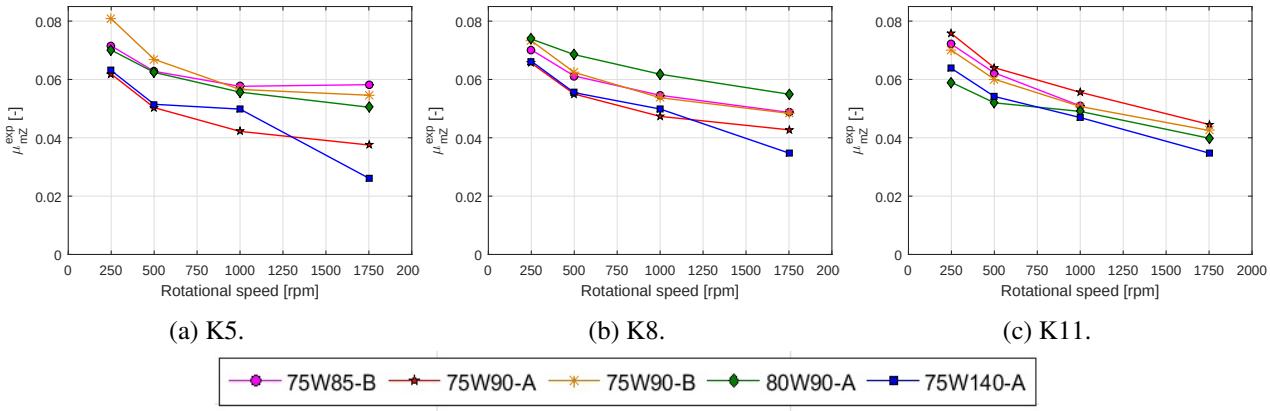

(a) K5. (b) K8. (c) K11.

Figure 7.18: Coefficient of friction based on experimental results (μ_{mZ}^{exp}) against the rotational speed for each load stage for A10 gears.

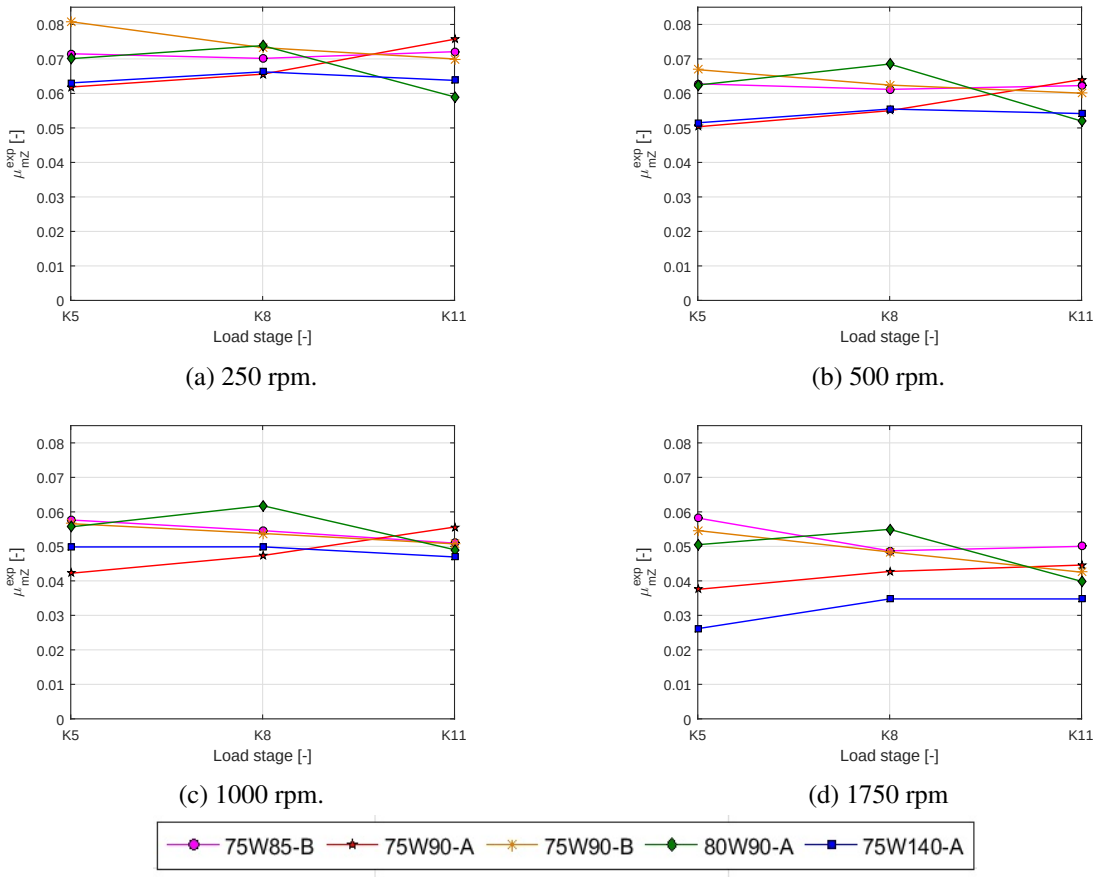

(a) 250 rpm. (b) 500 rpm.

(c) 1000 rpm. (d) 1750 rpm

Figure 7.19: Coefficient of friction based on experimental results (μ_{mZ}^{exp}) against the load stage for each rotational speed for A10 gears.

7.6.8. Schlenk coefficient of friction

Schlenk [Schlenk, 1994] proposed Equation (7.15) to calculate the average coefficient of friction along the path of contact. The equation was derived from twin disc tests lubricated with an additive free mineral oil. For such oil the lubricant parameter (X_L) is equal to 1. It included not only the oil viscosity but also the influence of the oil formulation, the applied load, the gear geometry, the velocity and the surface finishing.

$$\mu_{mZ} = 0.048 \cdot \left(\frac{F_{bt}/b}{\nu_{\sum C} \cdot \rho_{redC}} \right)^{0.2} \cdot \eta^{-0.05} \cdot R_a^{0.25} \cdot X_L \tag{7.15}$$

The experimental average coefficient of friction, μ_{mZ}^{exp}, calculated with Equation (7.14) can be correlated with those predicted by Equation (7.15). The difference between these two values was minimized using Equation (7.16), in order to determine the lubricant parameter (X_L) adjusted to each axle oil formulation.

$$error = \sum_{i=1}^{n} \left| \mu_{mz}^{i\ exp} - \mu_{mz}^{i\ Schlenk} \right| \tag{7.16}$$

To perform the minimization, the surface roughness which is the mean value of the composite surface roughness, before and after the run-in tests was made (see Table 7.3 and Figure 7.6). The average roughness required for the calculation is presented in Equation (7.17).

$$R_a = \frac{\frac{(R_{a1}+R_{a2})^{New}}{2} + \frac{(R_{a1}+R_{a2})^{Used}}{2}}{2} \tag{7.17}$$

Using this minimization approach, the lubricant parameter was calculated for each axle oil formulation. The results are presented in Figure 7.20 which shows the average coefficient of friction, experimental and predicted by Schlenk equation (at K5, K8 and K11 load stages). The correlation is acceptable but the influence of load is not well represented. The additive packages blended on the axle oils can modify the behaviour of the lubricant when load is applied and this seems to be the case here. Schlenk's equation shows a better correlation with the experimental results at K8 load stage for all the lubricants. For 75W90-A oil the Schlenk formula follows very well part of the experimental results (R^2=0.91). The 80W90-A oil at K11 load stage shows the worst correlation that is related to a different behaviour of the mineral base oil. In the case of 75W140-A oil, it is possible that full-film lubrication regime occurred at 1750 rpm, which can explain the different behaviour for K5, K8 and K11 load stages at 1750 rpm, and Schlenk equation is not suitable under full-film conditions.

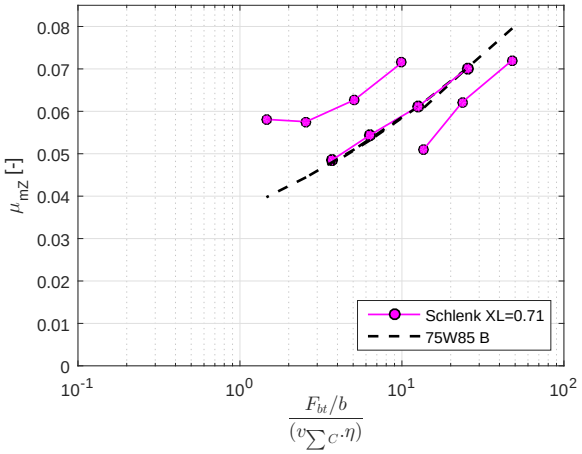

(a) 75W85-B.

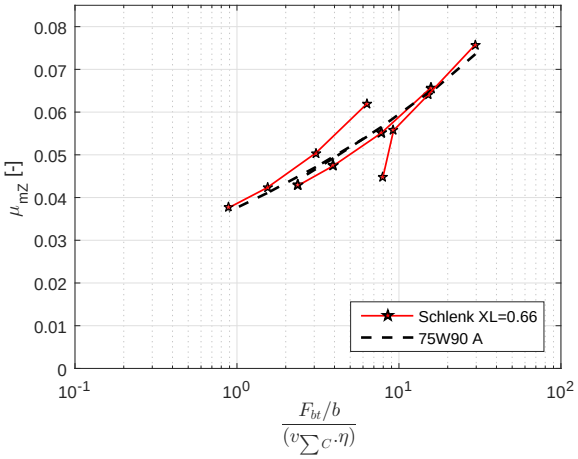

(b) 75W90-A.

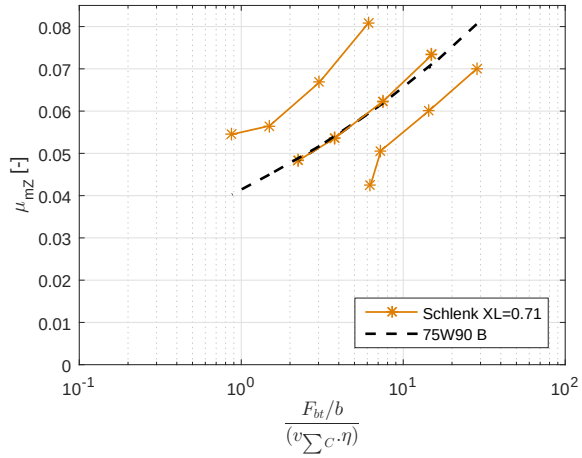

(c) 75W90-B.

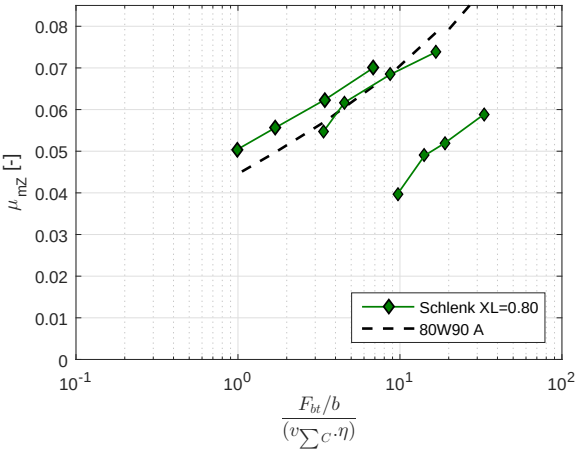

(d) 80W90-A

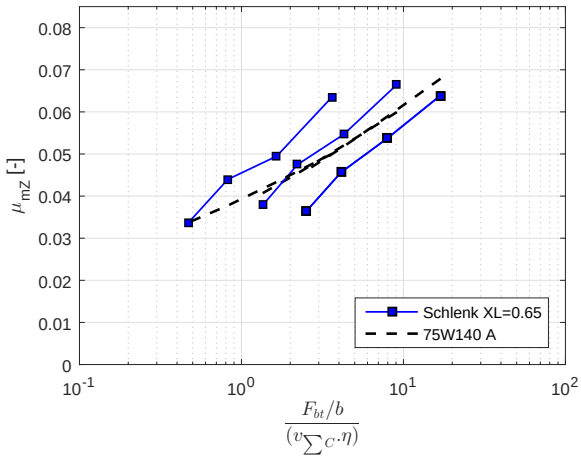

(e) 75W140-A.

Figure 7.20: Coefficient of friction determined based on experimental results vs. Schlenk equation adjusted for each axle gear oil as function of hydraulic parameter for A10 gears.

7.7. Calibrated power loss model

The results obtained permit the calibration of the model detailed in Chapter 5.

The model was summarized in Equation (7.18) in order to predict the different contribution of each power loss mechanism inside the gearbox. The different sources of power loss were quantified and the coefficient of friction was calibrated for each oil formulation.

$$P_V^i = \underbrace{P_{VZ0}}_{P_V^{1\ exp}-P_{VL}^1-P_{VD}} - \underbrace{P_{VZP}^i}_{P_V^{i\ exp}-P_{VL}^i-P_{VD}-P_{VZ0}} - \underbrace{P_{VL}^i}_{NewSKFModel} - \underbrace{P_{VD}}_{SimritEquation} \tag{7.18}$$

In order to quantify the actual power loss of the FZG gearbox, equation (7.19) should be applied.

$$P_V^i = \underbrace{P_{VZ0}}_{P_V^{1\ exp}-P_{VL}^1-P_{VD}} - \underbrace{P_{VZP}^i}_{P_{IN}\cdot H_V\cdot \mu_{mz}(X_L)} - \underbrace{P_{VL}^i}_{NewSKFModel} - \underbrace{P_{VD}}_{SimritEquation} \tag{7.19}$$

The coefficient of friction was already calculated with different approaches as presented in the previous sections, with the advantages and disadvantages of each method. For this work, the Schlenk equation was used for the power loss model calibration which is more interesting for design engineers and found in the standards. The lubricant parameter was determined for each axle oil formulation and given in Table 7.8. The rolling bearing losses were calibrated as discussed in Chapter 6. The no-load losses were determined using measurements performed because the existent models actually are not very accurate to predict the power losses.

Table 7.8: Lubricant parameter for each axle oil formulation.

Oil	X_L
75W85-B	0.71
75W90-A	0.66
75W90-B	0.71
80W90-A	0.80
75W140-A	0.65

Figure 7.21 (a) shows the weight of each power loss source in the overall gearbox efficiency (P_{VZP}, P_{VZ0}, P_{VL}, P_{VD}) for A10 gears, lubricated with 80W90-A axle oil, under an applied torque of 319 Nm. For A10 gear, all power losses increase with increasing rotational speed, as expected, and the meshing gear power loss (P_{VZP}) is dominant. The rolling bearing losses are important in the total power loss. The influence of the applied torque is presented in Figure 7.21 (b). The meshing gear power losses increase with the applied torque, as expected, and they are dominant in the case of A10 gear.

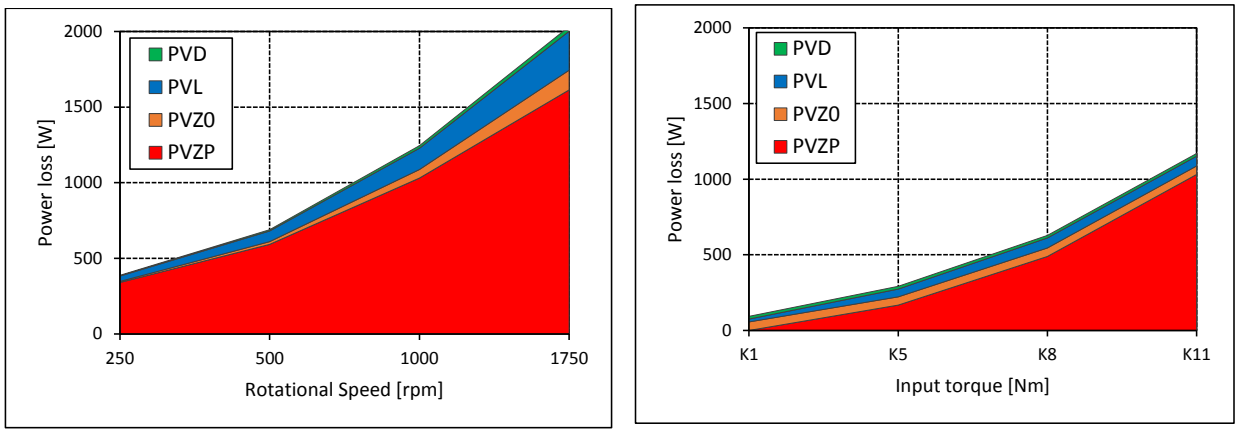

(a) Influence of speed at 319 Nm.

(b) Influence of load at 1000 rpm.

Figure 7.21: Evolution of each power loss source with 80W90-A oil for A10 gear geometry.

7.8. *Improving gearbox efficiency*

The gearbox efficiency is calculated using the torque installed in the system and the torque applied by the electric motor (T_L). The torque loss (T_L), that is also the torque applied by the electric motor to keep a constant operating speed, was measured on the wheel shaft. Thus, the global efficiency of the test rig is expressed in Equation (7.20).

$$\eta_{Global} = \frac{T_W - T_L}{T_W} \times 100 \tag{7.20}$$

During the test, the electric motor will put on the test rig the torque loss generated. Each shaft has a torque installed as presented on the diagram of Figure 7.22, where T_1 represents the torque installed on the pinion shaft and T_2 represents the torque installed on the wheel shaft. Both T_1 and T_2 are functions of the torque loss of the system and the initial static torque applied (T_W). The equilibrium of loads applied on shaft 2 is given by Equation (7.21):

$$T_2 = T_W - T_L \tag{7.21}$$

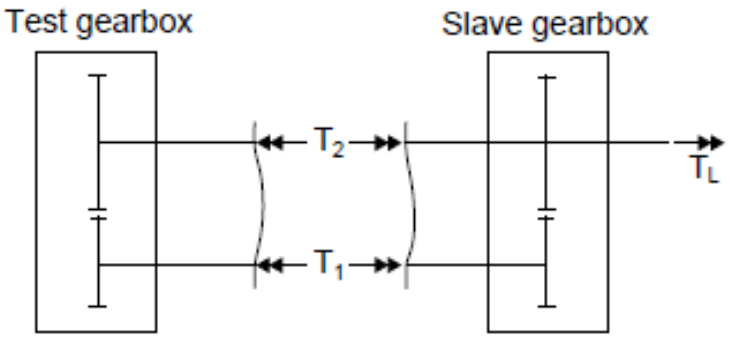

Figure 7.22: Torques circulating on the test rig [Fernandes, 2015].

In order to calculate the efficiency of the slave gearbox, it was assumed that the maximum torque is applied on motor shaft and is equal to the static torque applied on the test rig. In this way the slave gearbox efficiency is given by the Equations (7.22) and (7.23).

$$\eta_S \cdot T_W \cdot \omega_2 = T_1 \cdot \omega_1 \tag{7.22}$$

$$\eta_S = \frac{i \cdot T_1}{T_W} \tag{7.23}$$

The efficiency of the test gearbox is expressed in Equations (7.24) and (7.25).

$$\eta_T \cdot T_1 \cdot \omega_1 = T_2 \cdot \omega_2 \tag{7.24}$$

$$\eta_T = \frac{T_2}{i \cdot T_1} \tag{7.25}$$

The torque that circulates on shaft 1 is given by Equation (7.26).

$$T_1 = \frac{T_W - T_L}{i \cdot \eta_T} \tag{7.26}$$

The torque that circulates on shaft 2 is given by Equation (7.27).

$$T_2 = \eta_S \cdot \eta_T \cdot T_W \tag{7.27}$$

In the case of a system operated with the same gear geometry in both gearboxes, it can be considered that the slave and test gearbox efficiencies were equal and can be calculated using Equation (7.28).

$$\eta_T = \eta_S = \sqrt{\eta_{Global}} \tag{7.28}$$

Since the torque loss of the slave gearbox was measured and the global efficiency of a test rig is easily determined using Equation (7.20), the efficiency of the test gearbox can be calculated using Equation (7.29).

$$\eta_T = \frac{\eta_{Global}}{\eta_S} \tag{7.29}$$

In the case of different test gearbox assembly (different A10 gears), the efficiency of the test gearbox can be obtained through Equation (7.29) while maintaining the same slave gearbox.

Table 7.9 displays the efficiency values of the test gearbox lubricated with all axle gear oils. The efficiency maps of the FZG test gearbox assembled with A10 gears lubricated with axle gear oils are shown in Figure 7.23.

Since the efficiency under no-load conditions was small, the results of K1 load stage were not presented to not be compared with the other operating conditions. The torque influences the efficiency in the same way for all axle gear oils, high torque promote high efficiency.

It is interesting to observe that the efficiency maps have different curves shape, depending on the oil formulation used.

It is observed also that, a different oil formulation modifies the influence of the applied torque, mainly at low rotational speeds.

The extreme cases of performance will be considered, i.e. 80W90-A oil or 75W90-B oil and 75W90-A oil, that were already presented in section 7.6.3.

The gearbox efficiency can improve up to 0.56 % for the lower rotational speeds and until 0.51 % for higher operating speeds when 75W90-B oil is replaced by 75W90-A oil.

Independently of the operating conditions, replacing 80W90-A oil with 75W90-A oil can produce an efficiency improvement higher than 0.26 % and that improvement can achieve 0.46 % for higher rotational speeds.

For higher load, when 75W90-A oil is changed with 80W90-A oil an improvement of efficiency can be between 0.16 % to 0.51 %.

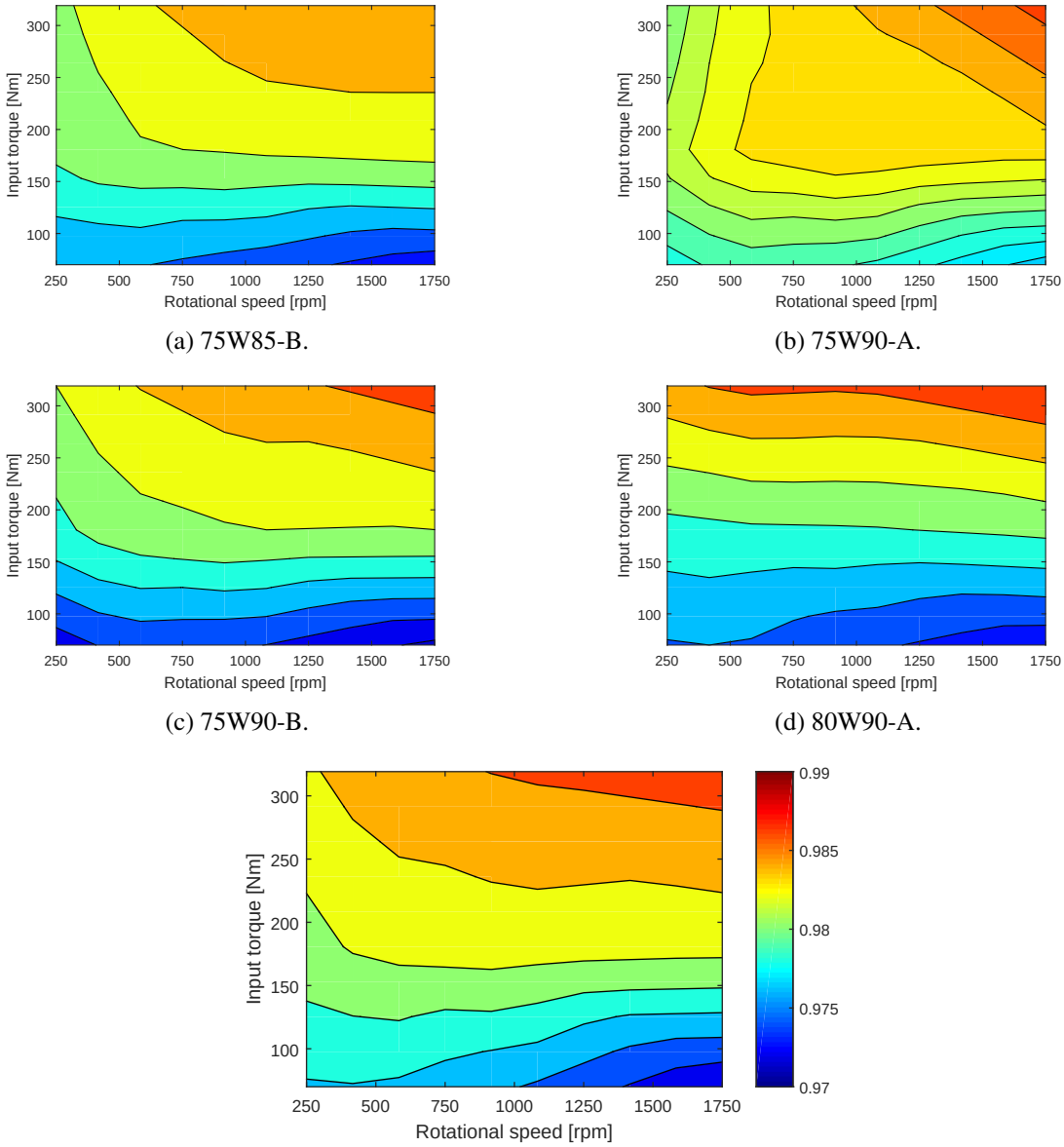

(a) 75W85-B.

(b) 75W90-A.

(c) 75W90-B.

(d) 80W90-A.

(e) 75W140-A.

Figure 7.23: Efficiency maps of a gearbox with A10 gear tests lubricated with different axle gear oils.

Table 7.9: Efficiency values η_T [%] of the test gearbox (A10 gears) for each test condition.

		75W85-B	75W90-A	75W90-B	80W90-A	75W140-A
250	K1	0.91	0.91	0.91	0.90	0.91
	K5	0.98	0.98	0.97	0.98	0.98
	K8	0.98	0.98	0.98	0.98	0.98
	K11	0.98	0.98	0.98	0.99	0.98
500	K1	0.86	0.86	0.87	0.86	0.85
	K5	0.98	0.98	0.97	0.98	0.98
	K8	0.98	0.98	0.98	0.98	0.98
	K11	0.98	0.98	0.98	0.99	0.99
1000	K1	0.82	0.82	0.82	0.81	0.84
	K5	0.98	0.98	0.97	0.97	0.98
	K8	0.98	0.98	0.98	0.98	0.98
	K11	0.99	0.98	0.99	0.99	0.99
1750	K1	0.80	0.76	0.76	0.75	0.60
	K5	0.97	0.98	0.97	0.97	0.97
	K8	0.98	0.98	0.98	0.98	0.98
	K11	–	0.99	0.99	0.99	0.99

7.9. Summary

The A10 gear geometry design lubricated with axle gear oils was discussed in details in this chapter. FZG gearbox power loss tests were performed using a slave gearbox characterized in terms of power loss in previous work, while in the test gearbox were assembled with A10 geometry.

The tests allow to understand the power loss behaviour of five axle gear oils and quantify the power loss of FZG slave gearbox. Furthermore, the results are necessary to calibrate a power loss model.

A deep study of coefficient of friction was done allowing to calibrate a power loss model. A lubricant parameter (X_L) that correlates the Schlenk coefficient of friction with the experimental results was determined for each oil formulation.

The experimental results presented clearly identify that the oil formulation is of great importance in the gearbox efficiency. Changing the oil from 80W90-A to 75W140-A, a reduction of power loss over 20 % was achieved for the lowest speed and highest loads. If 75W90-A is preferred over 80W90-A for all the speed range, the power loss reduction is higher than 8 %.

The influence of oil formulation was verified through the power loss trend which is presented as follows: $P_V^{80W90-A} > P_V^{75W90-B} > P_V^{75W85-B} > P_V^{75W90-A} > P_V^{75W140-A}$.

The outcome was great in terms of efficiency improvement, 0.5 % of efficiency improvement is feasible when replaced gear oils 80W90-A or 75W90-A with 75W90-A oil lubricating an A10 gear geometry.

8. Conclusions and future work

8.1. Conclusions

This thesis, discussed and planed to improve axle efficiency for passenger cars and light duty trucks through the study of the power loss mechanisms in axles, based on experimental evidence and modelling.

In Chapter 3, a physical and rheological characterization of different axle gear oils were presented. Density, viscosity and pressure-viscosity were measured. Chemical composition of different axle gear oil formulations was quantified.

The tribological properties of the five axle gear oils were revealed with film thickness in rolling/sliding contacts under boundary, mixed and full-film lubrication regimes and their friction behaviour through traction and Stribeck curves, presented in Chapter 4. Also in this chapter, the influence of axle gear oil formulation and additive package on rolling bearing surface failures and tribofilm generation were studied.

The multiple sources of gearbox power loss were discussed in Chapter 5, and a global power loss model structure was proposed to be calibrated through dedicated measurements of bearing and gear power loss.

The power losses of three types of rolling bearings lubricated with axle gear oils were measured in Chapter 6. The results clearly show that the oil formulation has an important influence in power loss. To better understand the results, as well as, to predict the actual rolling bearings power loss, the SKF model was implemented. The Thrust Ball Bearing (TBB) and Tapered Roller Bearing (TRB) power loss measurements showed that 75W85-B oil is less efficient than other formulations, under high loads and low rotational speeds. The 75W140-A oil lubricating the three rolling bearings type (TBB, RTB and TRB) is the most efficient formulation for low speeds, because the sliding torque, has a great influence. However, for higher speed the sliding torque starts to decrease, no matter the oil formulation, and the rolling torque becomes dominant. The rolling torque is only dependent on speed, bearing geometry and viscosity, so, the oils with intermediate viscosity (75W90-B, 80W90-A and 75W90-A) become the most efficient at high speeds, because they have the best balance between power loss dependency on viscosity and sliding coefficient of friction. This behaviour was observed

for TBB.

Chapter 7 presented power loss results of the FZG gearboxes. Type A gear geometry simulating hypoid gears found in axles were proposed and tested in a FZG machine.

For load stages above K1, The two 80W90-A and 75W90-B oils promoted the highest power loss, mainly at low speed (K5 and K8). The 75W90-A promoted the lowest power loss for all the speed range.

The rolling bearings showed that the 75W90-A oil is not better than the other formulations. The rolling bearings influence in the total power loss of the FZG gearboxes appeared to be evident for high load K11. The results show that 75W90-A oil should only be used for lower or moderate load for low and high speed where the gear losses are much lower than all the other power loss sources.

The average coefficient of friction in meshing gears was studied and under K8 load stage the oil formulations followed the trend: $\mu_{80W90-A} > \mu_{75W90-B} > \mu_{75W85-B} > \mu_{75W140-A} > \mu_{75W90-A}$. The results of the average coefficient of friction showed that the 75W90-A oil is better for gears under oil bath lubrication but the same is not true for bearings depending on the speed considered. The meshing gears coefficient of friction was calculated in order to complete a calibrated power loss model where the rolling bearing power loss model calibrated in Chapter 6, based on experimental work, takes part.

The power loss model proposed was validated, showing very good correlation with experimental results. Afterwards it was then used to study the influence of the operating conditions on each power loss source. It was found that gears and rolling bearings are affected by the speed or load in opposite way. The gears improve the efficiency with increasing speed while the rolling bearings improve the efficiency for increasing load.

8.2. Future work

The future improvements for this work of thesis can be suggested as follows:

- Perform torque loss tests on FZG test rig, lubricated with axle gear oils, under large ranges of the operating conditions-torque, speed and temperature. Standard gears (FZG-C, simulating conical gears) and low-loss gears (FZG-LL) can be tested in order to evaluate the influence of axle gear oil formulation and operating conditions on gear friction torque loss.
- Perform gear torque loss tests on the FZG test rig, lubricated with axle gear oils, under no-load conditions (very low torque), in order to measure the churning losses (spin losses) for large ranges of speed and temperature. Standard gears and low-loss gears are tested. Evaluate the influence of gear oil formulation and operating conditions on gear spin losses.
- Calculate the loss factor associated to each gear tooth design.

- Perform long term tests in gears (type FZG-A, FZG-C and FZG-LL) lubricated with axle gear oils. Asses influence of axle gear oil formulation and additive package on gear wear, under severe boundary film lubrication conditions.
- Follow-up of gear wear tests by oil condition monitoring techniques (ferrography, particle counting, viscosity, FTIR ...), evaluating lubricant degradation and gear wear.
- Design gear tooth geometries that minimize gear torque loss (Low-Loss Gear-LLG), for bevel and hypoid gears, considering module, number of teeth, pressure and helix angles, tooth width, profile shifts, tip relief ...
- Perform torque loss tests on a bevel gear test rig, lubricated with axle gear oils, under large ranges of the operating conditions-torque, speed and temperature. Evaluate the influence of axle gear oil formulation and operating conditions on the friction torque and spin losses in bevel gears.
- Develop a numerical model that predicts the gear loss factor, the coefficient of friction and the friction torque loss in bevel and hypoid gears. Correlate the model predictions with the experimental results.
- Perform torque loss tests on real differential (axle gear transmission) under wide ranges of operating torques and speeds, using different axle gear oil formulations.
- Perform torque loss tests on a modified differential, using high efficiency rolling bearings and Low-Loss conic and hypoid gears.
- Evaluate the cumulative influence of axle gear oil formulation, rolling bearing type and low-loss tooth geometry in decreasing differential torque loss.
- Perform torque loss tests on a modified differential, using high efficiency rolling bearing types (Angular Contact Bearing (ACB)) and Low-Loss conic and hypoid gears, under wide ranges of operating torques and speeds, using different axle gear oil formulations.
- Follow-up of differential tests by oil condition monitoring techniques (ferrography, particle counting, viscosity, FTIR ...), evaluating lubricant degradation and gear wear.
- Develop and validate a torque loss numerical model for axle gear transmissions (differentials), including the spin and friction losses in gears (bevel and hypoid) and rolling bearings, as well as the spin losses in seals, under dip lubrication.
- Correlate the experimental measurements and the numerical predictions for the torque loss in differentials, including the influence of axle gear oil formulation.

Bibliography

[sta, a] *ASTM D2270 -10e1 Standard Practice for Calculating Viscosity Index From Kinematic Viscosity at 40 and 100*, a. doi:10.1520/D2270-10E01. URL http://www.astm.org/Standards/D2270.htm.

[iso,] *Gears - FZG test procedures - Part 1: FZG test method A/8,3/90 for relative scuffing load-carrying capacity of Oils*, .

[sta, b] *Gears reducers - thermal capacity part 2: Thermal load-carrying capcity*, b.

[IIN,] *INA Walzlager KG, Basic principles rolling bearings, Friction and increases in temperature*, . URL http://medias.schaeffler.de/medias/en!hp.tg.cat/tg_hr*ST4_102160011;bhHLIZo_3h6b#ST4_102163723.

[sv1,] *SV-10 Vibro-viscometer*. Technical report, Zetasizer Mano Series technical note, . URL http://www.atomikateknik.com/pdf/SV-10%20Viscometer.pdf.

[vis,] *Viscosity Classifications*, . URL http://www.tribology-abc.com/abc/viscosity.htm.

[kat, 1976] *Simrit: Radialwellendichtringe, Kataog Nr. 100*, 1976.

[axl, 2000] *Wheeled vehicle drive lines, axles, and suspendion systems*, 2000. URL http://www.freeinfosociety.com/media/pdf/4463.pdf.

[gea, 2001] *Gears and gear drives*, 2001. URL https://www.google.pt/urlsa=t&rct=j&q=&esrc=s&source=web&cd=10&cad=rja&uact=8&ved=0CFIQFjAJ&url=http%3A%2F%2Fwww.emersonindustrial.com%2Fen-US%2Fdocumentcenter%2FPowerTransmissionSolutions%2FProductFundamentals%2Fgears2.pdf&ei=wPbRVIjGKMzzUKSqhMgF&usg=AFQjCNELa2RiCnIEoinYiXOTVH3Rifk_5g.

[DGM, 2002] *DGMK Information sheet - Short Test Procedure for the investigation of the micropitting load capacityof gear lubricants*, 2002.

[iso, 2004] *Gears - FZG test procedures - Part 2: FZG step load test A10/16,6/120 for relative scuffing load-carrying capacity of high EP Oils*, 2004.

[iso, 2005] *Gears - FZG test procedures - Part 3: FZG test method A/2, 8/50 for relative scuffing load-carrying capacity and wear characteristics of semifluid gear greases*, 2005.

[for, 2006] *Ford 2006 My SAE 5W-20 Engine Oil Recommendation*, 2006.

[sta, 2009] *ASTM D341-09, Standard Practice for Viscosity-Temperature Charts for Liquid Petroleum Products*, 2009. doi:10.1520/D0341-09. URL www.astm.org.

[NTN, (CAT. No. 9012/E)] *NTN, Rolling bearings handbook*. Technical report, (CAT. No. 9012/E).

[NSK, CAT. No. E728g] *NSK*. Technical report, CAT. No. E728g.

[Anderson and Maddock, 2008] Anderson, N. and Maddock, D. *Development of a Standardized Axle Efficiency Test Methodology*. In *2nd CTI Symposium, Automotive Transmissions, North America*, 2008.

[Anderson and Loewenthal, 1980] Anderson, N. E. and Loewenthal, S. H. *Spur-gear-system efficiency at part and full load*. Technical report, DTIC Document, 1980.

[Anderson and Loewenthal, 1982] Anderson, N. E. and Loewenthal, S. H. *Design of spur gears for improved efficiency*. *Journal of Mechanical Design*, 104(4):767–774, 1982.

[Andersson, 2014] Andersson, M. *Churning losses and efficiency in gearboxes*, 2014.

[Anuradha and Kumar, 2011] Anuradha, P. and Kumar, P. *New film thickness formula for shear thinning fluids in thin film elastohydrodynamic lubrication line contacts*. *Proceedings of the Institution of Mechanical Engineers, Part J: Journal of Engineering Tribology*, 225(4):173–179, 2011. Http://dx.doi.org/10.1177/1350650111399520.

[Archard and Kirk, 1961] Archard, J. and Kirk, M. *Lubrication at point contacts*. *Proceedings of the Royal Society of London. Series A. Mathematical and Physical Sciences*, 261(1307):532–550, 1961. Http://dx.doi.org/10.1098/rspa.1961.0094.

[Ariura et al., 1973] Ariura, Y., Ueno, T., SunAGA, T., and Sunamoto, S. *The lubricant churning loss in spur gear systems*. *Bulletin of JSME*, 16(95):881–892, 1973.

[of the Army and of the Air Force, 1956] of the Army, U. S. D. and of the Air Force, U. S. D. *Principles of Automotive Vehicles*. Number nos. 9-8000 in Air Force TO. Departments of the Army and the Air Force, 1956. URL https://books.google.pt/books?id=lSVuDKZ_-PoC.

[Bala et al., 2000a] Bala, V., Brandt, G., and Walters, D. *Fuel economy of multigrade gear lubricants*. *Industrial Lubrication and Tribology*, 52(4):165–173, 2000a. Http://dx.doi.org/10.1108/00368790010333610.

[Bala et al., 2000b] Bala, V., Rollin, A. J., and Brandt, G. *Rheological properties affecting the fuel economy of multigrade automotive gear lubricants*. Technical report, SAE Technical Paper, 2000b. Http://dx.doi.org/10.4271/2000-01-2051.

[Bassani and Ciulli, 1997] Bassani, R. and Ciulli, E. *Lubricant film thickness and shape using interferometry and image processing*. *Tribology Series*, 32:81–90, 1997.

[Bassani and Piccigallo, 1992] Bassani, R. and Piccigallo, B. *Hydrostatic lubrication*, volume 22. Elsevier, 1992.

[Benedict and Kelley, 1961] Benedict, G. and Kelley, B. *Instantaneous coefficients of gear tooth friction*. *ASLE transactions*, 4(1):59–70, 1961. Http://dx.doi.org/10.1080/05698196108972420.

[Bhandari, 2010] Bhandari, V. *Design of machine elements*. Tata McGraw-Hill Education, 2010.

[Bhushan, 2013] Bhushan, B. *Principles and applications of tribology*. John Wiley & Sons, 2013.

[Bjornen et al., 2003] Bjornen, K. K., Chambers, H., and DeGonia, D. *Development of a fuel efficient multipurpose 75W-90 gear lubricant*. Technical report, SAE Technical Paper, 2003. Http://dx.doi.org/10.4271/2003-01-1992.

[Boness, 1989] Boness, R. *Churning losses of discs and gears running partially submerged in oil*. In *Proc. ASME Int. Power Trans. Gearing Conf*, volume 1, pages 255–359, 1989.

[Brandao et al., 2009] Brandao, J., Meheux, M., Ville, F., and Seabra, J. *Experimental traction and Stribeck curves of mineral, PAO and ester based fully formulated gear oils*. In *IRF'2009*, page 14p, 2009.

[Brandao et al., 2011] Brandao, J. A., Meheux, M., Seabra, J. H., Ville, F., and Castro, M. *Traction curves and rheological parameters of fully formulated gear oils*. *Proceedings of the Institution of Mechanical Engineers, Part J: Journal of Engineering Tribology*, 225(7):577–593, 2011. Http://dx.doi.org/10.1177/1350650111405111.

[Bruce, 2012] Bruce, R. W. *Handbook of Lubrication and Tribology, Volume II: Theory and Design*, volume 2. CRC press, 2012.

[Buckingham, 1958] Buckingham, E. *Analytical Mechanics of Gears,(1949)*. *McGraw* Hill. Harris, L., Proceedings of the Institution of Mechanical Engineers*, 172:87112, 1958.

[Buckingham, 1988] Buckingham, E. *Analytical mechanics of gears*. Courier Corporation, 1988.

[Cameron and Gohar, 1966] Cameron, A. and Gohar, R. *Theoretical and experimental studies of the oil film in lubricated point contact*. *Proceedings of the Royal Society of London. Series A. Mathematical and Physical Sciences*, 291(1427):520–536, 1966. Http://dx.doi.org/10.1098/rspa.1966.0112.

[Cann et al., 1996] Cann, P., Spikes, H., and Hutchinson, J. *The development of a spacer layer imaging method (SLIM) for mapping elastohydrodynamic contacts*. *Tribology transactions*, 39(4):915–921, 1996. Http://dx.doi.org/10.1080/10402009608983612.

[Catalogue, 2005] Catalogue, S. G. *6000 EN*. *SKF, November*, 2005.

[Changenet et al., 2006] Changenet, C., Oviedo-Marlot, X., and Velex, P. *Power loss predictions in geared transmissions using thermal networks-applications to a six-speed manual gearbox*. *Journal of Mechanical Design*, 128(3):618–625, 2006. Http://dx.doi.org/10.1115/1.2181601.

[Changenet and Velex, 2007] Changenet, C. and Velex, P. *A model for the prediction of churning losses in geared transmissions -Preliminary results*. *Journal of Mechanical Design*, 1:128–133, 2007. Http://www.asme.org/about-asme/terms-of-use.

[Changenet and Velex, 2008] Changenet, C. and Velex, P. *Housing influence on churning losses in geared transmissions*. *Journal of Mechanical Design*, 130(6):062603, 2008. Http://dx.doi.org/10.1115/1.2900714.

[Chastain et al., 1995] Chastain, J., King, R. C., and Moulder, J. *Handbook of X-ray photoelectron spectroscopy: a reference book of standard spectra for identification and interpretation of XPS data*. Physical Electronics Eden Prairie, MN, 1995.

[Cheng and Lim, 2001] Cheng, Y. and Lim, T. C. *Vibration analysis of hypoid transmissions applying an exact geometry-based gear mesh theory*. *Journal of Sound and Vibration*, 240(3):519–543, 2001. Http://dx.doi.org/10.1006/jsvi.2000.3247.

[Cheng and Lim, 2003] Cheng, Y. and Lim, T. C. *Dynamics of hypoid gear transmission with nonlinear time-varying mesh characteristics*. *Journal of Mechanical Design*, 125(2):373–382, 2003. Http://dx.doi.org/10.1115/1.1564064.

[Chittenden et al., 1985] Chittenden, R., Dowson, D., Dunn, J., and Taylor, C. *A theoretical analysis of the isothermal elastohydrodynamic lubrication of concentrated contacts. II. General Case, with lubricant entrainment along either principal axis of the Hertzian contact ellipse or at some intermediate angle*. *Proceedings of the Royal Society of London. Series A, Mathematical and Physical Sciences*, pages 271–294, 1985. Http://dx.doi.org/10.1098/rspa.1985.0015.

[Coleman, 1975] Coleman, W. *Computing efficiency for bevel and hypoid gears*. *Machine Design*, 47(20):64–65, 1975.

[Conrado et al., 2007] Conrado, E., Höhn, B., Michaelis, K., and Klein, M. *Influence of oil supply on the scuffing load-carrying capacity of hypoid gears*. *Proceedings of the Institution of Mechanical Engineers, Part J: Journal of Engineering Tribology*, 221(8):851–858, 2007. Http://dx.doi.org/10.1243/13506501JET315.

[Corporation, 2014] Corporation, N. *How to test industrial and engine Oils*. *Machinery Lubrication*, 2014.

[Alder da Costa D'Ambros and Tinguy, 2012] Alder da Costa D'Ambros, R. V. and Tinguy, E. *Influence of Different Lubricant Parameters on Transmission Efficiency*. In W. J.Bartz, editor, *18th International Colloquium Tribology, Tribology - Industrial and Automotive Lubrication*, page 112, 2012.

[Cousseau et al., 2010] Cousseau, T., Graça, B., Campos, A., and Seabra, J. *Experimental measuring procedure for the friction torque in rolling bearings*. *Lubrication Science*, 22(4):133–147, 2010. Http://dx.doi.org/10.1002/ls.115.

[Croes and (K.U.Leuven),] Croes, J. and (K.U.Leuven), S. I. *D2.1 Document 1: Literature survey : gear losses*. Technical report, ESTOMAD, .

[Dawson, 1984] Dawson, P. *Windage loss in larger high-speed gears*. *Proceedings of the Institution of Mechanical Engineers, Part A: Journal of Power and Energy*, 198(1):51–59, 1984.

[De Gevigney et al., 2012] De Gevigney, J. D., Changenet, C., Ville, F., and Velex, P. *Thermal modelling of a back-to-back gearbox test machine: Application to the FZG test rig*. *Proceedings of the Institution of Mechanical Engineers, Part J: Journal of Engineering Tribology*, 226(6):501–515, 2012. Http://dx.doi.org/10.1177/1350650111433243.

[Dean et al., 1929] Dean, E., Davis, G., et al. *Viscosity variations of oils with temperature*. *Chemical and Metallurgical Engineering*, 36:618–619, 1929.

[Denny, 1998] Denny, C. *Mesh friction in gearing*. AGMA, 1998.

[Denton, 2011] Denton, T. *Automobile Mechanical and Electrical Systems*. Taylor & Francis, 2011. ISBN 9781136270383. URL https://books.google.pt/booksid=mXAQBAAAQBAJ.

[Diab et al., 2003] Diab, Y., Ville, F., Changenet, C., and Velex, P. *Windage losses in high speed gears: Preliminary experimental and theoretical results*. In *ASME 2003 International Design Engineering Technical Conferences and Computers and Information in Engineering Conference*, pages 941–947. American Society of Mechanical Engineers, 2003. Http://www.asme.org/about-asme/terms-of-use.

[Dowson and Higginson, 1959] Dowson, D. and Higginson, G. *A numerical solution to the elasto-hydrodynamic problem*. *Journal of Mechanical Engineering Science*, 1(1):6–15, 1959. Http://jms.sagepub.com/content/1/1/6.

[Dowson and Higginson, 1964] Dowson, D. and Higginson, G. *A theory of involute gear lubrication*. In *Proceeding of a Symposium Organized by the Mechanical Tests of Lubricants Panel of the Institute, Institute of Petroleum, Gear Lubrication, Elsevier, London*, volume 182, pages 8–15, 1964.

[Dowson and Higginson, 1966] Dowson, D. and Higginson, G. R. *Elasto-hydrodynamic lubrication: the fundamentals of roller and gear lubrication*, volume 23. Pergamon Press, 1966.

[Dowson and Toyoda, 1978] Dowson, D. and Toyoda, S. *A central film thickness formula for elastohydrodynamic line contacts*. *Elastohydrodynamics and Related Topics*, pages 60–67, 1978.

[Dowson, 1977] Dowson, G., D.and R.Higginson. *Elastohydrodinamic lubrication*. S. I. Editon. Pergamon Press Ltd., 1977.

[Drozdov, 1972] Drozdov, Y. N. *Thermal aspects of scoring in simultaneous rolling and sliding contact*. *Wear*, 20(2):201–209, 1972.

[Drozdov and Gavrikov, 1968] Drozdov, Y. N. and Gavrikov, Y. A. *Friction and scoring under the conditions of simultaneous rolling and sliding of bodies*. *Wear*, 11(4):291–302, 1968.

[Dyson, 1970] Dyson, A. *Frictional traction and lubricant rheology in elastohydrodynamic lubrication*. *Philosophical Transactions of the Royal Society of London. Series A, Mathematical and Physical Sciences*, 266(1170):1–33, 1970. Http://dx.doi.org/10.1098/rsta.1970.0001.

[Erjavec, 2010] Erjavec, J. *NATEF Standards Job Sheets Area A3, 3rd Edition*. Cengage Learning, 2010.

[Eschmann, 1985] Eschmann, P. *Ball and roller bearings - Theory, design and applications*, 1985.

[Evans and Snidle, 1983] Evans, H. and Snidle, R. *Analysis of elastohydrodynamic lubrication of elliptical contacts with rolling along the major axis*. *Proceedings of the Institution of Mechanical Engineers, Part C: Journal of Mechanical Engineering Science*, 197(3):209–211, 1983.

[Evans, 2014] Evans, S. D. *Delivering Axle Efficiency and Fuel Economy Through Optimised Fluid Design*. *SAE Technical Paper 2014-01-2799*, 2014. Http://dx.doi.org/10.4271/2014-01-2799.

[Fairley, 2009] Fairley, N. *CasaXPS manual 2.3. 15. Spectroscopy*. Acolyte Science, 2009.

[Fang et al., 2000] Fang, N., Chang, L., Webster, M., and Jackson, A. *A non-averaging method of determining the rheological properties of traction fluids*. *Tribology international*, 33(11):751–760, 2000.

[Fernandes et al., 2013a] Fernandes, C. M., Amaro, P. M., Martins, R. C., and Seabra, J. H. *Torque loss in cylindrical roller thrust bearings lubricated with wind turbine gear oils at constant temperature*. *Tribology International*, 67:72–80, 2013a. Http://dx.doi.org/10.1016/j.triboint.2013.06.016.

[Fernandes et al., 2013b] Fernandes, C. M., Amaro, P. M., Martins, R. C., and Seabra, J. H. *Torque loss in thrust ball bearings lubricated with wind turbine gear oils at constant temperature*. *Tribology International*, 66:194–202, 2013b. Http://dx.doi.org/10.1016/j.triboint.2013.05.002.

[Fernandes et al., 2014a] Fernandes, C. M., Marques, P. M., Martins, R. C., and Seabra, J. H. *Gearbox power loss. Part II: Friction losses in gears*. *Tribology International*, 2014a. Http://dx.doi.org/10.1016/j.triboint.2014.12.004.

[Fernandes et al., 2015] Fernandes, C. M., Marques, P. M., Martins, R. C., and Seabra, J. H. *Film thickness and traction curves of wind turbine gear oils*. *Tribology International*, 2015. Http://dx.doi.org/10.1016/j.triboint.2015.01.014.

[Fernandes et al., 2013c] Fernandes, C. M., Martins, R. C., and Seabra, J. H. *Friction torque of cylindrical roller thrust bearings lubricated with wind turbine gear oils*. *Tribology International*, 59(0):121 – 128, 2013c. ISSN 0301-679X. Http://dx.doi.org/10.1016/j.triboint.2012.05.030.

[Fernandes et al., 2013d] Fernandes, C. M., Martins, R. C., and Seabra, J. H. *Friction torque of thrust ball bearings lubricated with wind turbine gear oils*. *Tribology International*, 58:47–54, 2013d. Http://dx.doi.org/10.1016/j.triboint.2012.09.005.

[Fernandes et al., 2014b] Fernandes, C. M., Martins, R. C., and Seabra, J. H. *Torque loss of type C40 FZG gears lubricated with wind turbine gear oils*. *Tribology International*, 70(0):83 – 93, 2014b. ISSN 0301-679X. Http://dx.doi.org/10.1016/j.triboint.2013.10.003.

[Fernandes, 2015] Fernandes, C. M. d. C. G. *Power loss in rolling bearings and gears lubricated with wind turbine gear oils*. Ph.D. thesis, 2015.

[Flick, 1989] Flick, E. W. *Handbook of adhesives raw materials*. William Andrew, 1989.

[Fondelli et al., 2015] Fondelli, T., Andreini, A., Da Soghe, R., Facchini, B., and Cipolla, L. *Numerical Simulation of Oil Jet Lubrication for High Speed Gears*. *International Journal of Aerospace Engineering*, 2015, 2015. Http://dx.doi.org/10.1155/2015/752457.

[Forschungsvereinigung Antriebstechnik, 1993] Forschungsvereinigung Antriebstechnik, E. *FVA Research Project Nr*. Technical report, 54/I-IV: Test Procedure for the Investigation of the Micro-Pitting Capacity of Gear Lubricants, 1993.

[Garrett et al., 2001] Garrett, T., Newton, K., and Steeds, W. *The Motor Vehicle*. Butterworth-Heinemann, 2001.

[Gohar, 2001] Gohar, R. *Elastohydrodynamics*. World Scientific, 2001.

[Gold et al., 2001] Gold, J. W., Schmidt, A., dicke, H., Loos, H., and Aßmann, C. *Viscosity-Pressure-Temperature Behaviour of Mineral and Synthetic Oils*. *Journal of Synthetic Lubrication*, 18(1), 2001.

[Grossiord et al., 1999] Grossiord, C., Martin, J.-M., Le Mogne, T., Inoue, K., and Igarashi, J. *Friction-reducing mechanisms of molybdenum dithiocarbamate/zinc dithiophosphate combination: new insights in Mos2 genesis*. *Journal of Vacuum Science & Technology A*, 17(3):884–890, 1999. Http://dx.doi.org/10.1116/1.581660.

[Group, 2011] Group, S. *FAG, Bearings - online easy friction*. Technical report, 2011.

[Grubin and Vinogradova, 1949] Grubin, A. and Vinogradova, I. *Central scientific research institute for technology and mechanical engineering*. *Moscow (DSRI Translation, No. 337)*, 1949.

[Guangteng et al., 2000] Guangteng, G., Cann, P., Olver, A., and Spikes, H. *Lubricant film thickness in rough surface, mixed elastohydrodynamic contact*. *Journal of tribology*, 122(1):65–76, 2000. Http://dx.doi.org/10.1115/1.555330.

[Gupta et al., 1992] Gupta, P., Cheng, H., Zhu, D., Forster, N., and Schrand, J. *Viscoelastic effects in MIL-L-7808-Type lubricant, Part I: Analytical formulation*. *Tribology transactions*, 35(2):269–274, 1992. Http://dx.doi.org/10.1080/10402009208982117.

[Hammami et al., 2016] Hammami, M., Martins, R., Abbes, M. S., Haddar, M., and Seabra, J. *Axle Gear Oils: Tribological Characterization Under Full Film Lubrication*. *Tribology International*, pages –, 2016. ISSN 0301-679X. Http://dx.doi.org/10.1016/j.triboint.2016.05.051.

[Hammami et al., 2017] Hammami, M., Rodrigues, N., Fernandes, C., Martins, R., Seabra, J., Abbes, M. S., and Haddar, M. *Axle Gear Oils: Friction, Wear And Tribofilm Generation Under Boundary Lubrication Regime*. *Tribology International (2017)*, 2017. , http://dx.doi.org/10.1016/j.triboint.2017.04.018.

[Hamrock and Dowson, 1976] Hamrock, B. J. and Dowson, D. *Isothermal elastohydrodynamic lubrication of point contacts: part II Ellipticity parameter results*. *Journal of Tribology*, 98(3):375–381, 1976.

[Hamrock and Dowson, 1981] Hamrock, B. J. and Dowson, D. *Ball bearing lubrication: the elastohydrodynamics of elliptical contacts*, 1981.

[Hamrock and Dowson, 1981, 386] Hamrock, B. J. and Dowson, D. *Ball bearing lubrication*. John Wiley & Sons, 1981, 386.

[Hamrock et al., 2004] Hamrock, B. J., Schmid, S. R., and Jacobson, B. O. *Fundamentals of fluid film lubrication*. CRC press, 2004.

[Handschuh and Kilmain, 2003] Handschuh, R. F. and Kilmain, C. J. *Preliminary comparison of experimental and analytical efficiency results of high-speed helical gear trains*. In *ASME 2003 International Design Engineering Technical Conferences and Computers and Information in Engineering Conference*, pages 949–955. American Society of Mechanical Engineers, 2003.

[Harris, 1966] Harris, T. *Rolling bearing analysis*. Wiley, 1966.

[Harris and Kotzalas, 2006] Harris, T. A. and Kotzalas, M. N. *Advanced concepts of bearing technology: rolling bearing analysis*. CRC Press, 2006.

[Heingartner and Mba, 2003] Heingartner, P. and Mba, D. *Determining Power Losses in Helical Gear Mesh: Case Study*. In *ASME 2003 International Design Engineering Technical Conferences and Computers and Information in Engineering Conference*, pages 965–970. American Society of Mechanical Engineers, 2003.

[Henriot, 1980] Henriot, G. *Engrenages. Paris: Dunod*, 1980.

[Hillier and Coombes, 2004] Hillier, V. A. W. and Coombes, P. *Hillier's fundamentals of motor vehicle technology*. Nelson Thornes, 2004.

[Hobson, 1979] Hobson, D. *Axle Efficiency-Test Procedures and Results*. Technical report, SAE Technical Paper, 1979. Http://dx.doi.org/10.4271/790744.

[Höhn et al., 2011] Höhn, B., Michaelis, K., and Otto, H. *Flank load carrying capacity and power loss reduction by minimized lubrication*. *Gear Technology*, pages 53–62, 2011.

[Höhn et al., 2001] Höhn, B.-R., Michaelis, K., and Doleschel, A. *Frictional behavior of synthetic gear lubricants*. In G. Dalmaz, A. Lubrecht, D. Dowson, and M. Priest, editors, *Tribology research: From model experiment to Industrial Problem*. Elsevier, 2001.

[Höhn et al., 2009] Höhn, B.-R., Michaelis, K., and Hinterstoißer, M. *Optimization of gearbox efficiency*. *Goriva i maziva*, 48(4):462, 2009.

[Höhn et al., 2008] Höhn, B.-R., Michaelis, K., and Otto, H.-P. *Influence of immersion depth of dip lubricated gears on power loss, bulk temperature and scuffing load carrying capacity*. *International Journal of Mechanics and Materials in Design*, 4(2):145–156, 2008. Http://dx.doi.org/10.1007/s10999-007-9045-z.

[Hohn et al., 1996] Hohn, B.-R., Michaelis, K., and Vollmer, T. *Thermal Rating of Gear Drives: Balance Between Power Loss and Heat Dissipation*. *AGMA Technical Paper*, 1996.

[Höhn et al., June 2007] Höhn, B.-R., Michaelis, K., and Wimmer, A. *Low loss gears*, June 2007.

[Höhn and Steingröver, 1998] Höhn, B.-R. and Steingröver, K. *Local coefficients of friction in worm gear contacts*. AGMA, 1998.

[Hosokawa et al., 2009] Hosokawa, R. S., de Oliveira, R. A. A., Franco, D. M., and de Aguiar Vendrasco, A. *DOUBLE ROW REGULAR CONTACT BALL BEARING FOR AXLE DRIVES*. Technical report, SAE Technical Paper, 2009. Http://dx.doi.org/10.4271/2009-36-0055.

[Hurley, 2009] Hurley, J. D. *An Experimental Investigation of Thermal Behavior of an Automotive Rear Axle*. Ph.D. thesis, The Ohio State University, 2009.

[Jelaska, 2012] Jelaska, D. T. *Gears and gear drives*. John Wiley & Sons, 2012.

[Joachim et al., 2014] Joachim, F., Börner, J., and Kurz, N. *Power Losses in Transmissions, Axles, and Steering Systems*. In *Encyclopedia of Lubricants and Lubrication*, pages 1398–1411. Springer, 2014. Http://dx.doi.org/10.1007/978-3-642-22647-2.

[Joachim et al., 2011] Joachim, F. J., Kurz, N., and Börner, J. *Reduction of Power Losses in Transmissions and Gearings*. *Applied Mechanics and Materials*, 86:883–888, 2011. Http://dx.doi.org/10.4028/www.scientific.net/AMM.86.883.

[Johnston et al., 1991] Johnston, G., Wayte, R., and Spikes, H. *The measurement and study of very thin lubricant films in concentrated contacts*. *Tribology Transactions*, 34(2):187–194, 1991. Http://dx.doi.org/10.1080/10402009108982026.

[J.Shah, 2003] J.Shah, G. E. S. R. R., editor. *Fuels and Lubricants Handbook: Technology, Properties, Performance, and Testing*. ASTM International, 2003. URL https://books.google.pt/booksid=J_AkNu-Y1wQC.

[Kajdas et al., 1990] Kajdas, C., Wilusz, E., and Harvey, S. *Encyclopedia of tribology*, volume 15. Elsevier, 1990.

[Kakavas et al., 2016] Kakavas, I., Olver, A., and Dini, D. *Hypoid gear vehicle axle efficiency*. *Tribology International*, 101:314–323, 2016. Http://dx.doi.org/10.1016/j.triboint.2016.04.030.

[Katoh et al., 1983] Katoh, H., Inoh, T., and Umezawa, K. *Exact Measurement of Power Loss in Automotive Transmission and Axle for Fuel Economy*. Technical report, SAE Technical Paper, 1983. Http://dx.doi.org/10.4271/830573.

[Kelley and Lemanski, 1967] Kelley, B. and Lemanski, A. *Paper 11: Lubrication of Involute Gearing*. In *Proceedings of the Institution of Mechanical Engineers, Conference Proceedings*, volume 182, pages 173–184. SAGE Publications, 1967.

[Kerthe, 2012] Kerthe, R. *Oil can Talk: Oil Sensors Meet Lab Analysis*. In W. J.Bartz, editor, *18th International Colloquium Tribology, Tribology- Industrial and Automotive Lubrication*, page 21, 2012.

[Kettler, 2002] Kettler, J. *Ölsumpftemperatur von Planetengetrieben: Abschlußbericht; Forschungsvorhaben Nr. 313: Planetengetriebe-Sumpftemperatur*. FVA, 2002.

[K.Jacobs,] K.Jacobs. *Ultra High Vacuum Lab*, .

[Ko and Hosoi, 1984] Ko, Y. and Hosoi, K. *Measurements of Power Losses in Automobile Drive Train*. Technical report, SAE Technical Paper, 1984. Http://dx.doi.org/10.4271/840054.

[Kolekar, 2013] Kolekar, A. S. *Lubrication & efficiency of rear wheel drive axles in road vehicles*. Ph.D. thesis, 2013.

[Kolekar et al., 2013] Kolekar, A. S., Olver, A. V., Sworski, A. E., and Lockwood, F. E. *The efficiency of a hypoid axle a thermally coupled lubrication model*. *Tribology International*, 59(0):203 – 209, 2013. ISSN 0301-679X. Http://dx.doi.org/10.1016/j.triboint.2012.03.013.

[Kolivand and Kahraman, 2009] Kolivand, M. and Kahraman, A. *A load distribution model for hypoid gears using ease-off topography and shell theory*. *Mechanism and Machine Theory*, 44(10):1848–1865, 2009. Http://dx.doi.org/10.1016/j.mechmachtheory.2009.03.009.

[Kolivand et al., 2010] Kolivand, M., Li, S., and Kahraman, A. *Prediction of mechanical gear mesh efficiency of hypoid gear pairs*. *Mechanism*

and Machine Theory, 45(11):1568 – 1582, 2010. ISSN 0094-114X. Http://dx.doi.org/10.1016/j.mechmachtheory.2010.06.015.

[Krenzer, 1981] Krenzer, T. J. *Tooth contact analysis of spiral bevel and hypoid gears under load*. Technical report, SAE Technical Paper, 1981. Http://dx.doi.org/10.4271/810688.

[Ku et al., 1978] Ku, P., Staph, H., and Carper, H. *Frictional and thermal behaviors of sliding-rolling concentrated contacts*. *Journal of Tribology*, 100(1):121–128, 1978. Http://dx.doi.org/10.1115/1.3453101.

[Kubo et al., 1986] Kubo, K., Shimakawa, Y., and Kibukawa, M. *The effect of gear oil viscosity and friction reducer type on transmission efficiency*. *Tribology International*, 19(6):312 – 317, 1986. ISSN 0301-679X. Http://dx.doi.org/10.1016/0301-679X(86)90038-1.

[Larsson, 1997] Larsson, R. *Transient non-Newtonian elastohydrodynamic lubrication analysis of an involute spur gear*. *Wear*, 207(1–2):67 – 73, 1997. ISSN 0043-1648. Http://dx.doi.org/10.1016/S0043-1648(96)07484-4.

[Lauster and Boos, 1983] Lauster, E. and Boos, M. *Zum Wärmehaushalt Mechanischer Schaltgetriebe für Nutzfahrzeuge*. *VDI-Berichte*, (488):45–55, 1983.

[Law and Rowe, 1994] Law, D. and Rowe, C. *The design of fuel efficient automotive hypoid gear lubricants*. *Journal of Synthetic Lubrication*, 11(1):1–15, 1994.

[Lin et al., 2005] Lin, H., Burke, D. C., Binoniemi, R. R., Wenstrup, L., and Woodard, T. *Seal Friction Effect on Drive Axle Efficiency*. Technical report, SAE Technical Paper, 2005. Http://dx.doi.org/10.4271/2005-01-3779.

[Linke, 1996] Linke, H. *Stirnradverzahnung. Berechnumg. Werstoffe. Fertigung*, 1996.

[Litvin, 1989] Litvin, F. *Theory of Gearing, NASA RP-1212*. Technical report, AVSCOM TR-88-C-035, 1989.

[Ludwig, 2008] Ludwig, L. *Lubrication Selection for Enclosed Gear Drives*. *Machinery Lubrication*, 2008.

[Lugt and Morales-Espejel, 2011] Lugt, P. and Morales-Espejel, G. E. *A review of elastohydrodynamic lubrication theory*. *Tribology Transactions*, 54(3):470–496, 2011. Http://dx.doi.org/10.1080/10402004.2010.551804.

[Luke and Olver, 1999] Luke, P. and Olver, A. *A study of churning losses in dip-lubricated spur gears*. *Proceedings of the Institution of Mechanical Engineers, Part G: Journal of Aerospace Engineering*, 213(5):337–346, 1999. Http://dx.doi.org/10.1243/0954410991533061.

[Makhlouf and Aliofkhazraei, 2015] Makhlouf, A. S. H. and Aliofkhazraei, M. *Handbook of Materials Failure Analysis with Case Studies from the Chemicals, Concrete and Power Industries*. Butterworth-Heinemann, 2015.

[Mang, 2014] Mang, T. *Encyclopedia of Lubricants and Lubrication*. Springer Berlin, 2014.

[Mang et al., 2011] Mang, T., Bobzin, K., and Bartels, T. *Industrial tribology: tribosystems, friction, wear and surface engineering, lubrication*. John Wiley & Sons, 2011.

[Mang and Dresel, 2007] Mang, T. and Dresel, W. *Lubricants and lubrication*. John Wiley & Sons, 2007.

[Marchesse et al., 2011] Marchesse, Y., Changenet, C., Ville, F., and Velex, P. *Investigations on CFD simulations for predicting windage power losses in spur gears*. *Journal of Mechanical Design*, 133(2):024501, 2011.

[Marchesse et al., 2014] Marchesse, Y., Voeltzel, N., Changenet, C., Ville, F., and Velex, P. *Investigations on CFD simulation for predicting windage power losses generated by helical gears*. *Université de Lyon, ECAM Lyon, Laboratoire Énergétique, Lyon, France*, 2014.

[Marques et al., 2014] Marques, P. M., Fernandes, C. M., Martins, R. C., and Seabra, J. H. *Efficiency of a gearbox lubricated with wind turbine gear oils*. *Tribology International*, 71(0):7 – 16, 2014. ISSN 0301-679X. Http://dx.doi.org/10.1016/j.triboint.2013.10.017.

[Martin et al., 2000] Martin, J.-M., Grossiord, C., Le Mogne, T., and Igarashi, J. *Transfer films and friction under boundary lubrication*. *Wear*, 245(1):107–115, 2000.

[Martin, 1981] Martin, K. *The efficiency of involute spur gears*. *Journal of mechanical design*, 103(1):160–169, 1981.

[Martins et al., 2008a] Martins, R., Amaro, R., and Seabra, J. *Influence of low friction coatings on the scuffing load capacity of gears*. *Tribology International*, 41(4):234–243, 2008a. Http://dx.doi.org/10.1016/j.triboint.2007.05.008.

[Martins et al., 2008b] Martins, R., Cardoso, N., and Seabra, J. *Gear power loss performance of biodegradable low-toxicity ester-based oils*. *Proceedings of the Institution of Mechanical Engineers Part J-Journal of Engineering Tribology*, 222(J3):431–440, 2008b. doi:10.1243/13506501jet345. Http://dx.doi.org/10.1243/13506501JET345.

[Martins et al., 2006a] Martins, R., Seabra, J., Brito, A., Seyfert, C., and Luther, A., R.and Igartua. *Friction coefficient in FZG gears lubricated with industrial gear oils:Biodegradable ester vs. mineral oil*. *Tribology International*, 39(6):512–521, 2006a. Http://dx.doi.org/10.1016/j.triboint.2005.03.021.

[Martins et al., 2004] Martins, R., Seabra, J., Seyfert, C., Luther, R., Igartua, A., and Brito, A. *Power loss in FZG gears lubricated with industrial gear oils: biodegradableester vs. mineral oil*. In *Proceedings of the 31th "Leeds-Lyon Symposium" on Tribology*. Leeds, UK, 2004.

[Martins et al., 2005] Martins, R., Seabra, J., Seyfert, C., Luther, R., Igartua, A., and Brito, A. *Power Loss in FZG gears lubricated with industrial gear oils: Biodegradable Ester vs. Mineral oil*. In M. P. G. D. D. Dowson and A. A. Lubrecht, editors, *Tribology and Interface Engineering Series*, volume Volume 48, pages 421–430. Elsevier, 2005.

[Martins et al., 2006b] Martins, R. C., Moura, P. S., and Seabra, J. O. *MoS2/Ti low-friction coating for gears*. *Tribology International*, 39(12):1686–1697, 2006b. Http://dx.doi.org/10.1016/j.triboint.2006.02.065.

[Matsumoto and Morikawa, 2014] Matsumoto, S. and Morikawa, K. *The new estimation formula of coefficient of friction in rolling-sliding contact surface under mixed lubrication condition for the power loss reduction of power transmission gears, International*

Gear Conference 2014. In *Conference Proceedings*, volume 2, pages 1078–1088, 2014.

[Matsuyama et al., 2004] Matsuyama, H., Dodoro, H., Ogino, K., Ohshima, H., and Toda, K. *Development of Super-Low Friction Torque Tapered Roller Bearing for Improved Fuel Efficiency*. Technical report, SAE Technical Paper, 2004. Http://dx.doi.org/10.4271/2004-01-2674.

[Maurer, 1994] Maurer, J. V. *FVA Forschungsvorhaben Nr 44*, 1994.

[Mauz, 1987a] Mauz, W. *Hydraulische Verluste von Stirnradgetrieben bei Umfangsgeschwindigkeiten bis 60m/s*. na, 1987a.

[Mauz, 1987b] Mauz, W. *Hydraulische Verlute von Stirnradgetrieben bei Umfangsgeschwindigkeiten bis 60 m/s*. Ph.D. thesis, Dissertation Uni Stuttgart, 1987b.

[Michaelis, 1986] Michaelis, H. W. K. *Scoring tests of aircraft transmission lubricants at high temperatures*. *Journal of synthetic lubrication*, 3(2), 1986.

[Michaelis and Höhn, 1994] Michaelis, K. and Höhn, B.-R. *Influence of Lubricants on Power Loss of Cylindrical Gears©*. *Tribology transactions*, 37(1):161–167, 1994. Http://dx.doi.org/10.1080/10402009408983279.

[Mihailidis et al., 2002] Mihailidis, A., Bakolas, V., Panagiotidis, K., and Drivakos, N. *Prediction of the friction coefficient of spur gear pairs*. *VDI BERICHTE*, 1665:705–720, 2002.

[Misharin, 1958] Misharin, Y. A. *Influence of the friction condition on the magnitude of the friction coefficient in the case of rollers with sliding*. In *Proceedings of International Conference on Gearing, Mechanical Engineering, London*, pages 159–164, 1958.

[Mortier et al., 1992] Mortier, R. M., Orszulik, S. T., and Fox, M. F. *Chemistry and technology of lubricants*. Springer, 1992.

[Mostofi and Gohar, 1982] Mostofi, A. and Gohar, R. *Oil film thickness and pressure distribution in elastohydrodynamic point contacts*. *Journal of Mechanical Engineering Science*, 24(4):173–182, 1982. Http://jms.sagepub.com/content/24/4/173.

[NARUSE and HAIZUKA, 1978] NARUSE, C. and HAIZUKA, S. *Limiting Loads for Scoring and Coefficient of Friction on a Disk-Machine: Effects of Lubricating Oil, Specific Sliding and Sliding Velocity, in the Case of Steel/Steel*. *Bulletin of JSME*, 21(158):1311–1317, 1978.

[NARUSE et al., 1986] NARUSE, C., HAIZUKA, S., NEMOTO, R., and UMEZU, T. *Limiting Load for Scoring and Frictional Loss of Hypoid Gear: In Comparison with Spur Gear and Crossed Helical Gear, Using Mineral Oil and Synthetic Oil*. *Bulletin of JSME*, 29(253):2271–2280, 1986.

[Naunheimer, 2011] Naunheimer, B. J. W. a., H. Bertsche. *Automotive Transmissions: Fundamentals, Selection, Design and Application*. Springer Berlin Heidelberg, 2nd ed. edition, 2011. ISBN 978-3-642-16213-8,978-3-642-16214-5.

[Nijenbanning et al., 1994a] Nijenbanning, G., Venner, C., and Moes, H. *Film thickness in elastohydrodynamically lubricated elliptic contacts*. *Wear*, 176(2):217–229, 1994a.

[Nijenbanning et al., 1994b] Nijenbanning, G., Venner, C., and Moes, H. *Film thickness in elastohydrodynamically lubricated elliptic contacts*. *Wear*, 176(2):217–229, 1994b.

[OConnor et al., 1982] OConnor, B., Schiemann, L., and Johnson, R. *Axle Efficiency Response to Synthetic Lubricant Components*. Technical report, SAE Technical Paper, 1982. Http://dx.doi.org/10.4271/821181.

[O'donoghue and Cameron, 1966] O'donoghue, J. and Cameron, A. *Friction and temperature in rolling sliding contacts*. *ASLE TRANSACTIONS*, 9(2):186–194, 1966. Http://dx.doi.org/10.1080/05698196608972134.

[Ohlendorf, 1958] Ohlendorf, H. *Verlustleistung und Erwärmung von Stirnrädern*. Ph.D. thesis, Dissertation TU München, 1958.

[Oliveira et al., 2006] Oliveira, T., Martins, R., Seabra, J., Seyfert, C., and Igartua, A. *Efficiency tests of a transfer gearbox: biodegradable non-toxic ester vs.mineral oil*. *Mecânica Experimental*, (13):45–54, 2006.

[Palazzolo, 2009] Palazzolo, J. *High-performance Differentials, Axles & Drivelines*, 2009.

[Palmgren, 1959] Palmgren, A. *Ball and roller bearing engineering*. *Philadelphia: SKF Industries Inc., 1959*, 1, 1959.

[Parinam and Karan, 2014] Parinam, A. and Karan, R. *Analysis of Starved EHL Line Contacts for Lubricants with Linear Pressure Viscosity Dependence*. *International Journal of Advancements in Technology*, 5(1):11–27, 2014.

[von Petery, 2004] von Petery, G. *Fuel economy by custom-made: Bearings for differentials from BMW*. *ATZ worldwide*, 106(12):11–12, 2004.

[Petrusevich, 1951] Petrusevich, A. *Fundamental conclusions from the contact-hydrodynamic theory of lubrication*. *Izv. Akad. Nauk SSR (OTN)*, 2:209–233, 1951.

[Petry-Johnson et al., 2008] Petry-Johnson, T. T., Kahraman, A., Anderson, N., and Chase, D. *An experimental investigation of spur gear efficiency*. *Journal of Mechanical Design*, 130(6):062601, 2008. Http://dx.doi.org/10.1115/1.2898876.

[Pirro and Wessol, 2001] Pirro, D. and Wessol, A. *Lubrication fundamentals*. CRC Press, 2001.

[Pleguezuelos et al., 2010] Pleguezuelos, M., Pedrero, J., and Sánchez, M. *Simplified calculation method for the efficiency of involute helical gears*. In *New Trends in Mechanism Science*, pages 217–224. Springer, 2010. Http://dx.doi.org/10.1007/978-90-481-9689-0.

[Plint, 1967] Plint, M. A. *Third paper: traction in elastohydrodynamic contacts*. *Proceedings of the Institution of Mechanical Engineers*, 182(1):300–306, 1967.

[P.Nixon, 2006] P.Nixon, H. *The impact of Some Gear Lubricants on the Surface Durability of Rolling Element Bearings*. *SAE Technical Paper 2006-01-0357*, 2006. Http://dx.doi.org/10.4271/2006-01-0.57.

[Porrett et al., 1980] Porrett, D. C., Miles, S. D., Werderits, E. F., and Powell, D. L. *Development of a Laboratory Axle Efficiency Test*. Technical report, SAE Technical Paper, 1980. Http://dx.doi.org/10.4271/800804.

[Reynolds, 1886] Reynolds, O. *On the Theory of Lubrication and Its Application to Mr. Beauchamp Tower's Experiments, Including an Experimental Determination of the Viscosity of Olive Oil*. *Proceedings of the Royal Society of London*, 40(242-245):191–203, 1886.

[Rudnick, 2013] Rudnick, L. R. *Synthetics, mineral oils, and bio-based lubricants: chemistry and technology*. CRC press, 2013.

[Schlegel et al., 2009] Schlegel, C., Hösl, A., and Diel, S. *Detailed Loss Modelling of Vehicle Gearboxes*. In *Proceedings of the 7th Modelica Conference, Como, Italy*, 2009.

[Schlenk, 1994] Schlenk, L. *Unterscuchungen zur Fresstragfähigkeit von Grozahnrädern*. Ph.D. thesis, Dissertation TU München, 1994.

[Schwindaman, 2006] Schwindaman, S. *Beyond Suynthetics vs. Mineral Basestock or What Happened to the Application?*. *Lubrication Engineers, Leader in Lubricants*, 2006. URL http://www.lelubricants.com/lit/news/White%20Papers/beyond_synthetics_vs_mineral_basestock.pdf.

[Seabra et al., 2011] Seabra, J., Michaelis, K., Höhn, B.-R., and Hinterstoißer, M. *Influence factors on gearbox power loss*. *Industrial lubrication and tribology*, 63(1):46–55, 2011. Http://dx.doi.org/10.1108/00368791111101830.

[Seetharaman and Kahraman, 2009] Seetharaman, S. and Kahraman, A. *Load-independent spin power losses of a spur gear pair: model formulation*. *Journal of Tribology*, 131(2):022201, 2009. Http://dx.doi.org/10.1115/1.3085943.

[Seetharaman et al., 2009] Seetharaman, S., Kahraman, A., Moorhead, M., and Petry-Johnson, T. *Oil churning power losses of a gear pair: experiments and model validation*. *Journal of Tribology*, 131(2):022202, 2009. Http://dx.doi.org/10.1115/1.3085942.

[Shepard, 2013] Shepard, L. *Jeep, Dana & Chrysler Differentials: How to Rebuild the 8-1/4, 8-3/4, Dana 44 & 60 & AMC 20*, 2013.

[Shubkin, 1992] Shubkin, R. L. *Polyalphaolefins*. *CHEMICAL INDUSTRIES-NEW YORK-MARCEL DEKKER-*, 1992.

[Simmerrings and Seals,] Simmerrings, S. T. M. . and Seals, R. *Simrit Technichnical Manual 2007: Simmerrings and Rotary Seals*. *Technical Principales*, .

[Simon, 1981] Simon, V. *Elastohydrodynamic lubrication of hypoid gears*. *Journal of Mechanical Design*, 103(1):195–203, 1981.

[Simon, 1988] Simon, V. *Thermo-EHD analysis of lubrication of helical gears*. *Journal of Mechanical Design*, 110(3):330–336, 1988.

[Simon, 2000] Simon, V. *FEM stress analysis in hypoid gears*. *Mechanism and machine theory*, 35(9):1197–1220, 2000.

[SKF, 2013] SKF. *SKF Rolling Bearings General Catalogue*, 2013.

[Snidle and Evans, 1997] Snidle, R. and Evans, H. *Elastohydrodynamics of gears*. *Tribology Series*, 32:271–280, 1997.

[Speight and Exall, 2014] Speight, J. and Exall, D. I. *Refining Used Lubricating Oils*. CRC Press, 2014.

[Spindler and Von Petery, 2003] Spindler, D. and Von Petery, G. *Angular Contact Ball Bearings for a Rear Axle Differential*. Technical report, SAE Technical Paper, 2003. Http://dx.doi.org/10.4271/2003-01-3743.

[Stadtfeld, 2001] Stadtfeld, H. J. *The basics of spiral bevel gears*. *Gear Technology, February*, 2001.

[for Standardization. Technical Committee ISO/TC 57, 1996] for Standardization. Technical Committee ISO/TC 57, I. O. *ISO 4288. Geometrical Product Specifications (GPS). Surface Texture: Profile Method. Terms, Definitions and Surface Texture Parameters*. International Organization for Standardization, 1996.

[Stavytskyy et al., 2010] Stavytskyy, V., Nosko, P., Fil, P., Karpov, A., and Velychko, N. *Load-independent power losses of gear systems: A review*. *TEKA Kom. Mot. i Energ. Roln. B*, 10:205–213, 2010.

[Steffe and Daubert, 2006] Steffe, J. F. and Daubert, C. R. *Bioprocessing pipelines: rheology and analysis*. Freeman Press, 2006.

[Stokes, 1992] Stokes, A. *Manual Gearbox Design*. Butterworth-Heinemann, 1992. ISBN 9780750604178. URL http://books.google.pt/booksid=36SpQgAACAAJ.

[Stribeck and Schröter, 1903] Stribeck, R. and Schröter, M. *Die wesentlichen Eigenschaften der Gleit-und Rollenlager: Untersuchung einer Tandem-Verbundmaschine von 1000 PS*. Springer, 1903.

[Talbot et al., 2016] Talbot, D., Kahraman, A., Li, S., Singh, A., and Xu, H. *Development and Validation of an Automotive Axle Power Loss Model*. *Tribology Transactions*, 59(4):707–719, 2016. Http://dx.doi.org/10.1080/10402004.2015.1110862.

[Tallian, 1967] Tallian, T. *On competing failure modes in rolling contact*. *ASLE TRANSACTIONS*, 10(4):418–439, 1967. Http://dx.doi.org/10.1080/05698196708972201.

[Tan et al., 1991] Tan, J., Yamada, T., and Hattori, N. *Effects of sliding/rolling contact on worm gear lubrication*. In *Proceedings of JSME International Conference on Motion and Power Transmissions, Tokyo*, pages 1123–1127, 1991.

[Taylor et al., 1997] Taylor, C., Flamand, L., Dalmaz, G., Dowson, D., Childs, T., Berthier, Y., Georges, J., and Lubrecht, A. *Elastohydrodynamics-'96: fundamentals and applications in lubrication and traction*, volume 32. Elsevier, 1997.

[Terekhov, 1975] Terekhov, A. *Hydraulic losses in gearboxes with oil immersion*. *Russian Engineering Journal*, 55(5):7–11, 1975.

[Totten, 2012] Totten, G. E. *Handbook of Lubrication and Tribology: Volume I Application and Maintenance*, volume 1. CRC Press, 2012.

[Trachman et al., 1977] Trachman, E., Williams, R., and Sheng, P. *Orientation effects in the friction of a hard ellipsoid sliding on rubber*. *Journal of Applied Physics*, 48(8):3270–3273, 1977. Http://dx.doi.org/10.1063/1.324206.

[Vaishya and Houser, 1999] Vaishya, M. and Houser, D. R. *Modeling and measurement of sliding friction for gear analysis*. AGMA, 1999.

[Prakash del Valle, 2014] Prakash del Valle, C. *Thermal modelling of an FZG test gearbox*, 2014.

[Vijayakar, 2004] Vijayakar, S. *Calyx Hypoid Gear Model, User Manual*, 2004.

[Vinci et al., 2004] Vinci, J. N., Grisso, B. A., Schenkenberger, C., Qureshi, F. S., Gahagan, M. P., and Hasegawa, H. *Systematic formulation of efficient and durable axle lubricants for light trucks and sport utility vehicles*. Technical report, SAE Technical Paper, 2004. Http://dx.doi.org/10.4271/2004-01-3030.

[Walter, 1982] Walter, P. *Anwendungsgrenzen für die Tauchschmierung von Zahnradgetrieben, Plansch-und Quetschverluste bei Tauchschmierung: Forschungsvorhaben Nr. 44/I; Abschlußbericht*, 1982.

[Wang et al., 2007] Wang, J., Lim, T. C., and Li, M. *Dynamics of a hypoid gear pair considering the effects of time-varying mesh parameters and backlash nonlinearity*. *Journal of Sound and Vibration*, 308(1):302–329, 2007. Http://dx.doi.org/10.1016/j.jsv.2007.07.042.

[Warden et al., 2010] Warden, R., Brandt, A., Comfort, A., and Villahermosa, L. *Fuel Efficiency Effects of Lubricants in Military Vehicles*. Technical report, SAE Technical Paper, 2010. Http://dx.doi.org/10.4271/2010-01-2180.

[WILEY-VCH Verlag GmbH & Co. KGaA, 2007] WILEY-VCH Verlag GmbH & Co. KGaA, W. *Lubricants and Lubrication*, 2007.

[Willermet and Dixon, 1977] Willermet, P. and Dixon, L. *Fuel Economy-Contribution of the Rear Axle Lubricant*. Technical report, SAE Technical Paper, 1977. Http://dx.doi.org/10.4271/770835.

[Winter and Oster, 1987] Winter, H. and Oster, P. *Influence of the Lubricant on Pitting and Micro Pitting (grey Staining, Frosted Areas) Resistance of Case Carburized Gears: Test Procedures*. American Gear Manufacturers Association, 1987.

[Winter and Wech, 1988] Winter, H. and Wech, L. *Measurements and optimization of the efficiency of hypoid axle drives of vehicles*. Technical report, SAE Technical Paper, 1988. Http://dx.doi.org/10.4271/885127.

[Xu, 2005] Xu, H. *Development of a generalized mechanical efficiency prediction methodology for gear pairs*. Ph.D. thesis, The Ohio State University, 2005.

[Xu and Kahraman, 2007] Xu, H. and Kahraman, A. *Prediction of friction-related power losses of hypoid gear pairs*. *Proceedings of the Institution of Mechanical Engineers, Part K: Journal of Multi-body Dynamics*, 221(3):387–400, 2007. Http://dx.doi.org/10.1243/14644193JMBD48.

[Xu et al., 2007] Xu, H., Kahraman, A., Anderson, N., and Maddock, D. *Prediction of mechanical efficiency of parallel-axis gear pairs*. *Journal of Mechanical Design*, 129(1):58–68, 2007. Http://dx.doi.org/ 10.1115/1.2359478.

[Xu et al., 2012] Xu, H., Singh, A., Kahraman, A., Hurley, J., and Shon, S. *Effects of Bearing Preload, Oil Volume, and Operating Temperature on Axle Power Losses*. *Journal of Mechanical Design*, 134(5):054501, 2012. Http://dx.doi.org/10.1115/1.4006325.

[Xu et al., 2011] Xu, H., Singh, A., Maddock, D., Kahraman, A., and Hurley, J. *Thermal mapping of an automotive rear drive axle*. *SAE International Journal of Engines*, 4(2011-01-0718):888–901, 2011. Http://dx.doi.org/10.4271/2011-01-0718.

[Zhang and Gou, 1989] Zhang, P.-S. and Gou, J.-H. *Two new formulae to calculate the film thickness in elastohydrodynamic lubrication and an evaluation of Grubin's formula*. *Wear*, 130(2):357 – 366, 1989. ISSN 0043-1648. doi:http://dx.doi.org/10.1016/0043-1648(89)90189-0. URL http://www.sciencedirect.com/science/article/pii/0043164889901890.

A. Lubricants

A.1. Axle gear oil viscosity classifications

Table A.1: Axle and Manual Transmission Lubricant Viscosity Classification – SAE J306, 1998 [vis,].

Automotive Lubricant Viscosity Grades Gear Oils −Except SAE J306, 1998			
SAE Viscosity Grade	Maximum Temperature for a viscosity of 150,000 cP (°C)	Minimum Viscosity at (cSt) a 100 °C	Maximum Viscosity at (cSt) a 100 °C
	ASTM D 2983	ASTM D 445	ASTM D 445
70W	-55	4.1	–
75W	-40	4.1	–
80W	-26	7.0	–
85W	-12	11.0	–
80	–	7.0	<11.0
85	–	11.0	<13.5
90	–	13.5	<18.5
110	–	18.5	<24.0
140	–	24.0	<32.5
190	–	32.5	<41.0
250	–	41.0	–

Table A.2: U.S Military Axle and Manual Transmission Lubricant Viscosity Classification – MIL-PRF-2105E/SAE J2360, April 2001 [J.Shah, 2003].

Gear oil viscosity grade	Maximum Temperature for a viscosity of 150,000 cP (°C)	Minimum Viscosity at (cSt) a 100 °C	Maximum Viscosity at (cSt) a 100 °C	Channel point
	ASTM D 2983	ASTM D 445	ASTMD 445	FTM 3456
75W	-40	4.1	–	-45
80W-90	-26	13.5	<24.0	-35
85W-140	-12	24	<41.0	-20

A.2. API Classifications

Table A.3: API Gear Lubricant Service Designations − 1996 [Rudnick, 2013].

GL-1	Lubricants for this service are considered to be equivalent to straight mineral oil for anti-scoring properties. Inhibitors (oxidation, rust, foam) may be present in the oil. Designated for lubricant service for mild conditions and low unit pressures (automotive spiral and worm gear axles, low torque manual transmissions). The reference oil would be the CRC reference oil RGO-100.
GL-2	Lubricants for this service are lightly treated with anti-wear or mild EP additives (usually fatty acids or esters) for improved anti-scoring protection for automotive worm gears
GL-3	Lubricants for this service contain active anti-wear or mild EP additives for improved anti-scoring protection over the GL-2 level. Designated for manual transmissions (synchronized and non-synchronized) and lightly loaded axles (spiral bevel gears). The GL-3 CRC reference oil is RGO-104.
GL-4	Lubricants for this service contain active EP additives for passenger car or moderately loaded hypoid axle gears. Designated for synchronized and non-synchronized manual transmissions, spiral bevel axles, and moderate load hypoid axles. The GL-4 reference oil is the CRC RGO-105. Some test platforms are obsolete for the GL-4. The industry has allowed a half EP additive treat version of an approved GL-5 oil for this category.
GL-5	Lubricants for this service contain highly active EP additives for moderately or heavily loaded hypoid gears in axles for passenger cars and trucks. Similar to MIL-L-2105D performance requirements. Combined with API MT-1 for non-synchronized heavy-duty manual transmission service. The GL-5 uses a set of RGO reference oils for the various performance categories.
GL-6	Lubricants for this service contain up-treated levels of highly active EP additive for severe service involving high offset hypoid gear axles. An obsolete category designed for a single application.
MT-1	Lubricants for this service contain active anti-wear or EP additives for heavy-duty manual transmissions. Designated for non-synchronized heavy-duty transmissions, it must have minimum resistance to thermal/oxidative degradation and exhibit satisfactory performance with plate type synchronizers. This category has been combined with the GL-5 (MIL-L-2105D) to define the MIL-PRF-2105E/SAE2360 performance category.

A.3. Additives

A.3.1. Viscosity Index improvement

Viscosity Index improver are widely used in multigrade oils where the viscosity at high and low temperature is specified.

Since the viscosity of the lubricant clearly decreases at high temperature and oil lubrication ability deceases with low viscosity, the Viscosity Index improver are needed to keep the viscosity at acceptable levels and to provide a stable oil film even at high temperatures.

VI improver are long chain, high molecular weight polymers that increase the relative viscosity of the oil more at high temperature and at low temperatures. This is the result of the change in the physical configuration of the polymer with increasing temperature of the mixture. In cold oil, the viscosity is minimized because the polymer adopt a coiled form. In hot oil, the molecules tend to straighten out, and the interaction between these long molecules and the oil produces a proportionally greater thickening effect [Speight and Exall, 2014].

The most important VI improvers are methacrylate polymers and copolymers, acrylate polymers, olefin polymers and copolymers, and styrene butadiene copolymers. The amount of VI improvement from these materials depends on the molecular weight distribution of the polymer [Pirro and Wessol, 2001].

For the Newtonian fluids the viscosity is independents of the shear rate. The long molecules in VI improver are subject to degradation due to mechanical shearing in service. They align themselves in the direction of the stress, which reduces the resistance to flow. When the stress is removed, the molecules return to their usual random arrangement and the temporary viscosity loss is recovered. This effect can be beneficial due to the reduction of oil friction which makes an easier starting at cold weather [Pirro and Wessol, 2001].

A.3.2. Antiwear/extreme pressure additives

Automotive gear oils require different levels of antiwear and extreme pressure performance capabilities depending on the application. The predominant type of antiwear additive for automotive gear lubricants are phosphorus based active or nonactive systems. Then, the majority of EP additive for automotive gear lubricants, worldwide, are based on sulfur/phosphorus chemistry. These organic compounds react with metal surfaces in order to produce a protective films under boundary lubrication conditions [Totten, 2012]. These films are effective under low to moderate temperatures and loads. Furthermore, extreme pressure agents are more effective under heavy load and high temperature conditions.

So, the presence of antiwear/extreme pressure additives is prominent in gear oils, particularly with modern systems which operate under higher temperature, high contact pressure, longer drain intervals, and smaller sump size. Figure A.1 proves the effectiveness of antiwear/extreme pressure additives which compare the results of a used gear in L-37 test with an SAE 90 for GL-1 without those additives and SAE 80W90 for GL-5 gear oil that

contains those additives. It is clear that antiwear and extreme pressure additives are necessary to reduce fretting of metallic friction bodies and minimize material removal caused by wear [Mang, 2014].

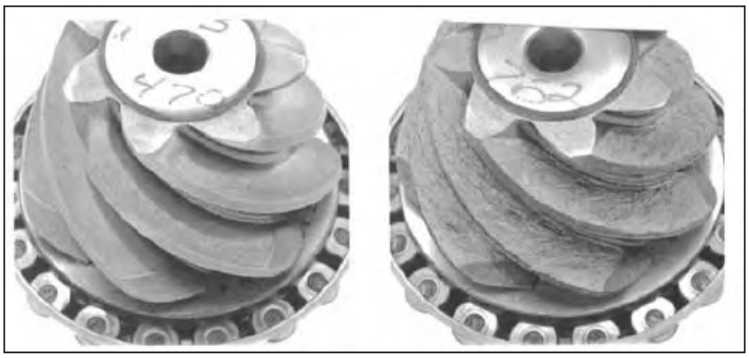

Figure A.1: Gear results from L-37 test [Totten, 2012].

The level of antiwear or EP additive needed for a specific application depends on the bulk oil viscosity and type of base stock used. Thus, higher SAE grades of axle gear oils generally require a lower additive treat for the same level of gear protection. PAO and ester based gear oils usually require an antiwear or EP additive overtreat for the same level of gear wear protection compared to using higher viscosity petroleum oil basestocks. Since, esters may compete with the additives on the metal surfaces, they may require more active additive package with higher concentration of antiwear or EP additive [Rudnick, 2013].

Most manual transmissions require only low levels of active or nonactive EP additive or antiwear additive for gear protection. Planetary, spiral bevel, and hypoid gear axle systems require active EP, either at the GL-4 or GL-5 additive level. The amount and the activity of the EP additive should be studied because it can have a negative impact on bearing life and elastomer durability in axles due to the conflict between EP additives and thermal stability.

A.3.3. Detergent and dispersant

Detergents and dispersants together correspond to 45 to 50 % of the total volume of lubricant additives manufactured. Detergents neutralize oxidation-derived acids as well as help suspend polar oxidation products in the lubricant.

A.3.4. Corrosion inhibitors

The lubricant carry out another role which is the prevention of system corrosion in environments where the contamination exist in the system like water. Corrosion inhibitors form a barrier film on the metallic surfaces of the mechanical equipment in order to protect them from attack of oxygen, water and other chemically active substances. Corrosion by organic

acids in oil can occur in the bearing for example. The corrosion inhibitors form a protective film on the bearing surfaces which do not allows the corrosive materials to reach or attack the metal. The film may be either adsorbed on the metal or chemically bonded to it. It has been found that the inclusion of highly alkaline materials in the oil will help neutralize these strong acids as they are formed, greatly reducing corrosive wear [Speight and Exall, 2014].

In order to prevent surfaces from corrosion, some inhibitors like basic sulfonates and futty amines can be used.

A.3.5. Oxidation inhibitors

Lubricating properties are reduced due to oxidation under high temperatures and long lubrication intervals. In fact, almost lubricants are sensitive to oxidation because they are made of hydrocarbon molecules in base oils which react with the oxygen present in the atmosphere at higher temperature resulting in peroxy or other radicals [Totten, 2012]. The oxidation reaction can be accelerated with the increase of temperature and the presence of metallic wear particles. The oxidation reaction produce the increase of oil viscosity, formation of sludge and varnish, corrosion of metallic parts and foaming. An antioxidant can act as a radical inhibitor of one of the steps of oxidation by neutralization of the free radicals. These are compounds such as phenol, alkaline earth phenolates and salicylates, and aromatic amines. In addition, an antioxidant destructive to oxidation products, such as hydroperoxide compounds which can initiate new oxidation chain reactions. It is a necessary additive for most lubricating oils [Speight and Exall, 2014]. So, using antioxidants additives can improve the lifetime.

A.3.6. Antifoaming agents

At low temperature, the churning action of gears in axles can be the source of air entrainment or foaming. Certain inhibitors are used such as silicone or alkyl polymethacrylate with low molecular weight in order to avoid foaming which is due to the presence of detergents and dispersing agents. These molecules are insoluble in oil and concentrate at the liquid–air interface. Their weak surface tension inhibits the formation of stable foam by rapid coalescence of air bubbles. Foaming not only enhances oxidation but also decreases the lubrication effect causing oil starvation. That's why a small quantity of antifoam additive is required to decrease the tendency of oil foaming.

B. Surface roughness

The topographies of the lower races of the roller thrust bearing RTB, were acquired data from a sample area with 5.8 mm of length (radial direction) and 0.8 mm of width. Figure B.1 shows the topographies of raceway of a new (a) and used (b) RTB, lubricated with axle gear oil 80W90-A. The differences between the topographies of the new and used RTB raceways are not significant. Table B.1, presents the 3D roughness parameters (S_a, S_q, S_p, S_v, S_z, S_{sk} and S_{ku}) of the new and used RTB (after 24 hours of testing).

From the surface topographies, it is possible to extract 2D roughness profiles across the contact track, in the radial direction. Figure B.2 shows examples of these roughness profiles for all raceways, new and used.

Table B.2, presents the 2D roughness parameters (R_a, R_q, R_{max}, R_z, R_{sk}, R_{ku}, R_{pk}, R_{vk}, M_{r1} and M_{r2}) of the new and used RTB raceways (after 24 hours of testing).

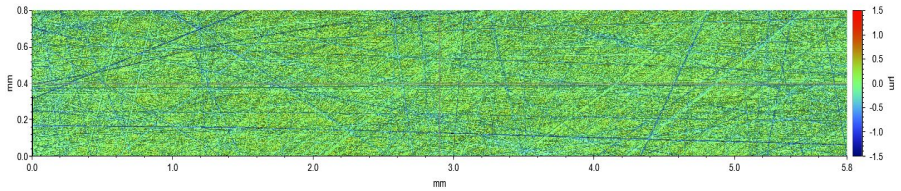

(a) New.

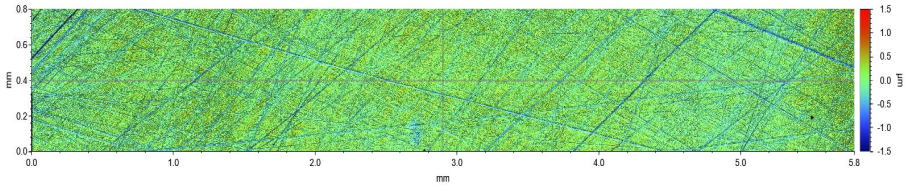

(b) 80W90-A.

Figure B.1: New and used RTB raceways surface analysis.

Table B.1: 3D roughness parameters on raceways.

Parameter	Units	New	75W85-B	75W90-A	75W90-B	80W90-A	75W140-A
S_a	[μm]	0.144	0.159	0.120	0.139	0.122	0.088
S_q	[μm]	0.193	0.218	0.166	0.190	0.167	0.125
S_p	[μm]	1.678	1.947	1.619	2.739	2.572	1.450
S_v	[μm]	-1.982	-2.981	-2.050	-2.210	-1.932	-7.006
S_z	[μm]	3.660	4.927	3.669	4.949	4.504	8.457
S_{sk}	[-]	-0.624	-0.918	-0.887	-0.678	-0.750	-0.895
S_{ku}	[-]	5.149	6.233	8.355	6.339	7.115	14.510

Table B.2: 2D roughness parameters on the raceways.

Parameter	Units	New	75W85-B	75W90-A	75W90-B	80W90-A	75W140-A
R_a	[μm]	0.118	0.153	0.107	0.125	0.107	0.082
R_q	[μm]	0.161	0.210	0.150	0.173	0.147	0.119
R_{max}	[μm]	1.722	1.988	1.842	1.849	1.634	1.590
R_z	[μm]	1.146	1.461	1.099	1.244	1.009	0.969
R_{sk}	[-]	-0.417	-0.910	-0.817	-0.723	-0.716	-0.833
R_{ku}	[-]	6.073	6.076	8.225	6.797	7.263	10.960
R_{pk}	[μm]	0.218	0.238	0.204	0.220	0.186	0.172
R_{vk}	[μm]	0.260	0.382	0.277	0.305	0.261	0.228
M_{r1}	[%]	9.678	8.366	9.608	9.211	8.982	10.219
M_{r2}	[%]	86.826	85.028	84.982	86.354	86.134	85.975

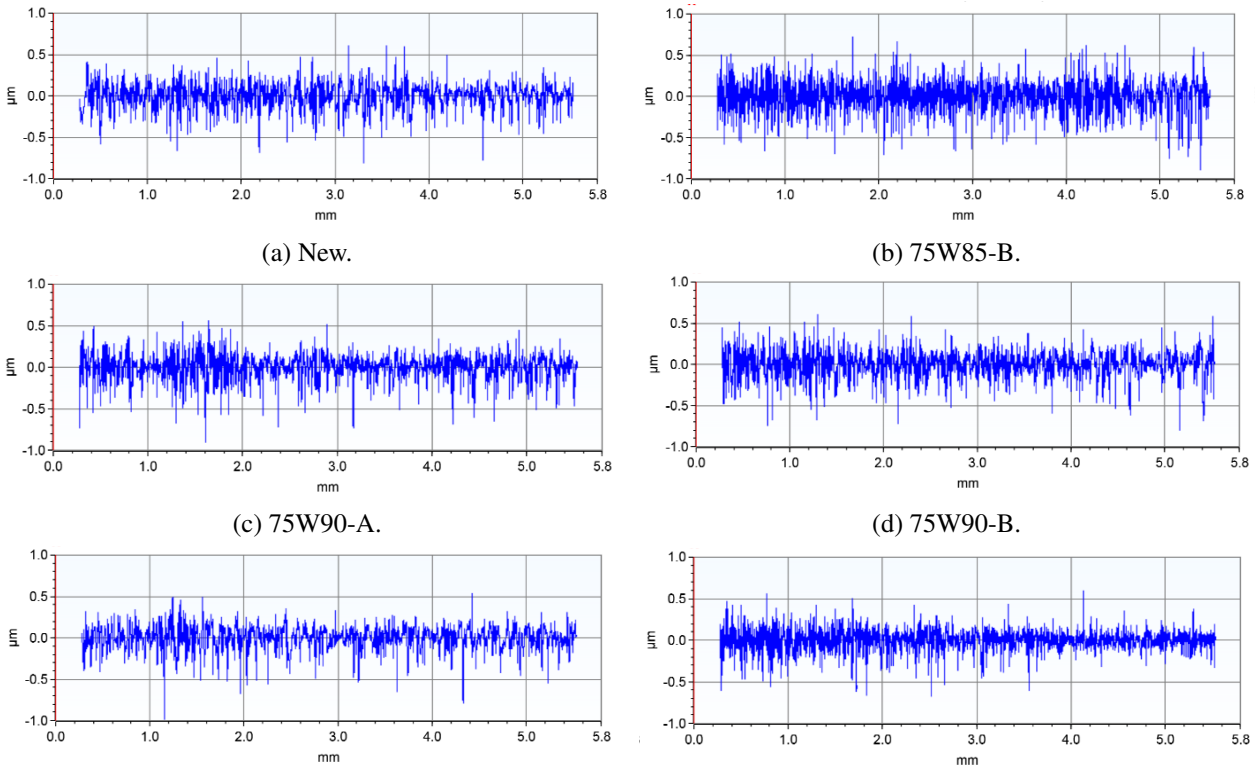

(a) New.

(b) 75W85-B.

(c) 75W90-A.

(d) 75W90-B.

(e) 80W90-A.

(f) 75W140-A.

Figure B.2: The roughness profile of the raceways.

C. Pre-test surface analyses XPS

Figures C.1 and C.2 display the curve fitting of C, O, Mg, P, S, Ca, Fe and Zn, XPS spectra recorded in tribofilms of the rollers submerged (S) and tested (M), respectively lubricated with oil 75W140-A. Figure C.3 presented the XPS spectra of rollers submerged (S) and tested (M) with the five axle gear oils.

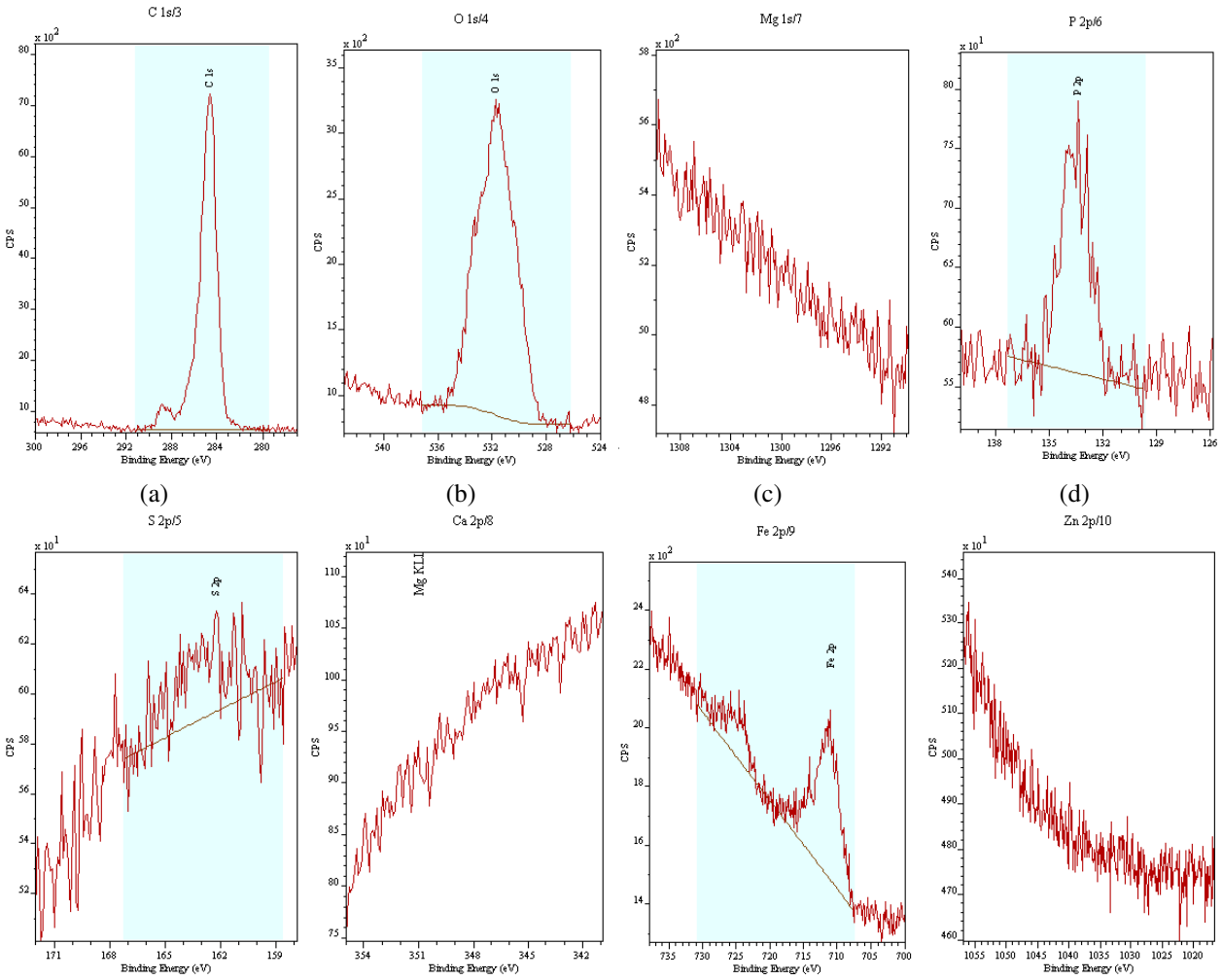

Figure C.1: C 1s/3, O 1s/4, Mg 1s/7, P 2p/5, S 2p/5, Ca 2p/8, Fe 2p/9 and Zn 2p/10 peaks curve fitting recorded in tribofilms of the rollers submerged (S) in oil 75W140-A.

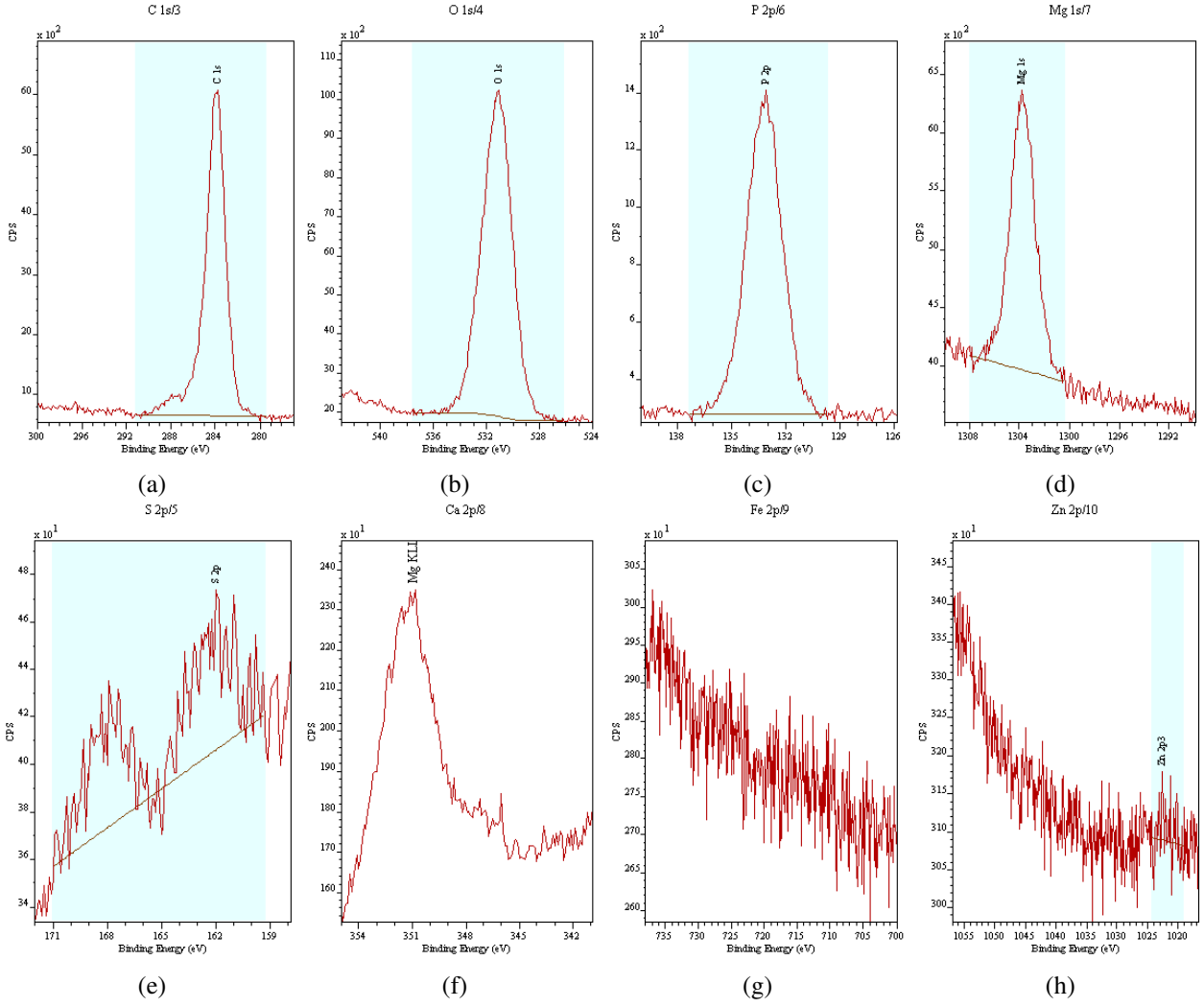

Figure C.2: C 1s/3, O1s/4, P 2p/6, Mg 1s/7, S2p/5, Ca 2p/8, Fe 2p/9 and Zn 2p/10 peaks curve fitting recorded in tribofilms generated on the tested rollers (M) lubricated with oil 75W140-A.

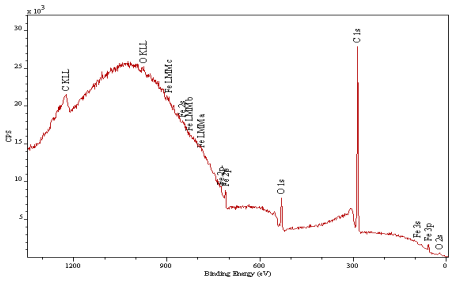

(a) 75W85-B (S).

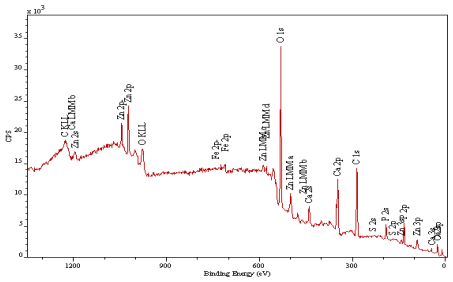

(b) 75W85-B (M).

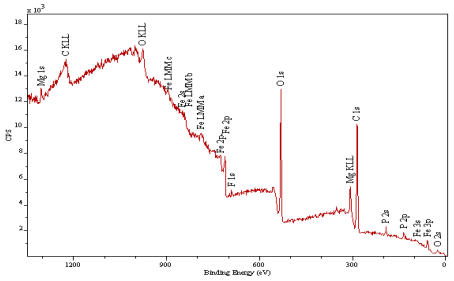

(c) 75W90-A (S).

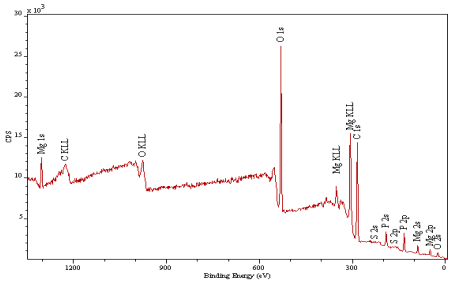

(d) 75W90-A (M).

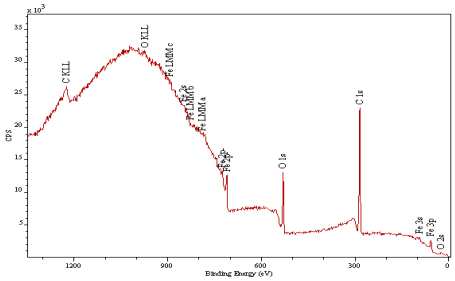

(e) 75W90-B (S).

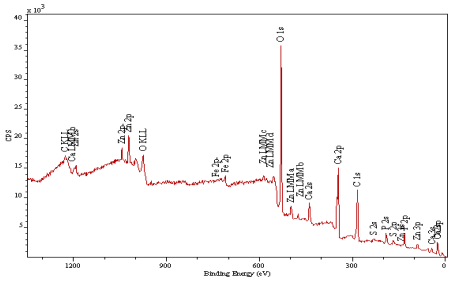

(f) 75W90-B (M).

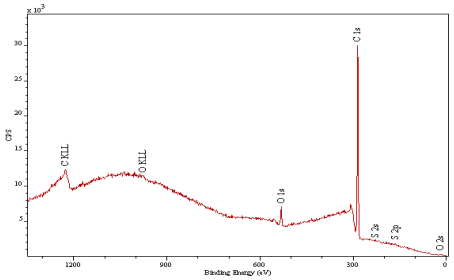

(g) 80W90-A (S).

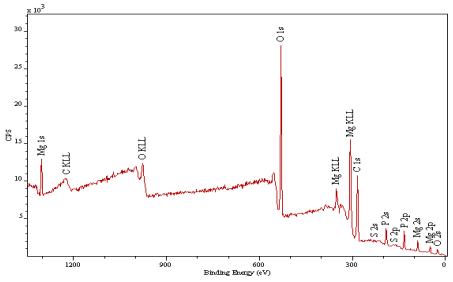

(h) 80W90-A (M).

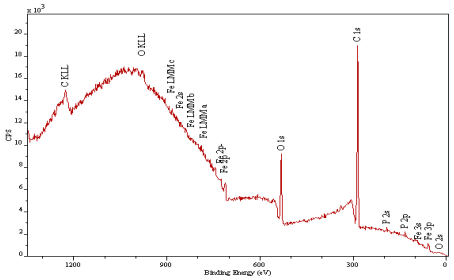

(i) 75W140-A (S).

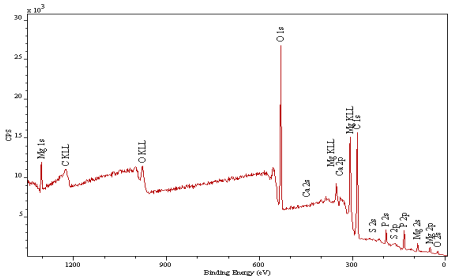

(j) 75W140-A (M).

Figure C.3: XPS spectra of the RTB 81107 rollers submerged (S) and tested (M) lubricated with all axle gear oils.

D. Traction curves

D.1. Traction curves for the operating temperature of T = 70 °C using smooth disc

The experimental traction curves were obtained for three oil operating temperatures and for three input speeds. In Figure 4.19 are presented the traction curves for the three entrainment speed at 40 °C and 100 °C allowing to understand the general trend, while Figure D.1 displays traction curves for the operating temperature of 70 °C at all input speeds.

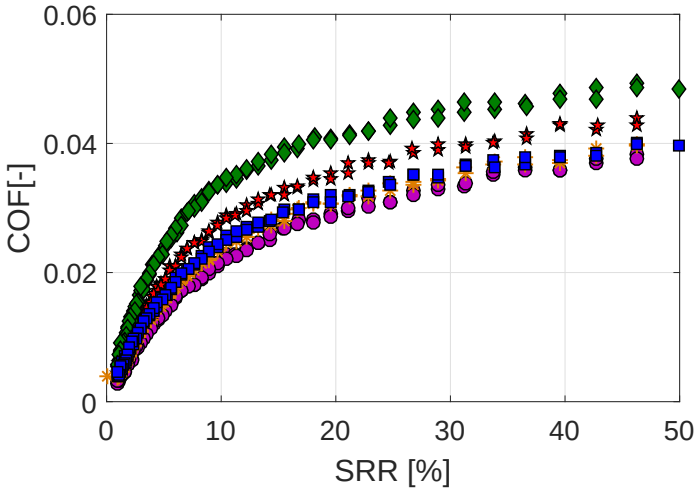

(a) T = 70 °C ; U = 0.5 m/s

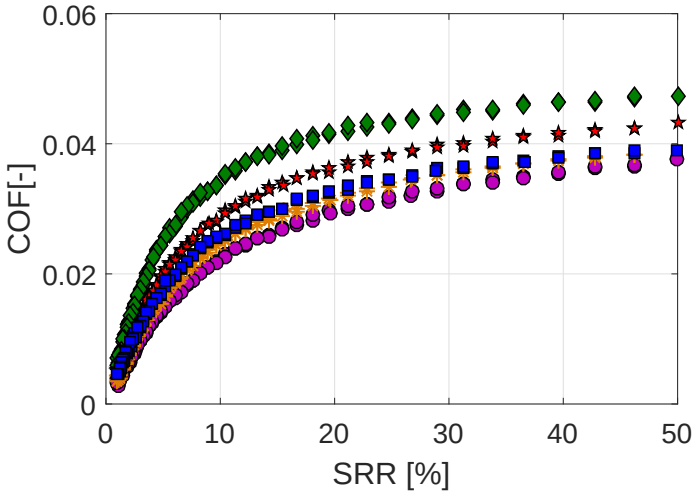

(b) T = 70 °C ; U = 1 m/s

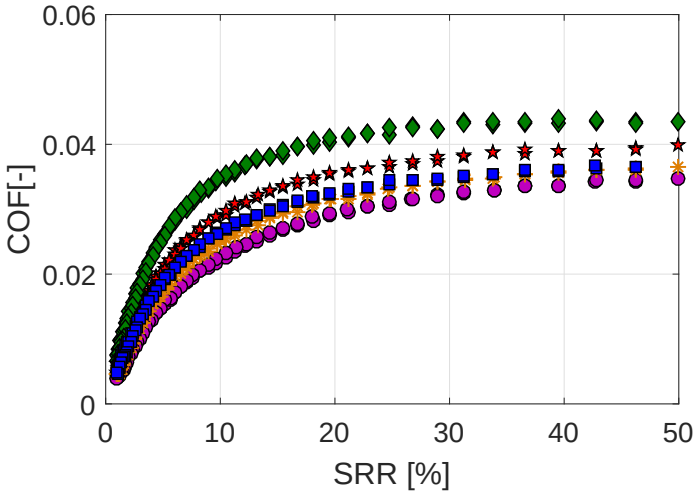

(c) T = 70 °C ; U = 2 m/s

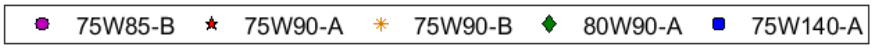

Figure D.1: Traction curves for the five axle gear oils using smooth disc: (a), (b), and (c) at 70 °C.

D.2. Traction curves for the operating temperature of T = 70 °C using rough disc

The experimental traction curves at 70 °C are shown in Figure D.2 Each subfigure plots the coefficient of friction (COF) versus the slide-to-roll ratio (SRR) for all five axle gear oils and for a certain combination of operating conditions (temperature and speed).

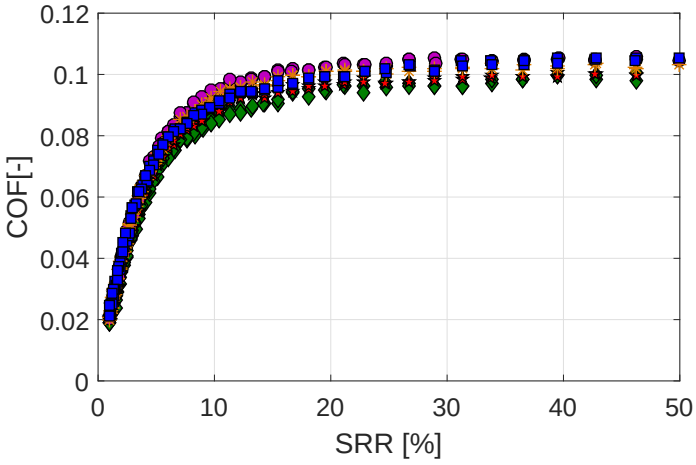

(a) T = 70 °C ; U = 0.5 m/s

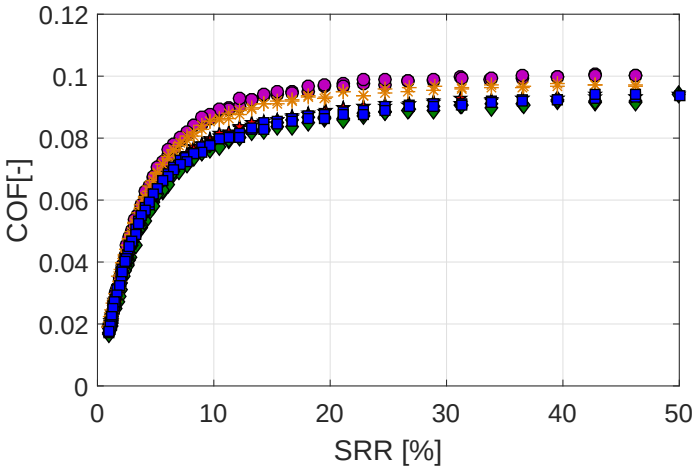

(b) T = 70 °C ; U = 1 m/s

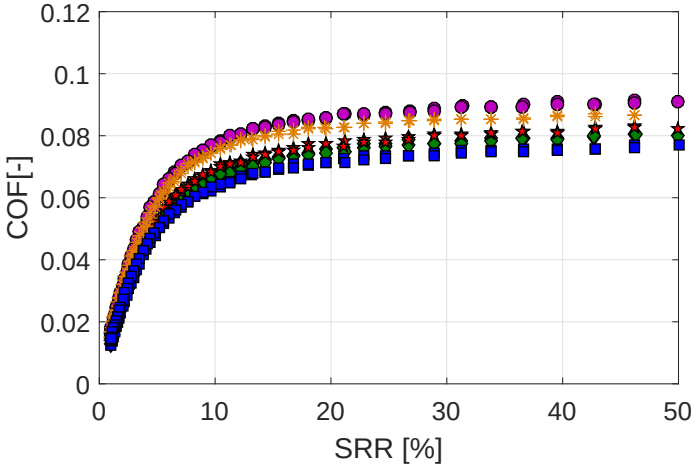

(c) T = 70 °C ; U = 2 m/s

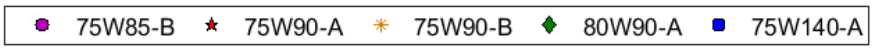

Figure D.2: Traction curves for the five axle gear oils using rough disc: (a), (b), and (c) at 70 °C.

E. SKF Friction Torque Model

The SKF rolling bearing friction torque model found in [Catalogue, 2005] is presented here with more details. In fact, all equations and constants will be specified for each rolling bearing type discussed in the present work depending on the rolling bearing assembly used.

The model divides the total friction torque of a rolling bearing in its true physical forms. It takes into account four different torque losses, the rolling torque (M_{rr}), the sliding torque (M_{sl}), the drag torque (M_{drag}) and the seals losses (M_{seal}) (see Equation (E.1)).

$$M_t = M'_{rr} + M_{sl} + M_{seal} + M_{drag} \tag{E.1}$$

E.1. Rolling Friction Torque - M'_{rr}

The rolling friction torque id calculated using Equation (E.2).

$$M'_{rr} = \phi_{ish} \cdot \phi_{rs} \cdot [G_{rr} \cdot (n \cdot \upsilon)^{0.6}] \tag{E.2}$$

where G_{rr} is the load distribution parameter presented in Table E.1 for different rolling bearing geometries. Different rolling bearing geometries were used for this work which are thrust ball bearing (TBB), cylindrical roller thrust bearing (RTB), angular contact ball bearing (ACBB), tapper roller bearing (TRB), four-point contact ball bearing (FPCB) and cylindrical roller bearing (CRB).

Table E.1: Bearing load constant G_{rr} for different rolling bearing geometries.

Rolling bearing	G_{rr}	$R1$	$R2$	$R3$
TBB 51107	$R1 \cdot d_m^{1,83} \cdot Fa^{0,54}$	1.03×10^{-6}	-	-
RTB 81107 TN	$R1 \cdot d_m^{2,38} \cdot Fa^{0,31}$	2.25×10^{-6}	-	-
ACBB 7203	$R1 \cdot d_m \cdot [Fr + Fg + R2 \cdot Fa]^{0,54}$	5.03×10^{-7}	1.97	1.9×10^{-12}
TRB 3320/28 X/Q	$R1 \cdot d_m^{2,38}(Fr + R2 \cdot Y \cdot Fa)^{0,31}$	2.38×10^{-6}	10.9	-
FCRB QJ 308	$R1 \cdot d_m^{1,97}(Fr + Fg + R2 \cdot Fa)^{0,54}$	4.78×10^{-7}	2.42	1.4×10^{-12}
CRB NJ 406	$R1 \cdot d_m^{2,41} \cdot Fr^{0,31}$	1.00×10^{-6}	-	-

As it is presented in Table E.1, in the angular contact ball bearing (ACBB) and in the four-point contact ball bearing (FCRB), the Fg is the centrifugal force and it is difined by Equation (E.3) and for tapper roller bearing (TRB), the Y is the calculation factor and it is equal to 1.7.

$$Fg = R3 \cdot d_m^4 \cdot n^2 \tag{E.3}$$

The rolling friction moment is also affected by two reduction factors, the inlet shear heating (ϕ_{ish}) and the kinematic replenishment/starvation (ϕ_{rs}).

The inlet shear heating occurs because not all the lubricant available in the bearing can go through the contact area. Only a small amount of it will recirculate in the inlet because of the reverse flow. This reverse flow generates heat, which lowers the viscosity of the lubricant, reduces film thickness and, therefore, lowers the rolling friction. This effect is taken into account in the SKF friction model by means of the inlet shear heating reduction factor ϕ_{ish}, which is calculated using Equation (E.4).

$$\phi_{ish} = \frac{1}{1 + 1.84 \cdot 10^{-9} \cdot (n \cdot d_m)^{1.28} \cdot \nu^{0.64}} \tag{E.4}$$

The kinematic replenishment/starvation is found in applications where the viscosity or speeds are high which hamper the replenishment of lubricant in the raceway. The kinematic starvation effect produces a reduction of the lubricant availability in the inlet of the contact which reduces the film thickness and the rolling friction. The replenishment/starvation effect is considered in the SKF friction model by means of the reduction factor ϕ_{rs}. This factor is a function of the lubricant supply mechanism as well and is calculated by Equation (E.5).

$$\phi_{rs} = \frac{1}{e^{K_{rs} \cdot \nu \cdot n \cdot (d+D) \cdot \sqrt{\frac{K_z}{2 \cdot (D-d)}}}} \tag{E.5}$$

where K_{rs} is the replenishment/starvation constant with value of 3×10^{-8} for low level oil bath and oil jet lubrication; and 6×10^{-8} for grease and oil-air lubrication. K_z is a bearing type related geometric constant.

The values are presented in Table E.2 for the different rolling bearing geometries.

Table E.2: Geometric constant K_z for different rolling bearing geometries.

Rolling bearing	K_z
TBB	3.8
RTB	4.4
ACBB	4.4
TRB	6
FPCB	3.1
CRB	5.1

E.2. Sliding Friction Torque - M_{sl}

The sliding friction torque is calculated in Equation (E.6).

$$M_{sl} = G_{sl} \cdot \mu_{sl} \tag{E.6}$$

The sliding friction torque depends mainly on the the sliding friction torque μ_{sl} and the bearing load constant G_{sl}.

Table E.3 depicts the bearing load constant G_{sl} influencing the sliding friction torque for the different rolling bearing geometries.

Table E.3: Bearing load constant G_{sl} for different rolling bearing geometries.

Rolling bearing	G_{sl}	$S1$	$S2$	$S3$
TBB 51107	$S1 \cdot d_m^{0,05} \cdot Fa^{4/3}$	1.6×10^{-2}	-	-
RTB 81107 TN	$S1 \cdot d_m^{0,62} \cdot Fa$	0.154	-	-
ACBB 7203	$S1 \cdot d_m^{0,26}((Fr+Fg)^{4/3} + S2 \cdot Fa^{4/3})$	1.3×10^{-2}	0.68	1.91×10^{-12}
TRB 320/28 X/Q	$S1 \cdot d_m^{0,82}(Fr + S2 \cdot Y \cdot Fa)$	0.014	2	-
FPCB QJ 308	$S1 \cdot d_m^{0,26}((Fr+Fg)^{4/3} + S2 \cdot Fa^{4/3})$	1.2×10^{-2}	0.9	1.4×10^{-12}
CRB NJ 406	$S1 \cdot d_m^{0,9} \cdot Fa + S2 \cdot d_m \cdot Fr$	0.16	0.0015	-

For the angular contact ball bearing (ACBB) and for the four-point contact ball bearing (FPCB), the Fg is the centrifugal force and it is given in Equation (E.7).

$$Fg = S3 \cdot d_m^4 \cdot n^2 \tag{E.7}$$

E.3. Drag Friction Torque - M_{drag}

The drag losses can be calculated by two Equations (E.8) and (E.9) for both ball bearings and roller bearings, respectively.

$$M_{drag} = 0.4 \cdot V_M . K_{ball} . d_m^5 . n^2 + 1.093 \times 10^{-7} \cdot n^2 \cdot d_m^3 \cdot (\frac{n \cdot d_m^2 \cdot f_t}{\nu})^{-1.379} \cdot R_s \tag{E.8}$$

$$M_{drag} = 4 \cdot V_M \cdot K_{roll} \cdot C_w \cdot B \cdot d_m^4 \cdot n^2 + 1.093 \times 10^{-7} \cdot n^2 \cdot d_m^3 \cdot (\frac{n \cdot d_m^2 \cdot f_t}{\nu})^{-1.379} \cdot R_s \tag{E.9}$$

where the rolling element related constants are given in Equations (E.10) and (E.11).

$$K_{ball} = \frac{i_{rw} \cdot K_Z \cdot (d+D)}{D-d} \times 10^{-12} \tag{E.10}$$

where i_{rw} is the number of ball rows.

$$K_{roll} = \frac{K_L \cdot K_Z \cdot (d+D)}{D-d} \times 10^{-12} \tag{E.11}$$

Table E.4 presents the constant K_L and the constant K_Z is presented in Table E.2.

Table E.4: Geometric constant K_L for different rolling bearing geometries.

Rolling bearing	K_L
TBB	-
RTB	0.43
ACBB	-
TRB	0.7
FPCB	-
CRB	0.65

The C_w factor is given by Equation (E.12) and l_D given by Equation (E.13).

$$C_w = 2.789 \times 10^{-10} \cdot l_D^3 - 2.786 \times 10^{-4} \times l_D^2 + 0.0195 \cdot l_D + 0.6439 \tag{E.12}$$

$$l_D = 5 \cdot \frac{K_L \cdot B}{d_m} \tag{E.13}$$

Other constants like f_t, R_s, t, and f_A are presented in details in Equations (E.14), (E.15), (E.16), (E.17) and (E.18).

$$f_t = sin(0.5t), \;\; when \;\; 0 \leq t \leq \pi \tag{E.14}$$

$$f_t = 1, \;\; when \;\; \pi \leq t \leq 2\pi) \tag{E.15}$$

$$R_s = 0.36 \cdot d_m^2 \cdot (t - sin\, t) \cdot f_A \tag{E.16}$$

$$t = 2 \cdot cos^{-1} \cdot \frac{(0.6 \cdot d_m - H)}{0.6 \cdot d_m} \;\; when \;\; H \geq d_m, \;\; use \;\; H = d_m \tag{E.17}$$

$$f_A = 0.05 \cdot \frac{K_Z \cdot (D+d)}{D-d} \tag{E.18}$$

Tunisian Republic
Ministry of Higher Education and Scientific Research

University of Sfax
National School of Engineers of Sfax

Doctoral School of Sciences and Technologies

Doctoral Thesis – Order Number:

University of Porto
Engineering Faculty

Doctoral Program in Mechanical Engineering

December 2017

Efficiency and Wear in Automotive Gear Transmissions

Hammami Maroua

الخلاصة: الهدف الرئيسي من هذا المشروع هو الزيادة إلى حد كبير في كفاءة الإرسال المحور. للوصول إلى هذا الهدف الطموح، تم درس فقدان الطاقة في المحامل والتروس مشحم بالزيوت تروس المحور، وتبين أن وضع النفط و هندسة التروس و المحامل لها تأثير كبير على فقدان الطاقة في علب التروس.....

Résumé : L'objectif principal du projet est d'augmenter de manière significative l'efficacité des transmissions d'essieux. Pour atteindre cet objectif ambitieux, on a étudié la perte de puissance dans les roulements et les engrenages lubrifiés avec des huiles pour engrenages d'essieu, montrant que la formulation d'huile ainsi que la géométrie des engrenages et de la géométrie des paliers à roulements ont une influence très importante sur les pertes de puissance des boites de vitesses.....

Abstract: The main goal of the project is to increase, significantly, the efficiency of axle transmissions. To reach such ambitious objective, the power loss in rolling bearings and gears lubricated with axle gear oils was studied, showing that the oil formulation and the gears and rolling bearings geometry have a very significant influence on the power loss of gearboxes.....

Resumo: O objetivo principal do projeto é aumentar significativamente a eficiência das transmissões de eixos. Para alcançar um objetivo tão ambicioso, estudou-se a perda de energia em rolamentos e engrenagens lubrificadas com óleos de engrenagens de eixos, mostrando que a formulação de óleo e a geometria das engrenagens e rolamentos têm uma influência muito significativa na perda de potência das caixas de engrenagens.....

المفاتيح: خصائص التريبولوجية؛ فيلم التشحيم؛ سلوك الاحتكاك؛ فقدان الطاقة؛ المحامل؛ التروس .
Mots clés: huiles essieu; propriétés tribologiques; film lubrifiant; Comportement au frottement; perte de puissance; roulements; engrenages...

Key-words: axle oils; tribological properties; lubricating film; friction behaviour; power loss; rolling bearings; gears……

Palavras-chave: óleos de eixo; Propriedades tribológicas; Filme lubrificante; Comportamento de fricção; Perda de energia; Rolamentos; Engrena .....